

Impact of New Seismic Design Provisions on Bridges in Mid-America: A PILOT POOLED FUNDS PROJECT

TPF-5(155)

FHWA, AR, GA, IL, IN, MO, TN

Authored by

Reginald DesRoches,

Professor and Associate Chair of Georgia Institute of Technology, Atlanta, GA

Jamie E. Padgett,

Assistant Professor, Rice University, Houston, TX

Oh-Sung Kwon

Assistant Professor, Missouri University of Science and Technology, Rolla, MO

Aman Mwafy,

Assistant Professor, United Arab Emirates University, Al Ain, UAE

Amr S. Elnashai,

Professor and Director of the MAE Centre, University of Illinois at Urbana-Champaign, Urbana, IL

Linda Kuo-Lin

Genex Systems LLC - Hampton, VA

J. Jerry Shen

Genex Systems LLC - Hampton, VA

Submitted to

FHWA COTR, W. Phillip Yen, Ph.D., P.E.

Office of Infrastructure, R&D, FHWA, McLean, VA

September 30, 2012

TABLE OF CONTENTS

Table of Contents	v
List of Tables	ix
List of Figures	xi
Chapter 1 Introduction	1
Background	1
Objectives	3
Work performed.....	3
Documental organization	4
Chapter 2 Seismic Hazard of the CSUS	7
2.1 Maps used in design guidelines	7
2.2 Procedures for obtaining design ground motion	9
AASHTO Standard Specifications—Division I-A	9
NCHRP 12-49 Recommendations	10
Impact from the NCHRP 12-49 Recommendations	10
AASHTO Guide Specifications 2007	27
FHWA Seismic Retrofitting Manual	31
Displacement capacity verification.....	32
2.2 Simulation of earthquake ground motion for the CSUS	32
Base response spectrum at rock sites	33
Site Response Spectrum Modification.....	36
2.3 Ground motion tools for bridge design and retrofitting.....	39
Product specifications and System requirement	40
User Instructions	40
Chapter 3 Seismic Vulnerability and Retrofit of Bridges in the Central and Southeastern United States	43
3.1 INTRODUCTION	43
3.2 Bridge Construction and Vulnerabilities	43
Bridge Construction	43
Vulnerability of Bridges	46
Past Earthquake Damage to Bridges.....	47
3.3 OVERVIEW OF BRIDGE RETROFIT IN CENTRAL AND SOUTHEASTERN UNITED STATES.....	48
3.3.1 COLUMN RETROFIT	51
Background	51
Examples of Column Retrofits.....	53
3.3.2 ISOLATION	56
Background	56
Examples of Isolation	58
3.3.3 LONGITUDINAL RESTRAINER BARS AND CABLES	60
Background	60
Examples of Longitudinal Restrainers.....	61
3.3.4 OTHER LONGITUDINAL RESTRAINT AND RESPONSE MODIFICATION DEVICES	65
Background	65

Examples of Other Longitudinal Restraint and Response Modification Devices.....	65
3.3.5 SHEAR KEYS	66
Background	66
Examples of Shear Keys	67
3.3.6 SEAT EXTENDERS AND CATCHER BLOCKS	68
Background	68
Examples of Seat Extenders and Catcher Blocks	69
3.3.7 BENT CAP RETROFIT	71
Background	71
Examples of Bent Cap Retrofits	71
3.4 Effect of Seismic Retrofit Bridge Performance	73
3.5 State-of-the-Art in Bridge Fragility	77
3.6 Application of Bridge Fragility Curve.....	82
3.6.1 Vulnerability Assessment	82
Reduction in Failure Probability.....	82
Median Value Shift of the Fragility and Comparison at Other Percentiles	83
3.6.2 Discussion of ideal retrofits for different bridges	84
MSC Steel	85
MSSS Concrete.....	85
3.6.3 Cost-Benefit Analysis	86
Chapter 4 Analytical Assessment and Comparison of Seismic Performance Evaluation Procedures for Bridge Structures	91
4.1 Introduction.....	91
4.2 Methods for Seismic Performance Evaluation	93
4.2.1 Inelastic Response History Analysis.....	93
4.2.2 Elastic Response History Analysis	95
4.2.3 Inelastic Response History Analysis of SDOF Model.....	97
4.2.4 Capacity Spectrum Analysis of SDOF Model	98
4.3 Application of Evaluation Procedures for Bridge Structures	99
4.3.1 Typical Highway Overcrossing Bridge in Central and Eastern U.S.....	100
4.3.1.1 Bridge Configuration	100
4.3.1.2 Analytical Models.....	101
Structural Model for Inelastic Response History Procedure.....	101
SDOF Model for Approximate Procedure.....	105
Capacity Spectrum Method.....	107
Elastic Analysis.....	107
4.3.1.3 Input Ground Motions.....	107
4.3.1.4 Analysis Results.....	108
Transverse Direction	108
Longitudinal Direction.....	111
4.3.2 Caruthersville Bridge	114
4.3.2.1 Bridge Configuration	114
4.3.2.2 Analytical Model	115
Structural Model for Inelastic Response History Procedure.....	115

Structural Models for Elastic Response History Procedure.....	117
4.3.2.3 Input Ground Motions.....	117
4.3.2.4 Results.....	118
Transverse Direction.....	120
Longitudinal Analysis.....	123
4.4 Assessment of Evaluation Procedure.....	126
Inelastic Response History Analysis.....	126
Elastic Response History Analysis.....	126
Inelastic SDOF Response History Analysis.....	127
Capacity Spectrum Methods.....	127
5 Summary and Recommendations.....	129
Development in design specifications.....	129
Ground motion simulation in CSUS.....	130
FHWA ground motion tool.....	130
Seismic Vulnerability and Retrofit of Bridges.....	131
Seismic Performance Evaluation Procedures.....	132
Acknowledgements.....	133
References.....	135
APPENDIX A: SEISMIC RETROFIT IN INDIANA.....	143
APPENDIX B: SEISMIC RETROFIT IN ILLINOIS.....	147
APPENDIX C: SEISMIC RETROFIT IN KENTUCKY.....	157
APPENDIX D: SEISMIC RETROFIT IN MISSOURI.....	159
APPENDIX E: SEISMIC RETROFIT IN TENNESSEE.....	169
APPENDIX F: SEISMIC RETROFIT IN TENNESSEE/ARKANSAS.....	189

LIST OF TABLES

Table 1 Equivalency of the Soil Profile Types and Site Classes ⁽⁵⁾	16
Table 2 Determination of seismic hazard level in NCHRP 12-49 recommendations	16
Table 3 Normalized one-second spectral acceleration ⁽⁸⁾	24
Table 4 Minimum service level required by AASHTO Division I-A and recommended by NCHRP 12-49	25
Table 5 Maximum allowed response reduction factor for concrete substructure	25
Table 6 Cost comparison of design based on NCHRP 12-49 recommendations and Standard specifications	26
Table 7 R-factors used in Illinois construction cost study	26
Table 8 Increase of construction cost in Missouri ⁽⁹⁾	27
Table 9 Implicit conservatism in current bridge design practice	29
Table 10 Empirical formulae for short-period response site coefficient ⁽¹⁸⁾	39
Table 11 Empirical formulae for long-period response site coefficient ⁽¹⁸⁾	39
Table 12 Bridge classes and their proportions in the Central and Southeastern US.....	44
Table 13 Summary of Vulnerable Components for Nine Bridge Classes – Deterministic Analyses	47
Table 14 MSSS Steel Retrofit Impact Summary	75
Table 15 MSC Steel Retrofit Impact Summary	76
Table 16 MSSS Concrete Retrofit Impact Summary	76
Table 17 MSC Concrete Retrofit Impact Summary	77
Table 18 Demand parameters of different bridge components considered in fragility development	79
Table 19 MSSS steel as-built and retrofitted bridge fragility curves.....	80
Table 20 MSC steel as-built and retrofitted bridge fragility curves.	80
Table 21 MSSS concrete as-built and retrofitted bridge fragility curves.	80
Table 22 MSC concrete as-built and retrofitted bridge fragility curves.	81
Table 23 Case study bridge dimensions.....	88
Table 24 Comparison of expected LCC for different retrofit measures and anticipated cost-benefit ratio (CBR) for sample MSC Concrete bridge located in Caruthersville, MO.	88
Table 25 Summary of ideal seismic retrofit based on highest cost-benefit ratio for the case study bridges at each location.	89
Table 26 Applied analysis methods for two bridge structures.....	99
Table 27 Recorded ground motions selected for fragility analysis.....	108
Table 28 Percentage of maximum transverse responses within 20% error bound	111
Table 29 Percentage of maximum longitudinal responses within 20% error bound	114
Table 30 Converged inelastic response history analysis.....	119

LIST OF FIGURES

Figure 1 Map. Transportation network	1
Figure 2 Map. Seismic hazard in the CSUS	2
Figure 3 Map. 1988 NEHRP map of 500-year return period PGA	7
Figure 4 Map. 1996 MCE maps for NEHRP Provisions and upper level events for FHWA Seismic Retrofitting Manual: 0.2-sec spectral acceleration (%g) with 2% probability of exceedance in 50 years (site: NEHRP B-C boundary)	8
Figure 5 Map. 1996 MCE maps for NEHRP Provisions and upper level events for FHWA Seismic Retrofitting Manual: 1.0-sec spectral acceleration (%g) with 2% probability of exceedance in 50 years (site: NEHRP B-C boundary)	8
Figure 6 Map. 1996 MCE maps for NEHRP Provisions and upper level events for FHWA Seismic Retrofitting Manual: 0.2-sec spectral acceleration (%g) with 5% probability of exceedance in 50 years (site: NEHRP B-C boundary)	8
Figure 7 Map. 1996 MCE maps for NEHRP Provisions and upper level events for FHWA Seismic Retrofitting Manual: 1.0-sec spectral acceleration (%g) with 5% probability of exceedance in 50 years (site: NEHRP B-C boundary)	9
Figure 8 Equation. C subscript s	9
Figure 9 Map. USGS regional workshops for earthquake hazard mapping	11
Figure 10 Map. Ratio between PGA of 2500-year return period and PGA of 500-year return period.....	11
Figure 11 Map. Comparison for long period response by 1-point and 2-point spectra (1996 USGS data): Long-period response ratio $S_1/1.2PGA$ (500-yr).....	12
Figure 12 Map. Comparison for long period response by 1-point and 2-point spectra (1996 USGS data): (b) Long-period response ratio $S_1/1.2PGA$ (2500-yr).....	13
Figure 13 Map. Comparison for short period response by 1-point and 2-point spectra (1996 USGS data): Short-period response ratio $S_s/2.5PGA$ (500-yr)	13
Figure 14 Map. Comparison for short period response by 1-point and 2-point spectra (1996 USGS data): Short-period response ratio $S_s/2.5PGA$ (2500-yr)	14
Figure 15 Map. Comparison of PGA values between 1988 and 1996 USGS maps: 1988 map (unit: percent of g).....	14
Figure 16 Map. Comparison of PGA values between 1988 and 1996 USGS maps: 1996 map (unit: g).....	15
Figure 17 Map. Ratio of long-period design spectral value (S_{D1}) for 2-point/1-point methods—Site B/S1	17
Figure 18 Map. Ratio of long-period design spectral value (S_{D1}) for 2-point/1-point methods—Site B/S1	17
Figure 19 Map. Ratio of short-period design spectral value (S_{Ds}) for 2-point/1-point methods—site B/S1	18
Figure 20 Map. Ratio of short-period design spectral value (S_{Ds}) for 2-point/1-point methods—site E/S4.....	18
Figure 21 Graph. Changed power of T in NCHRP 12-49 recommendations	19
Figure 22 Map. Ratio of spectral values between 2500-year return period and 500-year return period (2002 data)—PGA	19

Figure 23 Map. Ratio of spectral values between 2500-year return period and 500-year return period (2002 data)—Short period response (0.2-sec)	20
Figure 24 Map. Ratio of spectral values between 2500-year return period and 500-year return period (2002 data)—Long period response (1-sec).....	20
Figure 25 Map. Ratio of 2002 data to 1996 data—PGA 2500-year return period	20
Figure 26 Map. Ratio of 2002 data to 1996 data— S_s 2500-year return period	21
Figure 27 Map. Ratio of 2002 data to 1996 data— S_1 2500-year return period.....	21
Figure 28 Map. 500-year return period PGA from 1988 map	22
Figure 29 Map. 500-year return period PGA from 1996 update data.....	22
Figure 30 Map. Seismic Hazard Level in accordance with NCHRP 12-49 recommendations	22
Figure 31 Map. Seismic Hazard Level in accordance with NCHRP 12-49 recommendations	23
Figure 32 Graph. Map. Sample hazard curves in CSUS (Memphis) and western U.S. (Los Angeles)	24
Figure 33 Map. Sites for cost comparison of design based on NCHRP 12-49 recommendations and Standard specifications	26
Figure 34 Map. Sites to compare the increase of construction cost in Missouri (Contour: $S_1/1.2$ PGA—500-yr).....	27
Figure 35 Map. Ratio between PGA of 1000-year return period and PGA of 500-year return period.....	28
Figure 36 Map. Range of Applicability study in NCHRP 20-7 Task 193 ⁽⁸⁾ (GuideSpec). 30	
Figure 37 Map. Seismic Hazard Levels by NCHRP 12-49 recommendations.....	31
Figure 38 Map. Seismic Hazard Levels by Guide Specifications	31
Figure 39 Map. Seismic Hazard Levels by FHWA Seismic Retrofit Manual (left), Guide Specifications (middle), and NCHRP 12-49 recommendations (right).	32
Figure 40 Graph. Generic rock/stiff soil shear wave velocity profile used to produce USGS maps	34
Figure 41 Graph. Samples of ground motion relationships—Frankel et al., 1996	34
Figure 42 Graph. Samples of ground motion relationships— Atkinson and Boore, 1995 (2-corner)	35
Figure 43 Graph. Samples of ground motion relationships—Toro et al., 1997 (1-corner)	35
Figure 44 Graph. Samples of ground motion relationships—Atkinson and Boore, 2006(finite fault)	35
Figure 45 Graph. Rock motion (PGA) for four Illinois bridge sites.....	36
Figure 46 Graph. Comparison of UHRS to NEHRP spectra for Memphis, St. Louis, and Cabondale ⁽¹⁶⁾	37
Figure 47 Map. Locations where PSHA is performed to produce ground motions for the purpose of site amplification analysis ^(18,19)	38
Figure 48 Graph. Normalized site coefficients for varying soil layer thickness	38
Figure 49 Empirical formulae for modification of site coefficients	39
Figure 50 Screenshot. Opening screen of the ground motion tool	41
Figure 51 Screenshot. Return period and design/retrofitting documents	41
Figure 52 Screenshot. Site class.....	41
Figure 53 Screenshot. Design spectral values and display of the curve	42

Figure 54 Illustration. Typical Multi-Span Simply Supported Bridge in Mid-America (redrawn from TN Department of Transportation Bridge Plans)	45
Figure 55 Illustration. Rocker and Fixed Bearings Commonly Found in Mid-America Bridges (redrawn from IL Department of Transportation Bridge Plans).	45
Figure 56 Photo. Typical vulnerabilities found in bridges in the Central and Southeastern US, Including (a) short support lengths, (b) inadequate transverse reinforcement, and (c) inadequate bearings.....	46
Figure 57 Illustration. Analytical Model of Bridge Used in Nonlinear Dynamic Analysis.	47
Figure 58 Photo. Damage to steel girder bridges in past earthquake events: (a) pounding damage in Northridge, (b) column damage and (c) shifted superstructure in Kobe, and (d) bearing damage in Nisqually (courtesy of WDOT).	48
Figure 59 Photo. CSUS bridge retrofits: (a) steel jackets in TN, (b) elastomeric isolation bearings in IL, (c) restrainer cables in KY, (d) seat extenders and (e) shear keys in TN.	51
Figure 60 Graph. Effect of confinement on concrete.	52
Figure 61 Graph. Force deformation of column without and with steel jacket ⁽²⁹⁾	52
Figure 62 Illustration. Typical steel jacket retrofit details: (a) full height, (b) typical section.	53
Figure 63 Photo. Examples of (a) partial height steel jackets in MO and (b) full height steel jackets in TN.....	53
Figure 64 Photo. Concrete column overlay (a) during construction in TN and (b) as a partial encasement in IL.....	54
Figure 65 Photo. Other column retrofits with (a) cable wraps or (b and c) fiber composites performed in IL.	55
Figure 66 Photo. Column cable wraps, bent cap retrofits, restrainer bars (Poplar Street Complex - IL)	55
Figure 67 Photo. Steel jacket details (US40 Poplar Street – MO).....	56
Figure 68 Photo. (left) Typical elastomeric bearing adapted from Priestley et al. ⁽²⁹⁾ , (right) deformed bearing during experimental test.	57
Figure 69 Graph. Acceleration and displacement response spectrum showing the shift in periods with isolation systems.	58
Figure 70 Photo. Potentially vulnerable existing steel (a) fixed and (b) rocker bearings.	58
Figure 71 Photo. Elastomeric bearing isolation systems found in the CSUS.....	59
Figure 72 Photo. Sliding isolation systems used in the Central and Southeastern US.	59
Figure 73 Photo. (a) Elastomeric bearings with keeper plates, and (b) Bearings with dampers.	59
Figure 74 Illustration. Examples of restrainer connection details (a) (via the bent cap), or (b) from girder to girder.	61
Figure 75 Graph. Load-deformation from Caltrans restrainer cable testing ⁽³⁷⁾	61
Figure 76 Photo. Common CSUS restrainer cable retrofit details as performed in TN. ...	62
Figure 77 Photo. Examples of restrainer cables connected between adjacent girders.....	62
Figure 78 Photo. Example of restrainer cables wrapped around bent cap.	63
Figure 79 Photo. Example of high strength bar restrainers in the Central and Southeastern US.	63
Figure 80 Photo. Connection details for high strength restrainer bars.	64

Figure 81 Photo. Connection details for high strength restrainer bars used to restrain motion in the longitudinal and transverse directions.	64
Figure 82 Photo. Retrofits performed using bumper elements.	65
Figure 83 Photo. Application of shock transmission units at the intermediate span of a bridge.	66
Figure 84 Photo. Transverse restraint provided by (a) concrete shear keys and (b) keeper brackets.	67
Figure 85 Photo. Concrete block transverse shear keys in (a) Indiana (SR51 over White River/Carl Grey Memorial Bridge – IN) and (b) Missouri (Poplar Street Complex – MO).	67
Figure 86 Photo. (a) Concrete shear keys among other retrofits (Davies Plantation Road – TN) and (b) elevation view of shear key details.	68
Figure 87 Photo. (a) Steel transverse shear keys along with bent cap retrofit in MO (Poplar Street Complex – MO), and keeper bracket retrofits in TN (b) (SR59 – TN) and (c) (Chambers Chapel Road over I40 – TN).....	68
Figure 88 Illustration. Corbel and bracket seat extender details.....	69
Figure 89 Photo. (a) Traditional seat extender retrofit in TN (RT A026 over I40 – TN), (b) beam extender in MO, and (c) catcher block (Poplar Street Complex – MO).	70
Figure 90 Photo. Detail of steel bracket type seat extenders like those shown in Figure 89(a) (Rte A026 – TN).....	70
Figure 91 Photo. Steel seat extenders (Poplar Street Complex – MO).....	71
Figure 92 Photo. Bent cap retrofit using post tensioning rods.....	72
Figure 93 Photo. Bent cap retrofit focused on shear reinforcement and confinement of the bent cap end regions.....	72
Figure 94 Photo. Bent cap retrofits with reinforced concrete encasement.	73
Figure 95 Photo. Bent cap retrofits with reinforced steel encasement	73
Figure 96 Equation. Probability P_r subscript failure	77
Figure 97 Equation. Conditional probability P_r , bracket, “D greater than C” under the condition of IM, close bracket.	78
Figure 98 Equation. S subscript d.....	78
Figure 99 Equation. Conditional probability P_r , bracket, DS under the condition PGA, close bracket.....	79
Figure 100 Graph. Fragility curves for the MSSS Concrete girder bridge class, comparing the as-built and retrofitted bridge fragility for each damage state.	81
Figure 101 Graph. Comparison of as-built and retrofitted median fragility values for each damage state for the (a) MSSS Steel, (b) MSC Steel, and (c) MSC Concrete girder bridges.....	82
Figure 102 Graph. Fragility curves constructed from the lognormal parameters listed in Table 20 for the MSC steel bridge class, comparing the as-built and retrofitted failure probabilities.....	83
Figure 103 Graph. Illustration of (a) comparing the percent change in the median value and (b) comparing other percentiles for assessing retrofits.	84
Figure 104 Equation. PGA subscript x percent	84
Figure 105 Equation. Benefit subscript r.....	86
Figure 106 Equation. CBR subscript r.....	86
Figure 107 Equation. E, bracket, LCC, close bracket.....	87

Figure 108 Equation. P subscript T, f, j	87
Figure 109 Graph. Cost-benefit ratios for retrofit of the case-study bridges, at different locations.	89
Figure 110 Graph. Performance objectives of buildings and bridges.....	91
Figure 111 Illustration. Steel and concrete models used in inelastic response history analysis.....	94
Figure 112 Illustration. Discretization of reinforced concrete sections for frame analysis	95
Figure 113 Illustration. Modeling of gaps with asymmetric spring between two units ...	95
Figure 114 Equation. Δ subscript i	96
Figure 115 Equation. C for T less than T subscript a	96
Figure 116 Equation. C for T between T subscript a and T subscript b	96
Figure 117 Equation. C for T between T subscript b and T subscript c prime	96
Figure 118 Equation. C for T between T subscript c prime and T subscript c	96
Figure 119 Equation. C equals to 1 for T greater than T subscript c	96
Figure 120 Graph. Estimation of inelastic response from elastic response	97
Figure 121 Illustration. Configuration of the studied bridge	101
Figure 122 Illustration. Configuration of typical bents and foundations.....	102
Figure 123 Illustration. FE model of the bridge and connectivity of structural components	102
Figure 124 Graph. Analytical models of bridge components	104
Figure 125 Graph. Monotonic and cyclic pushover curves of bridge.....	106
Figure 126 Graph. Response of full inelastic and bilinear SDOF models in transverse direction	109
Figure 127 Graph. Maximum transverse response from different analysis methods	110
Figure 128 Graph. Maximum transverse responses from approximate methods (normalized by inelastic response history results)	111
Figure 129 Graph. Response of full inelastic and bilinear SDOF models in longitudinal direction	113
Figure 130 Graph. Maximum longitudinal response from various analysis methods	113
Figure 131 Graph. Maximum longitudinal responses from approximate methods (normalized by inelastic response history results)	114
Figure 132 Illustration. Overview of the Caruthersville Bridge ⁽⁷⁷⁾	115
Figure 133 Graph. Spring models for bridge bearings and expansion joints.....	116
Figure 134 Illustration. OpenSees model and sample results of Bent 2 foundation system	116
Figure 135 Graph. Input ground motions with 500 year return period.....	118
Figure 136 Illustration. Monitored bents during response history analysis.....	119
Figure 137 Illustration. Monitoring points at each bents	119
Figure 138 Graph. Sample transverse response history of bridge decks, GM2-500	121
Figure 139 Graph. Sample foundation response in transverse direction	122
Figure 140 Graph. Sample transverse hysteretic response of bridge piers	122
Figure 141 Graph. Normalized maximum transverse deck response from two elastic analyses.....	123
Figure 142 Graph. Sample longitudinal response history of bridge decks, GM2-1000 .	124
Figure 143 Graph. Sample foundation response in longitudinal direction	125

Figure 144 Graph. Sample longitudinal hysteretic response of bridge piers	125
Figure 145 Graph. Normalized maximum longitudinal deck response from two elastic analyses	126
Figure 146 Photo. Bearing retrofits and details in Indiana: Elastomeric bearing with keeper brackets (SR 66 at Diamond – IN)	143
Figure 147 Photo. Bearing retrofits and details in Indiana: Elastomeric Bearings (HW50 Red Skelton – IN)	143
Figure 148 Photo. Bearing retrofits and details in Indiana: Isomeric Bearing with Dampers (US 41 @ Eagle Creek –IN).....	144
Figure 149 Photo. Transverse restraining devices in Indiana: Transverse Shear Key (SR51 over White River / Carl Grey Memorial Bridge – IN)	144
Figure 150 Photo. Transverse restraining devices in Indiana: Transverse Restrainer Cables (SR51 over White River / Carl Grey Memorial Bridge – IN)	145
Figure 151 Photo. Transverse restraining devices in Indiana: Transverse Restrainer Bars (164 at County Road 800 - IN)	145
Figure 152 Photo. Poplar Street Retrofits in Illinois: Column Cable Wraps, Bent Cap Retrofits, Transverse Restrainer Bars (Poplar Street Complex - IL).....	147
Figure 153 Photo. Poplar Street Retrofits in Illinois: Details of Cable Column Wraps, Bent Cap Retrofits, Transverse Restrainer Bars (Rte 3 Poplar Street – IL)	147
Figure 154 Photo. Poplar Street Retrofits in Illinois: Bent Cap Retrofit, Longitudinal Restrainer Bars, and Transverse Restraint with Turnbuckles (Poplar Street Complex – IL)	148
Figure 155 Photo. Poplar Street Retrofits in Illinois: Cable Column Wraps, Bent Cap Retrofits, Restrainer Bars (Rte 70 Poplar Street – IL)	148
Figure 156 Photo. Poplar Street Retrofits in Illinois: Elevations (Rte 70 Poplar Street – IL)	149
Figure 157 Photo. Details of Column and Bent Cap Wraps in Illinois: Column Cable Wraps (Poplar Street Complex – IL)	149
Figure 158 Illustration. Details of Column and Bent Cap Wraps in Illinois: Cable Wraps (Rte 70 Poplar Street – IL).....	150
Figure 159 Illustration. Details of Column and Bent Cap Wraps in Illinois: Bent Cap Wraps (Rte 70 Poplar Street – IL)	150
Figure 160 Photo. Restrainer Bars and Bumpers in Illinois: Restrainer Bar (Poplar Street Complex - IL)	151
Figure 161 Illustration. Restrainer Bars and Bumpers in Illinois: Restrainer Bar Connections /Column Cable Wraps (Rte 70 Poplar Street – IL).....	151
Figure 162 Photo. Restrainer Bars and Bumpers in Illinois: Bumpers and Restrainer Bar (Poplar Street Complex - IL)	152
Figure 163 Illustration. Restrainer Bars and Bumpers in Illinois: Bumpers (Rte 3 Poplar Street – IL)	152
Figure 164 Photo. Restrainer Bars in Illinois: Restrainer Bar (Poplar Street Complex - IL)	153
Figure 165 Illustration. Restrainer Bars in Illinois: Detail of Typical Restrainer Bars (Rte 3 Poplar Street – IL).....	153
Figure 166 Illustration. Restrainer Bars in Illinois: Detail of Alternative Restrainer Bar Assembly (Rte 70 Poplar Street – IL).....	154

Figure 167 Photo. Column Retrofits in Illinois: Fiber Composite Retrofit (Poplar Street Complex – IL)..... 154

Figure 168 Photo. Column Retrofits in Illinois: Partial Column Encasement (Poplar Street Complex – IL)..... 155

Figure 169 Photo. Column Retrofits in Illinois: Fiber Composite Retrofit (Poplar Street Complex – IL)..... 155

Figure 170 Photo. Isolation in Illinois: Elastomeric Bearings and Restrainer Cables (Poplar Street Complex – IL)..... 156

Figure 171 Photo. Isolation in Illinois: Isolation Bearing (Poplar Street Complex – IL)..... 156

Figure 172 Photo. Different restrainer cable configurations in Kentucky: Restrainer Cables..... 157

Figure 173 Photo. Different restrainer cable configurations in Kentucky: Restrainer Cables..... 157

Figure 174 Photo. Different restrainer cable configurations in Kentucky: Restrainer Cables..... 158

Figure 175 Photo. Shear Key and Shock Transmission Unit Retrofits in Missouri: Shear Keys and Shock Transmission Units (Poplar Street Complex – MO)..... 159

Figure 176 Illustration. Shear Key and Shock Transmission Unit Retrofits in Missouri: Shock Transmission Unit and Shear Key (I70 Poplar Street – MO) 159

Figure 177 Illustration. Shear Key and Shock Transmission Unit Retrofits in Missouri: Shear Keys and Shock Transmission Units (I70 Poplar Street – MO) 160

Figure 178 Photo. Bumper, Bent Cap, and Shear Key Retrofits in Missouri: Bumpers (Poplar Street Complex – MO) 160

Figure 179 Illustration. Bumper, Bent Cap, and Shear Key Retrofits in Missouri: Bumpers (US40 Poplar Street – MO) 161

Figure 180 Illustration. Bumper, Bent Cap, and Shear Key Retrofits in Missouri: Transverse Shear Key (US40 Poplar Street – MO) 161

Figure 181 Photo. Bumper, Bent Cap, and Shear Key Retrofits in Missouri: Bent Cap Post-tension Retrofit 162

Figure 182 Photo. Longitudinal Bumper and Restrainer Retrofits in Missouri: Restrainer Bars and Bumpers (Poplar Street Complex – MO) 162

Figure 183 Illustration. Longitudinal Bumper and Restrainer Retrofits in Missouri: Bumper and Restrainer Cable (US40 Poplar Street – MO) 163

Figure 184 Photo. Longitudinal Bumper and Restrainer Retrofits in Missouri: Steel Jackets (Poplar Street Complex – MO) 163

Figure 185 Illustration. Longitudinal Bumper and Restrainer Retrofits in Missouri: Steel Jacket Details (US40 Poplar Street – MO) 164

Figure 186 Photo. Seat Extenders and Bent Cap Retrofit in Missouri: Beam Seat Extender (Poplar Street Complex – MO) 165

Figure 187 Illustration. Seat Extenders and Bent Cap Retrofit in Missouri: Seat Extender Section (US40 Poplar Street – MO)..... 165

Figure 188 Photo. Seat Extenders and Bent Cap Retrofit in Missouri: Bent Cap Retrofit (Poplar Street Complex – MO) 166

Figure 189 Photo. Seat Extender and Restrainer Rods in Missouri: Seat Extenders (Poplar Street Complex – MO)..... 166

Figure 190 Illustration. Seat Extender and Restrainer Rods in Missouri: Restrainers (US40 Poplar Street – MO).....	167
Figure 191 Illustration. Seat Extender and Restrainer Rods in Missouri: Seat Extender (US 40 Poplar Street – MO).....	167
Figure 192 Illustration. Replacement with Less Vulnerable Bearings in Missouri: Bearing Replacement (US40 Poplar Street – MO).....	168
Figure 193 Photo. The First Seismic Retrofit in Tennessee: First Retrofit in TN: “Uplift” and Longitudinal Restrainer Cables (SR 14 over CSX Railroad– TN)	169
Figure 194 Photo. The First Seismic Retrofit in Tennessee: First Retrofit in TN: “Deck Girder” Restrainer Cables (SR 14 over CSX Railroad – TN)	169
Figure 195 Illustration. The First Seismic Retrofit in Tennessee: Steel Jackets and Restrainer Cables (SR 14 over CSX Railroad – TN).....	170
Figure 196 Illustration. The First Seismic Retrofit in Tennessee: Restrainer Cables (SR14 over CSX Railroad – TN)	170
Figure 197 Illustration. The First Seismic Retrofit in Tennessee: Deck Girder Restrainer Cables (SR14 over CSX Railroad – TN)	171
Figure 198 Photo. Retrofit of Davies Plantation Road in Tennessee: Bent Cap Retrofit, Steel Jackets, and Shear Keys (Davies Plantation Road – TN)	171
Figure 199 Illustration. Retrofit of Davies Plantation Road in Tennessee: Shear Key (Davies Plantation Road – TN).....	172
Figure 200 Illustration. Details of Bent Cap and Column Retrofit in Tennessee: Bent Cap and Steel Casing (Davies Plantation Road – TN).....	173
Figure 201 Photo. Retrofit of Columns and Bearings in Tennessee: Painted Steel Jackets (I40 over SR 15 – TN)	174
Figure 202 Illustration. Retrofit of Columns and Bearings in Tennessee: Bearing Retrofit (I40 over SR 15 – TN)	174
Figure 203 Photo. Retrofit of Columns and Bearings in Tennessee: Bearing Retrofit (I40 over SR 15 – TN).....	175
Figure 204 Photo. Retrofit of Columns and Bent Caps in Tennessee: Steel Jackets and Bent Cap Retrofit (SR 196 over I40 – TN).....	175
Figure 205 Illustration. Retrofit of Columns and Bent Caps in Tennessee: Bent Cap Retrofit (SR 196 – TN)	176
Figure 206 Illustration. Retrofit of Columns and Bent Caps in Tennessee: Steel Jackets (SR196 – TN).....	176
Figure 207 Photo. Restrainer Cable Details in Tennessee: Restrainer Cables and Transverse Keeper Brackets (Chambers Chapel Road over I40 – TN).....	177
Figure 208 Illustration. Restrainer Cable Details in Tennessee: Connection for Cables (Chambers Chapel Road – TN).....	177
Figure 209 Illustration. Restrainer Cable Details in Tennessee: Restrainer Cable and Attachments (Chambers Chapel Road – TN)	178
Figure 210 Photo. Transverse Keeper Brackets (Shear Keys) in Tennessee: Transverse Keeper Brackets (Chambers Chapel Road over I40 – TN).....	178
Figure 211 Illustration. Transverse Keeper Brackets (Shear Keys) in Tennessee: Keeper Bracket Details – Type B(Chambers Chapel Road – TN).....	179
Figure 212 Photo. Transverse Keeper Brackets (Shear Keys) in Tennessee: Keeper Brackets (Chambers Chapel Road over I40 – TN)	180

Figure 213 Illustration. Transverse Keeper Brackets (Shear Keys) in Tennessee: Keeper Brackets - Type A (Chambers Chapel Road – TN)	181
Figure 214 Photo. Steel Jacket and Footing Retrofit in Tennessee: Steel Column Jackets (Chambers Chapel Road – TN).....	182
Figure 215 Illustration. Steel Jacket and Footing Retrofit in Tennessee: Steel Jacket Elevation (Chambers Chapel Road – TN)	182
Figure 216 Illustration. Steel Jacket and Footing Retrofit in Tennessee: Steel Column Jackets and Footing Retrofit (Chambers Chapel Road – TN)	183
Figure 217 Photo. Concrete Shear Keys in Tennessee: Concrete Shear Keys (SR59 over I40 – TN).....	183
Figure 218 Illustration. Concrete Shear Keys in Tennessee: Concrete Shear Key Details (SR59 – TN).....	184
Figure 219 Photo. Keeper Brackets in Tennessee: Keeper Brackets (SR59 – TN).....	185
Figure 220 Illustration. Keeper Brackets in Tennessee: Keeper Bracket Details (SR59 – TN).....	185
Figure 221 Photo. Restrainer Cables in Tennessee: Restrainer Cables (SR59 – TN)	186
Figure 222 Illustration. Restrainer Cables in Tennessee: Restrainer Cable Detail (SR59 – TN).....	186
Figure 223 Illustration. Restrainer Cables in Tennessee: Alternative Restrainer Cable Detail (SR 1 over I40 – TN)	187
Figure 224 Photo. Seat Extenders in Tennessee: Seat Extenders (RT A026 over I40 – TN)	187
Figure 225 Illustration. Seat Extenders in Tennessee: Detail of Seat Extenders (Rte A026 – TN).....	188
Figure 226 Photo. Isolation and Column Retrofit of the Hernando DeSoto Bridge Carrying I40 between Tennessee and Arkansas: Reinforced Concrete Encasement with Steel Jackets (Hernando DeSoto I40 over Mississippi River - TN)	189
Figure 227 Photo. Isolation and Column Retrofit of the Hernando DeSoto Bridge Carrying I40 between Tennessee and Arkansas: Friction Pendulum Isolation Bearing (Hernando DeSoto I40 Over Mississippi River – TN)	189
Figure 228 Photo. Isolation and Column Retrofit of the Hernando DeSoto Bridge Carrying I40 between Tennessee and Arkansas: Elastomeric Isolation Bearings (Hernando DeSoto I40 Over Mississippi River – TN)	190

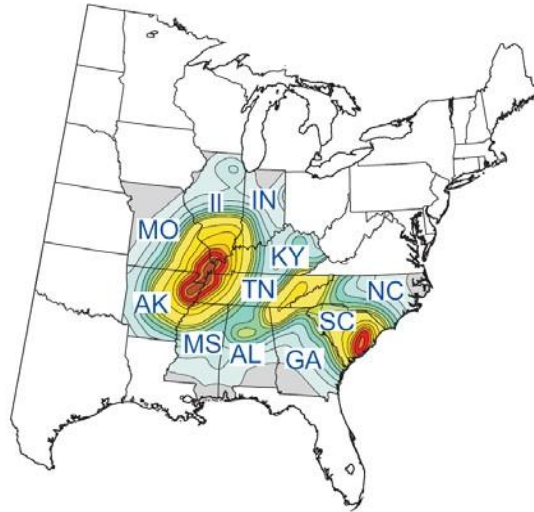


Figure 2 Map. Seismic hazard in the CSUS

In 1998, the National Cooperative Highway Research Program (NCHRP) initiated a study to develop a new set of seismic design provisions for highway bridges (NCHRP Project 12-49) for possible incorporation into the future AASHTO LRFD bridge design specifications. These recommended specifications provided the technical basis for a stand-alone set of provisions entitled "Recommended LRFD Guidelines for the Seismic Design of Highway Bridges" developed by a joint venture of the ATC and MCEER. The NCHRP project 12-49 was intended to reflect experience gained during recent damaging earthquakes and the results of research programs conducted in the US and elsewhere over the prior 10 years. The project was to incorporate the latest information regarding design, performance criteria, seismic hazard, site effects, and component design and detailing. Studies have shown that direct application of the proposed specifications may involve large number of bridges requiring seismic design, resulting in more cost for the states in the Central and Southeastern United States (CSUS). Such conflict in rational design requirement and practicality of new provisions had become a concern for state transportation authorities in this area.

Since the proposal of this project, further modifications had been made to the NCHRP 12-49 recommendations to address certain issues in the proposed design guidelines. In addition, the research results from the NCHRP 20-7 Task 193 "Development of LRFD Guidelines for the Seismic Design of Highway Bridges, Version 2" has been considered generally acceptable by AASHTO and became the candidate of the next generation seismic design provisions. The seismic design methodology recommended by the NCHRP 20-7 Task 193 (referred to as the AASHTO Guide Specifications, 2007, in this report) was significantly different from that used in the AASHTO Standard Specifications for Highway Bridges, Division I-A, and the AASHTO LRFD Bridge Specifications (seismic provisions in both documents were referred to as AASHTO Standard Specifications in this report). The AASHTO Guide Specifications intended to mitigate the impact on bridge design effort and cost by encouraging the use of advanced analysis methods and reduction of over-conservatism in the NCHRP 12-49 recommendations.

To address the seismic resilience issues for existing bridges, FHWA published the Seismic Retrofitting Manual for Highway Structures: Part 1-Bridges in 2006. This document was the product of a FHWA-funded program between 1992 and 2002 and reflected advancements in the practice of seismic retrofitting that had occurred since 1983. The FHWA Seismic Retrofitting Manual adopted a performance-based design concept, which provided rational basis for risk management under seismic events of different intensity. Two-level performance evaluation was given with specified performance level for bridges of different ages and importance categories.

New screening and prioritization methods were also provided in the 2006 FHWA Seismic Retrofitting Manual. In addition to the indices rating method from the 1983 and 1995 retrofitting manual, an “expected damage method” and a “seismic risk assessment method” were provided as alternatives. These methods required the use of fragility curves for specified bridge categories. While these new methods allowed more accurate and automated screening for bridge retrofitting, the calibration and customization of fragility curves for the specific bridge design and construction practice in the concerned area were critically important.

OBJECTIVES

The objectives of this research project are to apply a comprehensive methodology to design bridges in the CSUS - using the results of NCHRP 12-49 & NCHRP 20-7/ task 193 as a basis. The methodology would address:

1. Current source models and maps used for ground motion in the CSUS
2. Current site response models
3. Fragility models and network assessment to determine required level of seismic protection
4. Detailed analysis to derive retrofit design forces and deformations

WORK PERFORMED

- Comparison and synthesis of ground motion models
 - Investigated theoretical background of ground motion simulation used in existing and new seismic design.
 - Synthesized research documents on CSUS ground motion properties and simulation.
 - Reviewed reports related to seismic retrofitting practice and seismic analysis strategy to identify possible impact from ground motion models.
 - Obtained necessary information for expanding the design ground motion computer tools.
 - Extended literature search for more details on specific ground motion issues identified in previous studies (e.g. site effect).

- Developed graphical representations to compare the hazard level given by different sources and provisions.
- Development of seismic design and analysis tools for bridges in accordance with the knowledge obtained from the previous study.
 - Composed analysis tools to produce ground motion parameters used in latest design and retrofitting methods.
 - Expanded the ground motion analysis tool to cover all area in the scope of this study.
 - Expanded the computer analysis tool to cover majority of practical design/retrofitting jobs.
- Documentation of design and retrofit practice in CSUS
 - Completed documentation of retrofit practices in CSUS which included theory, retrofitting details, and applications of various retrofits
 - Continued review of Recommended LRFD Guidelines for the Seismic Design of Highway Bridges
- Fragility analysis study and application
 - Documentation of fragility analysis for Mid-America as-built and retrofitted bridges.
 - Development of framework using fragility curves for evaluating vulnerability and retrofit effectiveness.
- Comparison and evaluation of simplified analysis methods
 - Set up analytical framework for quantifying the effect of inelastic response of the soil on damage assessment of RC bridges, and identified necessary parameters through literature research.
 - Established analytical model for RC bridge and soil.
 - Analyzed bridge model with and without SSI/liquefaction and with model parameter variations.
 - Compared different methods of analysis and different modeling assumptions for simple bridges.
 - Reviewed and compared in detail between analysis results and code approach. Developed performance and comparison plots.
 - Reviewed liquefaction bridge fragilities and planned for publications.
- Organized a committee meeting to disseminate progress to sponsoring states and obtain comments.
- Report preparation and product dissemination

DOCUMENTAL ORGANIZATION

This report addresses the problems bridge engineers may encounter during the implementation of new design and retrofitting methods and necessary tools that simplify the transition from the outdated design and retrofitting practice. The ground motion characteristics and site response models were investigated and bridge performance fragility curves will be developed for representative states in the Central and Southeastern United States. Additional investigation into advanced analysis methods for bridges before and after retrofitting, and the use of network models will also be performed. It is believed that by addressing these four components using the latest tools and knowledge in

seismology, geotechnical engineering, transportation and structural engineering, the impact of the codes on seismic design might, in fact, be minimal.

Chapter 2 briefly introduces the method of establishing design ground motion in different design documents and the current practice of ground motion simulation. Comparisons are made to identify the impact from different design document and their practicality in the CSUS. Current ground motion simulation and site response analysis are investigated. A computer tools for obtaining design ground motion is developed.

Chapter 3 reports the investigation on the retrofitting practice in the CSUS. Bridge vulnerability to earthquakes and critical components are identified. The current practice in seismic retrofitting is examined and organized. Recommendations are made in assisting the selection of retrofitting methods.

Chapter 4 presents the study on evaluation procedures used in bridge design and retrofitting in CSUS. Several analytical evaluation procedures are compared via the application of the methods to two bridge structures. Analysis results from evaluation procedures with various level of simplification are compared. The importance of inelastic and dynamic analysis in assessment and design is revealed.

CHAPTER 2 SEISMIC HAZARD OF THE CSUS

2.1 MAPS USED IN DESIGN GUIDELINES

In the AASHTO Standard Specifications for Highway Bridges and LRFD Bridge Design Specifications, the maps developed by the U.S. Geological Survey (USGS) for the 1988 National Earthquake Hazards Reduction Program (NEHRP) provisions for the Development of Seismic Regulations for New Buildings were used. The maps provided peak ground acceleration values that depicted a 500-year return period for events exceeding the mapped values (Figure 3).

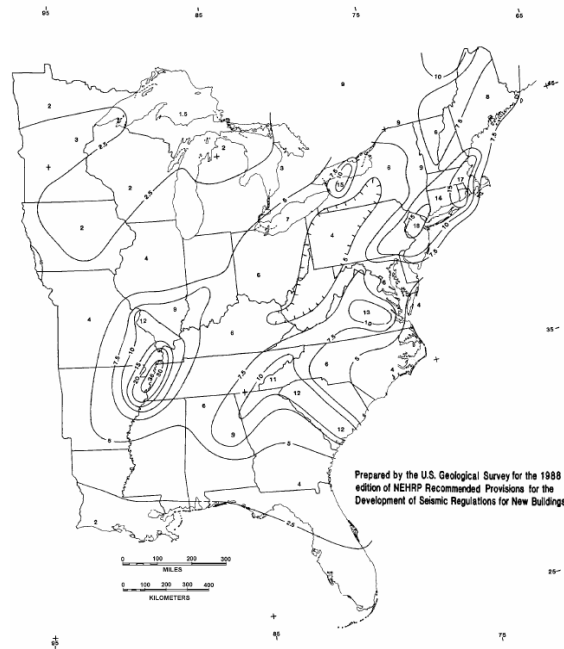


Figure 3 Map. 1988 NEHRP map of 500-year return period PGA

In order to support the 1994 NEHRP provisions for new buildings and 1997 building codes, the USGS developed a set of maps for maximum considered earthquakes that included spectral acceleration values for 2% probability of exceedance in 50 years at short and long structural periods (Figure 4 to Figure 7). In contrast with the 1988 seismic hazard map, which maps PGA of 500 year return period, the 1996 USGS National Seismic Hazard Maps provided several spectral values at different structural periods with 10%, 5%, and 2% probability of exceedance in 50 years, which are approximately equivalent to events of return period of 500-year, 1000-year, and 2500-year, respectively.

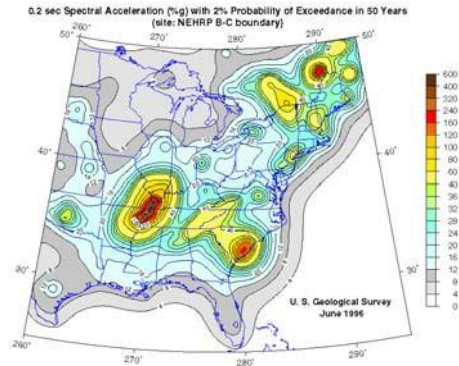


Figure 4 Map. 1996 MCE maps for NEHRP Provisions and upper level events for FHWA Seismic Retrofitting Manual: 0.2-sec spectral acceleration (%g) with 2% probability of exceedance in 50 years (site: NEHRP B-C boundary)

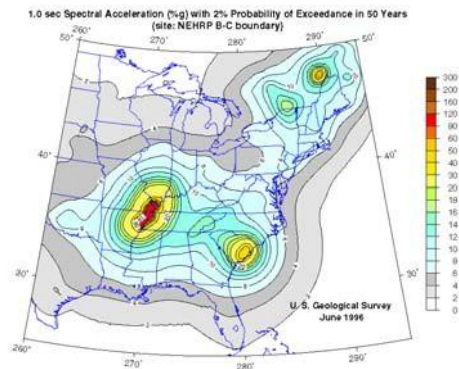


Figure 5 Map. 1996 MCE maps for NEHRP Provisions and upper level events for FHWA Seismic Retrofitting Manual: 1.0-sec spectral acceleration (%g) with 2% probability of exceedance in 50 years (site: NEHRP B-C boundary)

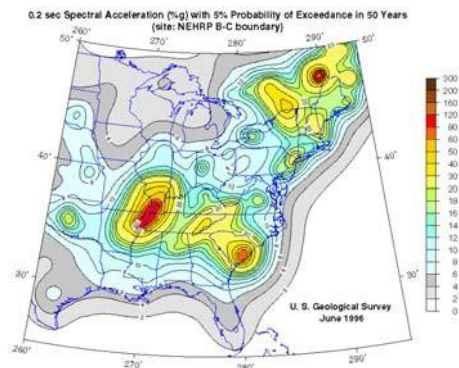


Figure 6 Map. 1996 MCE maps for NEHRP Provisions and upper level events for FHWA Seismic Retrofitting Manual: 0.2-sec spectral acceleration (%g) with 5% probability of exceedance in 50 years (site: NEHRP B-C boundary)

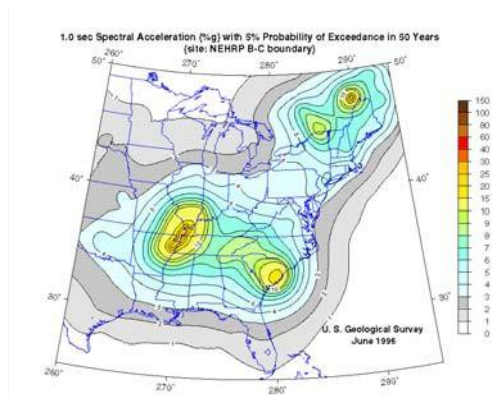


Figure 7 Map. 1996 MCE maps for NEHRP Provisions and upper level events for FHWA Seismic Retrofitting Manual: 1.0-sec spectral acceleration (%g) with 5% probability of exceedance in 50 years (site: NEHRP B-C boundary)

These maps were updated in 2002 and 2008 for the conterminous U.S. to include latest developments in seismological research. The 1996 MCE maps were adopted by the NCHRP 12-49 recommendations and the FHWA Seismic Retrofitting Manual while the 2002 maps were adopted by the AASHTO Guide Specifications. Mapped values of 1000-year return period events were used as upper level evaluation earthquakes in the FHWA Seismic Retrofitting Manual. The lower level evaluation earthquakes for FHWA Seismic Retrofitting Manual were 100-year return period events and were not available in 1996 data. A method is provided to obtain the lower level evaluation earthquake from 2002 seismic hazard data. However, the tool required for this method is not available for 2002 data anymore, but only available for 2008 data.

2.2 PROCEDURES FOR OBTAINING DESIGN GROUND MOTION

AASHTO Standard Specifications—Division I-A

The AASHTO LRFD Bridge Design Specification (equivalent of Division I-A of Standard Specification) identifies the Elastic Seismic Response Coefficient, C_s , through the Acceleration Coefficient, A , and Site Coefficient, S . The Acceleration Coefficient is the mapped peak ground acceleration of a rock site. The Seismic Response Coefficient, C_s , is given by

$$C_s = \frac{1.2AS}{T^{2/3}} \leq 2.5A$$

Figure 8 Equation. C subscript s

The Acceleration Coefficient is the mapped peak ground acceleration (PGA) at rock or stiff soil sites. The 1-second (considered “long period” in latest methods) response spectral acceleration at these sites are 1.2 times of the PGA. The long period spectral values of sites with deep soil (Type II), medium stiff clay/sand (Type III), and soft clay (Type IV) are amplified by factors of 1.2, 1.5, and 2.0, respectively. The short period response spectral values are 2.5 times of PGA regardless of the soil profile.

The mapped PGA is created by the USGS for the 1988 NEHRP provisions. It has a return period of 500 years. The seismic zone, which is used to determine appropriate analysis method, is determined by the PGA without consideration of soil profile.

NCHRP 12-49 Recommendations

The recommendations on design ground motion from the NCHRP 12-49 project is a major overhaul over the provisions from the AASHTO Standard Specifications. Changes directly related to ground motion include⁽¹⁾:

1. New seismic hazard mapped parameters—1996 updated map, S_s and S_1 .
2. New spectral shape
3. Improved site response factors
4. Hazard level and performance requirements

Some changes that do not directly change the procedure for obtaining ground motion parameters, but is related to the use of ground motion and assessment of earthquake demand/bridge capacity, include:

1. More economical design when advanced methods are being used
2. “No Seismic Demand Analysis” Design Concept
3. Capacity Spectrum Design Procedure
4. Displacement Capacity Verification (“Pushover”) Analysis
5. Liquefaction Hazard Assessment and Design
6. Seismic Isolation Provisions

The recommended provisions by NCHRP 12-49 project use two-level events for seismic performance evaluation: expected earthquake (EE, sometimes referred to as frequent earthquake or FE) and maximum considered earthquake (MCE).

The 3% probability of exceedance (PE) in 75 years event, which is approximately equivalent to the 2% PE in 50 year events used by NEHRP provisions, is used as MCE. NEHRP provisions for new buildings⁽²⁾ applies a two-third factor to this MCE to obtain the design spectrum. This was done under the condition that the provisions provide a 1.5 safety factor on collapse prevention. The NCHRP 12-49 provisions use the MCE without reduction as an attempt to better address the more critical displacement criteria for bridge collapse than for building collapse. This action is counterbalanced by a reduction of safety factor against collapse in the recommendation.

Impact from the NCHRP 12-49 Recommendations

1. The use of updated seismic hazard map

The updated USGS maps (1996) include the results from research work since the publication of previous maps. A series of seven workshops were convened to obtain regional consensus on the methodology used to produce seismic hazard maps (Figure 9). In this new map, the historical seismicity is smoothed and lower magnitude is used for pre-instrument earthquakes. A logic tree formalism is used to include a number of source models and attenuation relationship. These new maps represent more up-to-date knowledge in the United States.

The NCHRP 12-49 recommendations adopted events with 2500-year return period as the MCE. Compared to the acceleration coefficient, A , used in the AASHTO Standard Specifications, which is based on 500-year return period. Different levels of increase in the peak ground acceleration can be observed in different area. Figure 10 shows the ratio between PGA of 2500-year return period and PGA of 500-year return period. Most part of the concerned area has a 2500-year return period PGA 3~4 times as high as the 500-year return period PGA. A small area in the New Madrid Fault Zone exhibits a ratio of 6~8.



Figure 9 Map. USGS regional workshops for earthquake hazard mapping

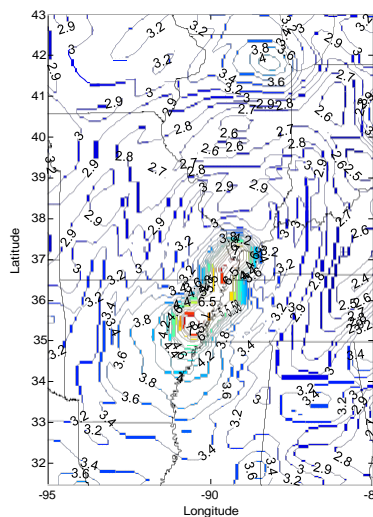


Figure 10 Map. Ratio between PGA of 2500-year return period and PGA of 500-year return period

2. Two-point spectral shape

The response spectra used in the AASHTO Standard Specifications are anchored at the PGA (zero second period) spectral value. The short period response is 2 or 2.5 times of PGA, while the long period response is $1.2S$ (S is the soil amplification factor) times of PGA. The two-point method has spectra anchored at mapped values for 0.2 sec (short period) and 1 sec (long period). This gives more flexibility to the spectral shape.

The impact to the design force from such change varies from place to place. A greatly simplified comparison is given in Figure 12 and Figure 12. These figures compare the long-period response (S_1) to 1.2 times of the PGA value from the map of 500-year return period (Figure 12) and 2500 year return period (Figure 12). The 1.2 times of PGA represents the 1-second site response of Soil Profile Type I using 1-point spectrum. S_1 is the mapped long-period response (1-second structural period) of Site Class B¹. The entire concerned area, with the exception of western Tennessee, has a ratio less than one. Figure 13 and Figure 14 show a similar comparison for the short-period response (0.2 second). The ratio of the entire area is less than one. This indicates that, without the soil amplification factors, a 2-point spectrum is generally lower than its one-point counterpart. It is important to note that, due to the changes on the soil amplification factors, the changes in design spectra are more complex than those presented in these figures. All maps in Figure 12 to Figure 14 are based on 1996 update of USGS seismic hazard data. For reference, the 1988 PGA map used by AASHTO Standard Specifications is compared to PGA of 500-year return period from 1996 USGS data in Figure 15 and Figure 16. The 500-year return period PGA values from 1996 map are somewhat lower than those from 1988 map in the entire area.

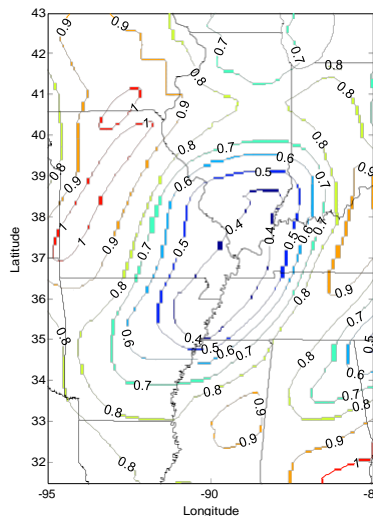


Figure 11 Map. Comparison for long period response by 1-point and 2-point spectra (1996 USGS data): Long-period response ratio $S_1/1.2PGA$ (500-yr)

¹ The site response for Soil Profile Type I and that for Site Class B are not completely equivalent. Soil Profile Type I includes Site Classes A, B, and part of C. This comparison is only done for the purpose of showing the difference from the mathematical forms of the design spectra formulae. Soil Profile Type I is compared to Site Class B because they both have the site coefficient of 1.

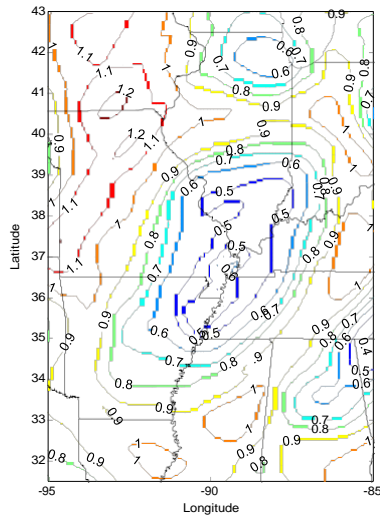


Figure 12 Map. Comparison for long period response by 1-point and 2-point spectra (1996 USGS data): (b) Long-period response ratio $S_1/1.2PGA$ (2500-yr)

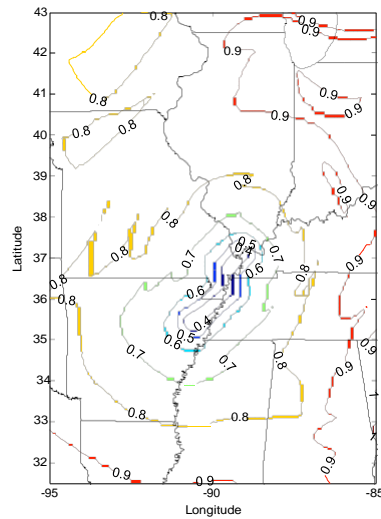


Figure 13 Map. Comparison for short period response by 1-point and 2-point spectra (1996 USGS data): Short-period response ratio $S_s/2.5PGA$ (500-yr)

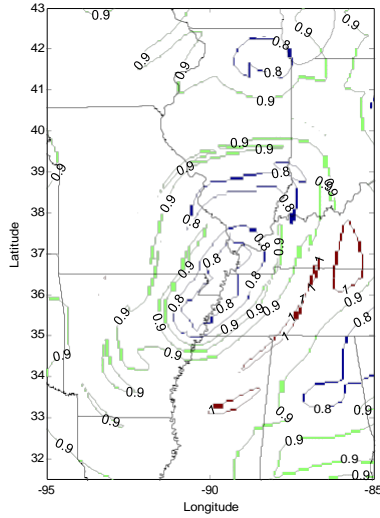


Figure 14 Map. Comparison for short period response by 1-point and 2-point spectra (1996 USGS data): Short-period response ratio $S_s/2.5PGA$ (2500-yr)

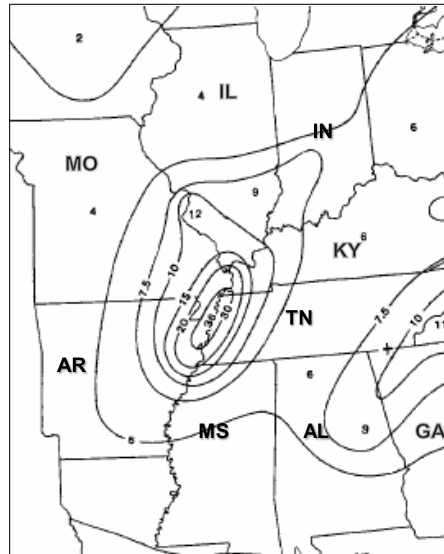
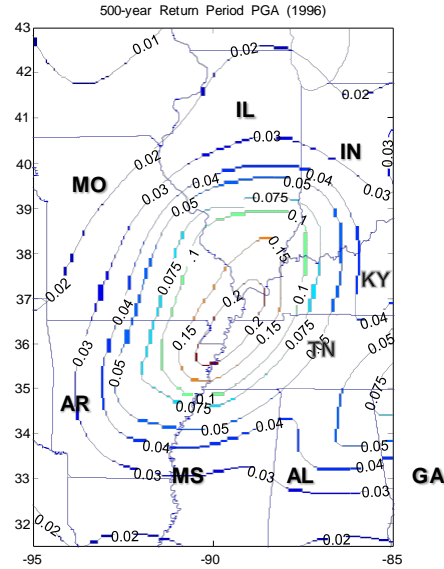


Figure 15 Map. Comparison of PGA values between 1988 and 1996 USGS maps: 1988 map (unit: percent of g)



**Figure 16 Map. Comparison of PGA values between 1988 and 1996 USGS maps:
1996 map (unit: g)**

3. Site amplification factors

The site coefficient, S , used in AASHTO Standard Specifications has departed from the building provisions since the adoption of the 1994 NEHRP Provisions. The new site coefficients in 1994 NEHRP provision (1997 UBC) are given in short-period (0.2 second or 0.3 second) and long period (1 second). Two new soil profiles are added. The coefficients are generally greater for softer soil profiles while nonlinear effect is taken into account and causes lower values at higher ground acceleration. Although bridges belong to a different class of structures than buildings, more consistent principles among building codes and bridge codes are favorable in maintaining reasonable seismic hazard risks of all infrastructural facilities⁽¹⁾.

The adoption of new site coefficients and soil profiles added another dimension to the difference between the ground motion specifications in new and old provisions. Figure 17 to Figure 20 show the ratio between design spectral values obtained with new and old site coefficients. These values are based on the 1996 update of USGS seismic hazard maps. Dobry et al.⁽⁵⁾ stipulates that the Site Classes A, B, and part of C are associated with the Soil Profile Type I (See Table 1). Site Classes C and D are associated with Soil Profile Types I and II. Site Classes E and F are associated with Soil Profile Types III and IV. For Such interweaved association shows the difficulty to compare the two systems. In Figure 17 to Figure 20, Site Class B is compared to Soil Profile I while Site Class E is compared to Soil Profile Type IV for their similarity in range of shear wave velocity. The figures show that the 2-point method with NEHRP site coefficients gives lower spectral values in higher seismicity area. This is consistent with the principle used in NEHRP 1994 provisions. It can also be noticed that the short-period response from the new method is more significantly enhanced at sites of softer soil profile.

The recommendations from the NCHRP 12-49 uses both short-period and long-period spectral values to determine the Seismic Hazard Level (SHL, Table 2), which, in turn, determines the design and analysis procedures and seismic detailing requirements. The higher design force for soft soil profile at short structural period potentially penalizes the short bridges in low seismicity area of the Mississippi Embayment. Since most values in Figure 17 to Figure 20 near the New Madrid Fault zone are significantly less than one, the design force is not increased due to the new shape of spectrum and site coefficient in moderate to high seismicity area (when the change in return period is not considered).

The new spectral acceleration level at long period range reduces with increasing structural period (T). Compared to the spectral shape of AASHTO Standard Specifications, which decreases with $T^{2/3}$, the new response spectral value drops faster along structural period (Figure 21). This has three effects on the bridge seismic design:

1. Bridges with longer natural period have lower seismic load.
2. Bridges with natural period between T_s and 1 second have higher seismic load.
3. T_s is longer if short-period and long-period design spectral acceleration (S_{DS} and S_{D1}) remain the same.

This effect is superimposed over the other effects of new spectra and may not always stand out and become significant for design.

Table 1 Equivalency of the Soil Profile Types and Site Classes⁽⁵⁾

Site class or soil profile type	Description	Shear wave velocity \bar{v} (m/sec)	SPT resistance \bar{N} or \bar{N}_{ch} (blows/ft)	Undrained shear strength \bar{s}_u (kPa)
S1	A	Hard rock	>1500	—
	B	Rock	760 – 1500	—
S1 and S2	C	Very dense soil/soft rock	360 – 760	>50
	D	Stiff soil	180 – 360	50 — 100
S3 and S4	E	Soft soil	<180	<50
	F	Special soils require site-specific evaluation	—	—

Table 2 Determination of seismic hazard level in NCHRP 12-49 recommendations

Seismic Hazard Level	Value of $F_v S_1$	Value of $F_a S_s$
I	$F_v S_1 \leq 0.15$	$F_a S_s \leq 0.15$
II	$0.15 < F_v S_1 \leq 0.25$	$0.15 < F_a S_s \leq 0.35$
III	$0.25 < F_v S_1 \leq 0.40$	$0.35 < F_a S_s \leq 0.60$
IV	$0.40 < F_v S_1$	$0.60 < F_a S_s$

Long period response ratio SD1/1.2SA (comparison for site B/S1, 2500 year return period)

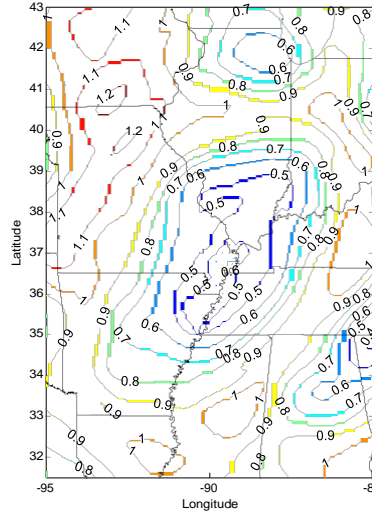


Figure 17 Map. Ratio of long-period design spectral value (S_{D1}) for 2-point/1-point methods—Site B/S1

Long period response ratio SD1/1.2SA (comparison for site E/S4, 2500 year return period)

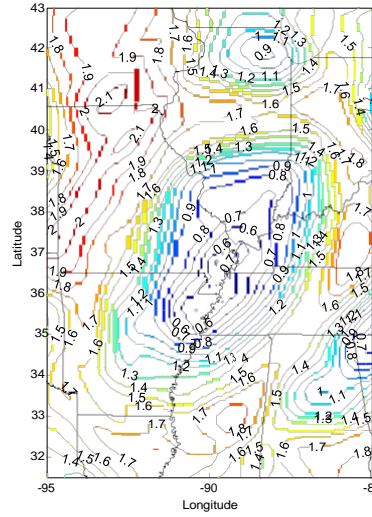


Figure 18 Map. Ratio of long-period design spectral value (S_{D1}) for 2-point/1-point methods—Site E/S4

Short period response ratio $S_{Ds}/2.5A$ (comparison for site B/S1, 2500 year return period)

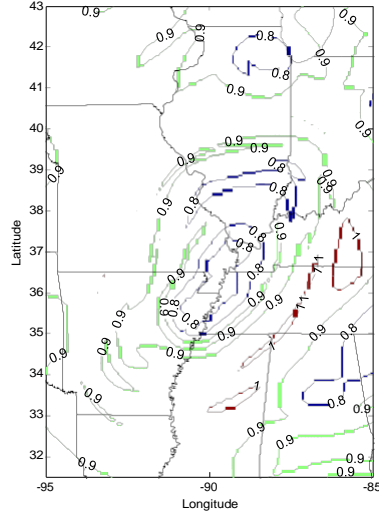


Figure 19 Map. Ratio of short-period design spectral value (S_{Ds}) for 2-point/1-point methods—site B/S1

Short period response ratio $SD1/1.2SA$ (comparison for site E/S4, 2500 year return period)

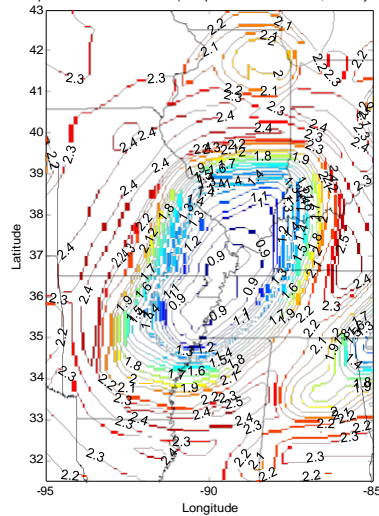


Figure 20 Map. Ratio of short-period design spectral value (S_{Ds}) for 2-point/1-point methods—site E/S4

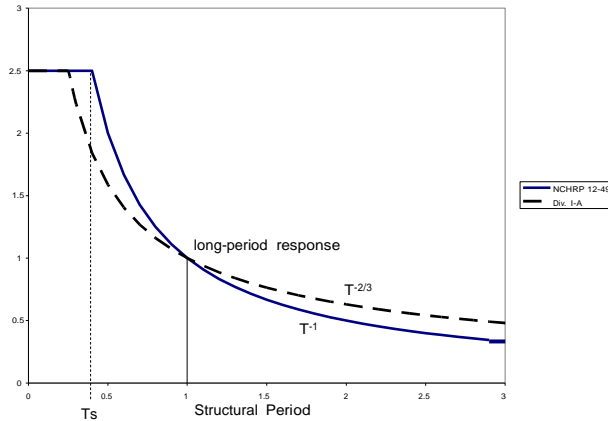


Figure 21 Graph. Changed power of T in NCHRP 12-49 recommendations

4. Hazard level and performance requirements

The use of updated seismic hazard data of 1996 generally reduces the ground motion intensity in the eastern U.S. by various degrees. Figure 15 and Figure 16 show that if the method specified in AASHTO Standard Specifications is used with the 1996 seismic hazard data, the design spectrum becomes approximately 30%~50% lower in lower seismicity zones in the concerned states, such as northern Illinois and western Missouri. This reduction is a result of advancement in seismic hazard analysis method and ground motion models used. Such reduction counteracts the increase from 500-year return period to 2500-year return period and makes the increase not as high as that shown in Figure 22 to Figure 24, which plots the increase of spectral values from 500-year return period to 2500-year return period. 2002 update of the ground motion includes new findings from ground motion research and exhibits relatively minor changes (Figure 25 to Figure 27).

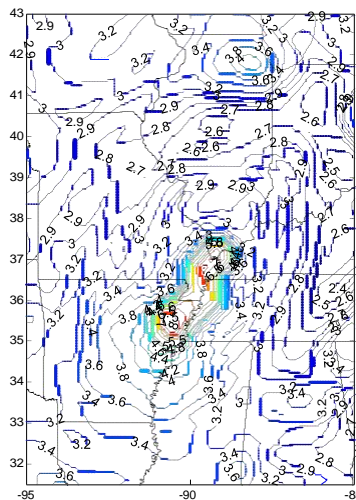


Figure 22 Map. Ratio of spectral values between 2500-year return period and 500-year return period (2002 data)—PGA

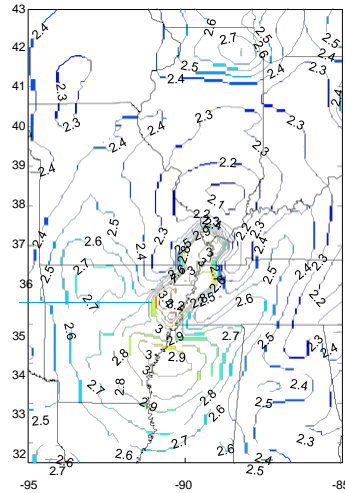


Figure 23 Map. Ratio of spectral values between 2500-year return period and 500-year return period (2002 data)—Short period response (0.2-sec)

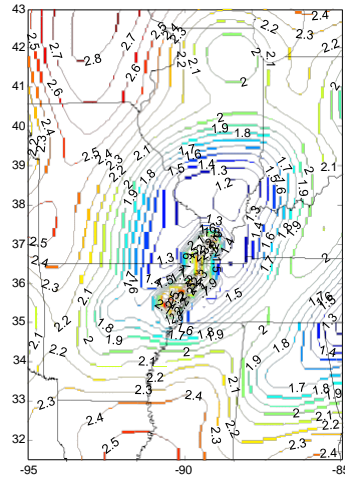


Figure 24 Map. Ratio of spectral values between 2500-year return period and 500-year return period (2002 data)—Long period response (1-sec)

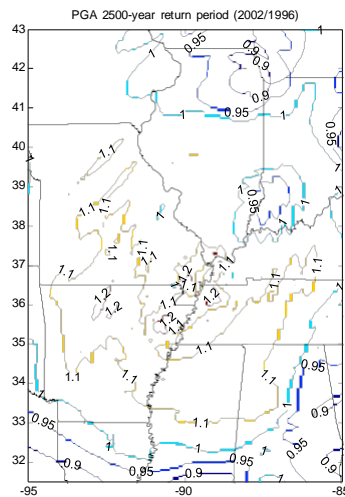


Figure 25 Map. Ratio of 2002 data to 1996 data—PGA 2500-year return period

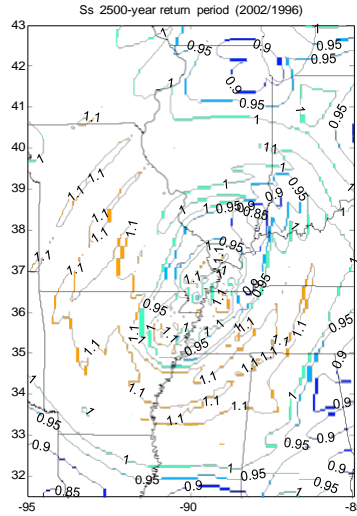


Figure 26 Map. Ratio of 2002 data to 1996 data—S_s 2500-year return period

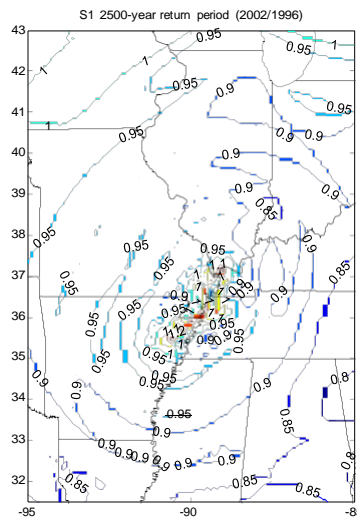


Figure 27 Map. Ratio of 2002 data to 1996 data—S₁ 2500-year return period

The reduction of spectral values in new data is more pronounced in the eastern seaboard⁽⁶⁾. Saadeghvairi⁽⁷⁾ found that the 2500-year return period ground motion in NCHRP 12-49 recommendations did not impose higher design requirements in New Jersey. Figure 28 and Figure 29 show the 1988 PGA map (500-year return period) in New Jersey area. Figure 30 and Figure 31 show that 1996 PGA data for 500-year return period in the same area. It is clear that the PGA values of 1996 map are 1/3~1/2.5 of those of 1988 map. This significant difference neutralizes the increase caused by the longer return period from NCHRP 12-49 recommendations. Figure 28 Figure 29 show the SHL for Site Class B and that for Site Class E. Only Class E sites have comparable size of area that requires seismic demand analysis to that of Standard Specifications shown in Figure 28.

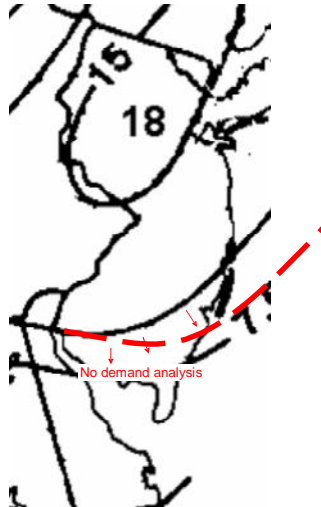


Figure 28 Map. 500-year return period PGA from 1988 map

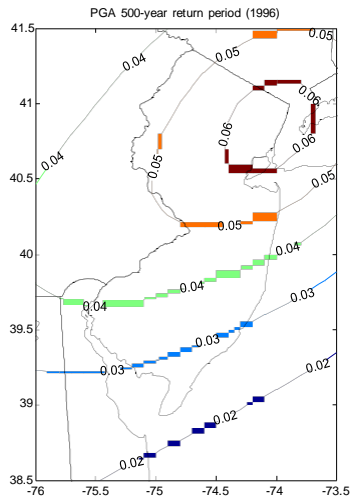


Figure 29 Map. 500-year return period PGA from 1996 update data

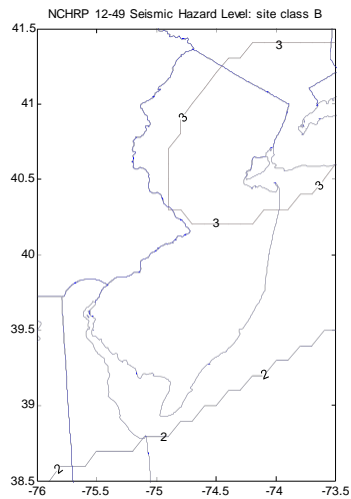


Figure 30 Map. Seismic Hazard Level in accordance with NCHRP 12-49 recommendations

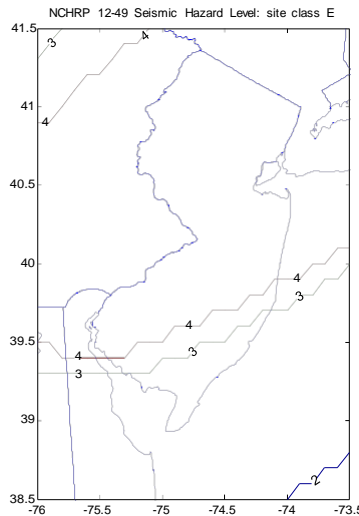


Figure 31 Map. Seismic Hazard Level in accordance with NCHRP 12-49 recommendations

The NCHRP 12-49 recommends the use of two earthquake levels to specify different performance objectives. The Maximum Considered Earthquake (MCE) represents a rare-occurrence event to assess the structural stability of bridges in the worst scenario. The Expected Earthquake (EE) is a normal event that is expected to be exceeded during the service life of the bridge. MCE and EE are characterized by return periods of 2462-year (using 2475-year USGS maps) and 108-year, respectively. Compared with the Western U.S. (WUS), seismic risk in the CSUS increases with return period much faster. This can be demonstrated by sample hazard curves shown in Figure 32. The peak ground acceleration of frequent events (on the left of the graph) at Memphis is much lower than that at Los Angeles. The rare events shown on the right end of the graph have similar intensity at the two locations. The seismic design of the bridges in CSUS is therefore often controlled by the MCE. Table 3 compares the typical long-period spectral values of different areas in the US normalized with spectral values of 474-year return period. It clearly shows the more significant impact from using ground motion with longer return period in the central and eastern U.S.

The MCE recommended by NCHRP 12-49 has a much longer return period (~2500-year) than that used by the AASHTO Standard Specifications (500-year). The corresponding ground motion parameters from NCHRP 12-49 are conceivably more severe. However, the performance objectives, design and analysis procedures, as well as detailing requirements are changed accordingly. The combined effect on bridge construction cost is not necessarily increased in the same scale as the design ground motion is. Table 4 shows a comparison of service level requirements in AASHTO Standard Specifications, NCHRP 12-49 recommendations, and AASHTO Guide Specifications under corresponding seismic hazard specified in each document. Although ground motion is the primary subject in this study, it is important to observe the difference in performance objectives because the effect from the changes in ground motion specifications may be offset by the changes in performance objectives.

Compared to the AASHTO Standard Specifications, the requirements for Life Safety performance level (for non-essential bridges) in NCHRP 12-49 recommendations are higher than those for essential/other bridges in the Standard Specifications and somewhat lower than those for critical bridges (no operational check for 500-year events). The requirements for Operational performance level are much higher than any requirements in the Standard Specifications.

The performance objectives in the Guide Specifications are very different from either of the other two documents. The only good reference is that they appear to lie between “critical” and “other” bridges in the Standard Specifications.

Both NCHRP 12-49 recommendations and the Guide Specifications contain incentives for the use of more advanced analysis method and better ductile structural behavior. In NCHRP 12-49 recommendations, the traditional force-based design approach is used with the option of using advanced displacement capacity check method, which allows a greater response modification factor (R-factor) as shown in Table 5. The Guide Specifications switches to displacement design for concrete substructure, therefore does not easily compare with either of the other documents. However, it is conceivable that it allows the designer to take advantage of displacement capacity of well-designed ductile structure/component in hope to produce more reliable and economical design.

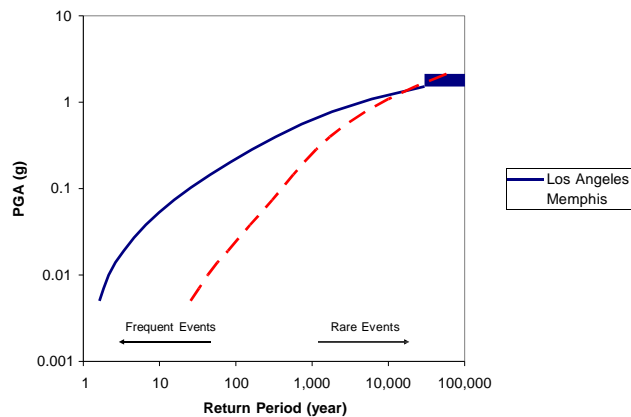


Figure 32 Graph. Map. Sample hazard curves in CSUS (Memphis) and western U.S. (Los Angeles)

Table 3 Normalized one-second spectral acceleration⁽⁸⁾

Return Period Years	Region				
	California	Pacific	Intermountain	Central US	Eastern US
474	1	1	1	1	1
1000	1.2	1.6	1.6	2.3	2.2
1500	1.4	2.2	2.0	3.5	3.4
2000	1.5	2.6	2.4	4.8	4.5
2500	1.6	3.0	2.7	6.1	5.7
Deterministic Cap	Yes	Yes	No	No	No

Table 4 Minimum service level required by AASHTO Division I-A and recommended by NCHRP 12-49

	Performance level	100 year return period earthquake	500 year return period earthquake	2500 year return period earthquake
Division I-A	Other	No provision	No collapse (implied)	No provision
	Essential	No provision	Open to emergency vehicle	No provision
	Critical	Fully operational (implied)	Fully operational (implied)	Fully operational
NCHRP 12-49	Life Safety	Fully operational	No provision	Open to emergency vehicle
	Operational	Fully operational	Fully operational (implied)	Fully operational
Guidespec	Non-essential	No collapse for 1000 year return period earthquakes		

Table 5 Maximum allowed response reduction factor for concrete substructure

Performance level		Wall piers	Columns	Vertical concrete piles
Division I-A	Other/Life safety	2.0	3 (single) 5 (multi)	3
	Critical/operational	1.5	1.5	1.5
NCHRP 12-49 (SDAP E)	Other/Life safety	3	6	6
	Critical/operational	1.5	2.5	2.5
Guidespec	Displacement design for concrete substructure			

A study on comparison of construction cost for three Illinois bridges showed significant difference with the combination of different ground motion specifications and different performance objective. In this study, the cost by NCHRP 12-49 recommendations is 2~5.5 times of the cost by the Standard Specifications⁽¹⁰⁾. It is important to observe that all three bridges are designed for “Operational” performance objectives and SDAP “D”, while the comparison is done with the “Essential” or “Other” importance categories in

Standard Specifications. The R-factors in SDAP D under Operational performance are between 1 and 1.5 (see Table 7). The design cannot take advantage of the possible high R-factors in NCHRP 12-49 recommendations. A study on typical bridge construction cost (Operational performance objectives, site class D) in Missouri⁽⁹⁾ shows that the use of 2500-year return period event increases the construction cost by 0~19% (see Table 8). These cases studies indicate that using the 2500-year return period ground motion specified in NCHRP 12-49 recommendations in this area with “Operational” performance objectives significantly increase design requirements and construction cost when the seismic force reduction offered in Seismic Design and Analysis Procedure E is not utilized.

Table 6 Cost comparison of design based on NCHRP 12-49 recommendations and Standard specifications

Bridge	Standard Specifications	NCHRP 12-49 (Operational)
Johnson County Bridge	\$123,930 (other)	\$243,650
St. Clair County Bridge	\$168,020 (other)	\$879,100
Pulaski County Bridge	\$165,340 (essential)	\$898,420

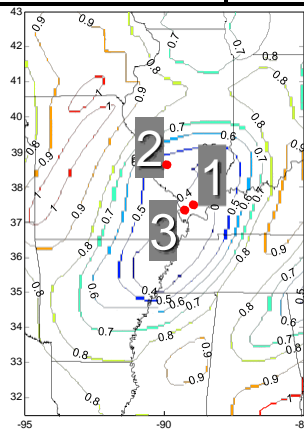
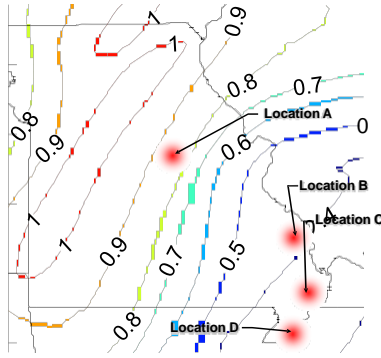


Figure 33 Map. Sites for cost comparison of design based on NCHRP 12-49 recommendations and Standard specifications

Table 7 R-factors used in Illinois construction cost study

Bridge	R-factor based on NCHRP 12-49 recommendations	R-factor based on Standard Specifications
Johnson County Bridge	1	2
St. Clair County Bridge	1.5	5
Pulaski County Bridge	1 longitudinal, 1.5 transverse	2 for flexural, 1 for shear



**Figure 34 Map. Sites to compare the increase of construction cost in Missouri
(Contour: $S_1/1.2$ PGA—500-yr)**

Table 8 Increase of construction cost in Missouri⁽⁹⁾

Bridge Site	Site Class	Increase of cost (%)	
		Sand Backfill	Clay Backfill
A	III (D)	0	0
B	III (D)	6	2
C	III (D)	7	7
D	III (D)	19	19

AASHTO Guide Specifications 2007

The recommendations from the NCHRP 12-49 project were submitted to AASHTO Bridge Subcommittee in 2002 for consideration of adoption. Some issues found in the trial design evaluation could not be resolved, and consequently the committee did not move forward on the adoption of the recommended design guidelines. Primary issues included seismic hazard level, increased seismic design effort required for bridges in some states, and complexity of the Guidelines for bridge engineers in the majority of states.

The AASHTO Guide Specifications adopted in 2007 is based on the research product and recommendation from the NCHRP 20-7 Project Task 193⁽⁸⁾: “Updating Recommended LRFD Guidelines for the Seismic Design of Highway Bridges.” This project utilizes the extensive technical studies completed under NCHRP Project 12-49 and reformats the guidelines to be more inline with the current practice in South Carolina Seismic Design Criteria in order to facilitate use by practicing engineers. Additionally, material from the Caltrans Seismic Design Criteria (SDC), ATC-32 and other state agencies is integrated into the guidelines as appropriate.

Research efforts related to ground motion in this project include:

1. Implementing 1996 MCE map with 2002 update.
2. Use factored map value to obtain required level before corresponding map is available.
3. Consideration of applying a reduction factor on the hazard intensity for existing bridges or bridges located in rural areas.

4. Check and modify implicit conservatism to ensure life safety for 1000yr return period event.

The primary changes related to ground motion include:

1. Single-level design earthquake with 7% probability of exceedance in 75 years (1000-year return period). Figure 35 shows increase of PGA from 500-year return period (Standard Specifications). Considerably lower values are observed compared to Figure 10.
2. Determining seismic hazard level by long-period design spectral value (as against by both long-period and short-period values in NCHRP 12-49 recommendations).

A number of implicit conservatisms in current bridge design practice are identified (

Table 9) to demonstrate the possible over-conservativeness of the choice of MCE and corresponding design and detailing requirements in NCHRP 12-49 recommendations. With adequate seat width and substructural ductility, a reduced MCE of 1000-year return period is justified.

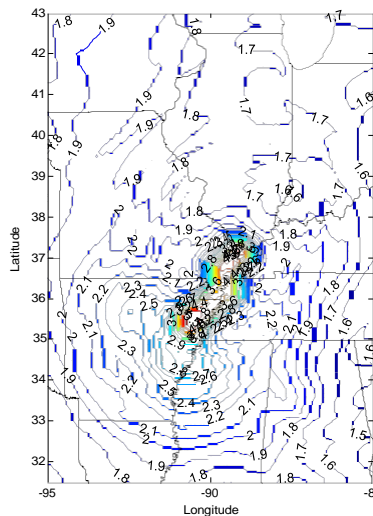


Figure 35 Map. Ratio between PGA of 1000-year return period and PGA of 500-year return period

Table 9 Implicit conservatism in current bridge design practice

Source of conservatism	Safety Factor
Computational vs. Experimental Displacement Capacity of Components	1.3
Effective Damping	1.2 to 1.5
Strain Rate Effect	1.2
Pushover Techniques Governed by First Plastic Hinge to Reach Ultimate Capacity	1.2 to 1.5
Out of Phase Displacement at Hinge Seat	To be addressed

The Seismic Hazard Level is used to determine the appropriate design procedures and requirements. It directly affects the amount of effort in seismic design and the learning curve of new design methodology. The NCHRP 20-7 (193) included a “Range of Applicability” study to verify that the hazard definition and corresponding design procedure used by the updated recommendations inflict comparable effort with current practice. Figure 36 shows that even under relatively high site amplification for Site Class D, the area that requires “Seismic Demand Analysis” by the NCHRP 20-7 (193) recommendations is of similar size to the “No Analysis” area by AASHTO Standard Specifications.

Figure 37 and Figure 38 compare the seismic hazard levels defined by the NCHRP 12-49 recommendations and those by AASHTO Guide Specifications. Three factors contribute to the change of the areas of different hazard levels:

1. The NCHRP 12-49 uses both S_{Ds} and S_{D1} to determine the Seismic Hazard Level. As described previously, for the same peak ground acceleration, the procedure that produces S_{Ds} yields greater values relative to those from AASHTO Standard Specifications. The seismic hazard level from NCHRP 12-49 is therefore pushed up by the relatively greater S_{Ds} values.
2. The Seismic Hazard Levels from NCHRP 12-49 are cut off at $S_{D1}=0.15, 0.25,$ and $0.40,$ while those from the Guide Specifications are cut off at $S_{D1}=0.15, 0.30,$ and $0.50.$
3. For determination of Seismic Hazard Level, the NCHRP 12-49 uses reduced site amplification factors for Site Class E when S_1 is less than or equal to 0.1. Effect of this reduction can be observed as the boundaries of Seismic Hazard Levels II and III do not expand from Site Class D to Site Class E (Figure 37, two plots on the right).

That is, the area enclosed by the blue contour line labeled “2” and the area enclosed by the green contour line labeled “3” do not expand.

The above observation shows that the AASHTO Guide Specifications (NCHRP 20-7 Task 193) preserves a similar level of design effort to that from the AASHTO Standard Specifications (in terms of ground motion specifications and hazard levels). Since the Guide Specifications has shifted from force design to displacement design, the observed characteristics of the ground motion do not directly translate to the construction cost of bridges. There has not been a clear indication as of how the construction cost compare between the Guide Specifications and the Standard Specifications. Further study is needed to investigate this issue.

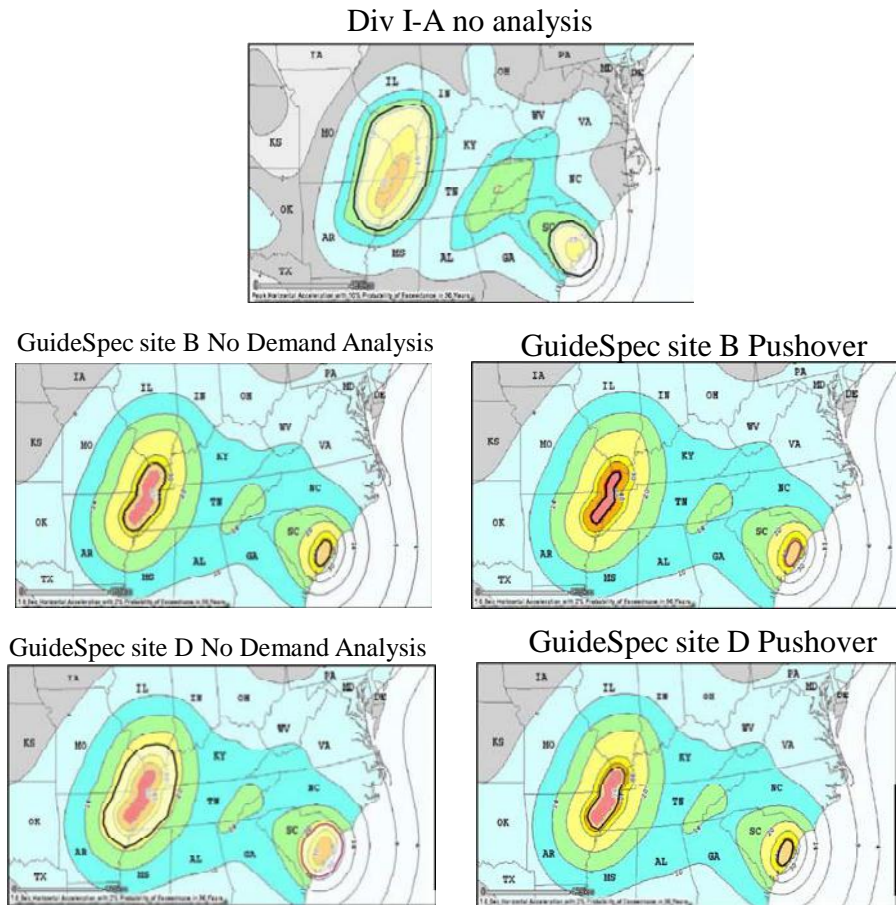


Figure 36 Map. Range of Applicability study in NCHRP 20-7 Task 193⁽⁸⁾(GuideSpec)

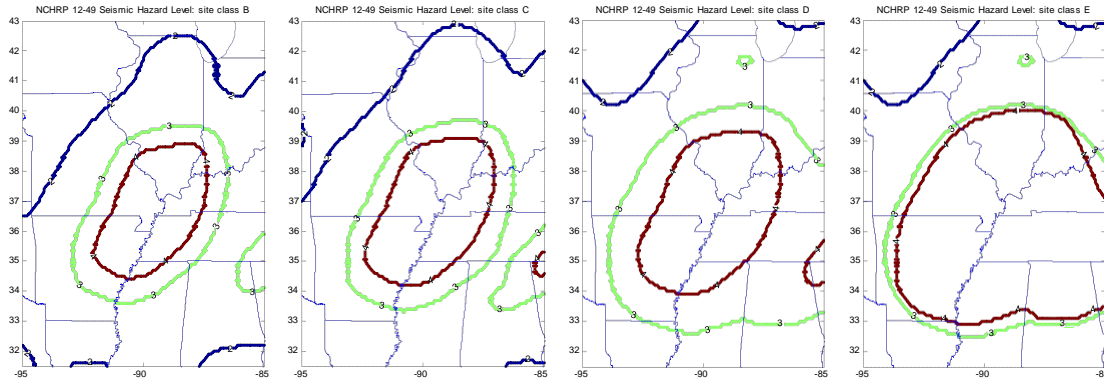


Figure 37 Map. Seismic Hazard Levels by NCHRP 12-49 recommendations

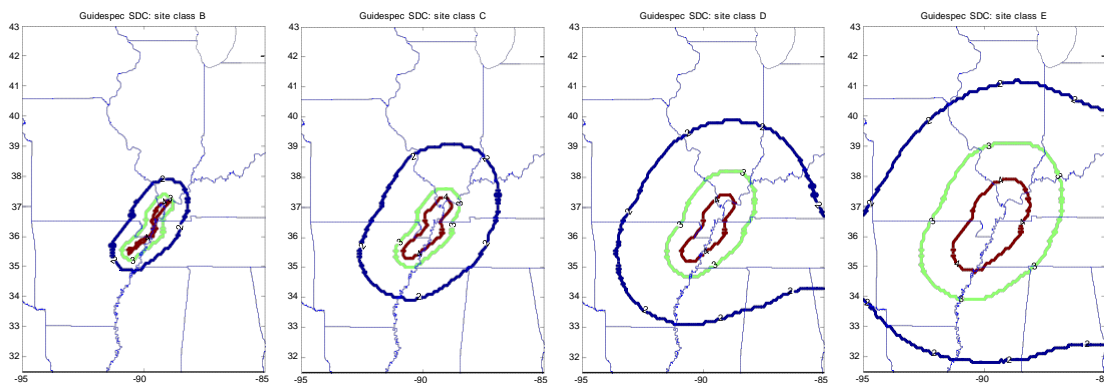


Figure 38 Map. Seismic Hazard Levels by Guide Specifications

FHWA Seismic Retrofitting Manual

The procedure to obtain ground motion in FHWA Seismic Retrofitting Manual is the same as that used in NCHRP `12-49 recommendations, except that the upper level events are 1000-year return period. Figure 39 shows the comparison of the FHWA Seismic Retrofitting Manual to AASHTO Guide Specifications and NCHRP 12-49 recommendations. The FHWA Seismic Retrofitting Manual has comparable “no demand analysis” are (SHL I and II: area beyond the green line labeled “3”) for Site Class E. For other Site Classes, the FHWA Seismic Retrofitting Manual has higher analysis requirements than the AASHTO Guide Specifications. This is due to the inclusion of short-period design spectral values in determination of SHL. When the comparison is strictly done in the seismic hazard definition, it appears that the retrofitting requirement is higher than the new design requirement by the Guide Specifications. However, it is possible that other procedural difference and detailing requirements may offset this unfavorable situation. Further trial design studies using these two documents may provide more insight in this issue.

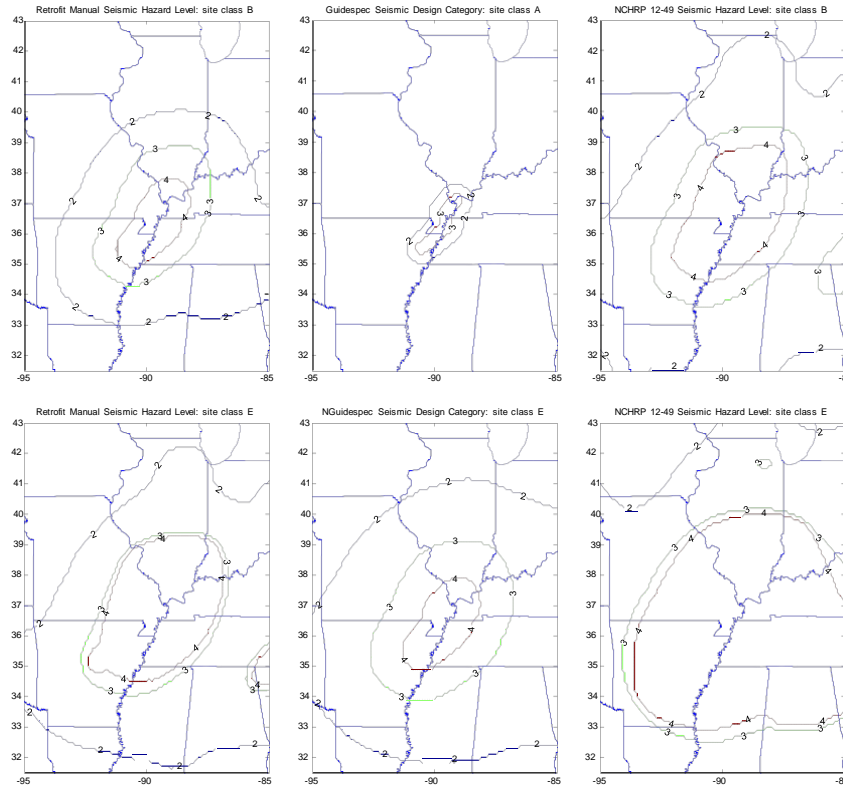


Figure 39 Map. Seismic Hazard Levels by FHWA Seismic Retrofit Manual (left), Guide Specifications (middle), and NCHRP 12-49 recommendations (right).

Displacement capacity verification

The NCHRP 12-49 recommendations and FHWA Retrofitting Manual encourages the use of explicit displacement capacity verification to benefit from the ductility of well-proportioned substructural components. In high seismicity area (SDC D), the AASHTO Guide Specifications requires the use of pushover analysis for displacement capacity verification. This method was not included in the AASHTO Standard Specifications and previous versions of FHWA Seismic Retrofitting Manual. Such new analysis requirement may increase the difficulty for implementation of the latest design and retrofitting documents in a broad range of the CSUS area. The FHWA has recently developed a computer tool for quickly conducting pushover analysis on a number of structural systems. Although this computer application is not developed under this pooled fund study, it will be available to the participating states free of charge.

2.2 SIMULATION OF EARTHQUAKE GROUND MOTION FOR THE CSUS

As progress in earthquake ground motion simulation is made, two questions may be asked for the CSUS area:

1. Is the current simulation method adequate for the specific geological and seismological conditions in this area?

2. Is the ground motion specifications in latest design procedure consistent with the most adequate simulation method for the CSUS?

The response spectrum used in design is reconstructed from national seismic hazard data in two separate steps: (1) obtaining spectrum for generic site condition, and (2) multiply spectral values by site coefficients. The PSHA result for generic rock site is usually used as the base spectrum. The site coefficient used in NCHRP 12-49 recommendations and AASHTO Guide Specifications are adopted from 1997 NEHRP Provisions. These coefficients modify the base spectrum to include the effect from the site condition. To answer the above questions, the procedures used to produce the base spectrum and the procedure to identify the site coefficients need to be investigated.

Base response spectrum at rock sites

The USGS seismic hazard maps for the CSUS are produced with Probabilistic Seismic Hazard Analysis (PSHA), which is suitable for a broad area of the country where clear tectonic mechanism that produces earthquakes is not accurately identified. PSHA includes the uncertainties that reside in all factors governing the ground motion intensity and characteristics at the bridge site. This includes the uncertainties in type of sources, source magnitude, source locations, and the path between source and the local rock base. The PSHA provides a rational basis for risk assessment in bridge design and is especially useful when limited earthquake records and tectonic activity data are available, which is a common condition in areas with fewer recent large earthquake activities. The method requires parameters that characterize the recurrence of all potential seismic sources surrounding the concerned site and modeling of the attenuation.

A PSHA involves stochastic modeling of a few components related to seismic events: source, path, and near-site condition⁽³⁾. A source model, an attenuation relationship, a rock/soil layer profile at the site, and uncertainties associated with all models are needed to obtain ground motion at the site stochastically. The USGS national seismic hazard data provide seismic hazard intensity based on a logic tree formalism, which includes a number of different models in each component. The identified seismic sources include historical events (gridded data or special zones), characteristic sources (fictitious fault ruptures), some regional sources, and large background zones. The source can be point source or faults with finite length. Two models⁽¹¹⁾ are used in 1996 update to characterize ground motions. In the 2002 update (used by Guide Specifications), three more models⁽¹²⁾ to include double-corner, finite-fault, and hybrid models. The path effect includes the attenuation and filtering from the crustal transmission of the seismic waves. The basic site condition is based on generic rock/stiff soil profile (see Figure 40). Modification factors (site coefficients) are used to modify the site spectra to the level associated with different site classes.

With a source model, attenuation relationship, and generic profile, a ground motion relationship can be developed. The spectral acceleration values at different periods from all considered magnitudes and distance are presented in such model. The results of the use of different models and source/attenuation/generic-profile parameters are different ground motion relationship equations. The choice of ground motion relationship should

represent the tectonic structure for the considered area. The relationship used in the CSUS can be considerably different from that used in western U.S.. Figure 41 to Figure 44 show the PGA ground motion relationship by Frankel et al.⁽¹¹⁾ (Figure 41), Atkinson and Boore⁽¹²⁾ (Figure 42), Toro et al.⁽¹³⁾ (Figure 43), and Atkinson and Boore⁽¹⁴⁾ (Figure 44). Frankel et al.⁽¹¹⁾ and Atkinson and Boore⁽¹⁴⁾ are developed for B/C boundary profile (firm rock) while the other two are for hard rock sites. Atkinson and Boore⁽¹²⁾ use 2-corner source model. Toro et al.⁽¹³⁾ use 1-corner source model. Atkinson and Boore⁽¹⁴⁾, use finite-fault model.

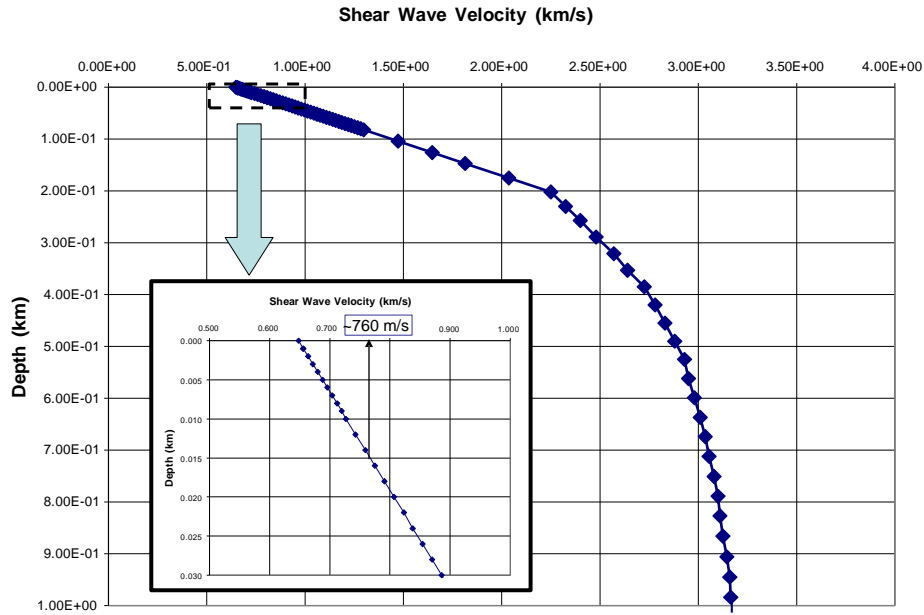


Figure 40 Graph. Generic rock/stiff soil shear wave velocity profile used to produce USGS maps

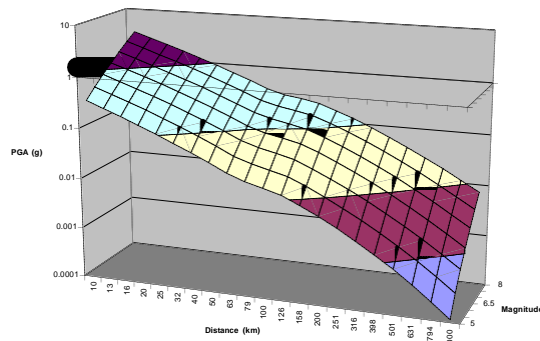


Figure 41 Graph. Samples of ground motion relationships—Frankel et al., 1996

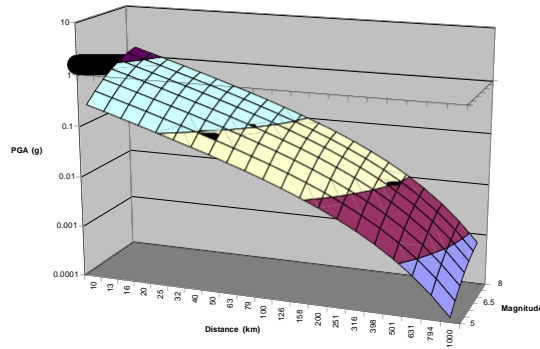


Figure 42 Graph. Samples of ground motion relationships— Atkinson and Boore, 1995 (2-corner)

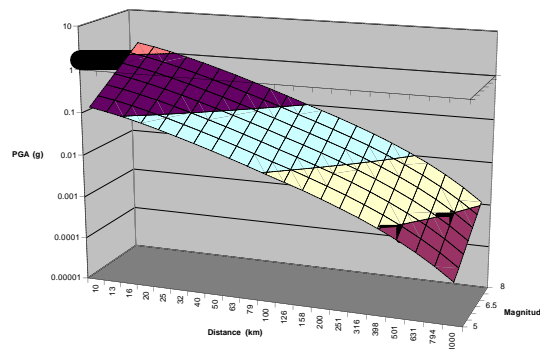


Figure 43 Graph. Samples of ground motion relationships—Toro et al., 1997 (1-corner)

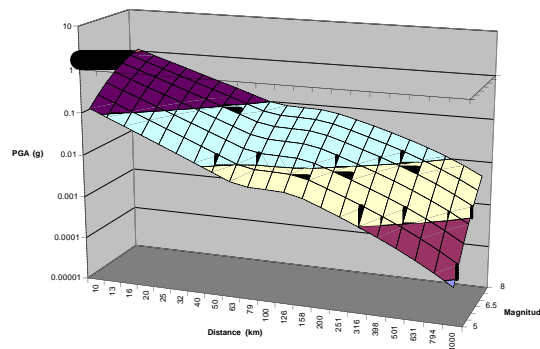


Figure 44 Graph. Samples of ground motion relationships—Atkinson and Boore, 2006(finite fault)

The logic tree formalism used by USGS seismic hazard maps is an effective way to address the uncertainty in modeling methodology. It includes multiple seismic hazard assessment schemes and gives weights based on the confidence to individual schemes from seismologists. It also provides a platform to promptly integrate latest seismological developments in every revision of the maps. For example, the 2-corner source model⁽¹²⁾ for the eastern U.S. yields significantly lower Fourier spectral values at intermediate frequencies than the traditional Brune 1-corner model, therefore relatively low response spectral values in some structural period range. This model is not included in the 1996

USGS seismic hazard data but is adopted in the 2002 update as it becomes broadly accepted. The PSHA procedure developed by Wen and Wu⁽¹⁶⁾ shows that the 500-year return period response spectrum is consistent with the USGS data, while the 2500-year return period response spectrum somewhat lower than USGS data. In a study on the LRFD seismic design of bridges in Illinois⁽¹⁰⁾, the PSHA is used to produce ground motion time history of rock sites. The peak ground acceleration of these ground motion records (2500-year return period) are found fairly consistent with those obtained from USGS seismic hazard data (MCE) at rock sites (see Figure 45). However, the ground motions of 1000-year return period from this study are found somewhat higher than those from USGS.

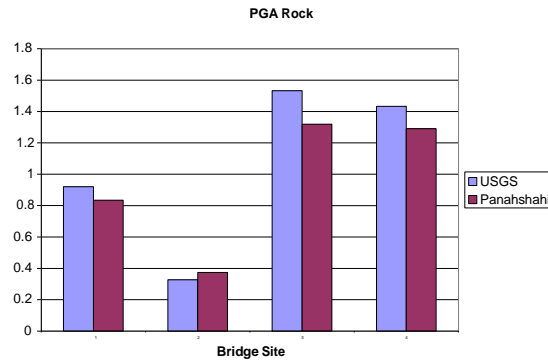


Figure 45 Graph. Rock motion (PGA) for four Illinois bridge sites

Site Response Spectrum Modification

The site coefficient used in NCHRP 12-49 recommendations and AASHTO Guide Specifications are adopted from 1997 NEHRP Provisions, which is calibrated primarily with recorded data from 1989 Loma Prieta Earthquake and 1985 Mexico City Earthquake, with some extrapolation using numerical analysis⁽⁵⁾. Verification with latest earthquake records has not shown significant inconsistency⁽¹⁵⁾.

The site response is, in fact, not simply dependent on rock spectrum values, as site coefficients used in NEHRP provisions, but also influenced by earthquake magnitude and distance. The development of the NEHRP site coefficients is not consistent with the PSHA that develops the rock motion. Several procedures have been developed to address this issue. Wen and Wu⁽¹⁶⁾ carried out PSHA to obtain ground motion at specific sites (Memphis, Tennessee, St. Louis, Missouri, and Carbondale, Illinois). The site effect is assessed by Quarter Wave Length method. A ground motion time history is produced in each simulation based on the Fourier spectra obtained from the ground motion model and site modification. The Uniform Hazard Response Spectra (UHRS) can be obtained from a large number of time history sets. Figure 46 shows the UHRS of the three sites, with thickness of soil layers of 1000m, 165m, 15.7m from left to right. It can be observed that thick soil layer tends to suppress the short-period response and produce a response spectrum generally lower than the NEHRP spectrum, with the exception of long-period response.

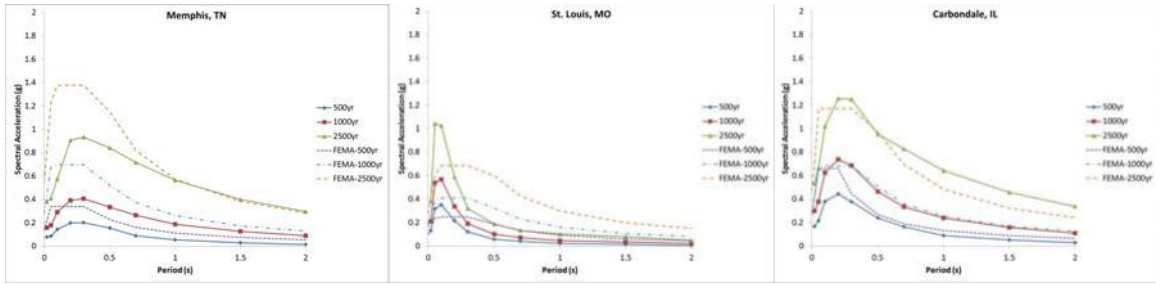


Figure 46 Graph. Comparison of UHRS to NEHRP spectra for Memphis, St. Louis, and Cabondale⁽¹⁶⁾

Romero and Rix⁽¹⁷⁾ used an equivalent linear method, which is capable of analyzing soil column resonance, to further characterize the effect of the deep soil layers in the Mississippi Embayment area. The result can be interpreted as:

1. The site effect of Mississippi Embayment Uplands is different from that of Lowlands.
2. The depth of soil deposits has a considerable impact on the site coefficients.
3. Nonlinear effect is important in this area (NEHRP site coefficients are based on empirical data in California and Mexico extrapolated by linear analysis.).

Two important implications from these conclusions on current application of site coefficients are:

1. The current site coefficients overestimate short-period response for earthquake sources in short distance.
2. The current site coefficients underestimates response of periods between 0.3 and 0.5 second.

These effects are further studied using one-dimensional nonlinear computation in recent studies^(18, 19) using nonlinear computation procedure in combination with the generic soil profiles for the Uplands and Lowlands developed by Romero and Rix⁽¹⁷⁾ and seismic hazard intensity of a number of locations (Figure 47). These studies explicitly include the soil layer vibration and nonlinear properties.

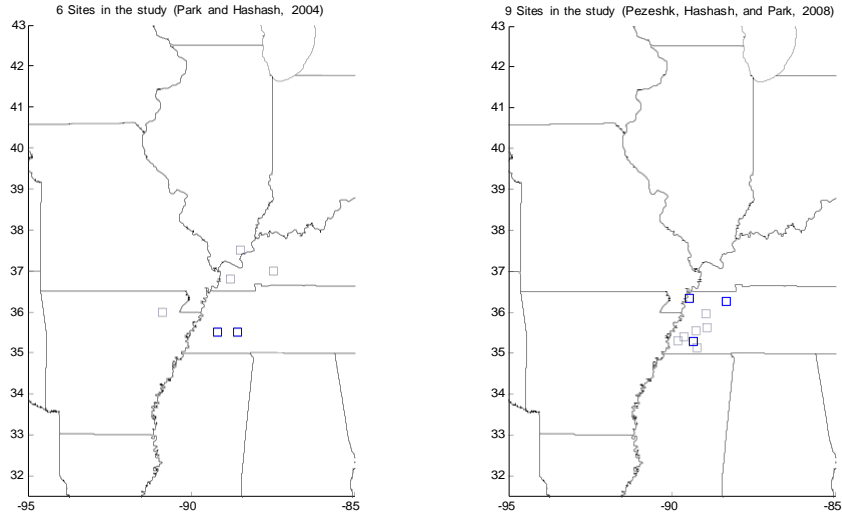


Figure 47 Map. Locations where PSHA is performed to produce ground motions for the purpose of site amplification analysis^(18, 19)

The sites studied show that the short-period response site coefficients, F_a , decrease with increasing soil layer thickness. Figure 48 shows the factor F_a normalized with the NEHRP site coefficient for Site Class D and the normalized long-period response site coefficient, F_v . A clear trend of F_a increasing along depth and F_v decreasing along depth can be observed.

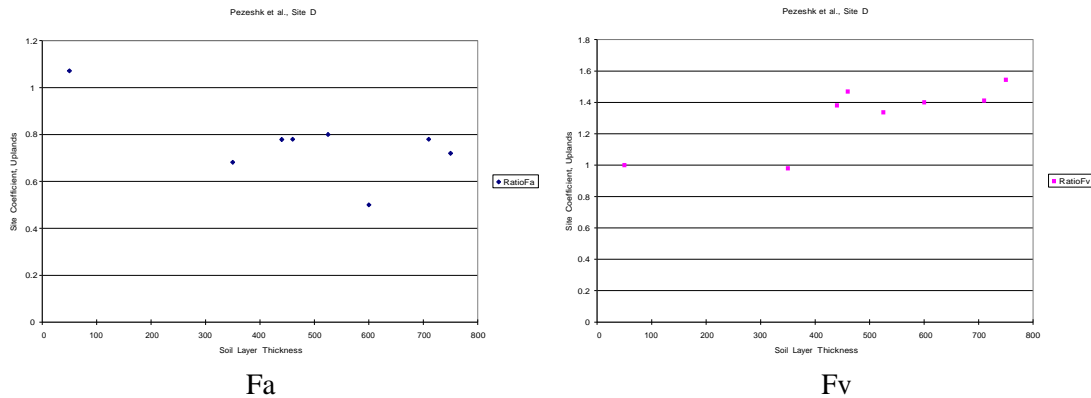


Figure 48 Graph. Normalized site coefficients for varying soil layer thickness

A matrix of site response amplification with varying seismic hazard and soil layer thickness was produced. Empirical formulae are provided by fitting the upper bound and lower bound of the data points with a few linear segments (Table 10 and Table 11). It is found that the formulae for Uplands and those for Lowlands are identical. This is in disagreement with the first finding from Romero and Rix⁽¹⁷⁾. This indicates that the depth and material properties are more predominant factors than the difference in the soil profile. Figure 49 shows the mean value of upper bound and lower bound formulae. The coefficients may exhibit more than 30% change (decrease for F_a and increase for F_v) at sites with deep soil layers under large earthquake ground motions. Note that this modification does not include the soil column resonant effect. It may underestimate

ground motions in the structural period range between 0.3 and 0.5 second. This falls in the area where the short-period and long-period response spectral curve meet (i.e. Ts). Future study is needed to address this issue.

Table 10 Empirical formulae for short-period response site coefficient⁽¹⁸⁾

Depth	Upper bound	Lower bound
0~30m	F_{a30}	F_{a30}
30m~300m	$F_{a30}-0.0006d$	$F_{a30}-0.001d$
300m~500m	$F_{a30}-0.18-0.00025(d-300)$	$F_{a30}-0.3-0.00025(d-300)$
500m~1000m	$F_{a30}-0.23-0.0001(d-500)$	$F_{a30}-0.35-0.0001(d-500)$

Table 11 Empirical formulae for long-period response site coefficient⁽¹⁸⁾

Depth	Upper bound	Lower bound
0~30m	F_{v30}	F_{v30}
30m~100m	$F_{v30}+0.003d$	$F_{v30}+0.001d$
100m~300m	$F_{v30}+0.3+0.001(d-100)$	$F_{v30}+0.1+0.001(d-100)$
300m~500m	$F_{v30}+0.5+0.00025(d-300)$	$F_{v30}+0.3+0.00025(d-300)$
500m~1000m	$F_{v30}+0.55+0.0001(d-500)$	$F_{v30}+0.35+0.0001(d-500)$

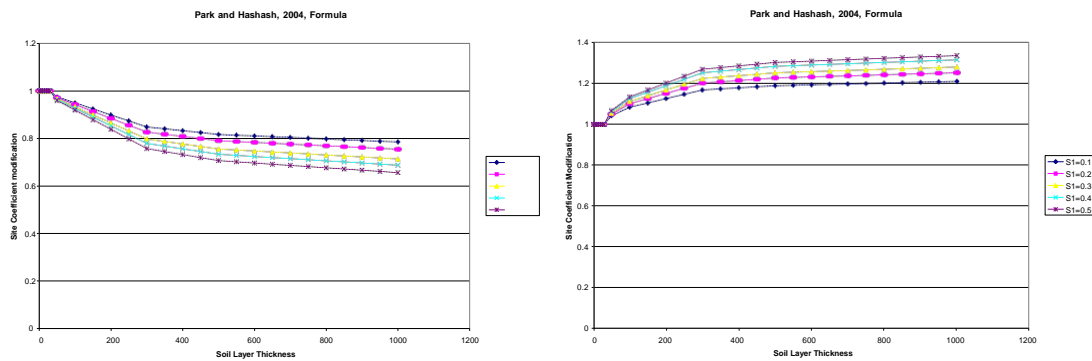


Figure 49 Empirical formulae for modification of site coefficients

2.3 GROUND MOTION TOOLS FOR BRIDGE DESIGN AND RETROFITTING

Bridge engineers are in need of adjusting to a few necessary changes in seismic hazard assessment:

1. The 1988 NEHRP seismic hazard maps are over two-decade old. Updated data are needed.
2. All recent design and retrofiting documents are adopting 2-point or 3-point spectra to better customize the design spectra for various types of seismic activities in the U.S.
3. A number of different levels of seismic hazard risk (measured by probability of exceedance or return period) are adopted by different design and retrofiting documents in different regions.

To assist bridge engineers in the concerned area of this study, the Office of Infrastructure R&D of FHWA produced a computer tool that provides a number of essential parameters related to seismic hazard used in bridge design and retrofiting. This tool is attached to this report for immediate application.

Product specifications and System requirement

The data included with this ground motion tool is the 2002 update of the USGS seismic hazard data. The site coefficients are calculated in compliance with the NEHRP site coefficients adopted by NCHRP 12-49 recommendations, AASHTO Guide Specifications, and FHWA Seismic Retrofitting Manual.

The FHWA ground motion tool is in the format of a Microsoft Excel spreadsheet. It requires the Microsoft Excel 2003 or later installed to the user's system.

User Instructions

1. The tool is opened by double-clicking the file "MidAmerica_Lat_Lon.xls" included with this report. A screen as shown in Figure 50 appears.
2. Enter the latitude and longitude in the corresponding boxes at the upper-left corner of the screen and hit enter. The valid range is 30~42.5 degrees in latitude and -95.7~-81 degrees in longitude. It is important to enter a negative number in longitude box.
3. Select a return period at the upper-right side of the screen that is associated with the appropriate document for design or retrofiting (Figure 51).
4. Select the site class on the left side of the screen (Figure 52).
5. The program shows:
6. Site coefficients: F_{pga} for peak ground acceleration, F_a for short-period response, and F_v for long-period response.
7. Base spectral values: PGA (peak ground acceleration), S_s (short-period response at 0.2 sec period), and S_1 (long-period response at 1 sec period).

8. Surface response spectral values: FpgaPGA (design peak ground acceleration), SDs (short-period design spectral value), and SD1 (long-period design spectral value).
9. Seismic Hazard Level (SHL, FHWA seismic retrofitting manual) I~IV. The SHL is displayed only when “100 years - FHWA retrofit” or “1000 years - FHWA retrofit” is selected in step 3.
10. Seismic Design Category (SDC, for AASHTO Guide Specifications) A~D. This is displayed only when the “1000 years – AASHTO Design” is selected in step 3.
11. Design spectral values and plot in 0.1 sec period interval (Figure 53).

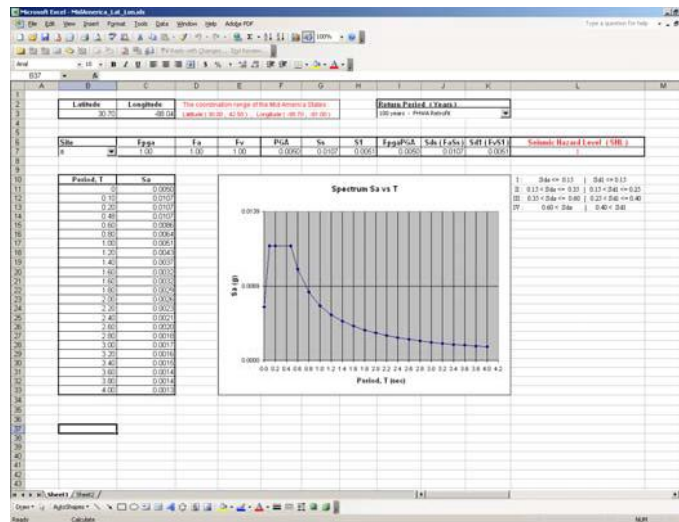


Figure 50 Screenshot. Opening screen of the ground motion tool

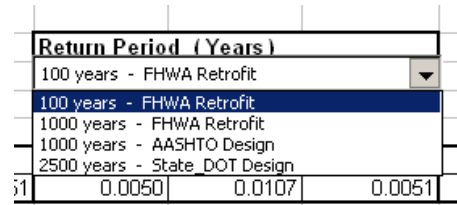


Figure 51 Screenshot. Return period and design/retrofitting documents

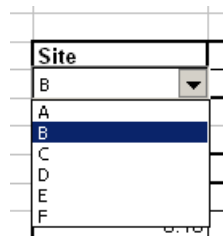


Figure 52 Screenshot. Site class

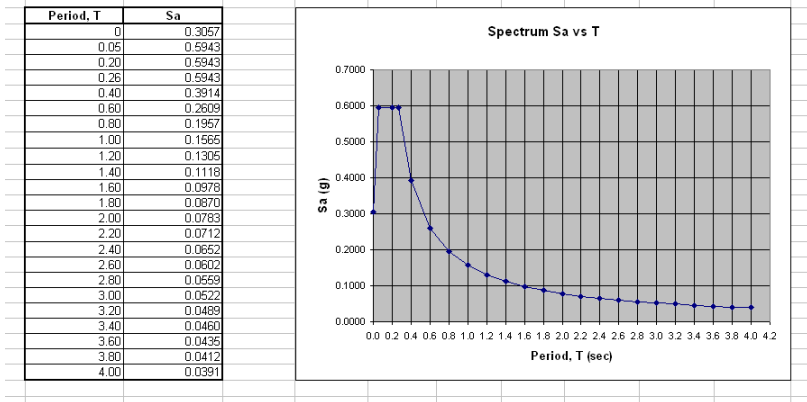


Figure 53 Screenshot. Design spectral values and display of the curve

CHAPTER 3 SEISMIC VULNERABILITY AND RETROFIT OF BRIDGES IN THE CENTRAL AND SOUTHEASTERN UNITED STATES

3.1 INTRODUCTION

Design of bridges in regions of low-to-moderate seismicity such as the Mid-America region of the United States share several common challenges;

- Very infrequent major or moderate earthquakes, leading to little understanding of large earthquake characteristics;
- Lack of adequate seismic design in typical structures;
- Vague understanding of earthquake source and mechanism; and
- Ground motion that attenuates less, leading to more wide-spread damage area compared to high seismic regions.

In addition, the absence of strong ground shaking in Mid-America, and the adoption of the 10% probability of exceedance in 50 years ground motion criteria led to significantly lower design forces for Mid-America compared to the west coast. To assess the vulnerability of bridges in Mid-American (Central and Southeastern US), detailed analysis of the common bridge types in this region are performed.

3.2 BRIDGE CONSTRUCTION AND VULNERABILITIES

Bridge Construction

To better understand the seismic risk to bridges in Mid-America, a detailed inventory of the bridge types in the region is compiled. Using the National Bridge Inventory database and specific bridge plans obtained from various state departments of transportation, a detailed inventory study is performed. In the 11 states considered in the analysis, it is found that there are over 163,000 bridges. Table 12 shows the breakdown of the bridges by bridge type and material. It is shown that 10 bridge types comprise approximately 90% of the bridges in the Central and Southeastern US. The largest group in the inventory is the Multi-Span Simply Supported Concrete Girder bridge, which makes up nearly 20% of the bridges in the CSUS bridge inventory.

The construction year of the different bridge types was also analyzed. Since seismic design details were not used until approximately 1990, the age of the bridges is a good indication of the potential vulnerability to seismic loads. It was found that approximately 80-85% of the bridges in the CSUS were built prior to 1990.

Table 12 Bridge classes and their proportions in the Central and Southeastern US

Bridge Class	Number	Percentage
Multi-Span Continuous Concrete Girder	10,638	6.5%
Multi-Span Continuous Steel Girder	21,625	13.2%
Multi-Span Continuous Slab	5,955	3.6%
Multi-Span Continuous Concrete Box Girder	916	0.6%
Multi-Span Simply Supported Concrete Girder	30,923	18.9%
Multi-Span Simply Supported Steel Girder	18,477	11.3%
Multi-Span Simply Supported Slab	9,981	6.1%
Multi-Span Simply Supported Concrete Box Girder	4,909	3.0%
Single-Span Concrete Girder	22,793	13.9%
Single-Span Steel Girder	18,281	11.2%
Other	18,945	11.7%
Total	163,433	100%

(based on 2005 NBI Database).

Most bridges in the CSUS are composite steel girder and concrete deck or composite prestressed girder and concrete deck, as shown in Figure 54. The girders are typically supported by single or multi-column bents which are supported on pile foundations in areas of poor soils. The girders are typically supported on steel bearings, pot bearings, or elastomeric bearings. These bridge types differ from those found in the West Coast, where most bridges consist of multiple frames with box girder decks. Subsequently, their seismic performance and effective retrofit strategies are not well understood. Based on previous studies, the most likely vulnerable parts of the bridge are the following;

- Substructure (below grade): Pile caps most likely have inadequate reinforcement to ensure plastic hinging in the columns.
- Substructure: insufficient lap splices, and inadequate transverse reinforcement, leading to limited ductility capacity and low shear strength⁽²⁰⁾.

- Superstructure: Steel bearings (Figure 55) lack ductility, and seat widths are inadequate to ensure against unseating.

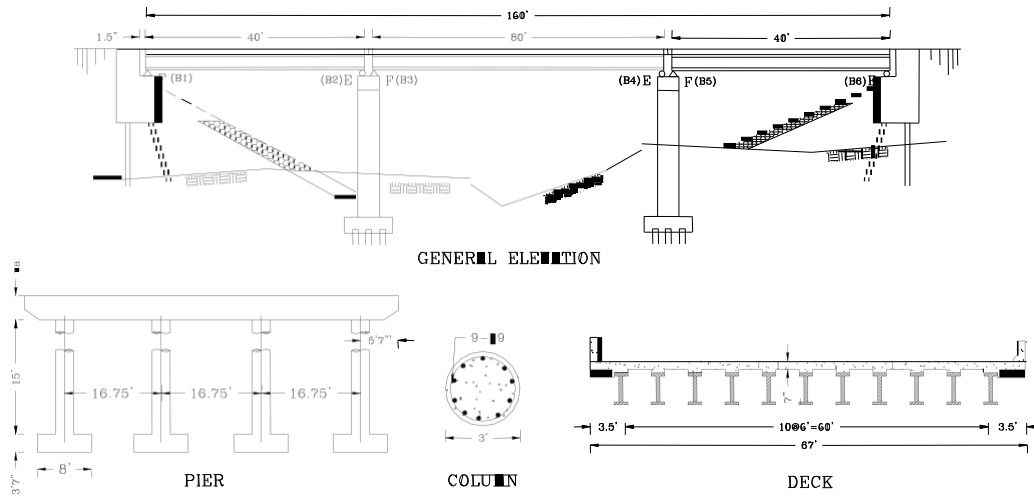


Figure 54 Illustration. Typical Multi-Span Simply Supported Bridge in Mid-America (redrawn from TN Department of Transportation Bridge Plans)

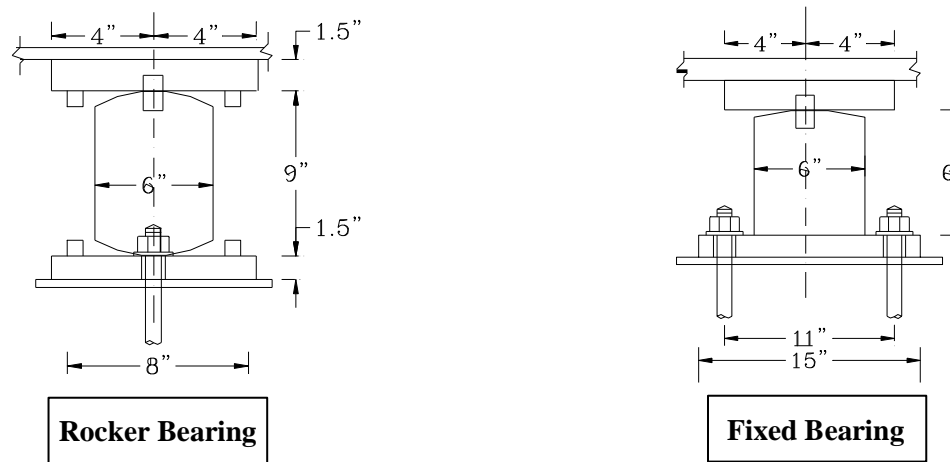


Figure 55 Illustration. Rocker and Fixed Bearings Commonly Found in Mid-America Bridges (redrawn from IL Department of Transportation Bridge Plans).

Vulnerability of Bridges

Since many of the bridges in the CSUS were designed without consideration of seismic forces, they are susceptible to significant damage and/or collapse during a moderate to strong earthquake. The vulnerability in these bridges includes inadequate reinforcement in pile caps, inadequate transverse reinforcement in columns, insufficient splice and anchorage lengths in reinforcement, and nonductile steel fixed and rocker bearings (See Figure 56 for examples). In addition, many of the bridges have very short support length, increasing their vulnerability to collapse at the intermediate piers and abutments. Finally, bridges located on liquefiable soils are susceptible to damage due to large and often times differential displacements.

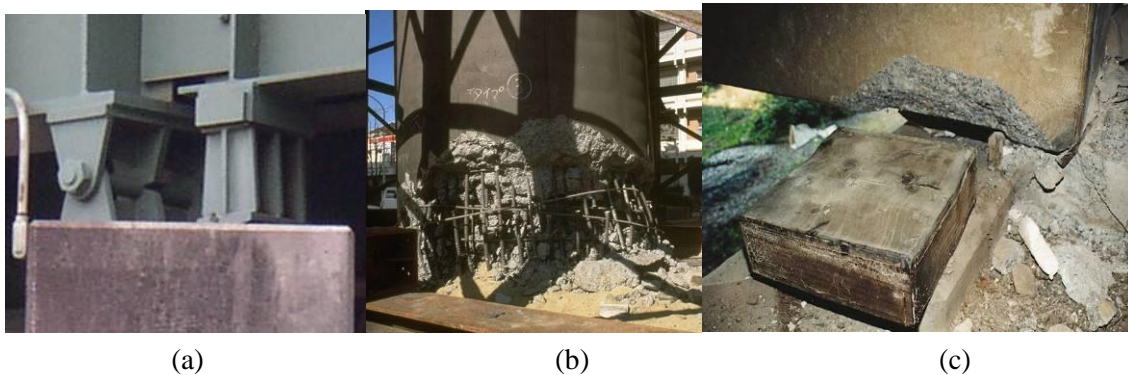


Figure 56 Photo. Typical vulnerabilities found in bridges in the Central and Southeastern US, Including (a) short support lengths, (b) inadequate transverse reinforcement, and (c) inadequate bearings.

Based on detailed analysis of the common bridge types in the Mid-America region (Figure 57), it is found that non-seismically designed columns in the Central US results in vulnerability in most bridge types (Table 13). Other common vulnerabilities include fixed and expansion bearings (in steel bridges), and transverse abutments in most multi-span bridges.

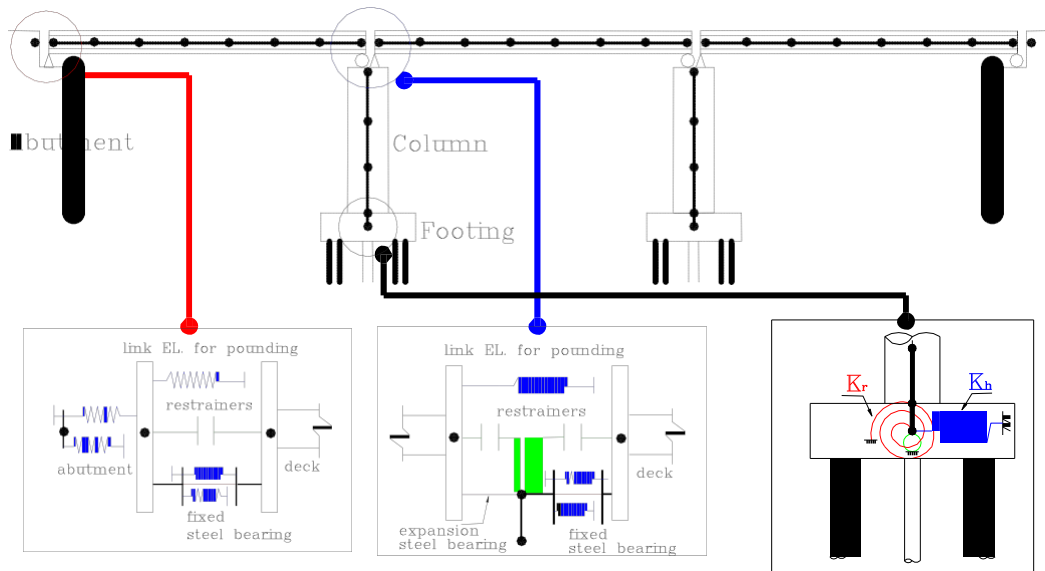


Figure 57 Illustration. Analytical Model of Bridge Used in Nonlinear Dynamic Analysis.

Table 13 Summary of Vulnerable Components for Nine Bridge Classes – Deterministic Analyses

Bridge Type	Vulnerable Bridge Components							
	Col	^a Fxd-Long	^a Fxd-Tran	^b Exp-Long	^b Exp-Tran	^c Ab-Pass	^c Ab-Act	^c Ab-Tran
MSC Concrete	X	X		X				X
MSC Slab	X						X	X
MSC Steel	X	X	X	X	X	X		X
MSSS Concrete	X	X		X			X	X
MSSS Concrete-Box	X						X	X
MSSS Slab	X						X	X
MSSS Steel	X	X	X	X	X			
SS Concrete								
SS Steel				X	X			

^aFixed Bearings

^bExpansion Bearings

^cAbutments

Past Earthquake Damage to Bridges

While most of the damage in recent earthquakes in the US have been to CA-type box-girder bridges, there have been examples of damage to steel bridges similar to those found in the CSUS in past earthquake events (Figure 58). The state of California has hundreds of steel girder bridges, several of which experienced damage during the 1994 Northridge earthquake. Typical damage included pounding damage, failure of bearings and fracture of anchor bolts, and damage to piers and abutments. A number of steel bridges were damaged in the 1995 Hyogoken-Nanbu (Kobe, Japan) earthquake. These

bridges have details and characteristics that are similar to the steel girder bridges found in North America and particularly the Central and Eastern US. Damage to non-seismically detailed reinforced concrete substructures included flexural failure of columns due to inadequate confinement and shear failures due to inadequate shear reinforcement. There was a significant amount of observed damage to steel bearings, as well as excessive deck displacements as a consequence of bearing failure and the loss of connection between the superstructure and substructure. Approximately 8 steel girder bridges were damaged in the 2001 Nisqually Earthquake in the state of Washington. These bridges were often constructed prior to 1975 and suffered bearing damage, spalling of concrete columns, and cracking at the abutments.

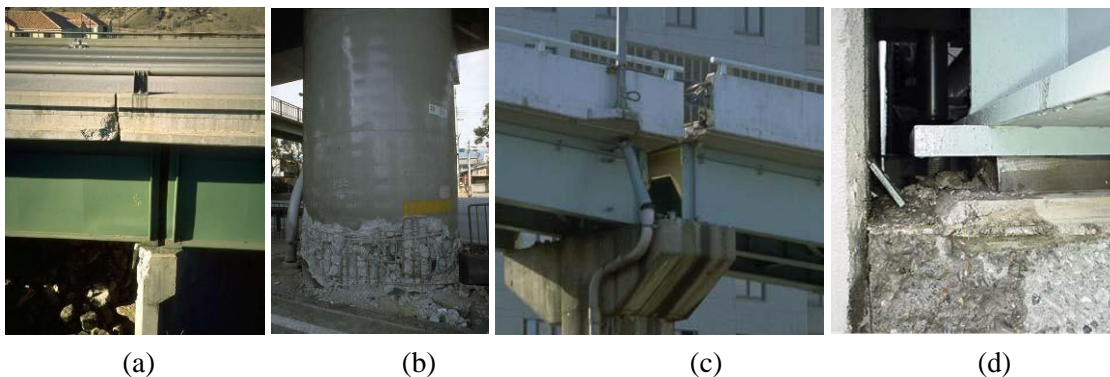


Figure 58 Photo. Damage to steel girder bridges in past earthquake events: (a) pounding damage in Northridge, (b) column damage and (c) shifted superstructure in Kobe, and (d) bearing damage in Nisqually (courtesy of WDOT).

3.3 OVERVIEW OF BRIDGE RETROFIT IN CENTRAL AND SOUTHEASTERN UNITED STATES

Bridge retrofit activities are at a more mature stage in west coast states such as California, which were primarily motivated by past earthquake events, such as the 1971 San Fernando earthquake. Awareness of the potential seismic hazard in the Central and Southeastern US has more recently increased and has precipitated seismic retrofit activities in some CSUS states. The Central US Earthquake Consortium (CUSEC) collaborated with the US Department of Transportation to prepare a monograph that helps to increase the awareness of the earthquake risk to transportation systems in the Central US⁽²¹⁾, focusing on the vulnerable regions of Arkansas, Illinois, Indiana, Kentucky, Mississippi, Missouri, and Tennessee. They discuss and encourage mitigation

efforts, including development or adoption of sufficient design criteria, and bridge retrofit programs that implement technologies that are new and innovative in the CSUS community. Additionally, the authors of this paper have conducted a review of the state-of-practice in seismic retrofit for the region.

Protection of a number of different bridge components using a range of measures have been considered or adopted in the region. A subset of retrofit measures are identified for assessment in this paper based on typical practice in the CSUS and/or having been identified as potentially viable retrofit measures for CSUS bridge types based on past studies^(22, 23, 24, 25, 26). Characteristic CSUS bridge deficiencies have been recognized as inadequately detailed columns with limited ductility capacity and low shear strength, brittle steel bearings, short seat widths, and inadequately reinforced pile caps among others⁽²⁷⁾. As such, general column retrofits often include some type of encasement to improve the shear or flexural strength, flexural confinement and ductility capacity, or lap splice performance. Steel jackets, such as those shown in Figure 59(a) from Tennessee are a common measure which will be included in this study. Isolation is another potential approach to limit the forces transferred to the substructure and replace existing seismically vulnerable bearings. Figure 59(b) shows an application of elastomeric isolation bearings in Illinois. Avoiding unseating and collapse of bridge spans is a primary concern for most CSUS states, who seek to promote life safety and avoid complete bridge damage. The use of restrainer cables (Figure 59(c) in Kentucky) and seat extenders (Figure 59(d)) are both common retrofit measures across several states in the CSUS. Some retrofit measures which specifically target lateral restraint or limit excessive transverse motion have been used. Typically these take the form of concrete shear keys (Figure 59(e)), though steel keeper brackets or transverse bumpers are also used. The five retrofit measures identified above will be evaluated as a part of this work and cover a range of common bridge retrofits. It is noted that this list is not fully comprehensive, as other measures such as shock transmission units, FRP column wraps, other types of isolation bearings, etc. have already been used in practice in the CSUS and may be considered in future projects.

Little technical support has been offered to date for evaluating the impact of the various retrofit measures on the seismic performance of bridges in the CSUS region or selecting measures appropriate for these bridges. There is a strong need for a comparative assessment of the viability of various retrofit strategies for typical CSUS bridges. In addition to posing a discussion of the array of different retrofit options that are available

for bridges, the recent edition of the *Seismic Retrofitting Manual for Highway Bridges*⁽²⁸⁾ has noted the potential application of fragility curves for assessing bridge vulnerability, prioritizing bridges for retrofit, and performing seismic risk assessments. Building on this philosophy, fragility curves for retrofitted CSUS bridge classes also offer an approach for selecting appropriate measures for further detailed assessment. One advantage of this approach is the ability to capture the impact of retrofit on the bridge system vulnerability. Most of the retrofit measures noted above tend to target a particular response quantity, such as the restrainers which aim to reduce deck displacements and bearing deformations. However, there may be inadvertent affects on other components such as the columns or abutments. This is a particularly important consideration in the CSUS because of the number of different deficiencies that may be present in a single non-seismically designed bridge class, or may be impacted by the common retrofit measures in either a positive or negative fashion. For more details on retrofits, see Appendices.

Examples of the current state of practice in seismic retrofit of bridges in the Central and Southeastern US is presented below. This includes protection of a number of different bridge components using a range of retrofit measures and approaches, including:

1. Colum Retrofits
2. Isolation
3. Restrainers
4. Other Longitudinal Restraint and Response Modification
5. Shear Keys
6. Seat Extenders and Catcher Blocks
7. Bent Retrofits

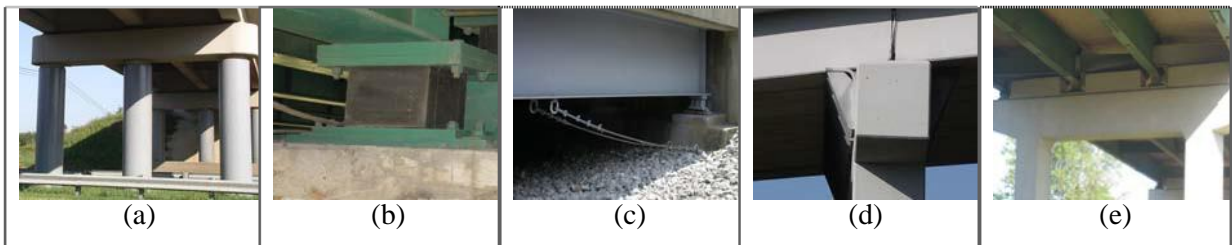


Figure 59 Photo. CSUS bridge retrofits: (a) steel jackets in TN, (b) elastomeric isolation bearings in IL, (c) restrainer cables in KY, (d) seat extenders and (e) shear keys in TN.

3.3.1 COLUMN RETROFIT

Background

CSUS columns have been found to be particularly vulnerable due to insufficient lap splices and inadequate transverse reinforcement, leading to limited ductility capacity and low shear strength. Figure 60 illustrates the effect of confinement on concrete, indicating the negative impact of having limited transverse reinforcement in columns and motivating the use of column confinement through jacketing or other measures.

Confinement results in an increase in compressive strength and ultimate strain capacity in the concrete. Steel jacketing has been used as a retrofit measure to enhance the flexural ductility, shear strength, or performance of lap splices in reinforced concrete bridge columns. Extensive proof-of-concept testing of steel jacketed bridge columns was performed in the early 1990s (see Figure 61), and several hundred bridges in the US had been retrofit with this technology by the mid 1990s. A review of the state-of-practice in the CSUS has revealed that this is the most common column retrofit in the CSUS, as well. Figure 62 details a typical cross section of a circular column retrofit by a steel jacket, and the full height configuration which is assumed for this study. The steel jackets are typically A36 steel casings and a space of about 2 inches is provided at the ends of the column to prevent the jacket from bearing on adjacent members. This serves to avoid undesirable flexural strength enhancement in which larger shears and moments may be transferred to the footings and cap beams under seismic loading⁽²⁹⁾. The minimum recommended shell thickness for steel jackets is 0.40 inches for handling of the shells during construction, and is often found to be sufficient to provide for needed confinement of lap splices and enhanced flexural confinement of typical CSUS highway overpass bridges. While the effect is not intended, experimental testing by Chai et al. has revealed that the steel jacket increases column stiffness by approximately 10 to 15% for partial height⁽²²⁾ and 20 to 40% for full height jackets⁽²⁹⁾. While steel jacketing is one of the most common column retrofit used in the CSUS, examples of other measures of encasement or column enhancement are also discussed below.

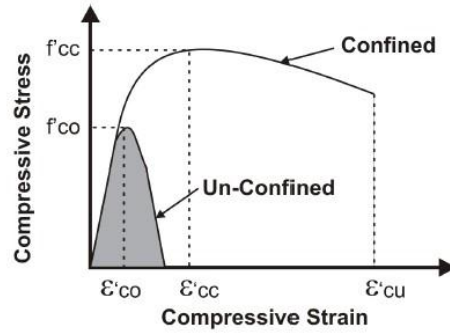


Figure 60 Graph. Effect of confinement on concrete.

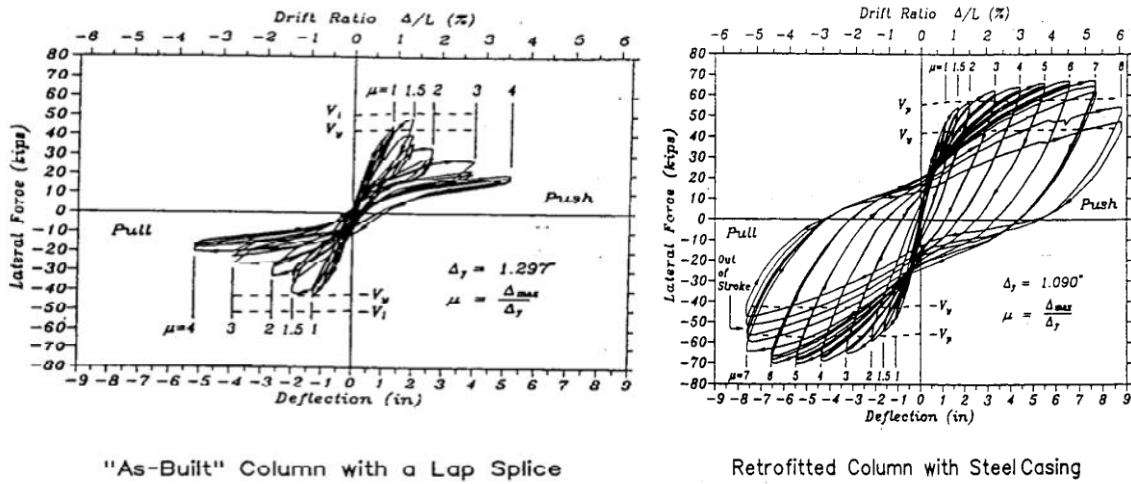


Figure 61 Graph. Force deformation of column without and with steel jacket⁽²⁹⁾.

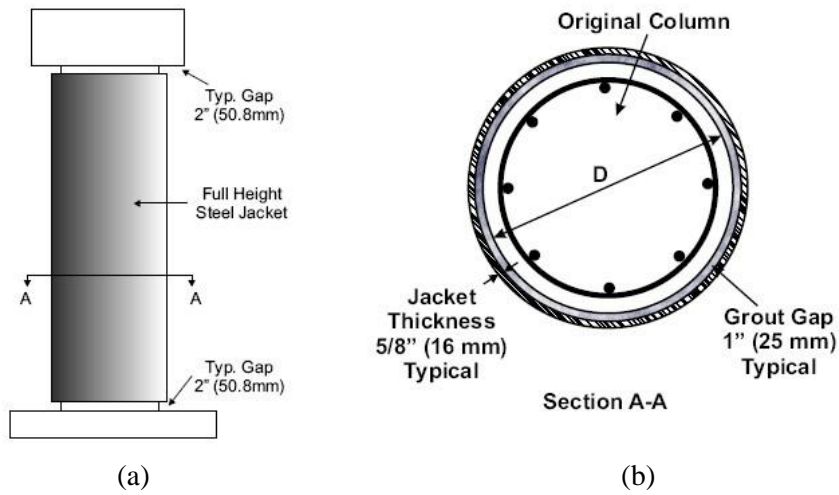


Figure 62 Illustration. Typical steel jacket retrofit details: (a) full height, (b) typical section.

Examples of Column Retrofits

States in the CSUS region have used a number of different approaches to target the improved performance of non-seismically detailed columns. A vast majority of the columns in typical CSUS bridges are concrete columns, for which a variety of retrofit measures have been proposed. While full column replacement is sometimes an option, states often adopt less costly and less invasive alternatives. The general retrofit strategy for these columns often includes some sort of encasement in order to improve the shear or flexural strength, flexural confinement and ductility capacity, or lap splice performance.

Steel jackets are a common approach to retrofitting deficient columns in the CSUS. Partial column casings often target the plastic hinge regions by providing enhanced confinement for increased ductility capacity, or target locations of the lap splices for improved bond transfer. Full height jackets also improve the shear strength of the column. Examples of a partial height steel jacket in St. Louis, MO and full height column retrofit in Tennessee are shown in Figure 63. Over a dozen bridges in Tennessee have been retrofit with these jackets.

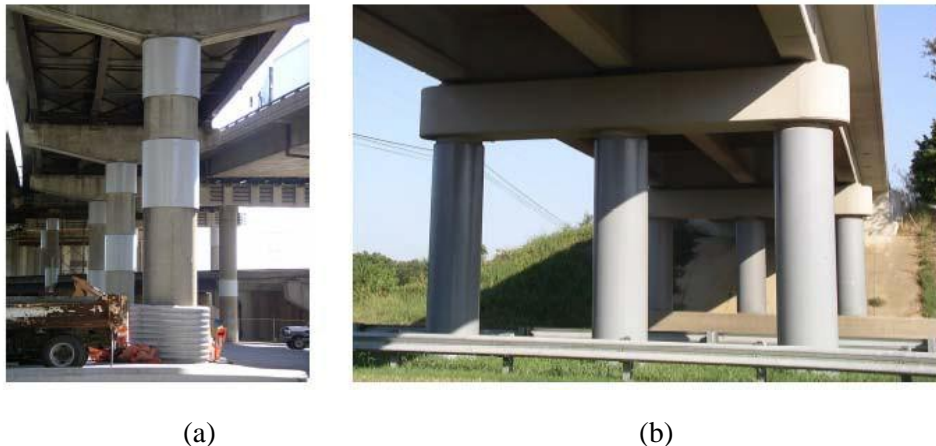


Figure 63 Photo. Examples of (a) partial height steel jackets in MO and (b) full height steel jackets in TN.

Concrete overlays are often used to provide confinement for enhanced ductility capacity, and less often as measures to increase a column's flexural strength since this is not often required or desired. Both longitudinal and transverse reinforcement may be provided in these casings, and in some instances the concrete overlay is used in conjunction with a steel jacket retrofit. The construction of a concrete encasement in Memphis, TN is shown in Figure 64(a) and a completed partial height encasement in Illinois is shown in Figure 64(b). Other column retrofit measures which have been performed in some states but are less common on average include cable column wraps (or external prestressing), and jacketing by fiber composite wraps, which may be continuous or applied in strips. Examples of these column retrofits performed by the Illinois DOT are shown in Figure 65. Figure 66 shows sample details of cable column wraps on the Poplar Street Complex in IL, while Figure 67 shows the cross section of a typical partial steel jacket in MO. The main objective in most cases is to provide confinement for the concrete columns.



Figure 64 Photo. Concrete column overlay (a) during construction in TN and (b) as a partial encasement in IL.



(a)



(b)

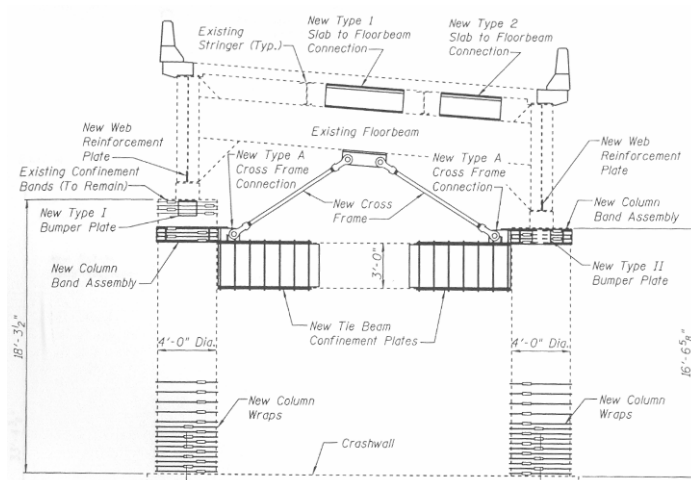


(c)

Figure 65 Photo. Other column retrofits with (a) cable wraps or (b and c) fiber composites performed in IL.



(a) Column cable wraps among other retrofits (Poplar Street Complex - IL)

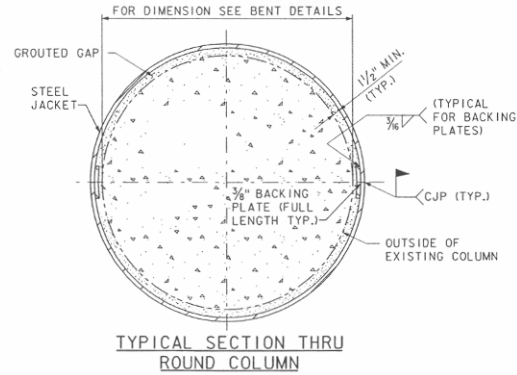


(b) Details of column cable wraps, bent cap retrofits, restrainer bars (Rte 70 Poplar Street – IL)

Figure 66 Photo. Column cable wraps, bent cap retrofits, restrainer bars (Poplar Street Complex - IL)



(a) Partial steel jackets (Poplar Street Complex – MO)



(b) Steel jacket details (US40 Poplar Street – MO)

Figure 67 Photo. Steel jacket details (US40 Poplar Street – MO)

3.3.2 ISOLATION

Background

Elastomeric bearings (or laminated-rubber bearings) are a form of isolation bearings that have been used in bridge and building construction for over 35 years⁽³⁰⁾, and have been used in some CSUS retrofit projects. The general concept of isolation is to shift the natural period of the structure out of the region of dominant earthquake energy, to increase the damping, and to limit the forces transferred from the superstructure to the substructure⁽³¹⁾. It is often adopted as a retrofit scheme because isolation systems tend to reduce the need for costly retrofit of deficient pier and foundation elements. Koh and Kelly⁽³²⁾ have identified elastomeric bearings as the simplest method of isolation, making them prime candidates for retrofit of typical CSUS bridges. Elastomeric bearings are composed of horizontal layers of elastomer separated and reinforced by thin layers of steel (steel shims) as shown in Figure 68. These types of isolation bearings are commonly found in the CSUS, along with a similar elastomeric bearing having a lead core often referred to as a lead rubber bearing (LRB).

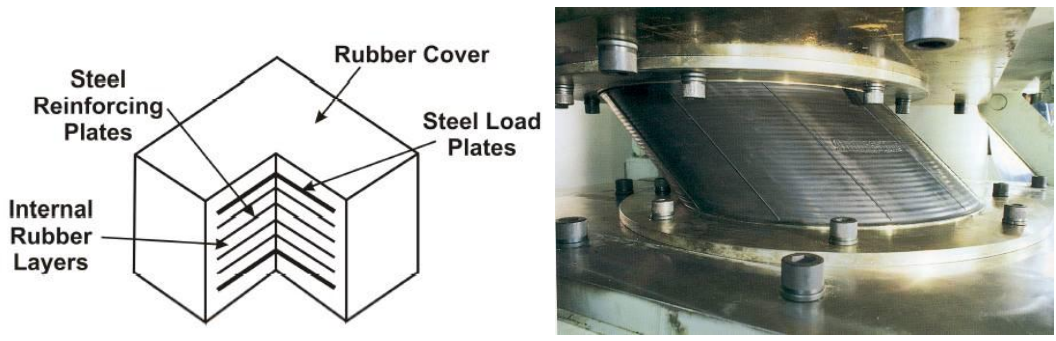


Figure 68 Photo. (left) Typical elastomeric bearing adapted from Priestley et al.⁽²⁹⁾, (right) deformed bearing during experimental test.

The period shift in structures base isolated structures results in a significant reduction in forces transferred to vulnerable substructure components of a bridge. However, the period lengthening is also typically coupled with increases in displacements, as shown in Figure 69. These displacements can be reduced by the use of damping systems, either built into the isolator (i.e. lead-rubber bearings), or in parallel with the isolators.

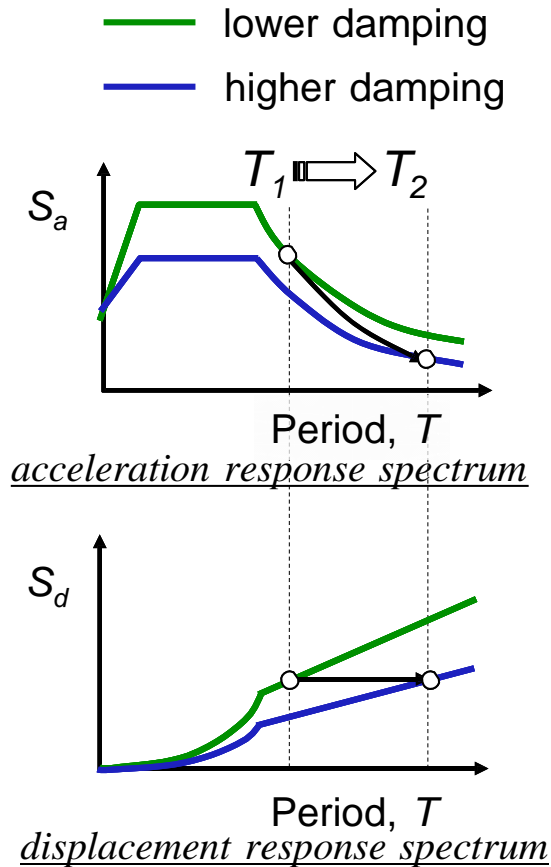


Figure 69 Graph. Acceleration and displacement response spectrum showing the shift in periods with isolation systems.

Examples of Isolation

Isolation strategies are adopted to limit the forces transferred to deficient substructure elements and as a means to replace existing bearings. While the replacement of existing vulnerable bearings, such as those shown in Figure 70, with isolation bearings is slightly more intrusive than other measures, several states have employed this retrofit approach. States in the Central and Southeastern US have performed retrofit with a relatively limited number of bearing types. Laminated elastomeric bearings have been used in several states, as shown in Figure 71. Others have used energy dissipating sliding or friction pendulum bearings, as shown in Figure 72. Figure 73 shows an illustration of elastomeric bearings with keeper plates and dampers.

Previous research has shown that elastomeric bearings can have a significant increase in stiffness when subjected to cold temperatures. This should be considered when using these systems in areas of extreme cold temperature.



(a)



(b)

Figure 70 Photo. Potentially vulnerable existing steel (a) fixed and (b) rocker bearings.



(a)



(b)

Figure 71 Photo. Elastomeric bearing isolation systems found in the CSUS.



(a)



(b)

Figure 72 Photo. Sliding isolation systems used in the Central and Southeastern US.



(a)



(b)

Figure 73 Photo. (a) Elastomeric bearings with keeper plates, and (b) Bearings with dampers.

3.3.3 LONGITUDINAL RESTRAINER BARS AND CABLES

Background

Restrainer cables are one potential device for unseating prevention, which serves to limit relative hinge displacement and prevent collapse of bridge spans. They are often employed in bridges with insufficient support lengths (such as those in the CSUS) at the intermediate columns or abutments. In general, restrainer cables are either directly connected between adjacent girders, or can be connected to or through the bent cap, as shown in Figure 74. The use of restrainer cable retrofits has been a common approach on the West Coast since the 1970s following the 1971 San Fernando earthquake, and has been found to be a relatively simple and inexpensive retrofit measure to reduce the vulnerability to unseating⁽²⁹⁾. Experience from previously installed retrofits in the Los Angeles area has shown that despite some pull-through failure, most restrainer cables performed adequately in the 1994 Northridge earthquake^(33,34), as did most of those in the Oakland area in the 1989 Loma Prieta earthquake⁽³⁵⁾.

Restrainer cables are often designed as 0.75 inch diameter cables with an effective area of 0.22 sq. inches, and a length between 5 ft. and 10 ft. Due to ambient temperature conditions, the slack may also vary between 0 and 0.75 inches, which could significantly effect the response of the bridge⁽³⁶⁾. Testing by the California Department of Transportation⁽³⁷⁾ has revealed that the elastic modulus of these high strength steel cables is $E=10,000$ ksi and that the yield force is approximately $F_y=39$ kips, corresponding to a stress of 176 ksi. Figure 75 shows the test data for a typical 3/4" restrainer cable and a 1 1/4" restrainer bar.

Over 200 bridges have been retrofit with steel restrainer cables in the state of Tennessee alone, and a number of similar retrofit projects have been performed in other Central and Southeastern US states.

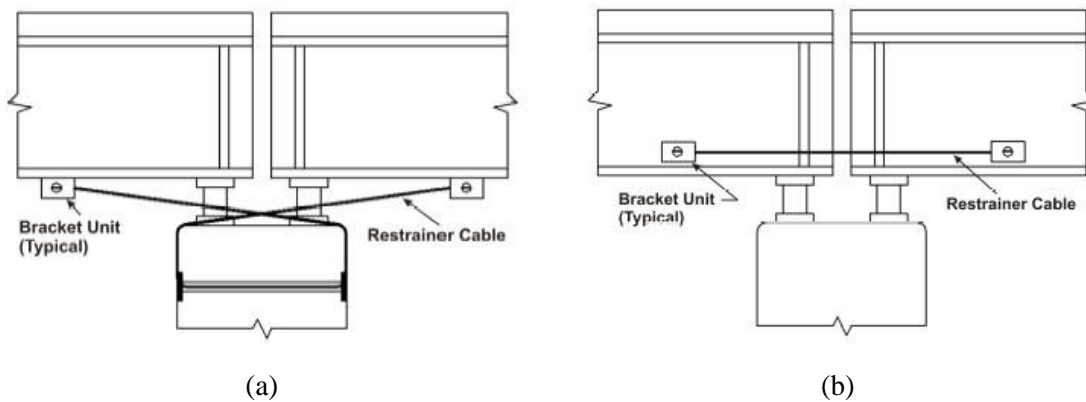


Figure 74 Illustration. Examples of restrainer connection details (a) (via the bent cap), or (b) from girder to girder.

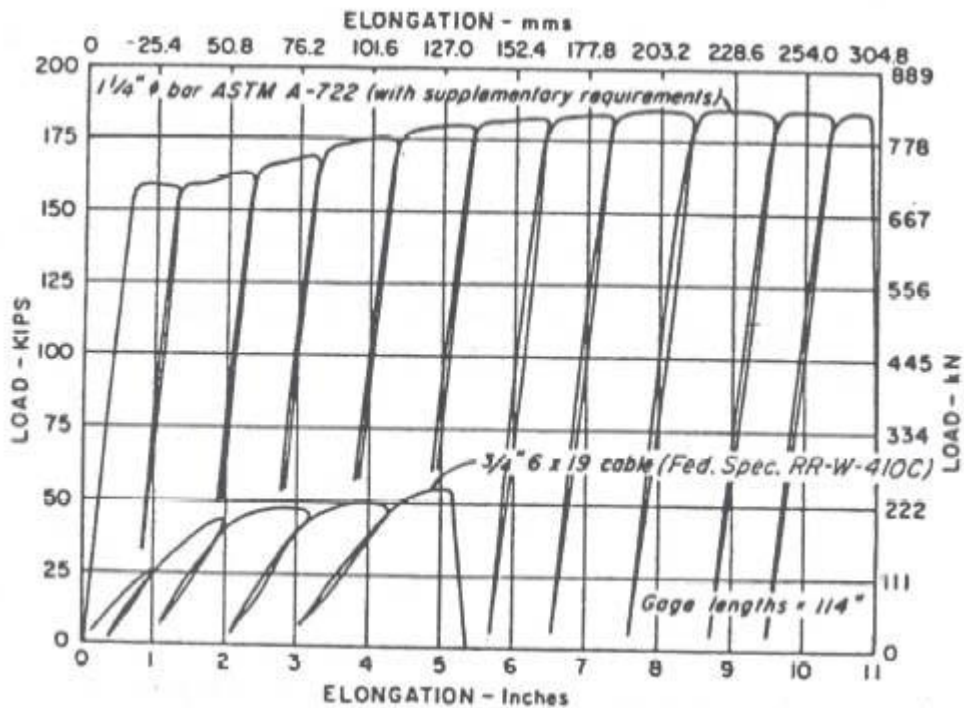


Figure 75 Graph. Load-deformation from Caltrans restrainer cable testing⁽³⁷⁾.

Examples of Longitudinal Restrainers

Longitudinal restrainers are often implemented at the expansion joints between adjacent decks or at the deck-abutment interface to limit deck displacement and reduce the potential for span unseating. In the CSUS, these restrainers often take the form of cable restrainers or bar restrainers. For simply supported bridges, as are typical in the CSUS,

cables may be anchored to the girder and then directly connected to the abutment or bent, as shown in Figure 76. An alternate configuration would be for the cables to be mounted directly between adjacent girders as shown in Figure 77, however this has been recognized as a less appropriate method for bridges with short seat widths⁽³⁸⁾. Restrainer cables can also be wrapped around the bent cap and anchored to the bottom flange of the support girder, as shown in Figure 78.



Figure 76 Photo. Common CSUS restrainer cable retrofit details as performed in TN.



Figure 77 Photo. Examples of restrainer cables connected between adjacent girders.



Figure 78 Photo. Example of restrainer cables wrapped around bent cap.

Another type of restrainer is high strength bar restrainers, which are often stiffer yet more ductile than the cable restrainers, as was shown in Figure 75 above. These have been used less frequently in the CSUS yet examples exist in different arrangements in Illinois and Missouri. Figure 79(a) shows an example of inclined restrainer bars connected from the girder flange to the column, while Figure 79(b) shows an example of restrainer bars connected directly from girder to girder. Figure 80 the details of the connection of restrainer bars for the interior girders. Finally, Figure 81 shows the application of restrainer bars where the bars act in both the longitudinal and transverse direction.

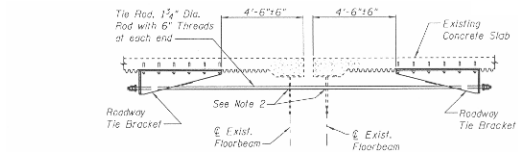


(a)

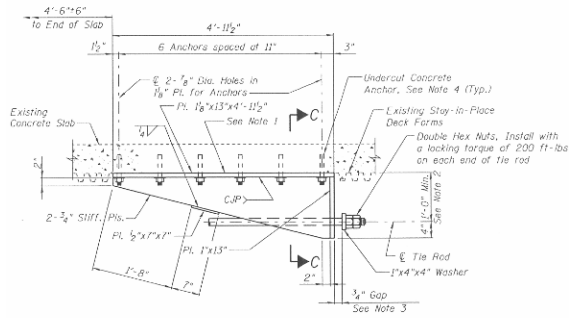


(b)

Figure 79 Photo. Example of high strength bar restrainers in the Central and Southeastern US.



ELEVATION - ROADWAY TIE



ROADWAY TIE BRACKET DETAIL



Figure 80 Photo. Connection details for high strength restrainer bars.

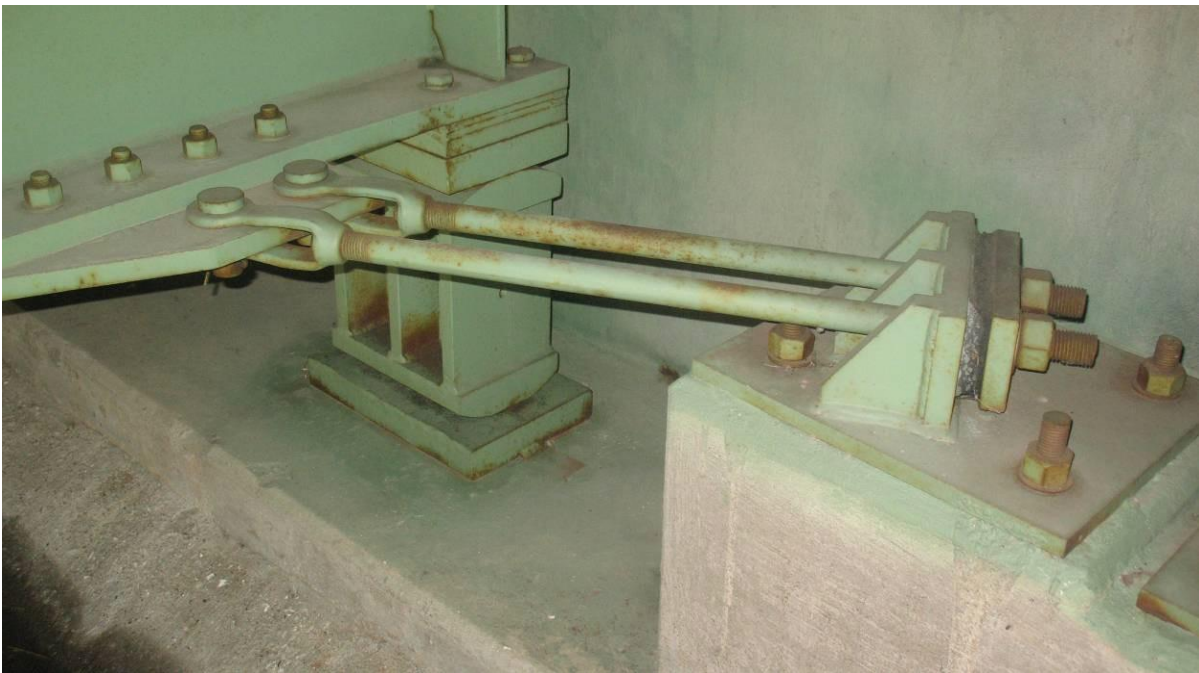


Figure 81 Photo. Connection details for high strength restrainer bars used to restrain motion in the longitudinal and transverse directions.

3.3.4 OTHER LONGITUDINAL RESTRAINT AND RESPONSE MODIFICATION DEVICES

Background

Other devices that modify the longitudinal response of bridges have been employed in bridge retrofit, often to either prevent excessive movement of the superstructure or to provide energy dissipation. A relatively simple alternative method to restrainer cables is the use of stoppers, or bumper blocks. Bumpers may be used in conjunction with restrainer bars or used alone. The bumpers serve a similar role as restrainer cables with the goal of limiting longitudinal motion of the superstructure.

Shock transmission units (STUs) have also been used to modify the longitudinal response. These devices allow for slow motion, such as thermal movements, yet rigidly restrict rapid motion, such as that induced by earthquake loading. These retrofits all serve as displacement limitation devices and provide load transfer at the location of implementation.

Examples of Other Longitudinal Restraint and Response Modification Devices

Figure 82 shows the application of bumper elements in multi-span bridges in the Central and Southeastern US. The bumper elements, constructed of structural steel beams, are typically placed on both sides of the bent cap with a gap typically ranging from 2-6 inches.



Figure 82 Photo. Retrofits performed using bumper elements.

Figure 83 shows the application of shock transmission units in a bridge in St. Louis, MO. These units form a longitudinal lock (or restraint) in the event of a sudden large motion.



Figure 83 Photo. Application of shock transmission units at the intermediate span of a bridge.

3.3.5 SHEAR KEYS

Background

Many of the retrofit measures indicated above primarily impact the response and vulnerability of a bridge in the longitudinal direction. However, typical CSUS bridges may also suffer damage due to excessive motion or demands in the transverse direction. As such, the use of shear key retrofits have been identified as being present in a number of CSUS bridges. The shear keys serve to restrain the deck motion when a bridge is excited in the transverse direction and facilitate shear force transfer to the substructure. These devices are often concrete blocks provided at each bearing location. An initial gap is often provided before the shear key engages in the transverse direction which may be on the order of ½ inch. Care must be taken when designing the shear keys to limit the forces transferred to the substructure. Oftentimes, the shear strength of the shear keys is limited to a fraction of the shear strength of the columns and the blocks are checked to ensure shear, rather than flexural, governs failure. Other forms of transverse shear keys include keeper brackets and transverse bumpers of various details shown below.

Examples of Shear Keys

Transverse restraint of the superstructure is often provided to keep the superstructure from sliding off its supports should the bearings fail in the transverse direction, and is recommended for common CSUS conditions such as when high steel rocker bearings are used, or limited transverse seat is available⁽²⁸⁾. Shear keys often take the form of reinforced concrete blocks doweled into the bent beam, which have been used in TN and MO among other states (Figure 84(a)). In some cases they are added as keeper brackets to the bearing assembly, as shown in Figure 84(b), and less often as transverse steel bumper assemblies. Figure 85 shows examples of concrete shear keys, including details for a sample shear key retrofit in TN (Figure 86). Additional examples of steel shear keys and keeper plates used in MO and TN, respectively, are shown in Figure 87.



Figure 84 Photo. Transverse restraint provided by (a) concrete shear keys and (b) keeper brackets.



Figure 85 Photo. Concrete block transverse shear keys in (a) Indiana (SR51 over White River/Carl Grey Memorial Bridge – IN) and (b) Missouri (Poplar Street Complex – MO).

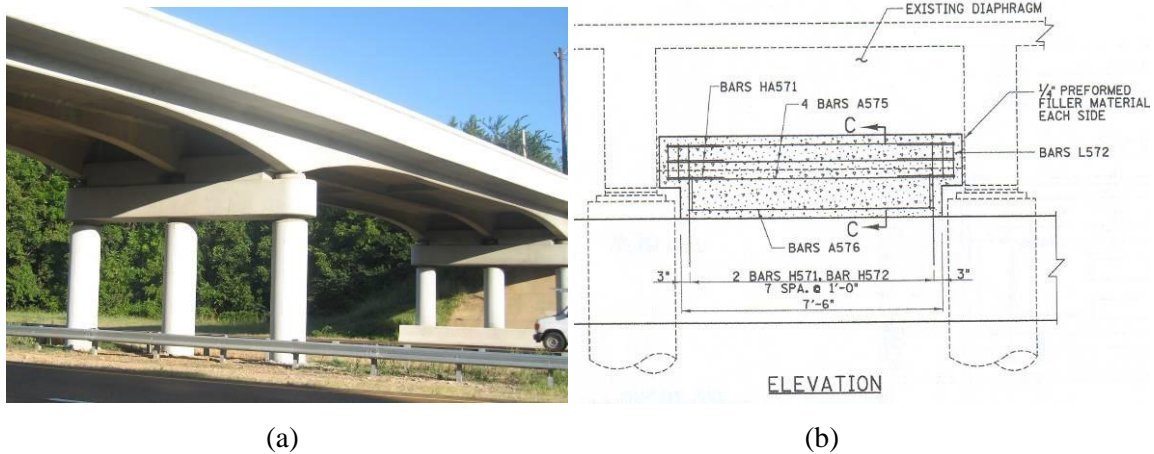


Figure 86 Photo. (a) Concrete shear keys among other retrofits (Davies Plantation Road – TN) and (b) elevation view of shear key details.

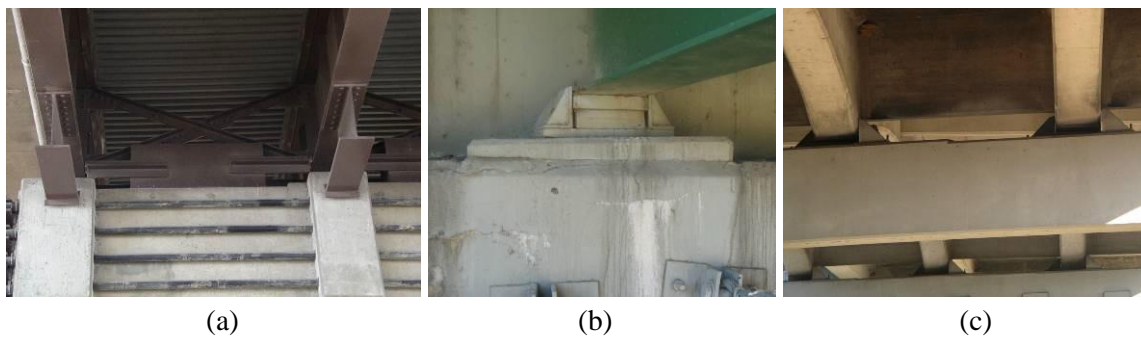


Figure 87 Photo. (a) Steel transverse shear keys along with bent cap retrofit in MO (Poplar Street Complex – MO), and keeper bracket retrofits in TN (b) (SR59 – TN) and (c) (Chambers Chapel Road over I40 – TN)

3.3.6 SEAT EXTENDERS AND CATCHER BLOCKS

Background

Seat extenders are an alternate method of preventing unseating of spans by providing an extended effective seat length, and have been found to be fairly common retrofits in the CSUS. Hipley⁽³⁹⁾ has deemed them the simplest and least expensive means of preventing unseating and allowing the superstructure to float over the substructure. As a retrofit measure, seat extenders serve primarily to increase the capacity of the bridge to sustain longitudinal displacement without collapse due to unseating. Rather than alter the response of the bridge in the longitudinal direction, they serve as a failsafe to deck collapse by providing an extended support length. They do not protect other bridge components from damage. Most commonly, the seat length for a simply supported

bridge may be extended at the abutment or bent through the addition of a concrete corbel or steel bracket as illustrated in Figure 88. However, other configurations have also been observed in the Central US. Catcher blocks are a very similar retrofit measure. However, rather than extending the seat length, catcher blocks may be provided to catch the girder should high-type bearings become unstable.

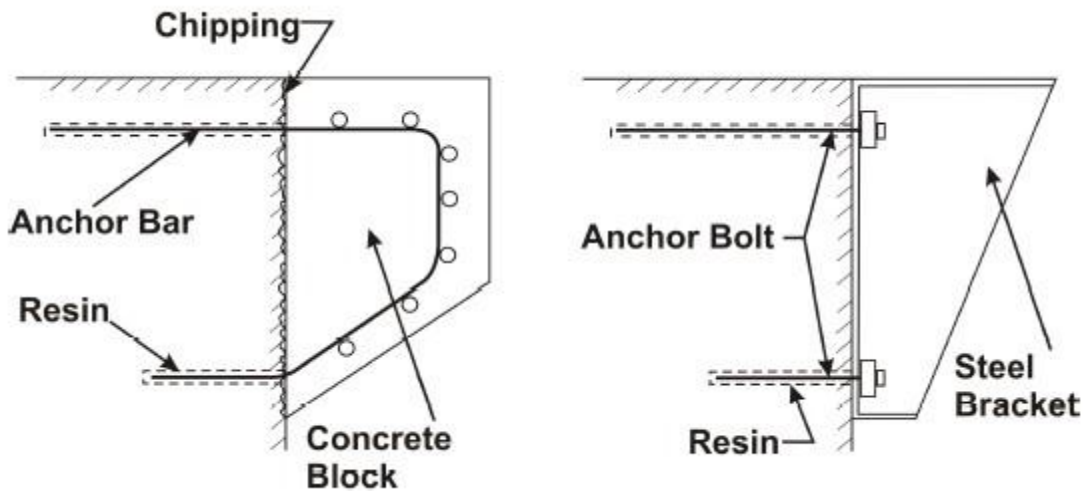


Figure 88 Illustration. Corbel and bracket seat extender details.

Examples of Seat Extenders and Catcher Blocks

Since many of the bridges in the CSUS have relatively short seat widths and unseating is a concern, the use of seat extenders is a popular retrofit measure. Tennessee has performed a number of retrofits with seat extenders in bridges crossing I-40, as shown in Figure 89(a). Typical details for the steel bracket type seat extenders are shown in Figure 90. Figure 89(b) and Figure 91 show less conventional seat extender details used on US40 in Missouri. Catcher blocks perform a similar function of supporting the span given it has fallen off of its bearing or the bearing has failed, and have also been used in MO. However, catcher blocks are elevated to a height just under the girders and are often used either when the deck is supported by tall bearings, and/or there is not sufficient room to anchor seat extenders as in Figure 89(c).



(a)

(b)

(c)

Figure 89 Photo. (a) Traditional seat extender retrofit in TN (RT A026 over I40 – TN), (b) beam extender in MO, and (c) catcher block (Poplar Street Complex – MO).

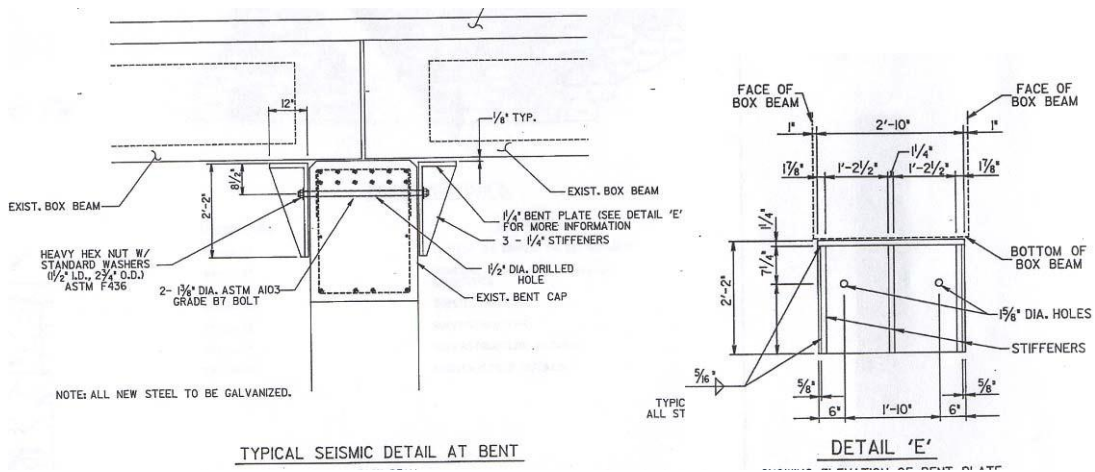


Figure 90 Photo. Detail of steel bracket type seat extenders like those shown in Figure 89(a) (Rte A026 – TN).



Figure 91 Photo. Steel seat extenders (Poplar Street Complex – MO).

3.3.7 BENT CAP RETROFIT

Background

Bent caps which serve to transfer loading from the bearings to the columns may be deficiently reinforced for either shear or flexural loading. The general approach to bent cap retrofit is to enhance the shear or flexural strength to sufficient levels such that the columns form plastic hinges before damage occurs in the bent beam⁽²⁹⁾. The most common measures for retrofitting the bent caps include providing pre-stressing of the beam through external tendons, providing external shear reinforcement, adding reinforced concrete bolsters to the existing cap beam face to increase the level of shear and flexural reinforcement, or completely encasing and reinforcing the beam.

Examples of Bent Cap Retrofits

Figure 92 below shows an example of a bent cap retrofit using post tensioning rods placed around the outsides of the bent cap. The post tensioning essentially enhances the strength of the bent cap by providing an axial compression force on the beam. Figure 93 shows another retrofit approach, which uses external shear reinforcement via steel plates connected by steel rods at the ends of the bent caps. Figure 94 illustrates an example of bent cap retrofit by adding reinforced concrete bolsters to the existing cap beam face to increase the level of shear and flexural reinforcement, while Figure 95 shows an example of completely encasing and reinforcing the beam.



Figure 92 Photo. Bent cap retrofit using post tensioning rods.



Figure 93 Photo. Bent cap retrofit focused on shear reinforcement and confinement of the bent cap end regions.



Figure 94 Photo. Bent cap retrofits with reinforced concrete encasement.



Figure 95 Photo. Bent cap retrofits with reinforced steel encasement

3.4 EFFECT OF SEISMIC RETROFIT BRIDGE PERFORMANCE

The component responses that are evaluated as a part of the deterministic performance analysis are presented in Table 14, along with their abbreviations. The results of the deterministic seismic performance evaluation for the MSSS Steel, MSC Steel, MSSS

Concrete, and MSC Concrete are summarized in Table 14 to Table 17, respectively. These tables indicate the initial level of component response from time history analysis using the suite of Wen and Wu ground motions for the as-built bridge of each type. The impact of the different retrofit measures on the component response is identified based on whether the response was increased, decreased, or if the retrofit had a negligible effect. These summaries are anticipated to provide insight on the impact of different retrofit measures on the seismic response of each bridge type and their component response levels. It is noted, however, that these results are for a specific uniform hazard level (2% in 50 years) using ground motions developed for Memphis, TN.

The MSSS Steel girder bridge tends to have relatively high demands placed on the fixed and expansion bearings in the longitudinal direction and column demands indicative of potential damage. Since the typical MSSS Steel girder bridge exhibits predominant response and vulnerability in the longitudinal direction, the shear keys have little impact. The steel jackets provide ample capacity improvement in the columns and significantly reduce the likelihood for column damage in the MSSS Steel girder bridge, yet do not impact the response of other vulnerable components, such as the bearings. The restrainer cables reduce the rocker bearing deformations yet have little effect on the fixed bearings because of the initial slack in the cables. The column demands are slightly reduced by use of the cables yet increase the active deformation of the abutments. The elastomeric bearings are highly effective in reducing potential component damage, and offer a potentially viable retrofit option. They considerably reduce the column demands by isolating the superstructure, and diminish the likelihood for bearing damage by replacing the vulnerable steel bearings with flexible isolation bearings. However, there are issues with increased pounding at the abutments.

The MSC Concrete girder bridge is heavier than the steel bridge and has relatively large deck displacements, bearing, and column demands. It is noted, however, that the bearings used in this bridge are more flexible than the steel bearings and can sustain larger deformations before damage is expected to occur. The mean peak expansion bearing deformations are reduced by roughly 20% with the restrainer cables and fixed bearings by only about 10%, because of the large inertial deck loads that tend to yield the restrainer cables and limit their effectiveness. The fairly high transverse bearing deformations are considerably reduced by use of the shear keys, yet this retrofit leads to an increase in abutment deformations in the transverse direction. It is interesting to note that the use of steel jackets in the MSC Concrete bridge slightly increases the transverse

bearing deformations, which is attributed to the redistribution of forces due to slight stiffening of the columns from jacketing. Isolation of the superstructure by use of the elastomeric isolation bearings reduces the active deformations of the abutments considerably, and the demands placed on the columns (particularly in the longitudinal direction), yet still leads to an increase in the passive and transverse abutment deformations.

Table 14 MSSS Steel Retrofit Impact Summary

Component	Response Level	Impact of Retrofit on Response			
	As-Built	Restrainer Cable	Elastomeric Bearing	Steel Jacket	Shear Key
Exp-Long	High	-	N/A	=	=
Exp-Tran	Low	=	N/A	=	=
Fb-Long	High	=	N/A	=	=
Fb-Tran	Medium	=	N/A	=	=
Col-Ductility-Long	Medium	-	-	=	=
Col-Ductility-Tran	Medium	=	=	=	=
Ab-Act	Low	+	-	=	=
Ab-Pass	Low	=	+	=	=
Ab-Tran	Low	=	+	=	=

* Increased (+), Reduced (-), Negligible impact (=)

Table 15 MSC Steel Retrofit Impact Summary

Component	Response Level	Impact of Retrofit on Response			
	As-Built	Restrainer Cable	Elastomeric Bearing	Steel Jacket	Shear Key
Exp-Long	High	-	N/A	=	=
Exp-Tran	High	=	N/A	=	-
Fb-Long	Low	=	N/A	=	=
Fb-Tran	Medium	=	N/A	=	-
Col-Ductility-Long	High	-	-	=	=
Col-Ductility-Tran	Medium	=	-	-	=
Ab-Act	Low	+	=	=	=
Ab-Pass	Medium	=	+	=	=
Ab-Tran	Low	=	+	=	+

* Increased (+), Reduced (-), Negligible impact (=)

Table 16MSSS Concrete Retrofit Impact Summary

Component	Response Level	Impact of Retrofit on Response			
	As-Built	Restrainer Cable	Elastomeric Bearing	Steel Jacket	Shear Key
Exp-Long	Medium	-	N/A	=	=
Exp-Tran	High	=	N/A	+	-
Fb-Long	Medium	=	N/A	=	=
Fb-Tran	High	=	N/A	=	-
Col-Ductility-Long	Medium	+	-	-	=
Col-Ductility-Tran	Low	=	+	-	+
Ab-Act	Low	=	-	=	=
Ab-Pass	Low	=	+	=	=
Ab-Tran	Low	=	+	=	=

* Increased (+), Reduced (-), Negligible impact (=)

Table 17 MSC Concrete Retrofit Impact Summary

Component	Response Level		Impact of Retrofit on Response			
	As-Built		Restrainer Cable	Elastomeric Bearing	Steel Jacket	Shear Key
Exp-Long	Medium		-	N/A	=	=
Exp-Tran	Medium		=	N/A	+	-
Fb-Long	Medium		=	N/A	=	=
Fb-Tran	Medium		=	N/A	+	-
Col-Ductility-Long	Medium		=	-	=	=
Col-Ductility-Tran	Medium		=	-	=	-
Ab-Act	Low		=	-	=	=
Ab-Pass	Low		-	+	=	=
Ab-Tran	Low		=	+	=	+

* Increased (+), Reduced (-), Negligible impact (=)

3.5 STATE-OF-THE-ART IN BRIDGE FRAGILITY

The focus of this paper is on comparing the conclusions that may be derived from evaluating the fragility curves for different bridge classes, and investigating the sources of ideal retrofit selection. Therefore only a brief overview of the fragility methodology itself is provided herein. Further details on the analytical methodology may be found elsewhere⁽⁴⁰⁾.

The general form of a seismic fragility may simply be expressed as the conditional probability shown in Figure 96:

$$Pr_{failure} = P[D > C | IM]$$

Figure 96 Equation. Probability Pr subscript failure

where D is the seismic demand placed on the structural component, C is the capacity or limit state of the component, and IM is the intensity measure of the ground motion. When the demand and capacity are both assumed to follow a lognormal distribution, a closed form solution for the fragility may be presented as (Figure 97):

$$P[D > C | IM] = \Phi \left[\frac{\ln \left(\frac{S_d}{S_c} \right)}{\sqrt{\beta_{d|IM}^2 + \beta_c^2}} \right]$$

Figure 97 Equation. Conditional probability P, bracket, “D greater than C” under the condition of IM, close bracket.

where $\Phi[\bullet]$ is the standard normal cumulative distribution function, S_c is the median value of the structural capacity (or the limit state), β_c is its associated logarithmic standard deviation of structural capacity, S_d is the median value of seismic demand, and $\beta_{d|IM}$ is the associated logarithmic standard deviation for the demand. These parameters must be estimated in the development of the fragility curves.

The seismic demand in both the longitudinal and transverse directions placed on various critical components within the bridge (listed in Table 18) is estimated through the establishment of probabilistic seismic demand models. Peak responses of the components found through nonlinear time history analysis are related to the ground motion intensity, assumed to be peak ground acceleration in this study. Following the work by Cornell et al.⁽⁴¹⁾, an estimate of the median of the seismic demand can be assumed to follow a power form as shown in (Figure 98):

$$S_d = aIM^b$$

Figure 98 Equation. S subscript d

where a and b are regression coefficients. The dispersion is also estimated through regression analysis. Various sources of uncertainty are accounted for in this analysis, such as ground motion, modeling, and geometric parameters.

The seismic demand must be compared to a capacity estimate as indicated by the fragility definition in (Figure 96). The seismic capacity reflects the limit upon which a given level of damage occurs and level of functionality is realized. The capacity estimates (median and dispersions) presented by Nielson and DesRoches⁽⁴²⁾ are used in this study, with some limit states altered for the various retrofits. These limit states were derived such that the limit states for various components are functionally equal. Upon achieving the slight, moderate, extensive, or complete damage state, a given level of traffic carrying capacity and restoration may be assumed.

Fragility models for the various bridge components can be assessed through (2). However, in order to evaluate the overall impact of retrofit on bridge system performance, system fragility curves must be derived considering the contribution of the critical components. As such, the system fragility for classes of CSUS retrofitted bridges is evaluated through a Monte Carlo simulation. Correlation between the demands placed on various components is assessed to define a joint probability distribution for demand, and the demand model is integrated across all failure domains (defined by the capacity estimates). This allows for assessment of the probability of achieving various damage states for the retrofitted bridge system, which is greater than any one component.

Table 18 Demand parameters of different bridge components considered in fragility development.

Component	Associated Demand Parameter	Abbreviation
Column	Column curvature ductility demand	μ_ϕ
Expansion Bearing	Longitudinal expansion bearing deformation	ex_L
Expansion Bearing	Transverse expansion bearing deformation	ex_T
Fixed Bearing	Longitudinal fixed bearing deformation	fx_L
Fixed Bearing	Transverse fixed bearing deformation	fx_T
Abutment	Active abutment deformation	abut_A
Abutment	Passive abutment deformation	abut_P
Abutment	Transverse abutment deformation	abut_T

These fragility curves are of the form

$$P[DS | PGA] = \Phi \left(\frac{\ln(PGA) - \ln(med_{sys})}{\beta_{sys}} \right)$$

Figure 99 Equation. Conditional probability P, bracket, DS under the condition PGA, close bracket

where med_{sys} is the median value of the system fragility (in units of g PGA), and β_{sys} is the dispersion, or logarithmic standard deviation, of the system fragility. The fragility statement gives the probability of meeting or exceeding damage state DS

Table 19 MSSS steel as-built and retrofitted bridge fragility curves.

Retrofit Condition	Slight		Moderate		Extensive		Complete	
	med _{sys}	β _{sys}						
As-Built	0.25	0.45	0.47	0.40	0.60	0.44	0.91	0.50
Steel Jackets	0.26	0.44	0.50	0.38	0.65	0.42	1.03	0.50
Elastomeric Isolation Bearings	0.39	0.61	0.62	0.59	0.83	0.63	1.27	0.64
Restrainer Cables	0.26	0.45	0.48	0.39	0.63	0.42	1.02	0.49
Seat Extenders	0.25	0.46	0.47	0.40	0.61	0.44	1.15	0.49
Shear Keys	0.25	0.46	0.46	0.41	0.59	0.44	0.89	0.50
Restrainer Cables & Shear Keys	0.25	0.45	0.48	0.40	0.63	0.42	1.00	0.49
Seat Extenders & Shear Keys	0.25	0.45	0.46	0.40	0.60	0.44	1.13	0.49

Table 20 MSC steel as-built and retrofitted bridge fragility curves.

Retrofit Condition	Slight		Moderate		Extensive		Complete	
	med _{sys}	β _{sys}						
As-Built	0.19	0.56	0.36	0.54	0.44	0.56	0.57	0.59
Steel Jackets	0.20	0.57	0.40	0.56	0.50	0.58	0.67	0.62
Elastomeric Isolation Bearings	0.26	0.72	0.43	0.70	0.56	0.71	0.92	0.73
Restrainer Cables	0.20	0.57	0.37	0.55	0.49	0.57	0.67	0.60
Seat Extenders	0.19	0.56	0.36	0.54	0.44	0.56	0.69	0.58
Shear Keys	0.21	0.56	0.41	0.56	0.50	0.59	0.62	0.62
Restrainer Cables & Shear Keys	0.21	0.57	0.41	0.57	0.53	0.59	0.69	0.61
Seat Extenders & Shear Keys	0.21	0.56	0.41	0.56	0.51	0.59	0.80	0.61

Table 21 MSSS concrete as-built and retrofitted bridge fragility curves.

Retrofit Condition	Slight		Moderate		Extensive		Complete	
	med _{sys}	β _{sys}						
As-Built	0.21	0.71	0.65	0.63	0.94	0.65	1.32	0.66
Steel Jackets	0.22	0.74	0.84	0.73	1.25	0.71	1.85	0.74
Elastomeric Isolation Bearings	0.34	0.68	0.65	0.62	0.99	0.66	1.54	0.65
Restrainer Cables	0.21	0.73	0.69	0.67	1.04	0.68	1.49	0.69
Seat Extenders	0.21	0.70	0.67	0.62	0.96	0.64	1.74	0.67
Shear Keys	0.22	0.68	0.63	0.59	0.86	0.62	1.15	0.64
Restrainer Cables & Shear Keys	0.22	0.69	0.67	0.63	1.00	0.65	1.41	0.67
Seat Extenders & Shear Keys	0.22	0.68	0.66	0.60	0.89	0.63	1.60	0.66

Table 22 MSC concrete as-built and retrofitted bridge fragility curves.

Retrofit Condition	Slight		Moderate		Extensive		Complete	
	med _{sys}	β _{sys}						
As-Built	0.16	0.86	0.59	0.69	0.85	0.69	1.18	0.69
Steel Jackets	0.16	0.88	0.69	0.78	0.99	0.73	1.42	0.74
Elastomeric Isolation Bearings	0.47	0.66	0.77	0.64	1.03	0.70	1.38	0.70
Restrainer Cables	0.16	0.79	0.57	0.69	0.86	0.67	1.24	0.66
Seat Extenders	0.16	0.86	0.59	0.69	0.85	0.68	1.54	0.68
Shear Keys	0.16	0.82	0.58	0.69	0.84	0.67	1.19	0.69
Restrainer Cables & Shear Keys	0.16	0.76	0.57	0.69	0.88	0.67	1.33	0.67
Seat Extenders & Shear Keys	0.16	0.84	0.57	0.69	0.84	0.67	1.62	0.69

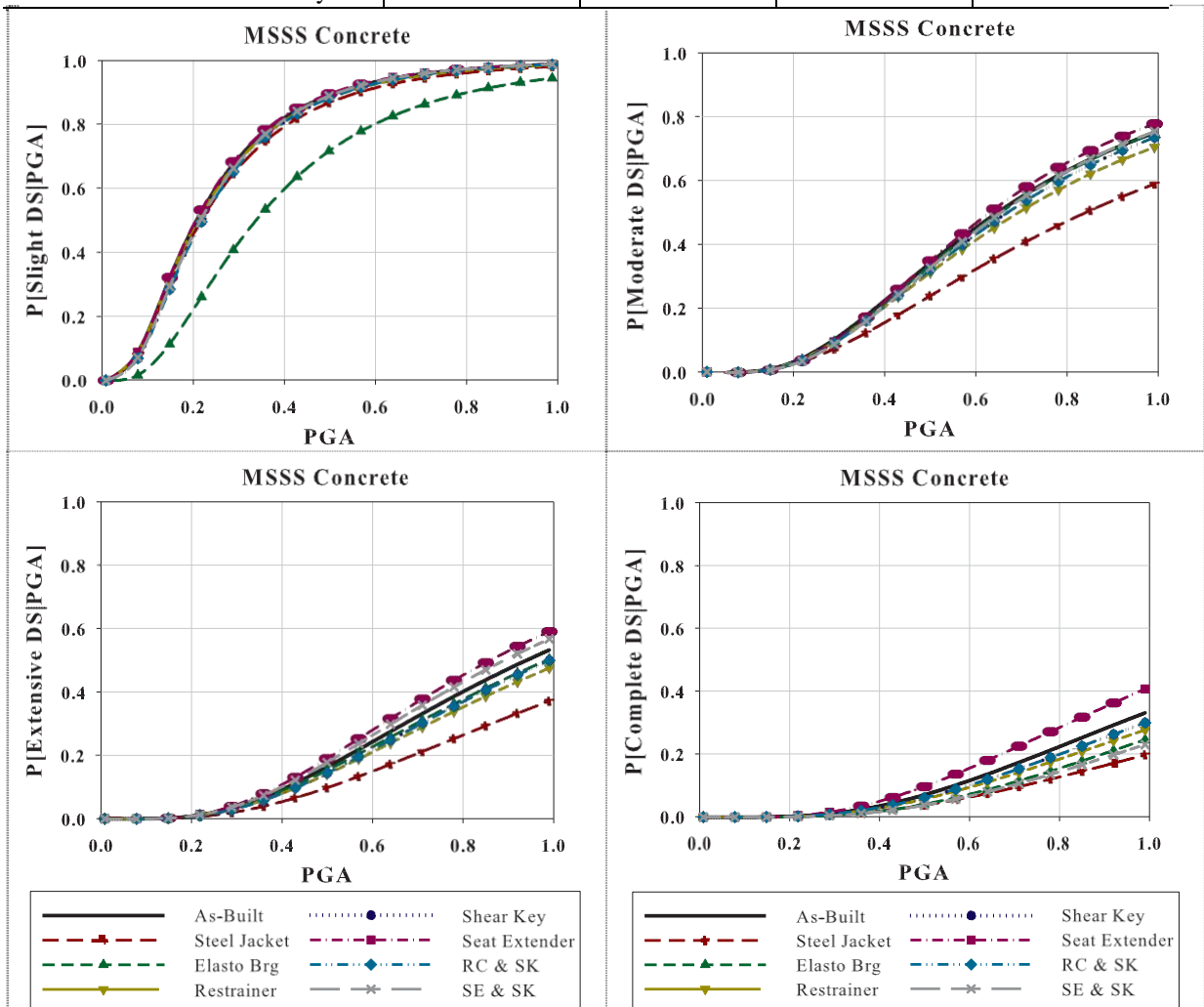


Figure 100 Graph. Fragility curves for the MSSS Concrete girder bridge class, comparing the as-built and retrofitted bridge fragility for each damage state.

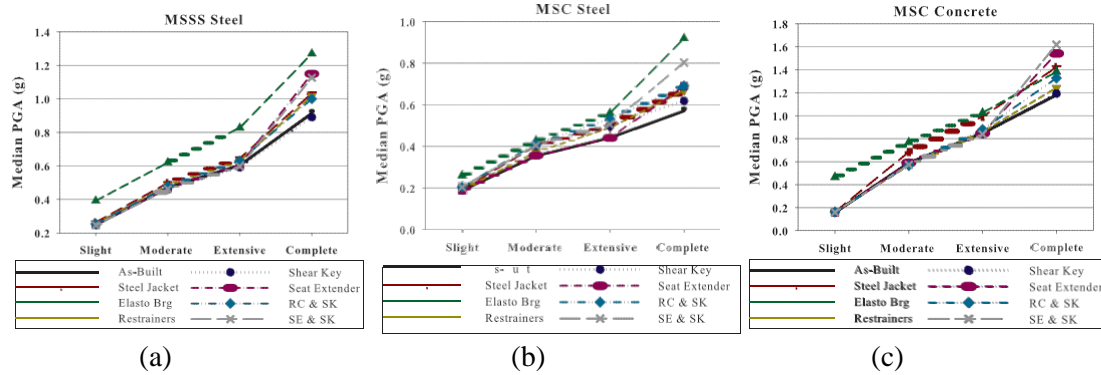


Figure 101 Graph. Comparison of as-built and retrofitted median fragility values for each damage state for the (a) MSSS Steel, (b) MSC Steel, and (c) MSC Concrete girder bridges.

3.6 APPLICATION OF BRIDGE FRAGILITY CURVE

3.6.1 Vulnerability Assessment

Reduction in Failure Probability

The fragility curves presented above depict the probability of failure (stated as meeting or exceeding a particular damage state) conditioned upon the peak ground acceleration of the earthquake event, as shown in Figure 102. For a given scenario event or target PGA level, one can extract the retrofit measure that most effectively reduces the probability of failure. It is noted that the dispersion, characterizing uncertainty modeled by the fragility, may have a significant impact in the selection at very high and low levels of PGA.

However, as an example, if one aims to reduce the potential for complete damage in the MSC steel bridge at a target design event with 0.6g PGA, the curve is then entered vertically at that value. The as-built bridge has roughly a 53% probability of complete damage. The use of the seat extenders, combined seat extenders and shear keys, and elastomeric isolation bearings result in the probability being reduced to 40%, 31%, and 27%, respectively.

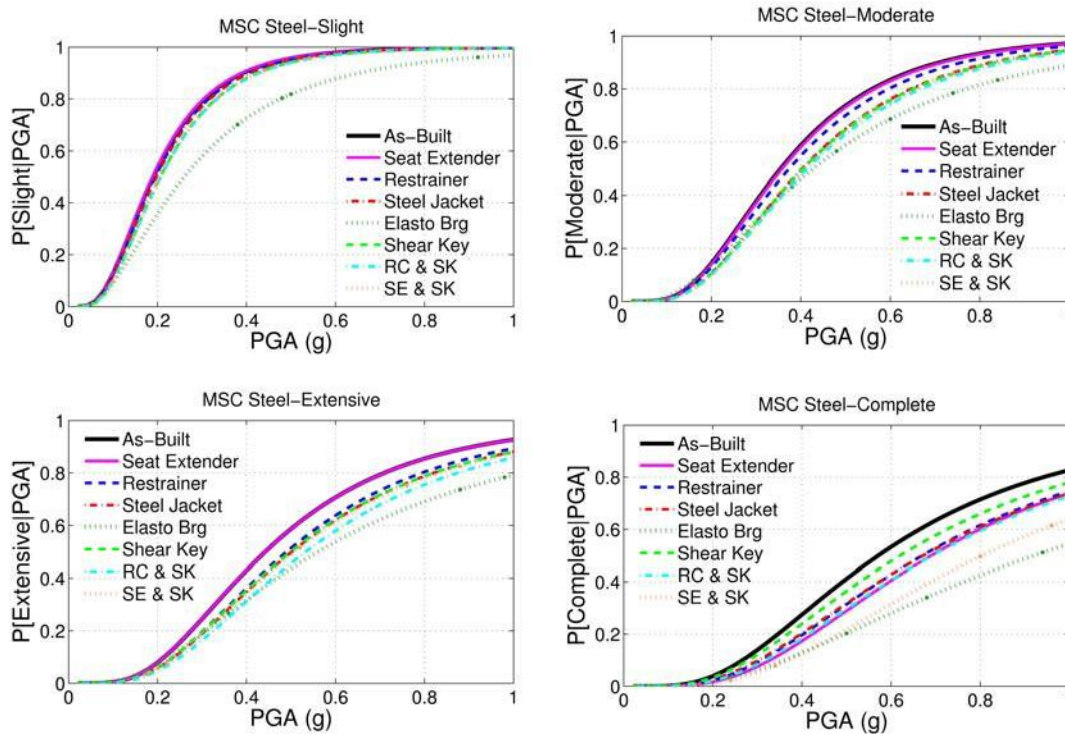


Figure 102 Graph. Fragility curves constructed from the lognormal parameters listed in Table 20 for the MSC steel bridge class, comparing the as-built and retrofitted failure probabilities.

Median Value Shift of the Fragility and Comparison at Other Percentiles

One of the simplest ways of comparing the different retrofit measures is to evaluate the relative change in the median value of the fragility estimate. This eliminates the need to select a particular ground motion intensity and allows for quick screening and comparison of the retrofits. It is noted that the impact on the dispersion is neglected in such an approach, however. A positive percent change in the median indicates a shift of the median value indicative of a less vulnerable structure, while a negative change in the median value indicates a more vulnerable structure (Figure 103). Key conclusions from such a comparison reveal for the complete damage state that elastomeric bearings are most effective for the MSC steel bridge with a median value increase of 61%; and the steel jackets are the most effective for the MSSS concrete bridge with an increase of 40%.

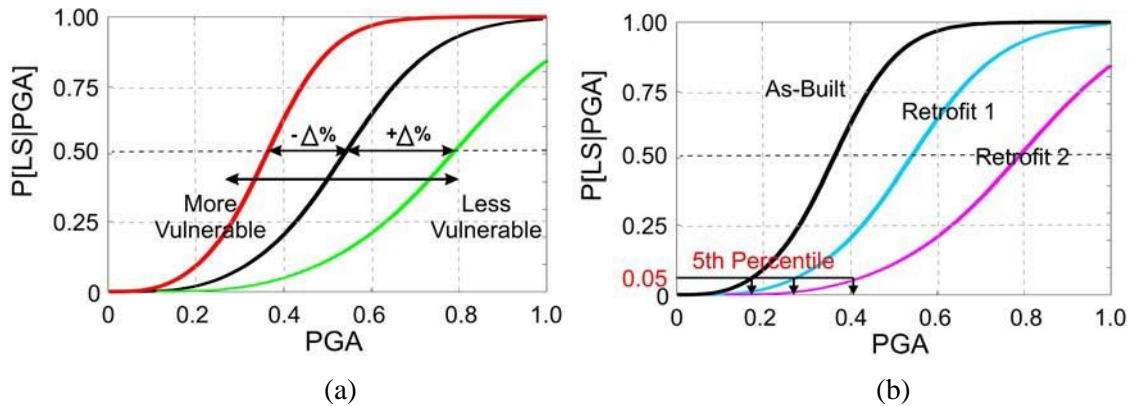


Figure 103 Graph. Illustration of (a) comparing the percent change in the median value and (b) comparing other percentiles for assessing retrofits.

While comparing median values of the fragility for the as-built bridge with various retrofit measure provides a quick approach for screening retrofits, there are some noted limitations. This does not capture the impact of different retrofits on the dispersion, which could affect the failure probability, and the likely impact of retrofit for higher probability events. It may therefore be desirable to evaluate other percentiles (in addition to the 50th percentile represented by comparing median values). For example entering at the 5th percentile would provide insight as to what level of earthquake could be experienced to avoid damage 95% of the time, with and without retrofit. Comparison of the PGA at a percentile of $x\%$, $PGA_{x\%}$, can be found by:

$$PGA_{x\%} = med_{sys} \cdot \exp(\beta_{sys} \cdot \Phi^{-1}(x\%))$$

Figure 104 Equation. PGA subscript x percent

where all constituents have been previously defined. For the MSSS concrete bridge, the $PGA_{5\%}$ increases from 0.45g to 0.55g using the steel jackets, and to 0.58g with the seat extenders.

3.6.2 Discussion of ideal retrofits for different bridges

The sections above have presented several approaches for comparing retrofit measures for common bridge classes using bridge fragility curves. Other options not discussed or considered in the findings presented in this report include their application in region seismic risk assessment for comparing mitigation strategies, or cost-benefit analyses. General findings are presented herein as to which retrofit measures are the most effective

in improving the fragility alone, on the basis of median value shift of the system fragility, which implies in general a reduction in the conditional failure probability. A comparison is made between retrofit measures appropriate for the MSSS concrete girder bridge class relative to the MSC steel bridges.

MSC Steel

The MSC Steel Girder bridge is the most vulnerable bridge type in the CEUS inventory. The steel bearings in this bridge are a primary concern because such bearing types require only limited deformation before being damaged. However, the fixed bearings above the columns are not as vulnerable as the expansion bearings at the far ends of the continuous bridge deck, due to the large expansion joint at the deck ends. In addition, larger demands are placed on the columns of this bridge because of the inertial loads of the continuous deck acting in unison. The elastomeric bearings, therefore, are effective in replacing the more vulnerable steel expansion bearings. However, since all of the bearings act similarly in order to isolate the superstructure from the substructure, the demands are fairly high causing them to be slightly more vulnerable than the original fixed bearings (which are not required to deform considerably).

The expansion bearings are also vulnerable to damage in the transverse direction which is part of the explanation for the synergistic improvement of the performance of the MSC Steel bridge with seat extenders and shear keys. While the steel jackets have a significant impact on reducing the column vulnerability, their inability to affect other components results in limited improvement for the bridge system fragility. The restrainer cables offer a slight improvement in the vulnerability of the expansion bearings. However, they transfer forces from the cables, to the abutments, increasing the system vulnerability.

MSSS Concrete

The concrete girder bridge class has considerably less vulnerable bearings than its steel counterpart, yet has a larger mass. The relative vulnerability of various components in this as-built bridge varies considerably depending on the damage state. This helps to explain why different retrofits have a varying effect at the different damage states. For example, at the slight damage state, the longitudinal fixed and expansion bearings as well as the abutments in active action are the most susceptible to damage. Hence, the elastomeric bearings are particularly effective because they both replace the bearings and reduce the active demands placed on the abutments.

Beyond the limit of moderate damage, the columns tend to become more vulnerable and the steel jacketing becomes particularly effective. The elastomeric bearings are not as effective beyond the slight damage state as one might have expected, because of the increased vulnerability of the abutments in the transverse direction due to pounding of the heavier deck against the wingwall. It is also interesting to note that the use of shear keys actually increases the system vulnerability at the higher damage states. This is because the bearings of the bridge are not particularly susceptible to the higher levels of damage in the transverse direction, so there is negligible positive effect realized. Instead the shear keys actually result in more vulnerable columns due to the inertial loads transferred when the bridge is excited in the transverse direction.

3.6.3 Cost-Benefit Analysis

A cost-benefit analysis is a well known tool for comparing alternative investments, though is frequently used in scenario driven applications. The model presented above, however, presents an opportunity to assess the cost effectiveness of bridge retrofit through a risk-based framework. The fragility curves coupled with probabilistic seismic hazard curves and costs estimated from bridge damage allow for assessment of economic losses with and without the retrofit in place. The benefit of a particular retrofit, r , is evaluated as the difference between the present value of the losses without retrofit, $LCC_{as-built}$, and the present value of the losses with retrofit, LCC_r , as shown in Figure 105:

$$Benefit_r = E[LCC_{as-built}] - E[LCC_r]$$

Figure 105 Equation. Benefit subscript r

The cost-benefit ratio (CBR_r) for a particular retrofit is then assessed as the ratio between the net present value of the investment in retrofit ($Benefit_r$), and the initial cost of the retrofit ($Cost_r$):

$$CBR_r = \frac{Benefit_r}{Cost_r}$$

Figure 106 Equation. CBR subscript r

The CBR is a measure of the financial return for each dollar invested in the seismic retrofit. A CBR greater than one indicates a positive return on investment, and the retrofit

with the largest CBR has a larger savings in losses over the remaining life, per dollar investigated in mitigation. It is noted that a CBR less than one may still be favorable in certain cases due to non-monetary benefits of retrofit and social responsibility, such as loss of life avoided.

With the assumption that earthquake occurrence is modeled as a Poisson process, the expected value of the life-cycle costs due to seismic damage in present day dollars can be expressed as follows:

$$E[LCC] = \frac{1}{\alpha T} (1 - e^{-\alpha T}) \sum_{j=1}^4 (-C_j [\ln(1 - P_{Tfj}) - \ln(1 - P_{Tfj+1})])$$

Figure 107 Equation. E, bracket, LCC, close bracket

where, j is the damage state, α is an inflation adjusted discount ratio assumed as 3%, T is the remaining service life of the bridge, C_j is the cost associated with damage state j , and P_{Tfj} is the T -year probability of exceeding damage state j , estimated as:

$$P_{Tfj} = 1 - (1 - P_{Aj})^T$$

Figure 108 Equation. P subscript T, f, j

The cost-benefit analysis method presented above is applied in a case study assessment of retrofit evaluation for four non-seismically designed highway bridges in Mid-America. The case study bridges selected from each bridge class, including dimensions and dynamic periods, used in the present analysis is given in Table 23. For the bridge retrofit assessments presented, the remaining life of the bridge, T , is assumed to be 50 years for all of the bridges as a base case for comparison. Costs associated with repair from each damage state, C_j , are estimated as a fraction of the replacement cost using the repair cost ratios estimated by Basoz and Mander. The replacement costs for each bridge are estimated based on regional bridge construction costs. As a simple approach to acknowledge and account for these indirect losses, the total cost of losses associated with each damage state is assumed to be 13 times larger than the estimated repair costs. A sample of the steps in the cost-benefit analysis is shown in Table 24 for the MSC concrete bridge located in Caruthersville, MO.

Table 23 Case study bridge dimensions.

Bridge Type	End Span Length (m)	Mid Span Length (m)	Deck Width (m)	Column Height (m)	No. of Girders
MSC Concrete	12.2	22.6	12.8	3.93	8
MSSS Concrete	12.2	13.4	10.4	4.23	5
MSC Steel	22.3	22.3	10.3	4.08	5
MSSS Steel	12.2	13.7	10.5	4.02	5

Table 24 Comparison of expected LCC for different retrofit measures and anticipated cost-benefit ratio (CBR) for sample MSC Concrete bridge located in Caruthersville, MO.

Retrofit	Expected LCC (\$)	Benefit (\$)	Cost (\$)	CBR
As-Built	91915	---	---	---
Steel jacket	79051	12864	36000	0.36
Elastomeric bearing	65760	26155	21912	1.19
Restrainer cable (RC)	87101	4841	11280	0.43
Shear key (SK)	91251	664	23250	0.03
Seat extender (SE)	76601	15314	9000	1.70
SE+SK	76639	15276	32250	0.47
RC+SK	84123	7792	34530	0.23

The bar charts in Figure 109 reveal which retrofit measure is the most cost-effective, having the highest CBR. The effect of siting the bridges in different hazard conditions is evaluated by considering the Caruthersville, MO and Charleston, SC hazard curves in the central and southeastern US, as well as a West Coast hazard curve in Los Angeles, CA. A total of seven different retrofit options were evaluated. Table 25 provides a summary of the most cost effective retrofit for each bridge type and location. The results indicate a natural shift in magnitude of losses and retrofit cost-benefit ratio with increasing seismic hazard. However, they also indicate that due to the relative effect of different retrofit measures at different damage states (exhibited in the fragility model), as well as the nature of the local seismic hazard, the most cost-effective bridge retrofit may differ by location. For example, a relatively cheap retrofit measure with seat extenders, which is particularly effective in mitigating complete damage, tends to be more cost-effective in CSUS locations than in the West Coast example. Additionally, the findings underscore the fact that more costly initial investments in retrofit, such as the use of isolation, may be warranted for some bridge types, such as the MSSS Steel bridge. This is due to the superior effectiveness of the elastomeric bearings in reducing the fragility at all damage

states and its translated impact on reducing the LCC. While the results presented herein are specific to the case study example, the model can be extended to other bridge types, retrofit measures, or locations for screening cost-effective investments in seismic upgrade.

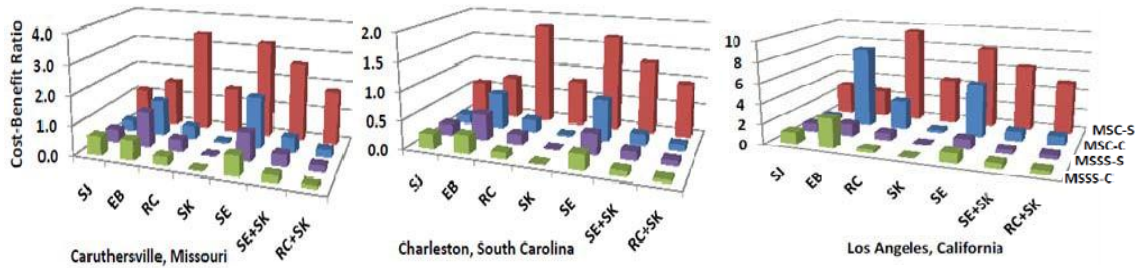


Figure 109 Graph. Cost-benefit ratios for retrofit of the case-study bridges, at different locations.

Table 25 Summary of ideal seismic retrofit based on highest cost-benefit ratio for the case study bridges at each location.

Bridge	Caruthersville, MO	Charleston, SC	Los Angeles, CA
MSC Concrete	SE	SE	EB
MSC Steel	RC	RC	RC
MSSS Concrete	SE	EB	EB
MSSS Steel	EB	EB	EB

Note: SE=seat extenders; RC=restrainer cables; EB=elastomeric bearings

CHAPTER 4 ANALYTICAL ASSESSMENT AND COMPARISON OF SEISMIC PERFORMANCE EVALUATION PROCEDURES FOR BRIDGE STRUCTURES

4.1 INTRODUCTION

The limit state, or more recently-termed performance-based, seismic design and evaluation method requires structures to satisfy different performance criteria for different levels of seismic excitation. For instance, structures may suffer minor damage but should be operational under frequent earthquakes with low intensity. Under infrequent earthquakes with large intensity, structures should not collapse to protect people. The performance criteria for diverse structural types are suggested in literatures, for example, reinforce concrete structure⁽⁴³⁾, concrete and masonry wall buildings⁽⁴⁴⁾, steel structures⁽⁴⁵⁾, and bridge structures⁽²⁸⁾ as each structural configuration has different performance objective. Buildings and bridges also have different performance objective, Figure 110. To evaluate structural performance with the multi-level performance criteria, it is essential to employ analysis methods which can distinguish the subtle differences of structural responses at different excitation level.

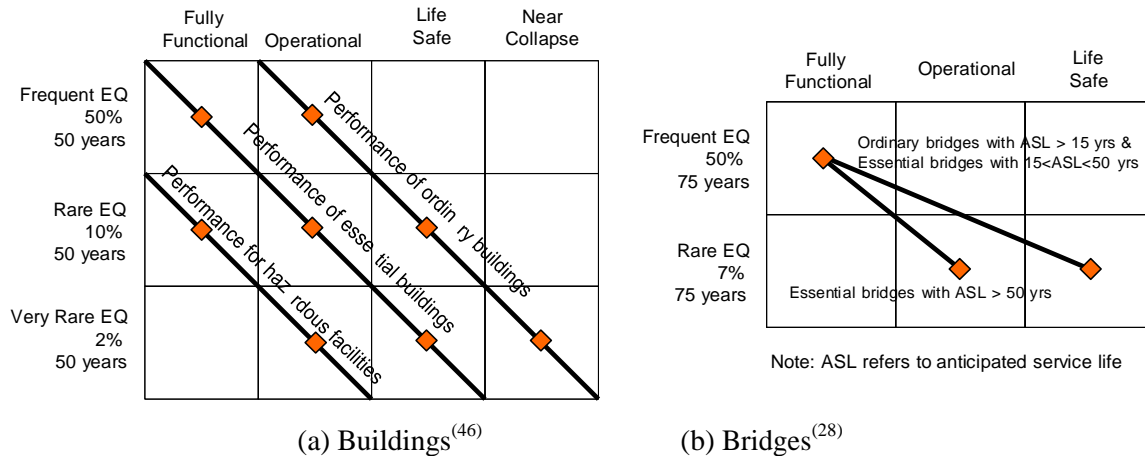


Figure 110 Graph. Performance objectives of buildings and bridges

The majority of structures are designed to behave in the inelastic range under the design earthquake to optimize construction cost and structural performance. Exceptions include hazardous facilities, such as nuclear plant or natural gas storage tanks, the failure of which may lead to devastating consequences. As structures are designed to behave in inelastic range, seismic performance of structures can be most realistically evaluated through inelastic response history analysis. This approach requires accurate

representation of the inelastic and nonlinear characteristics of structural elements, gaps, foundation, and supporting soil. Even though this approach is most realistic, it has not been commonly adopted in practice due to large modeling efforts, lack of data for inelastic model, and expensive computational costs in comparison with simplified approximate approaches.

With the above difficulties in inelastic response history analysis, several approximate methods have been commonly adopted. For instance, an inelastic system can be represented with an equivalent linear system. In this approach, secant stiffness and increased damping are adopted to take account reduced stiffness and increased damping of inelastic system. Method C in bridge retrofitting⁽²⁸⁾ adopts similar concept by reducing flexural stiffness to $0.5EI$ of original structural element and by increasing damping.

On the other hand, there are elastic approaches where initial stiffness and damping are used for the response history analysis and displacement modification factors are applied to take into account increased displacements of inelastic system. The modification factors are mainly function of structural period, ductility demand, and hysteretic characteristics of a system. This method was first proposed by Veletsos and Newmark⁽⁴⁷⁾ followed by many variations. C_1 factor in FEMA 356⁽⁴⁸⁾ and C_d factor in FEMA 450⁽⁴⁹⁾ are in this category.

In addition to the above response history analysis methods, there exist several variations of static pushover methods for seismic capacity estimation and capacity spectrum methods for seismic demand estimation. The pushover analysis is based on inelastic response of a single mode. To take account higher mode effects, multi-mode pushover analysis⁽⁵⁰⁾, adaptive pushover analysis^(51, 52, 53, and 54), and energy based pushover analysis⁽⁵⁵⁾ methods are developed.

The above simplified approaches encompass many approximations which can result in inaccurate, often non-conservative, structural response estimations. The approximation in the above approaches includes: simplification of MDOF system to SDOF system, linearization of inelastic structural responses, and demand estimation without consideration of element capacity, among many others. Hence, the applicability of the above approximate methods highly depends on the magnitude, frequency content of the input ground motion, and hysteretic characteristics of structures.

Furthermore, most of the approximate methods have been developed and verified with building structures. For example, the damping modification factor, β , in the capacity spectrum method in ATC-40⁽⁴³⁾ is derived from typical hysteretic behavior of buildings. Modal pushover analysis (MPA) by Chopra and Goel⁽⁵⁰⁾ is verified with building structures where the first two to three modes have 80 ~ 90% of the modal participation factors.

Bridge structures are inherently and fundamentally different from building structures. In regular highway bridges, mass is concentrated in the deck which mostly remains elastic during earthquake. Bents and decks are often connected with bearings which do not transfer moment. As a footprint of bridge structure is relatively smaller than that of building structures, the effect of soil-structure interaction can be more significant than that of building structures. Because of these reasons, the simplified approaches, which have been developed and assessed mainly for building structures, call for thorough evaluation before application to bridge structures.

The following sections will summarize the theoretical background of approximate methods. Inelastic response history analysis and several approximate methods are applied to evaluate seismic response of two bridge structures. The analysis results from approximate methods are compared with those from inelastic response history analysis method.

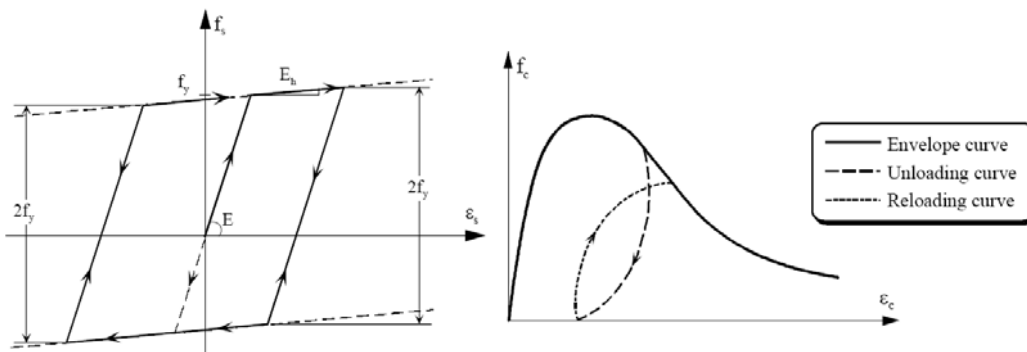
4.2 METHODS FOR SEISMIC PERFORMANCE EVALUATION

In this study, approximate methods including elastic response history analysis, capacity spectrum methods, and SDOF representation of bridge response are compared with inelastic response history analysis. The details of each approximate method employed in this study are described below.

4.2.1 Inelastic Response History Analysis

Usually, material inelasticity as well as geometric nonlinearity is considered in the inelastic response history analysis. A bilinear model is used to idealize steel members and reinforcement. In this model, the loading and unloading in the elastic range follow a linear function with constant stiffness represented by the Young's modulus of steel. In the post-elastic range, a kinematic hardening rule for the yield surface defined by a linear relationship is assumed, as shown in Figure 111(a). A uniaxial constant 'active' confinement concrete model based on the model of Mander et al.⁽⁵⁶⁾ is used to represent

concrete material. The model, which incorporates the influence of confinement effects on the peak stress and strain as well as on the post-peak stress-strain relationship, can provide a good estimation of the cyclic response of RC members under cyclic and dynamic loading. The model requires material parameters such as ultimate compressive strength of unconfined concrete (f_c), tensile strength (f_t), crushing strain (ϵ_c) and the confinement factors (K). Figure 111(b) shows a typical stress-strain relationship for concrete under cyclic loading. As a platform for the inelastic response history analysis, inelastic seismic assessment platform, Zeus-NL⁽⁵⁷⁾, is used.



(a) Bilinear steel model with kinematic strain hardening (b) Behavior of concrete under cyclic loading

Figure 111 Illustration. Steel and concrete models used in inelastic response history analysis

In Zeus-NL, the inelastic uniaxial material models represent hysteretic behavior of individual fibers which consists a frame section. The forces and moments at a section are obtained by integrating the inelastic responses of individual fibers, Figure 112. The Eulerian approach towards geometric inelasticity is employed at the element level. Therefore, full account is taken of the spread of inelasticity along the member length and across the section depth as well as the effect of large member deformations. Since the sectional response is calculated at each loading step from inelastic material models that account for stiffness and strength degradation, there is no need to make assumptions on the moment-curvature response as commonly required by other analysis tools.

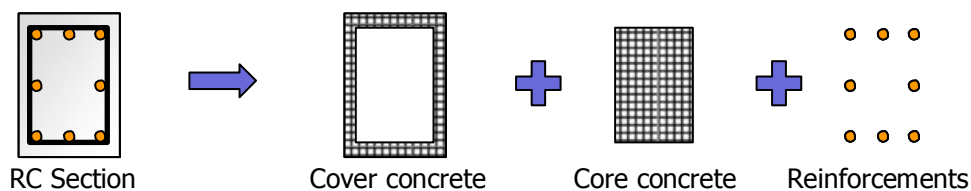


Figure 112 Illustration. Discretization of reinforced concrete sections for frame analysis

Foundations are represented with trilinear springs whose properties are identified from three-dimensional finite element analysis of soil and foundation system. Details about foundation models are presented in the examples. Gaps between decks and between deck and abutments are represented with asymmetric springs which have very large stiffness when gaps are closed between two units. The springs have negligible stiffness when gaps are open (Figure 113).

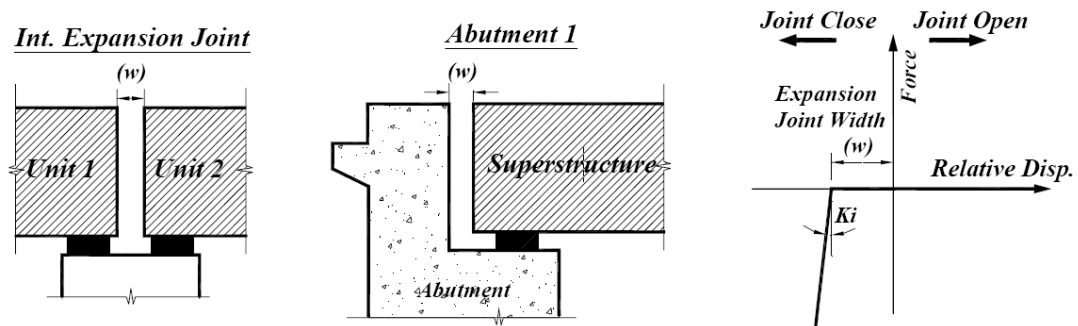


Figure 113 Illustration. Modeling of gaps with asymmetric spring between two units

4.2.2 Elastic Response History Analysis

Inelastic response of a structure can be generally characterized with two features: period elongation and energy dissipation. The natural periods of inelastic system elongate as structures' deformation increases. As a displacement response spectrum has larger amplitude at longer period range, the response of a inelastic system generally increases with inelastic excursion of structural response. On the other hand, the inelastic response dissipates seismic energy which decreases structural response. Hence when an inelastic system is modeled with elastic model, the period elongation and energy dissipation needs to be appropriately modeled.

There are mainly two categories of methods which use elastic response history analysis to represent response of inelastic system. The first category is multiplying elastic response with displacement modification factors. In this approach, an elastic system with same initial stiffness and damping of inelastic system is used for analysis. The response from elastic system, point (B) in Figure 120, is multiplied with a factor to get approximate value of inelastic system, point (A) in Figure 120. As the inelasticity of a structure can be characterized with many parameters, such as post yield stiffness, stiffness degradation,

strength degradation, pinching, P- δ effect, among many others, researchers proposed several expressions for the modification factor. The development of these modification factors are originated from the study by Velotsos and Newmark⁽⁴⁷⁾. For an elasto-perfectly system, the relationship between the maximum elastic response, Δ_e , and the maximum inelastic response, Δ_i , is proposed by Newmark and Hall⁽⁵⁸⁾.

$$\Delta_i = C\Delta_e$$

Figure 114 Equation. Delta subscript i

where C is modification factor as below.

$$C = \mu, T < T_a = 1/33s$$

Figure 115 Equation. C for T less than T subscript a

$$C = \mu / (2\mu - 1)^\beta, T_a \leq T < T_b = 0.125s$$

Figure 116 Equation. C for T between T subscript a and T subscript b

$$C = \mu / \sqrt{2\mu - 1}, T_b \leq T < T_c$$

Figure 117 Equation. C for T between T subscript b and T subscript c prime

$$C = T_c / T, T_c \leq T < T_c$$

Figure 118 Equation. C for T between T subscript c prime and T subscript c

$$C = 1, T \geq T_c$$

Figure 119 Equation. C equals to 1 for T greater than T subscript c

where T_c is a corner period. The above expressions are developed based on numerous analyses of SDOF systems. The above equations imply that the maximum elastic response and maximum inelastic response are similar at long period range while at short period, it needs modification factors larger than 1. It is worth noting that the ductility demand is not known without running inelastic analysis. Hence the above equations can be useful for design purpose, where the structure's ductility can be partially controlled through design, but cannot be directly applied to evaluation of existing structures as ductility demand is not known a priori. In the seismic regulations for new buildings, FEMA 450⁽⁴⁹⁾, modification factors are suggested as a function of structural type.

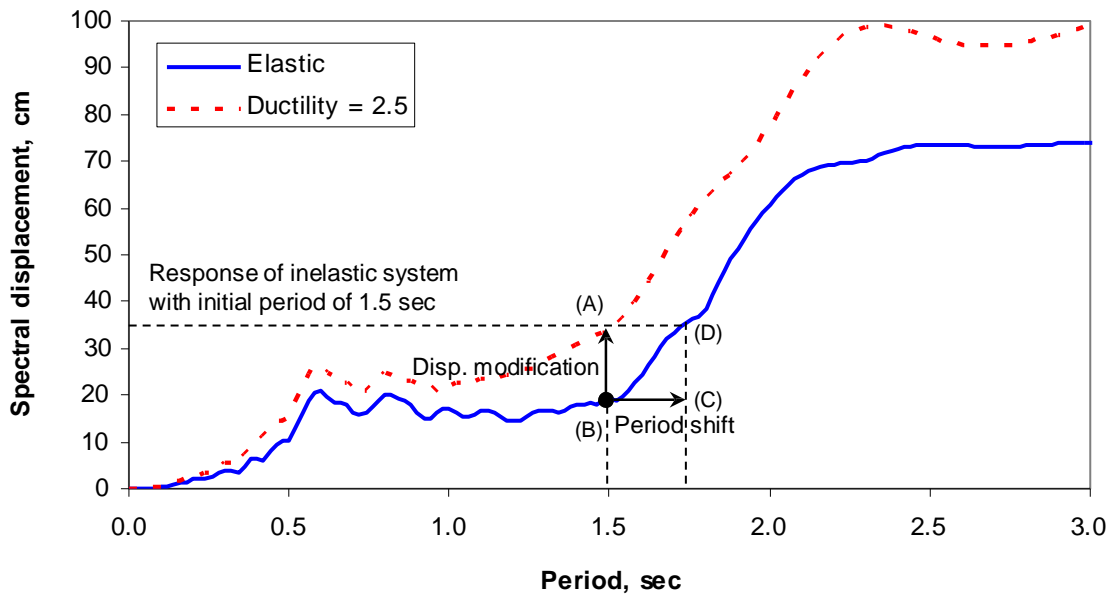


Figure 120 Graph. Estimation of inelastic response from elastic response

The second categories of methods which can approximately take account the inelasticity of a structural system is shifting structural period to longer period range. If a structural period increases from point (B) to (C) in Figure 120, for example, spectral displacement of a system increases. Then the amplitude of maximum elastic response of the system, point (D) in Figure 120, is similar to the maximum response of the inelastic system, point (A). Methods in this category include, Rosenblueth and Herra⁽⁵⁹⁾, Gulken and Sozen⁽⁶⁰⁾, Hadjian⁽⁶¹⁾, Kowalsky⁽⁶²⁾, among many others.

The *Seismic Retrofitting Manual for Highway Bridges*⁽²⁸⁾ allows elastic response history analysis in Method C. The manual suggests that the flexural rigidity of reinforced concrete piers should to be reduced to $0.5E_cI_g$ to take account cracking and yielding. The manual also allows the use of equivalent viscous damping when secant stiffness is used in the analysis. In this study, the response history analysis of a bridge with $0.5E_cI_g$ will be compared with the responses of elastic system with $1.0E_cI_g$ and inelastic system in subsequent sections of this report.

4.2.3 Inelastic Response History Analysis of SDOF Model

While a complex bridge, such as the second example in this study, needs hundreds of modes to have modal participation factor of 90%, a regular bridge with limited number of continuous spans mostly need a single mode to model vibration of the bridge. Hence a bridge with a few spans, such as the first example in this study, can be confidently

modeled with a single degree of freedom system. The inelastic characteristics of the SDOF system can be obtained from the pushover analysis of the bridge with the 1st mode load distribution pattern. Then the response of the inelastic SDOF system can be used to estimate response of a bridge.

This approach can be applied to estimate seismic response including multi-mode effects as suggested by Chopra and Goel⁽⁵⁰⁾. In Chopra and Goel⁽⁵⁰⁾, pushover analyses with higher mode load distribution pattern are conducted. The pushover curves from the analysis are used to model two or three inelastic SDOF systems. Then the maximum responses of the inelastic SDOF systems are combined using appropriate combination rule. This approach is not conceptually accurate as superposition of inelastic response is not theoretically correct. But numerical studies proved that the results from this approach are practically acceptable. This multi mode pushover analysis approach, so called as MPA method, has been verified through building structures whose response are governed by the first few modes. Recently, Paraskeva et al.⁽⁶³⁾ applied the MPA approach to a curved bridge. One of the shortcomings of the approach, as stated in Paraskeva et al.⁽⁶³⁾, is how the monitoring point is defined during pushover analysis. The pushover curve can be dramatically different depending on the selection of monitoring point. To overcome the weakness of arbitrary selection of monitoring point, Hernández-Montes et al.⁽⁵⁵⁾ proposed energy based pushover analysis where displacement of pushover curve is estimated from the total work during the pushover analysis.

In this study, only SDOF representation of a regular bridge is investigated as the multi-mode pushover approach is not well established for bridge structures. The method is applied to the first bridge example.

4.2.4 Capacity Spectrum Analysis of SDOF Model

Capacity spectrum method can be used to approximate response of inelastic SDOF system. In this method, a pushover curve is converted to capacity spectrum. Earthquake load is represented with response spectrum in spectral displacement vs spectral acceleration domain. In an elastic system, the intersection of the capacity curve and the demand curve is identical to theoretical structural response.

If a structures' response is in inelastic range, elastic response spectrum needs to be reduced to represent inelastic seismic demand. ATC-40 (1997) proposed to use equivalent damping to reduce seismic demand. In this approach, maximum elastic

response is obtained from capacity spectrum method. Then equivalent damping is calculated based on the maximum response. Reduced response spectrum with the equivalent damping is plotted over capacity curve to estimate inelastic response. This procedure is iterated until the response converges.

Chopra and Goel⁽⁶⁴⁾ showed that in the ATC-40⁽⁴³⁾ approach, where equivalent damping is used to reduce seismic demand, convergence is not achieved in many cases, results are inaccurate, and a parameter, κ , in the equivalent damping is based on judgment. Hence they proposed to use constant ductility response spectrum to represent inelasticity in structural response.

In this study, the two capacity spectrum methods in ATC-40⁽⁴³⁾ and Chopra and Goel⁽⁶⁴⁾ are applied to estimate the transverse response of the first bridge example. The capacity spectrum method is not applied to evaluate the longitudinal bridge response as the bridge capacity curve in longitudinal direction is very different from conventional capacity curve due to bearings, gaps, and abutment.

4.3 APPLICATION OF EVALUATION PROCEDURES FOR BRIDGE STRUCTURES

Two bridges are used as reference structures. The first bridge is a highway overcrossing bridge in Central and Eastern United States. This bridge represents one of the most common bridge configurations in the area. Several approximate procedures are employed in addition to inelastic response history analysis. The second bridge is a complex 59-span bridge. For the analysis of the second bridge, two elastic response history analyses with initial stiffness of $0.5E_cI_g$ and $1.0E_cI_g$ and inelastic response history analysis are conducted. Adopted analysis methods for each bridge are summarized in Table 26. Bridge configurations, analytical models, and analysis results are presented in the subsequent sections.

Table 26 Applied analysis methods for two bridge structures

Bridge	Analyzed direction	Analysis methods	Ground motions
Regular four span bridge (Section 3.1)	Transverse	Inelastic response history	30 artificial 30 recorded
		Elastic response history, $0.5E_cI_g$	
		Elastic response history, $1.0E_cI_g$	
		Bilinear SDOF response history	

		Capacity spectrum ⁽⁴³⁾	
		Capacity spectrum ⁽⁶⁴⁾	
		Inelastic response history	
		Elastic response history, $0.5E_cI_g$	
	Longitudinal	Elastic response history, $1.0E_cI_g$	30 artificial 30 recorded
		SDOF system with a bilinear spring	
		SDOF system with multiple springs	
		Inelastic response history	
	Transverse	Elastic response history, $0.5E_cI_g$	9 artificial
		Elastic response history, $1.0E_cI_g$	
		Inelastic response history	
Complex multi-span bridge (Section 3.2)	Longitudinal	Elastic response history, $0.5E_cI_g$	9 artificial
		Elastic response history, $1.0E_cI_g$	

4.3.1 Typical Highway Overcrossing Bridge in Central and Eastern U.S

4.3.1.1 Bridge Configuration

A highway overcrossing bridge in Southern Illinois is selected as a reference structure. The bridge is located about 110 km from the New Madrid Seismic Fault. The selected bridge is a multi-span continuous steel girder bridge which is the third most common configuration (13 %) of the entire bridge inventory in the area after multi-span simply supported concrete girder bridges (19%) and single-span concrete girder bridges (SSC, 14%)⁽⁶⁵⁾. The bridge consists of three bents and continuous steel girders as illustrated in Figure 121. Deck is supported on fixed bearings at Bent 2 and on expansion bearings at Bent 1, Bent 3, and abutments. Each bent consists of three circular piers supported by a pile cap and 10 steel piles. The piles at Bent 2 are battered toward the abutments to resist moment transferred from longitudinal movement of the deck. Each abutment in the reference bridge is supported on six steel piles, two of which are battered toward the bridge. Five boring tests were conducted at the site. The boring test results showed that a bedrock is located at an average depth of 4.57 m (15 ft) below the bottom of pile caps. The soil layers consist predominantly of very stiff to hard clays. For further information about the bridge, a reference is made to Kwon and Elnashai⁽⁶⁶⁾.

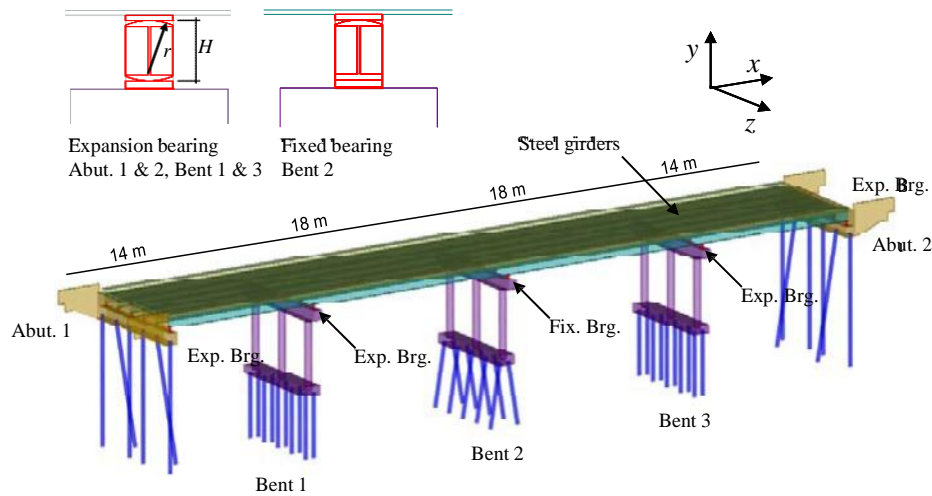


Figure 121 Illustration. Configuration of the studied bridge

4.3.1.2 Analytical Models

Structural Model for Inelastic Response History Procedure

The superstructure of the reference bridge consists of a concrete deck on top of six continuous steel girders. The substructure consists of three piers supported on steel pile foundations. The dimension and configuration of a typical bent and foundation is presented in Figure 122. The steel girders, decks, cross beams of bents, and piers are modeled in ZEUS-NL⁽⁵⁷⁾ using cubic frame elements, as shown in Figure 123. Fiber-based elements are used to model each frame element. In fiber-based frame analysis it is typically assumed that concrete sections are initially uncracked, and bond-slip effects are ignored. Thus, in general, the fiber-based frame analysis tends to show larger initial stiffness than the real structure. When the ground shaking intensity is large enough to crack concrete sections, however, the fiber-based frame analysis is very reliable, especially for frames with flexural failure.

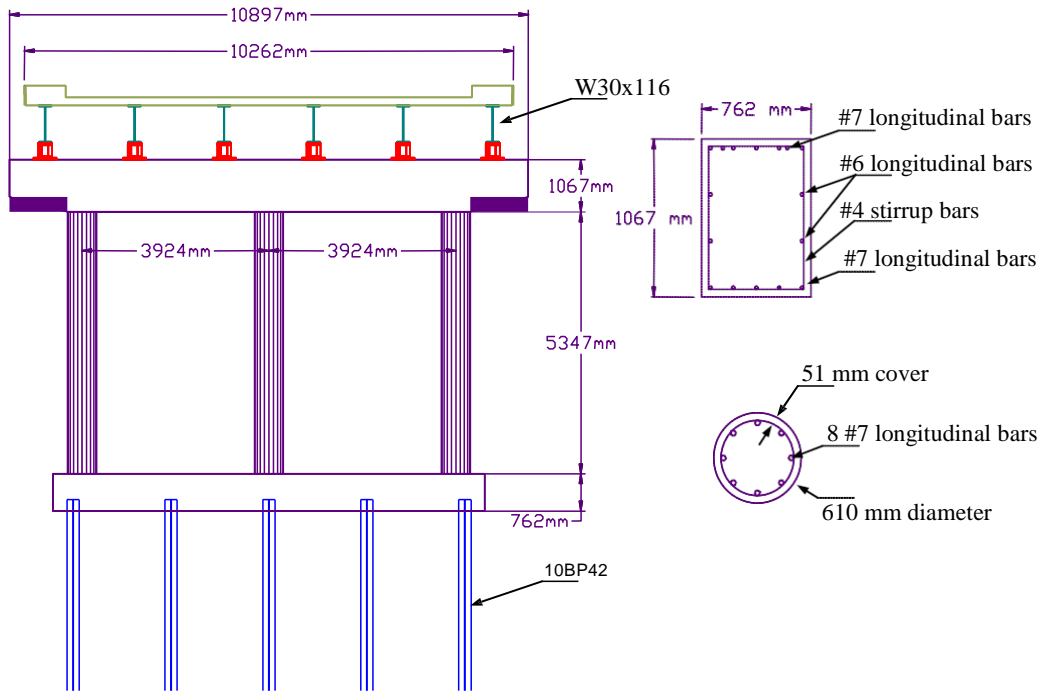


Figure 122 Illustration. Configuration of typical bents and foundations

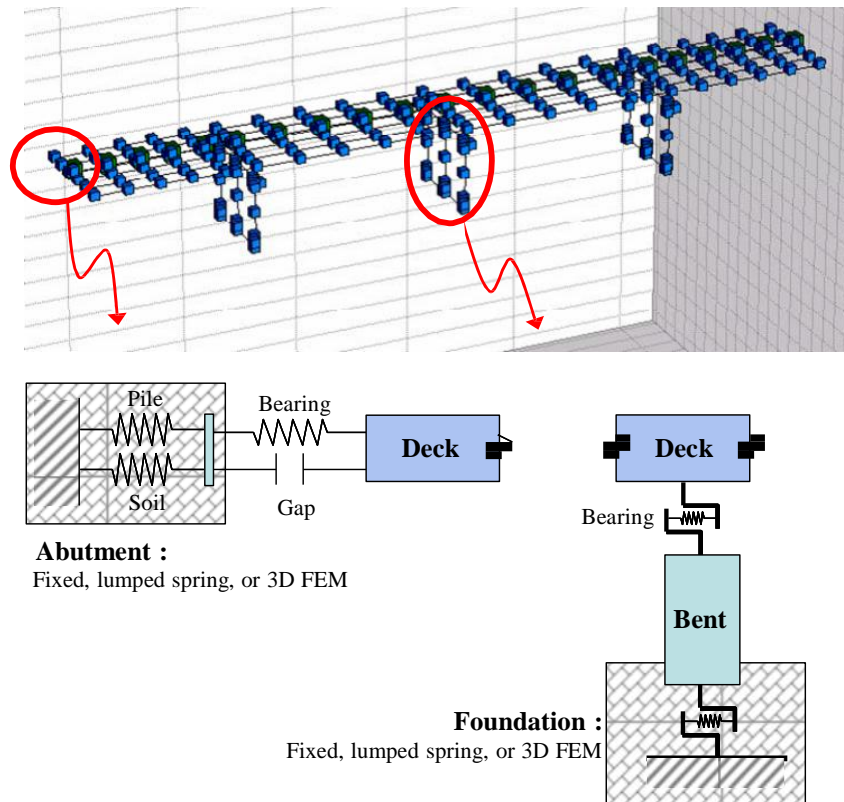
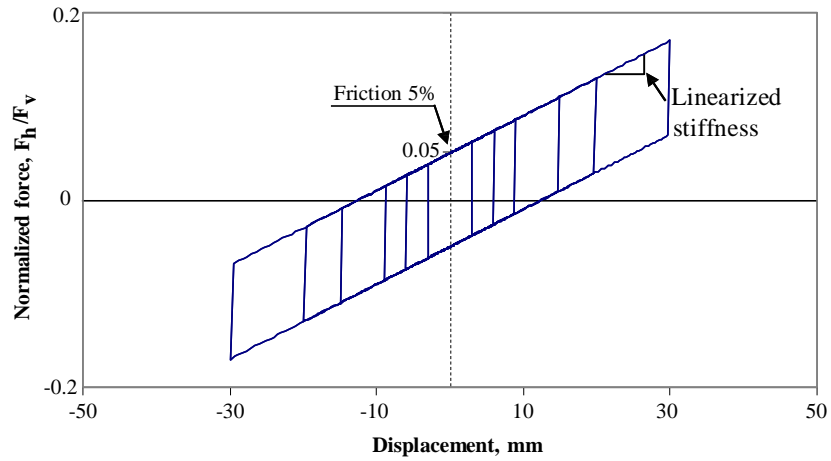


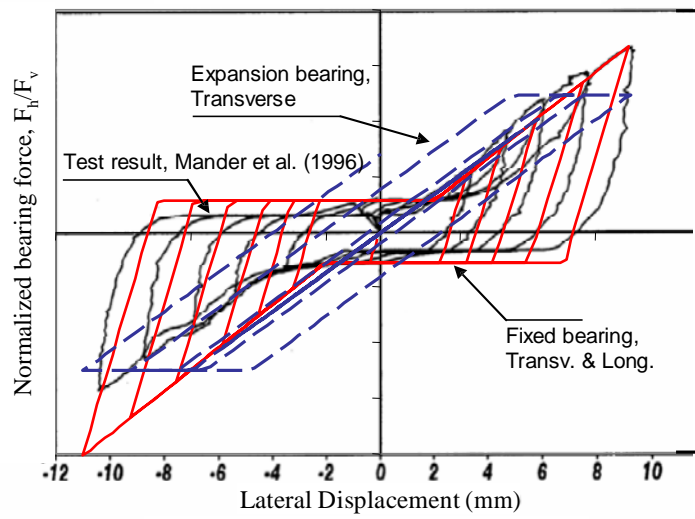
Figure 123 Illustration. FE model of the bridge and connectivity of structural components

Two types of bearings are used in the bridge (Figure 121). The expansion bearings are typical segmental rocker-type units. The longitudinal stiffness of this type of bearing increases with the relative displacement between two plates at top and bottom. A linearized segment of the inelastic displacement-force relationship is used for response history analysis. In this study, the longitudinal stiffness of expansion bearings includes a frictional coefficient of 0.05 consistent with the findings of Mazroi et al.⁽⁶⁷⁾. Figure 124(a) presents the hysteretic behavior of expansion bearings in the longitudinal direction. Mander et al.⁽⁶⁸⁾ tested bearings taken from existing bridges. Among the several types of tested bearings, the behavior of low-type bearings is expected to be similar to the transverse response of the reference bridge bearings. The movement at all of these bearings is restrained by pintle pins and pintle holes which act as shear key connections. The study showed that the behavior of bearings in the transverse direction is controlled by the contact and separation of pintle pins to bearing plates and bearing plates to anchor bolts. Until the gaps between these elements are closed, constant friction is observed. Then, the resisting force increases with the Figure 124(b) compares the test result of low-type sliding bearings and the behavior of the idealized trilinear model. In the absence of further experimental data, the behavior of fixed bearings in transverse and longitudinal directions is assumed to be similar to the transverse direction test of low-type bearing by Mander et al.⁽⁶⁸⁾. For the modeling of expansion bearings in transverse direction, bilinear models are used. It is assumed that the bearings yield when shear force at pintle pins reaches shear strength capacity.

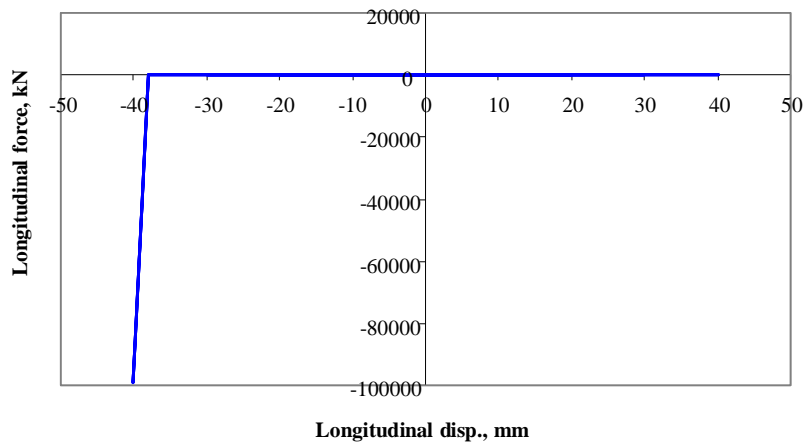
The design drawings of the bridge show that there is a 38 mm of gap between the deck and abutments at a temperature of 50°F. Neglecting the variation of the length of the superstructure with temperature variation, the gaps are modeled as asymmetric springs such that the spring has no resistance on tensile loading, and they become stiff when the gap closes. The hysteretic behavior of a gap element used in the bridge model is shown in Figure 124(c).



(a) Expansion bearing model in longitudinal direction



(b) Low-type bearing behavior in transverse direction



(c) Hysteretic behavior of gap elements

Figure 124 Graph. Analytical models of bridge components

The inelastic characteristics of the soil-pile-foundation systems are obtained from a three-dimensional FE analysis of soil-pile-foundation system using realistic soil material models in OpenSees⁽⁶⁹⁾. Boring log data shows that the soil of the bridge site predominantly consists of stiff to hard clay. Thus the subsoil layers are assumed to be pressure-independent material with soil properties of stiff clay proposed by the developer of the soil material model, Yang and Elgamal⁽⁷⁰⁾. Due to lack of information on embankment properties, the material properties of the embankments are taken from those of a similar study conducted by Kwon and Elnashai⁽⁷¹⁾. The stiffness and strength of foundations identified from pushover analyses of these models are used in the inelastic structural model.

SDOF Model for Approximate Procedure

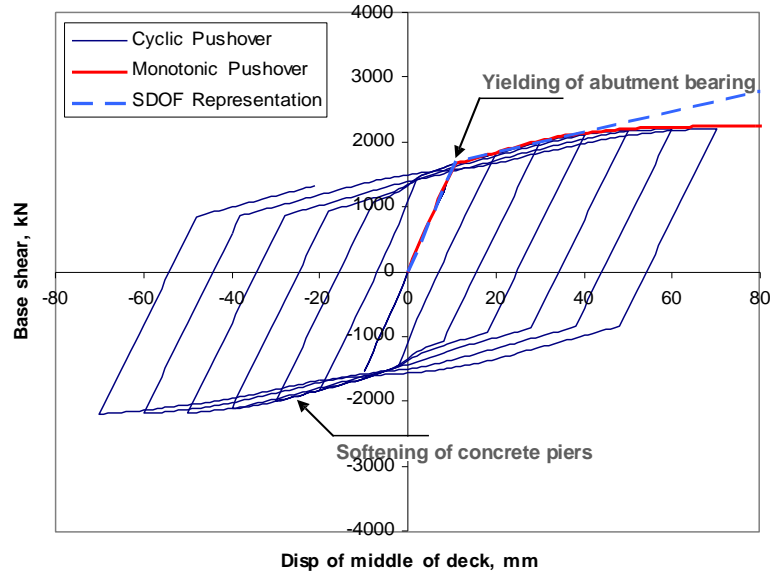
The bridge is a very regular structure. The geometry of the bridge shows that the first mode response will predominantly govern the bridge response. Thus a SDOF representation of the bridge in longitudinal and in transverse directions may sufficiently replicate the dynamic response of the bridge structure. The stiffness and strength of the SDOF system are identified from pushover analysis. To accurately represent the cyclic behavior of the bridge response, cyclic pushover analyses are conducted in transverse direction and in longitudinal direction. Transverse direction response shows clear yielding and softening behavior. The yielding point in the pushover curve, Figure 125(a) is from the yielding of abutment bearings in Figure 124(b). After yielding at bearings, concrete piers are gradually softened due to cracking and yielding of reinforcements. The transverse directional response of the bridge is represented as SDOF system whose pushover curve is modeled as dashed line in Figure 125(a). The mass of the SDOF representation is determined such that the period of the SDOF system is identical to the period of the 1st mode of the bridge in transverse direction.

A similar procedure is used in the longitudinal direction. Monotonic and cyclic pushover analyses are conducted. The response of the bridge in longitudinal direction can be characterized with friction of bearings, opening and closing of gaps, and large stiffness of abutments. Hence SDOF system with bilinear spring, which can model only initial stiffness and friction of bearings, may not be sufficient. To represent longitudinal response, two different SDOF systems are used.

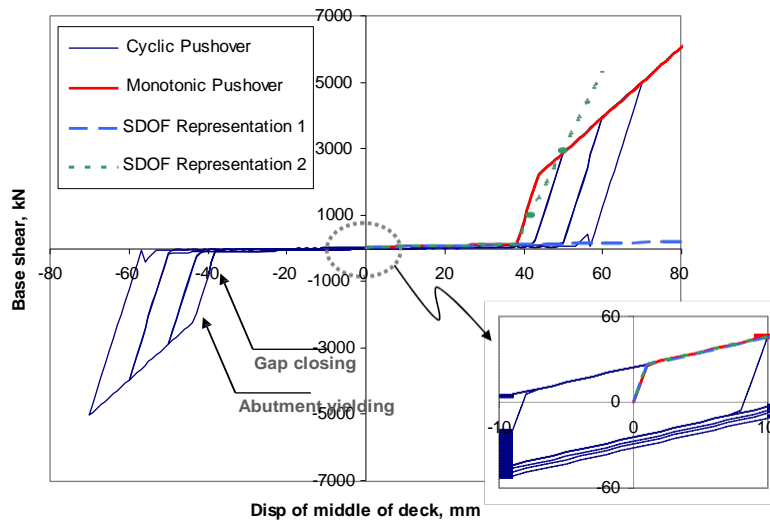
- SDOF system with a bilinear spring: This system can represent initial stiffness and friction.

- SDOF system with combination of multiple springs: This system can represent initial stiffness, friction, and closing and opening of gaps.

The pushover curves of the above two SDOF systems are overlapped with pushover curve of the bridge in longitudinal direction in Figure 125(b). Same damping values are used with inelastic model.



(a) Transverse direction



(b) Longitudinal direction

Figure 125 Graph. Monotonic and cyclic pushover curves of bridge

Capacity Spectrum Method

Capacity spectrum methods are adopted to analyze the bridge in transverse direction. Pushover curves in Figure 125(a) are used as capacity curve of the structure. Response spectrum of input ground motions are used as demand curve. Two capacity spectrum methods, ATC-40⁽⁴³⁾ and Chopra and Goel⁽⁶⁴⁾, are used. In the ATC-40 method, the inelastic seismic demand is obtained by reducing elastic seismic demand using equivalent damping. As the cyclic pushover curve of the bridge, Figure 125(a), does not show pinching, stiffness degradation or strength degradation, damping modification factor, κ , is assumed to be 1.0.

The capacity spectrum method is not applied for the analysis in longitudinal direction as the methods were developed and verified with softening systems while the pushover curve of the bridge in longitudinal direction shows hardening behavior due to opening and closing of gaps and large stiffness of abutments which cannot be found in building structures.

Elastic Analysis

Seismic retrofitting manual for highway bridges⁽²⁸⁾ suggests $0.5 E_c I_g$ as initial stiffness for reinforced concrete column and beams subjected to yielding. For the elastic analysis of the bridge, $0.5 E_c I_g$ is used for concrete bents. For the purpose of comparison, $1.0 E_c I_g$ is also used to understand the effect of linearized stiffness. For all inelastic spring elements, such as gaps, bearings, and foundations, initial stiffness are used. Thus bearings in the elastic bridge model tend to have large stiffness.

4.3.1.3 Input Ground Motions

Due to the infrequent nature of earthquakes within the Central and Eastern U.S., ground motion records, especially from large earthquakes, do not exist. Therefore, artificial ground motion records are used in conjunction with ground motion records from other sites. A total of 60 ground motions, 30 artificial ground motions and 30 recorded ground motions, are used for the fragility analysis. The artificial ground motions generated for Paducah, Kentucky⁽⁷²⁾, which is about 60 km from the studied region, are used in this study. The artificial ground motions were generated for three return periods, 475, 975, and 2,475 years. The selection criteria of the recorded motions include magnitude (~ 6.5), distance (20 to 120 km), and site condition (B). The distance range is broad such that the PGA of the recorded motion can cover a wide range of seismic intensity. PGA of the recorded and artificial ground motions range from 0.05g to 0.74g which covers from

elastic response to fully inelastic response of the bridge. The list of the selected ground motions is presented in Table 27.

Table 27 Recorded ground motions selected for fragility analysis

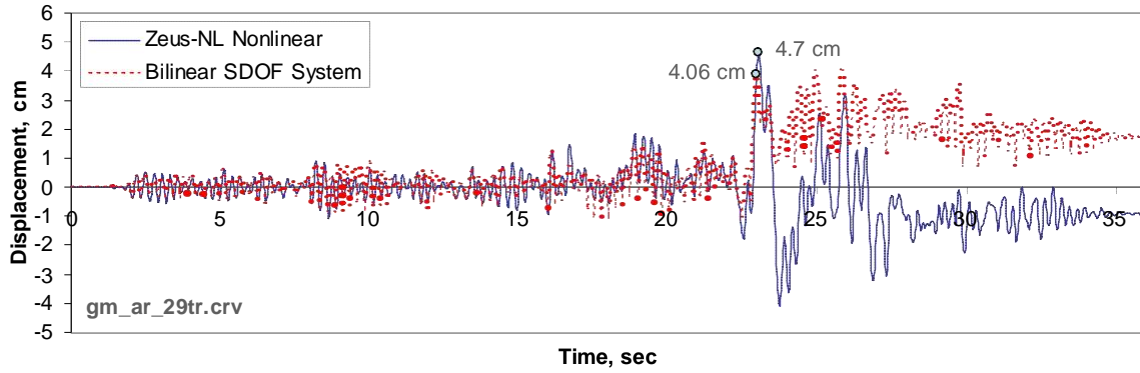
Date	Earthquake	M	Station	Distance, km	PGA,g	
					Comp. 1	Comp. 2
1/17/1994 12:31	Northridge	6.7	14403 LA - 116th St School	41.9	0.21	0.13
2/9/1971 14:00	San Fernando	6.6	24278 Castaic - Old Ridge Route	24.9	0.32	0.27
10/18/1989 0:05	Loma Prieta	6.9	58262 Belmont - Envirotech	49.9	0.11	0.11
1/17/1994 12:31	Northridge	6.7	24157 LA - Baldwin Hills	31.3	0.24	0.17
11/8/1980 10:27	Trinidad, California	7.2	1498 Rio Dell Overpass, E Ground	71.9	0.16	0.13
6/28/1992 11:58	Landers	7.3	23559 Barstow	36.1	0.13	0.14
9/20/1999 1:47	Chi-Chi, Taiwan	7.6	CHY022	71.6	0.07	0.04
9/20/1999 1:47	Chi-Chi, Taiwan	7.6	CHY079	55.0	0.05	0.04
6/28/1992 11:58	Landers	7.3	23 Coolwater	21.2	0.42	0.28
4/25/1992 18:06	Cape Mendocino	7.1	89509 Eureka - Myrtle & West	44.6	0.15	0.18
1/17/1994 12:31	Northridge	6.7	Featherly Park - Pk Maint Bldg	84.2	0.10	0.10
10/18/1989 0:05	Loma Prieta	6.9	1678 Golden Gate Bridge	85.1	0.23	0.12
10/18/1989 0:05	Loma Prieta	6.9	1678 Golden Gate Bridge	85.1	0.12	0.23
1/17/1994 12:31	Northridge	6.7	14196 Inglewood - Union Oil	44.7	0.09	0.10
1/17/1994 12:31	Northridge	6.7	Beverly Hills - 12520 Mulhol	20.8	0.62	0.44
1/17/1994 12:31	Northridge	6.7	24400 LA - Obregon Park	37.9	0.36	0.56
1/17/1994 12:31	Northridge	6.7	24400 LA - Obregon Park	37.9	0.56	0.35
1/17/1994 12:31	Northridge	6.7	24278 Castaic - Old Ridge Route	22.6	0.57	0.51
2/9/1971 14:00	San Fernando	6.6	80053 Pasadena - CIT Athenaeum	31.7	0.09	0.11
7/21/1952 11:53	Kern County	7.4	283 Santa Barbara Courthouse	87.0	0.09	0.13
10/18/1989 0:05	Loma Prieta	6.9	47189 SAGO South - Surface	34.7	0.07	0.07
4/25/1992 18:06	Cape Mendocino	7.1	89530 Shelter Cove Airport	33.8	0.23	0.19
4/25/1992 18:06	Cape Mendocino	7.1	89530 Shelter Cove Airport	33.8	0.19	0.23
9/20/1999 1:47	Chi-Chi, Taiwan	7.6	TCU034	33.0	0.25	0.11
9/20/1999 1:47	Chi-Chi, Taiwan	7.6	TCU045	24.1	0.51	0.47
9/20/1999 1:47	Chi-Chi, Taiwan	7.6	TCU047	33.0	0.41	0.30
9/20/1999 1:47	Chi-Chi, Taiwan	7.6	TCU047	33.0	0.30	0.41
9/20/1999 1:47	Chi-Chi, Taiwan	7.6	TCU095	43.4	0.38	0.71
1/17/1994 12:31	Northridge	6.7	24605 LA - Univ. Hospital	34.6	0.49	0.21
2/9/1971 14:00	San Fernando	6.6	290 Wrightwood - 6074 Park Dr	60.3	0.06	0.04

4.3.1.4 Analysis Results

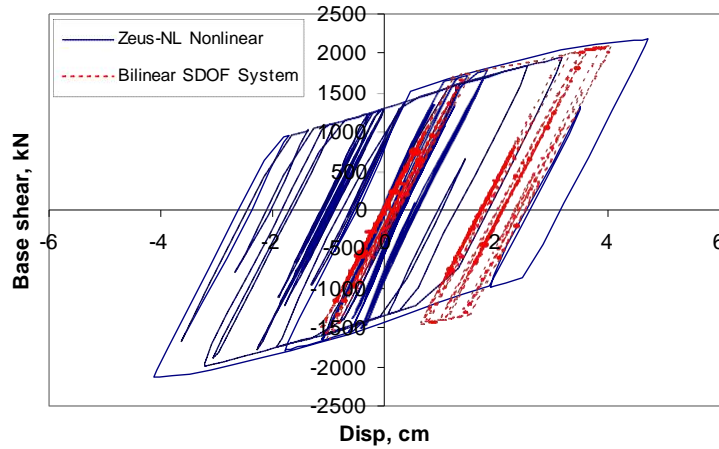
Transverse Direction

Sample inelastic response history analysis results are presented in Figure 126. The solid line in Figure 126(a) represents analysis results from full inelastic model in Zeus-NL while the dashed line in Figure 126(b) is from bilinear SDOF system introduced in the previous section. It can be observed from the figure that responses from full inelastic model are similar to bilinear model at low amplitude vibration. As amplitude of vibration increases, the differences between the two models increase. Even though the maximum responses are similar, permanent drift and response history are different from each other.

As the objective of this study focuses on maximum responses, however, maximum responses of each analysis methods are collected and summarized in Figure 127 as a function of PGA level.



(a) Response history



(b) Hysteretic response curve

Figure 126 Graph. Response of full inelastic and bilinear SDOF models in transverse direction

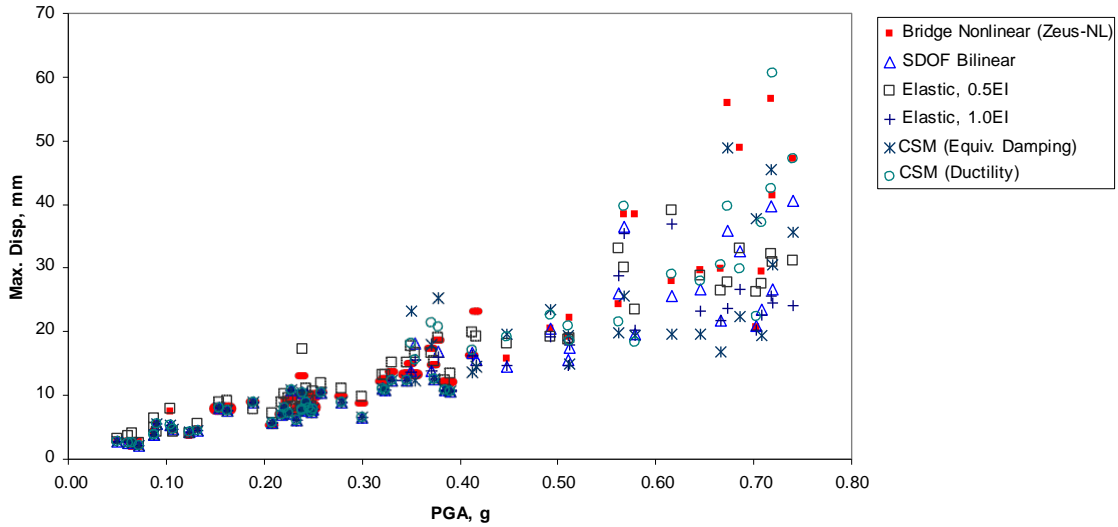


Figure 127 Graph. Maximum transverse response from different analysis methods

It is worth noting that for low intensity ground motion, for example PGA with 0.25g or less, results from several methods are very similar (Figure 127). At this PGA range, the model for SDOF bilinear analysis, elastic analysis with $1.0E_cI_g$, and capacity spectrum methods (CSM) are mostly in the elastic range. These methods are theoretically identical in the elastic range when higher-mode effects are not considered. As the intensity of ground motion increases, the differences from each methods increase.

The maximum responses from approximate methods are normalized by the maximum response from inelastic response history analysis of full inelastic model in Figure 128. To quantify the accuracy of the each method, ground motion intensities are grouped in three PGA ranges, 0~0.25g, 0.25~0.50g, and 0.50~0.75g. Note that these ranges are based on judgment. If different bridge structures is analyzed which yield at very low intensity level or very large intensity level, the above PGA ranges need to be modified. For each PGA range, it is assumed that $\pm 20\%$ of difference from the results of inelastic response history analysis is practically acceptable. Thus accuracy of each approximate method is quantified by estimating percentage of the acceptable responses from approximate methods for each PGA range.

Table 28 summarizes accuracy of each method as a function of the specified PGA range. At low intensity level, 0~0.25 g, elastic response with $0.5 E_c I_g$ shows lowest accuracy. This method tends to overestimate bridge response. At this PGA range, the bridge structure may remain in the elastic range thus assuming low secant stiffness for elastic response history analysis may not be necessary. At intermediate PGA level, capacity

spectrum methods show lowest accuracy. The bilinear SDOF representation of the bridge and two elastic analyses with $0.5E_cI_g$ and $1.0E_cI_g$ have similar accuracy. At large intensity level, all approximate methods show equal or less than 60% of accuracy. Among the evaluated approximate methods, SDOF representation and capacity spectrum method by Chopra and Goel⁽⁶⁴⁾ have highest accuracy. It is worth noting that all approximate methods tend to underestimate maximum responses at large intensity level which may result in non-conservative seismic performance evaluation.

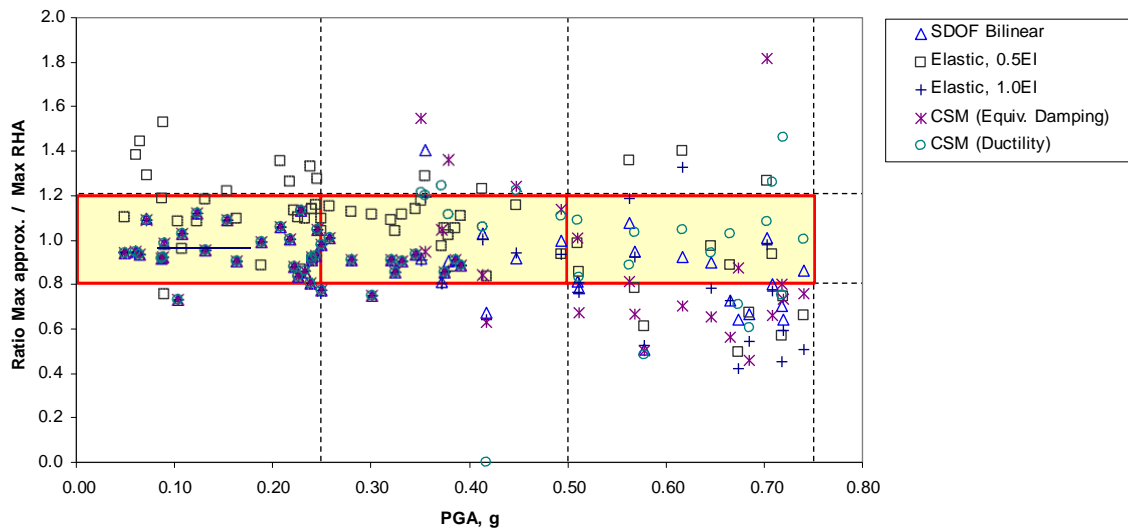


Figure 128 Graph. Maximum transverse responses from approximate methods (normalized by inelastic response history results)

Table 28 Percentage of maximum transverse responses within 20% error bound

PGA Level	SDOF Bilinear	0.5EI Elastic	1.0EI Elastic	CSM Equiv. Damp.	CSM Ductility
0.00 ~ 0.25 g	93% (2, 25, 0)	63% (1, 17, 9)	93% (2, 25, 0)	93% (2, 25, 0)	93% (2, 25, 0)
0.25 ~ 0.50 g	83% (2, 15, 1)	89% (0, 16, 2)	89% (2, 16, 0)	72% (2, 13, 3)	72% (2, 13, 3)
0.50 ~ 0.75 g	53% (7, 15, 0)	33% (7, 5, 3)	27% (10, 4, 1)	27% (10, 4, 1)	60% (4, 9, 2)

Notation: $a\% (b, c, d)$

a : percentage of acceptable response within 20% of error bound. $a = c/(b+c+d)$

b : number responses lower than 80% of the maximum response from NRHA

c : number responses within 20% from the maximum response from NRHA

d : number responses larger than 120% of the maximum response from NRHA

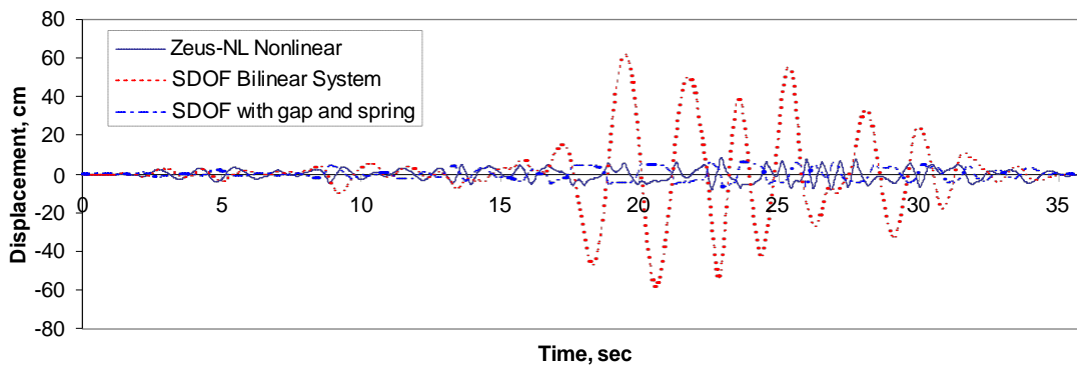
NRHA refers to inelastic response history analysis.

Longitudinal Direction

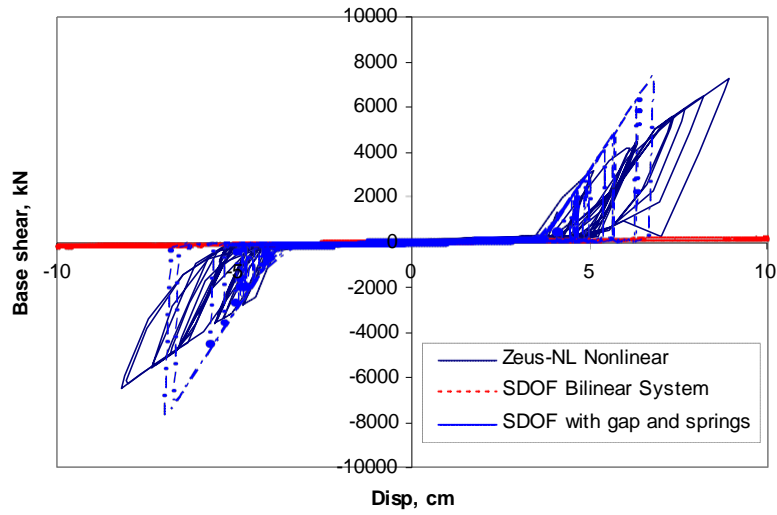
Example response history analysis results in longitudinal direction are presented in Figure 129. For SDOF representation, two different models are used. The first one is

bilinear representation which cannot model gaps and abutments. The second model is SDOF model with combination of multiple springs which can represent the two components. Figure 129(a) illustrates that the maximum response from inelastic model of the full bridge is bounded in certain displacement limit. This boundary is defined by gaps between deck and abutment. As the bilinear SDOF model cannot represent these features, the response can be unreasonably larger than actual inelastic response. The response from the SDOF model with gap and abutment springs is bounded as shown in Figure 129(a). Figure 129(b) presents displacement – force history from response history analysis of two SDOF systems and full inelastic response history model. Note that the SDOF system with bearing and gap model can reasonably represent the response of the full bridge.

The maximum responses from approximate methods are compared with those from inelastic response history analysis (Figure 130). In the longitudinal analysis, two elastic analysis of the whole system are conducted in addition to two SDOF response history analyses. Figure 131 presents normalized maximum responses from approximate methods. It can be easily observed that the accuracy of the approximate methods is much lower in longitudinal direction than in transverse direction presented in Figure 128. This difference can be mainly contributed to the actions of bearings, gaps, and abutments in longitudinal direction. The accuracy of approximate methods in longitudinal direction is quantified in Table 29 following the procedure for the transverse direction. Among the four approximate methods, the SDOF model with GAP and abutment springs has the highest accuracy for all PGA level. All other methods tend to be inaccurate and overestimate the response.



(a) Response history



(b) Hysteretic response curve

Figure 129 Graph. Response of full inelastic and bilinear SDOF models in longitudinal direction

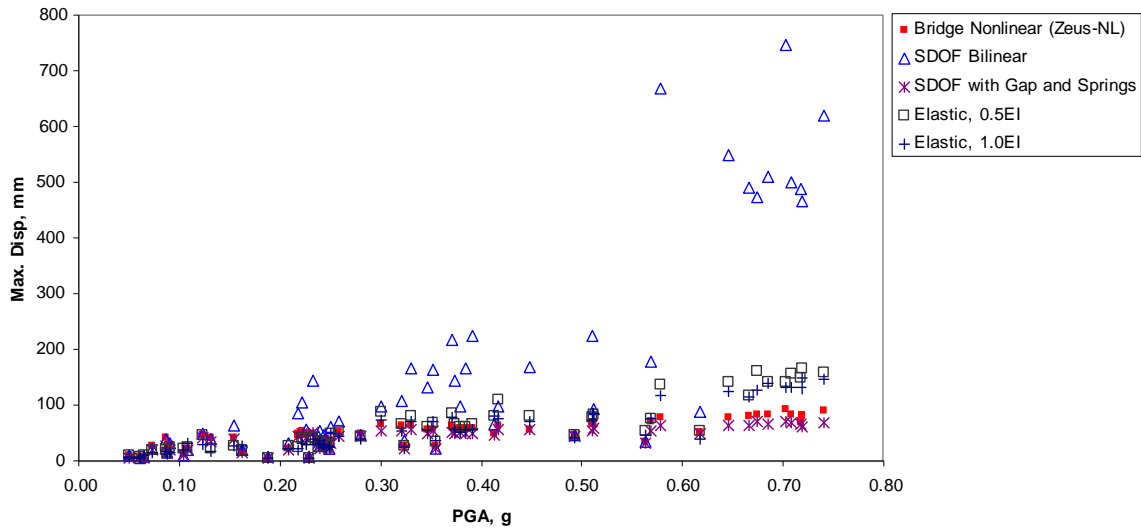


Figure 130 Graph. Maximum longitudinal response from various analysis methods

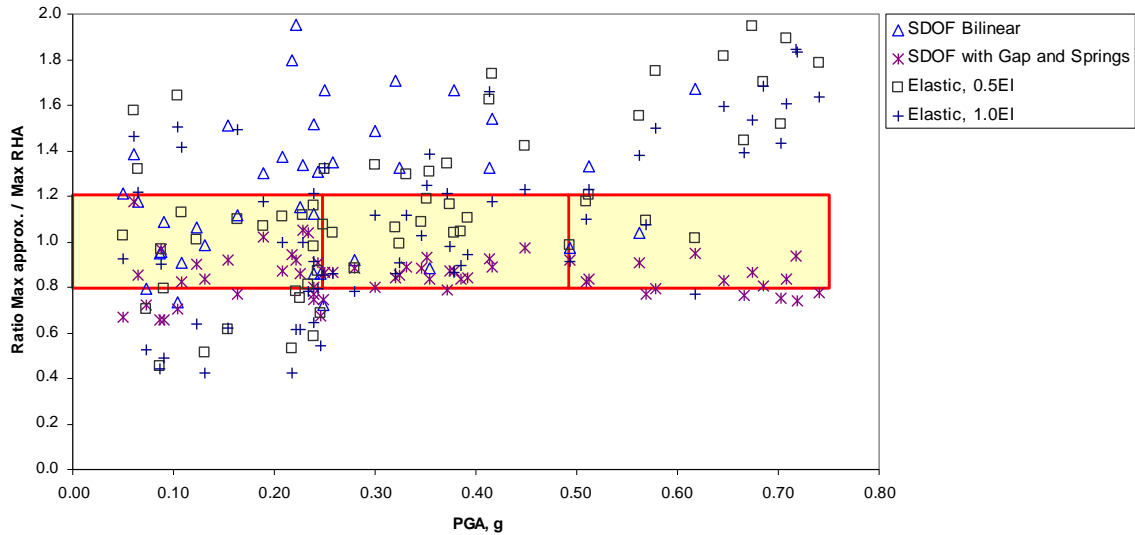


Figure 131 Graph. Maximum longitudinal responses from approximate methods (normalized by inelastic response history results)

Table 29 Percentage of maximum longitudinal responses within 20% error bound

PGA Level	SDOF Bilinear	SDOF w/ Gap & Springs	0.5EI Elastic	1.0EI Elastic
0.00 ~ 0.25 g	44% (3, 12, 12)	63% (10, 17, 0)	48% (10, 13, 14)	26% (13, 7, 7)
0.25 ~ 0.50 g	17% (0, 3, 15)	94% (1, 17, 0)	61% (0, 11, 7)	67% (1, 12, 5)
0.50 ~ 0.75 g	7% (0, 1, 14)	60% (6, 9, 0)	13% (0, 2, 13)	7% (1, 1, 13)

Notation: $a\%$ (b, c, d)

a : percentage of acceptable response within 20% of error bound. $a = c/(b+c+d)$

b : number responses lower than 80% of the maximum response from NRHA

c : number responses within 20% from the maximum response from NRHA

d : number responses larger than 120% of the maximum response from NRHA

NRHA refers to inelastic response history analysis.

4.3.2 Caruthersville Bridge

4.3.2.1 Bridge Configuration

The second example in this study is a 59-span complex bridge. The bridge, Caruthersville Bridge, carries route I-155 over the Mississippi River between Pemiscot County, Missouri and Dyer County, Tennessee. The superstructure consists of eleven units separated by expansion joints and supported on a variety of elastomeric and steel bearings. The main channel crossing is composed of two-span asymmetrical cantilever steel truss and ten-span steel girders, while approach spans are precast prestressed

concrete girders (Figure 132). The substructure includes piers on deep caissons and bents on steel friction piles driven into the near surface silty sands and clayey materials. Bedrock is located 2,700 feet below the sand, gravel, and hard clay strata.

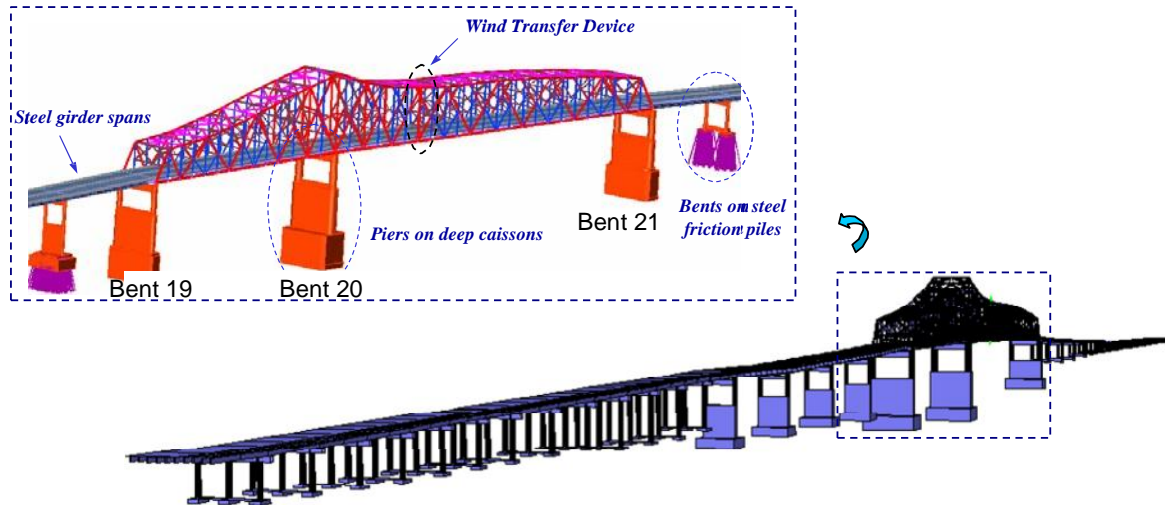


Figure 132 Illustration. Overview of the Caruthersville Bridge⁽⁷⁷⁾

4.3.2.2 Analytical Model

Structural Model for Inelastic Response History Procedure

Detailed three-dimensional dynamic response simulations of the entire bridge including foundations and soil effects are undertaken using a number of analytical platforms. The finite element analysis program, ZEUS-NL⁽⁵⁷⁾, is employed for elastic and inelastic analysis of the structure. The Pacific Earthquake Engineering Research (PEER) Center analysis platform OpenSees⁽⁷³⁾ is used for an inelastic simulation of the foundation and the underlying sub-strata.

Equivalent gravity loads and mass are distributed on the superstructure and along the piers height. The total weight of the bridge is 351,275 kip, which includes superstructure, substructure, non-structural members, pile caps and caissons. As a result of the several deficiencies observed in structural members in the latest available inspection report of the bridge and the lack of reliable information confirming the actual material characteristics, nominal material properties are used in analysis. A bilinear model and a uniaxial constant ‘active’ confinement concrete model are used to idealize steel and concrete, respectively. Bridge bearings and expansion joints are realistically modeled using ZEUS-NL joint

elements. Figure 133 shows the models adopted for the expansion bearings, bronze self-lubricating bearings and structural gaps. The bearing idealizations follow the analytical models suggested by Mander et al.⁽⁶⁸⁾, while a tri-linear asymmetric elasto-plastic idealization capable of representing the slippage and collision are employed to model bridge gaps (e.g. Mwafy et al.⁽⁷⁴⁾).

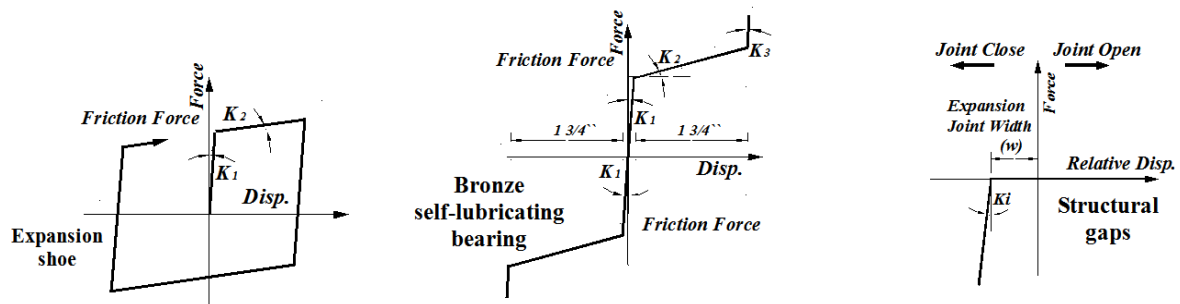


Figure 133 Graph. Spring models for bridge bearings and expansion joints

Based on the soil profile, number of piles and batter angle, thirteen soil-foundation profiles are idealized using OpenSees⁽⁷³⁾. The number of piles of different footings varies from 9 to 112, depending on the supporting loads, while Bent 19, 20, and 21 are supported on massive caisson. The foundation and soil medium are all modeled with 8 node brick elements. Figure 134 describes the OpenSees model and sample results of the Bent 2 foundation system under the effect of cyclic loadings. Trilinear idealizations are adopted to simplify the monotonic pushover curves of different foundation classes to be used as inelastic soil springs for inelastic analysis of the bridge. For further information regarding the bridge model, reference is made to Elnashai et al.⁽⁷⁵⁾.

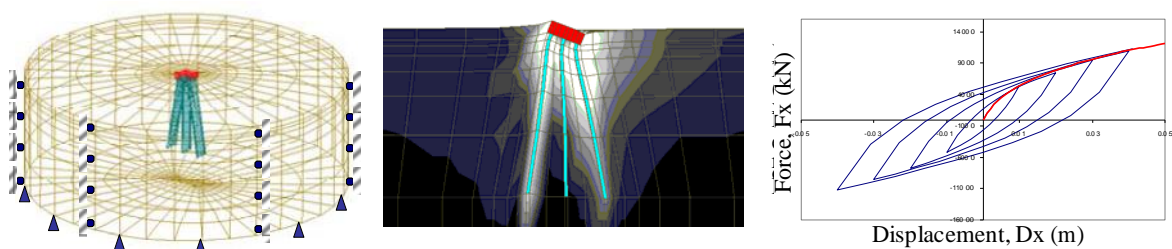


Figure 134 Illustration. OpenSees model and sample results of Bent 2 foundation system

Structural Models for Elastic Response History Procedure

Models for elastic response history analyses are identical to the inelastic model except that initial stiffness is used for bearings and foundations, and $0.5E_cI_g$ and $1.0E_cI_g$ are used for bents.

4.3.2.3 Input Ground Motions

Probabilistic Seismic Hazard Analyses (PSHA) for hard rock site conditions were performed for the bridge⁽⁷²⁾. The results of the analyses include hazard curves, uniform hazard spectra (UHS) and suites of ground motions compatible with the UHS for hard rock site conditions. Three hazard levels were considered in the analysis, 10%, 5%, and 2% of probability of exceedance in 50 years, corresponding to return periods of 500, 1000 and 2500 years. The PSHA analysis provided 10 records of spectrum compatible ground motion time series for each of the three hazard levels - 10%, 5%, and 2% of probability of exceedance in 50 years - corresponding to return periods of 500, 1000 and 2500 years. Three records (1, 2 & 3) were selected from the 10 records for propagation through the thick embayment deposits. Using the selected bedrock motion, one-dimensional seismic site response analyses were conducted to account for the influence of the thick deposits on the computed ground motion⁽⁷⁶⁾. Given the length of the structure, ground motion incoherence, including wave passage, was included in the propagated ground motion. In this study, however, uniform ground excitation is assumed to focus on the difference in inelastic analysis and elastic analysis. Total nine ground motions, three ground motions in three return periods, are used for longitudinal analysis and transverse analysis. Figure 135 shows sample input ground motions with 500 year return period.

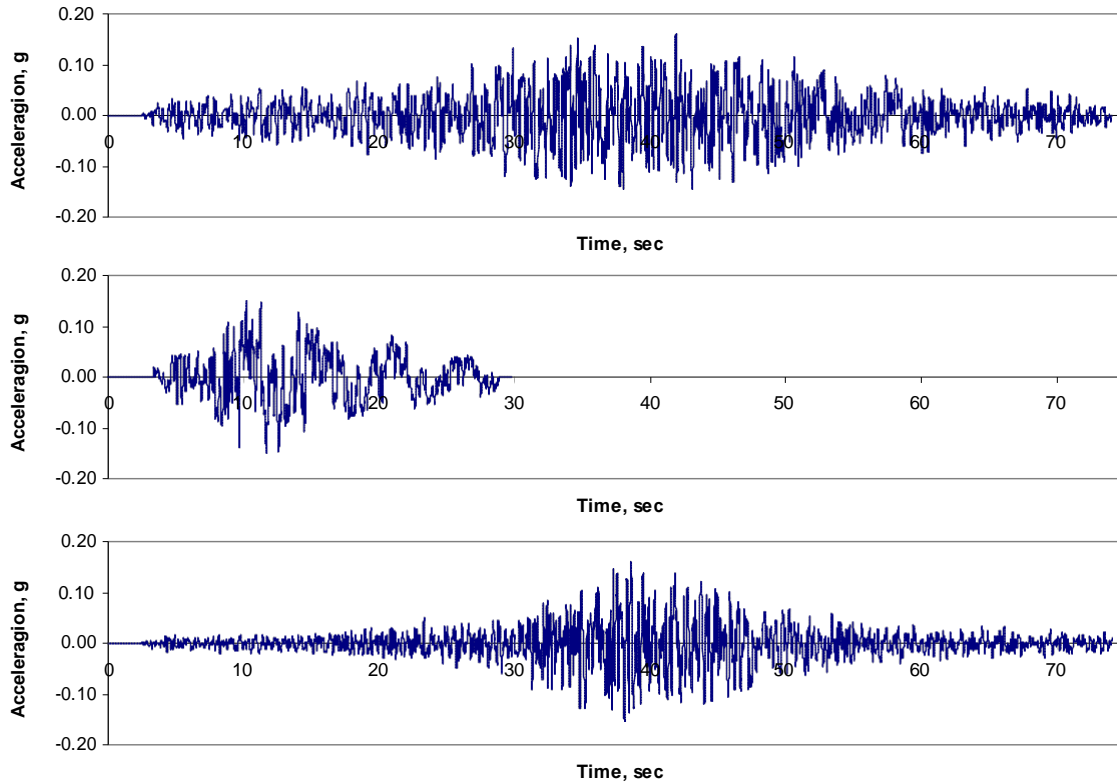


Figure 135 Graph. Input ground motions with 500 year return period

4.3.2.4 Results

A total of 54 analyses are conducted. Three different models; inelastic, elastic with bent stiffness of $0.5E_cI_g$, and elastic with bent stiffness of $1.0E_cI_g$, are subjected to 9 ground motions in longitudinal and transverse directions. Out of the 18 analysis for inelastic structural model, seven analyses are completed successfully without divergence issue. The remaining eleven analyses could not be completed due to numerical stability of the analytical model, indicating a level of deformation corresponding to complete collapse, especially at gaps and joints. The seven successful analyses are sufficient to show the differences between inelastic analysis and elastic analysis. In Table 30, analysis cases with shaded background represent analyses that are used to compare the effect of different analytical approaches. Analysis results of 15 representative bents in Figure 136 are monitored including forces at foundations, piers, and bearings. Figure 137 depicts monitored values of the bridge.

Table 30 Converged inelastic response history analysis

Direction	Ground Motion	Total duration	Converged duration		
			0.5EI	1.0EI	Inelastic
L	GM1-0500	74.03	74.00	74.00	74.00
L	GM1-1000	74.03	74.03	74.00	41.38
L	GM1-2500	73.00	73.00	73.00	37.78
L	GM2-0500	29.82	29.00	29.00	29.00
L	GM2-1000	30.20	29.00	29.00	29.00
L	GM2-2500	29.80	29.03	29.00	12.00
L	GM3-0500	74.50	74.00	74.00	74.00
L	GM3-1000	74.50	74.03	74.00	37.25
L	GM3-2500	79.20	79.03	79.00	36.83
T	GM1-0500	74.03	72.78	72.75	72.75
T	GM1-1000	74.03	26.98	19.25	32.15
T	GM1-2500	73.00	13.55	15.08	33.20
T	GM2-0500	29.82	29.00	29.00	29.00
T	GM2-1000	30.20	29.03	13.15	10.70
T	GM2-2500	29.80	12.20	15.40	9.18
T	GM3-0500	74.50	74.00	74.00	74.00
T	GM3-1000	74.50	36.45	52.90	36.28
T	GM3-2500	79.20	29.43	29.43	79.00

Note that only shaded analysis cases are converged for all 0.5EI, 1.0EI, and inelastic analysis

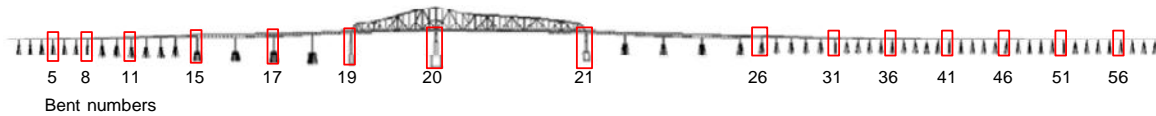


Figure 136 Illustration. Monitored bents during response history analysis

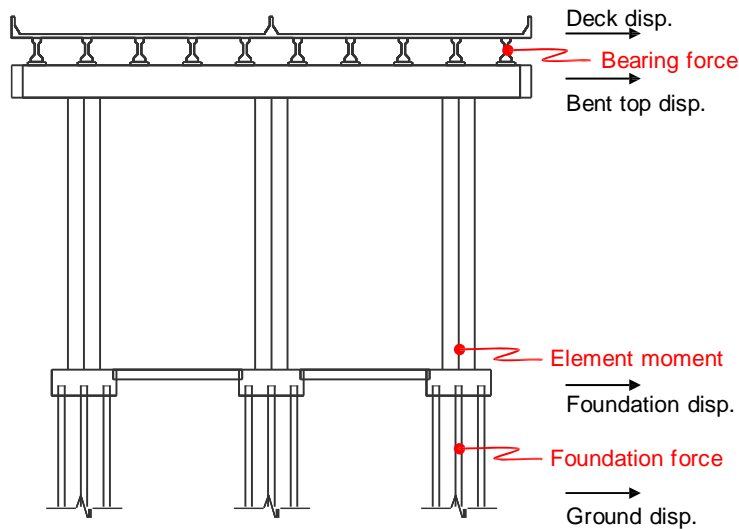


Figure 137 Illustration. Monitoring points at each bents

Transverse Direction

A sample transverse response history of the bridge subjected to ground motion GM2-500 is depicted in Figure 138. The figure shows bridge deck response at Bent 8, 17, and 21. It can be observed from the figure that response history from inelastic analysis and elastic analysis with $1.0 E_c I_g$ are similar in terms of frequency content and amplitude. The amplitude of elastic response with $0.5 E_c I_g$ is larger than inelastic response. From this observation, it can be noted that the intensity of the ground motion does not cause severe inelasticity to inelastic structure. In addition, the stiffness of elastic model with $0.5 E_c I_g$ does not represent the response of the bridge well in comparison with elastic model with $1.0 E_c I_g$ at this intensity level.

Figure 139 depicts sample foundation response of the bridge. Most of the foundation remained elastic. Only a few foundation of the bridge subjected to ground motion with 500 year return period yielded in transverse direction. As noted earlier, the displacement-force relationship of the foundation of the elastic models follow the initial stiffness of inelastic foundation model.

Figure 140 presents displacement of bent defined as the difference between bent top displacement and foundation displacement and bending moment at the bottom of each pier, Figure 137. Note that at this ground motion level in transverse direction, the bents do not yield significantly. Also it can be observed that the displacement-force relationship of $1.0 E_c I_g$ model is very close to the initial stiffness while that of $0.5 E_c I_g$ model is very close to secant stiffness at maximum displacement level.

The maximum response of decks at each monitored bent are normalized with the maximum response from inelastic response history analysis and plotted in Figure 141. Responses from three ground motions are plotted together in the same figure. At this ground motion level, it can be clearly seen that the elastic model with $0.5 E_c I_g$ overestimates response for all bents and the elastic model with $1.0 E_c I_g$ underestimates response of most of the bents.

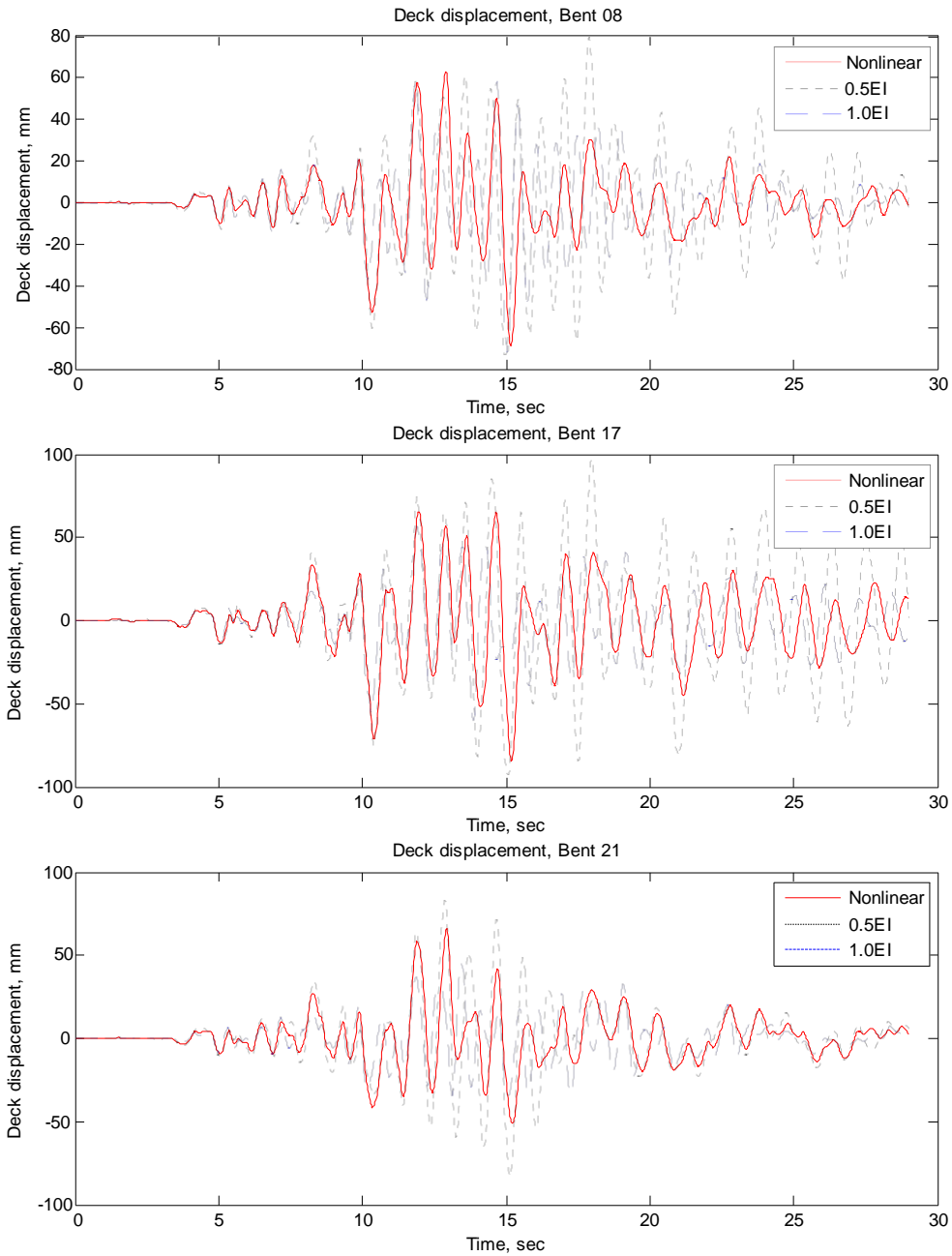


Figure 138 Graph. Sample transverse response history of bridge decks, GM2-500

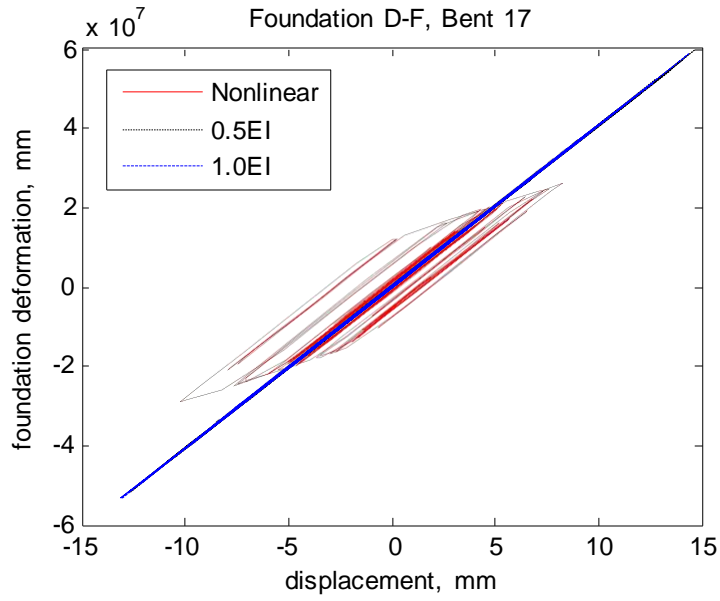


Figure 139 Graph. Sample foundation response in transverse direction

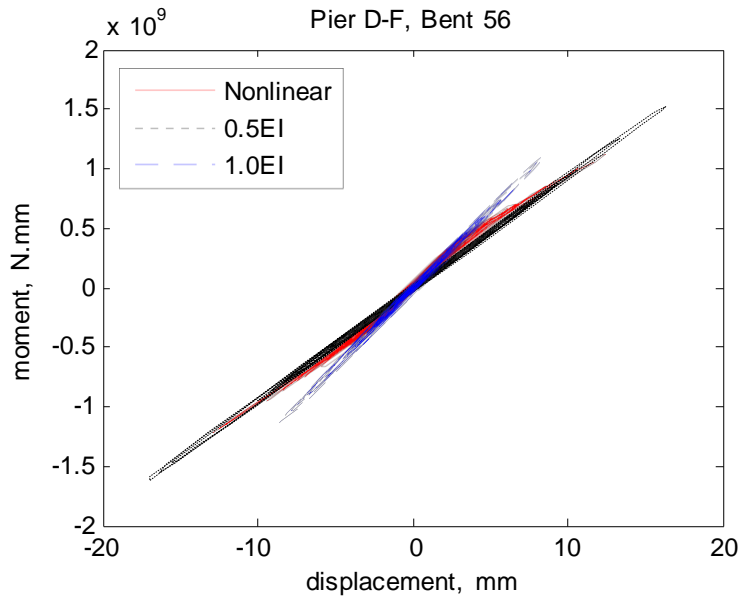


Figure 140 Graph. Sample transverse hysteretic response of bridge piers

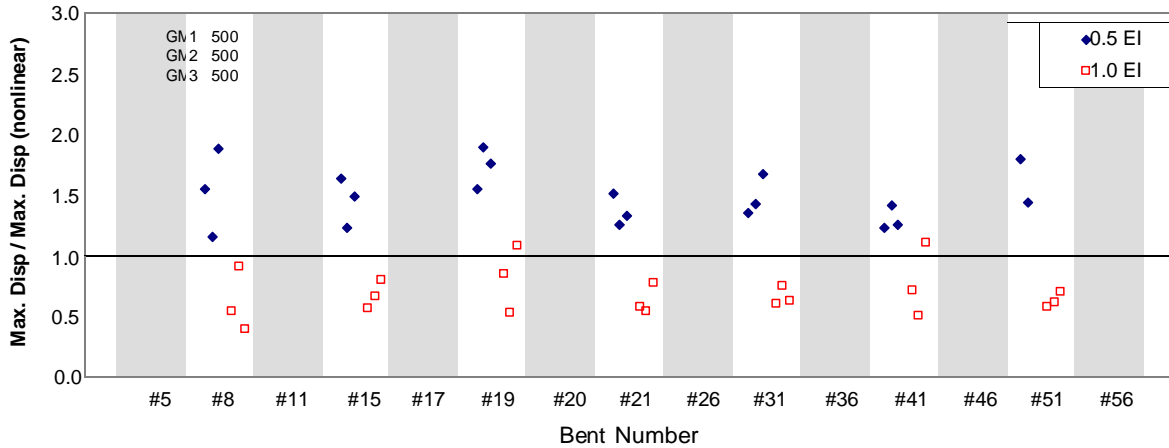


Figure 141 Graph. Normalized maximum transverse deck response from two elastic analyses

Longitudinal Analysis

The inelastic analysis of the bridge subjected to ground motion with 1000 year return period was successfully completed. Figure 142 presents response history of bridge decks at different bents subjected to GM2-1000. Unlike transverse response in Figure 138, the longitudinal response from inelastic analysis shows clearly different frequency content from the response of elastic response history analyses.

At this ground motion level, most of the foundations remain in range. A few foundations experience inelastic deformation as shown in Figure 143. Most piers show inelastic responses. As presented in Figure 144, the moment-displacement relationship of $1.0E_cI_g$ model matches initial stiffness of the inelastic model. Stiffness of $0.5E_cI_g$ is between that of $1.0E_cI_g$ model and secant stiffness of inelastic model at maximum displacement. It can be observed that the inelastic model, in general, shows much less stiffness than $0.5E_cI_g$ during inelastic deformation.

Normalized maximum longitudinal responses are presented in Figure 145. It can be noted that both elastic analysis with $0.5E_cI_g$ and $1.0E_cI_g$ underestimate bridge responses at most bents except Bents 15, 17, and 19.

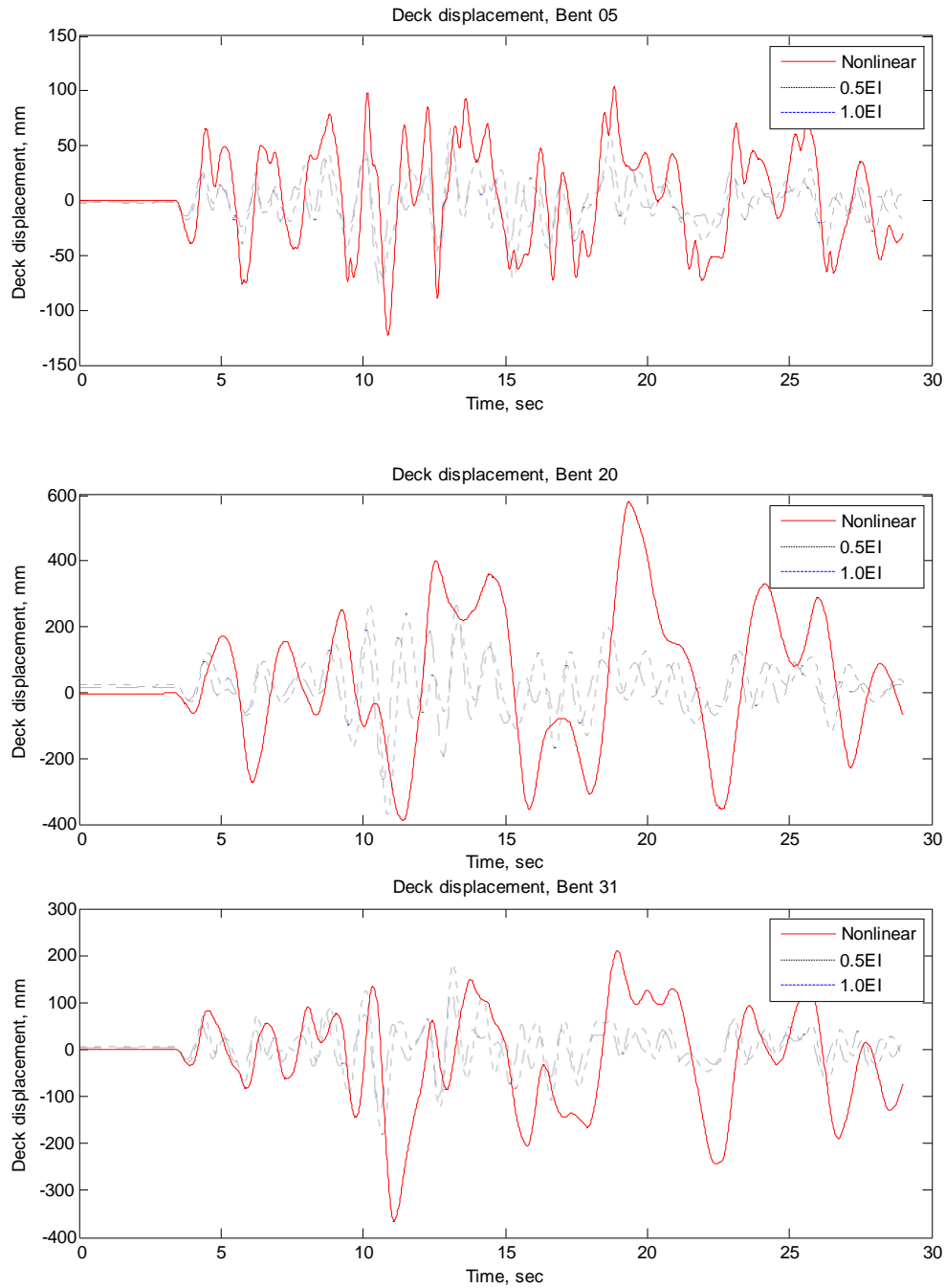


Figure 142 Graph. Sample longitudinal response history of bridge decks, GM2-1000

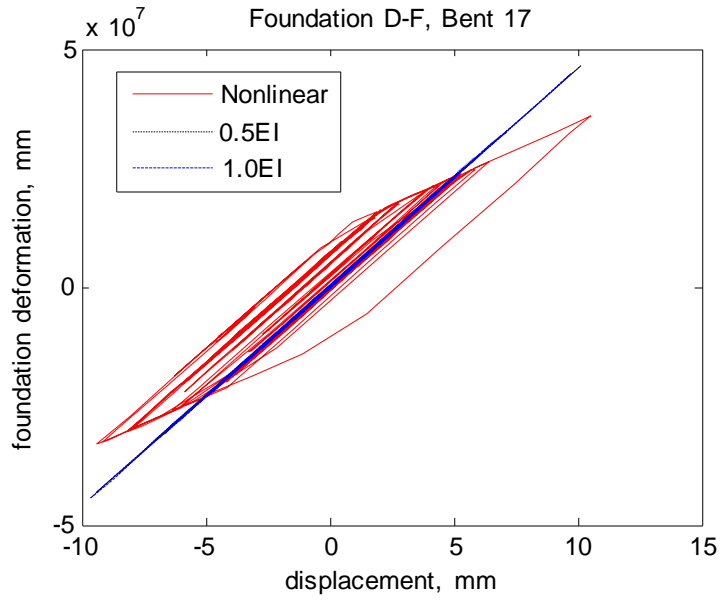


Figure 143 Graph. Sample foundation response in longitudinal direction

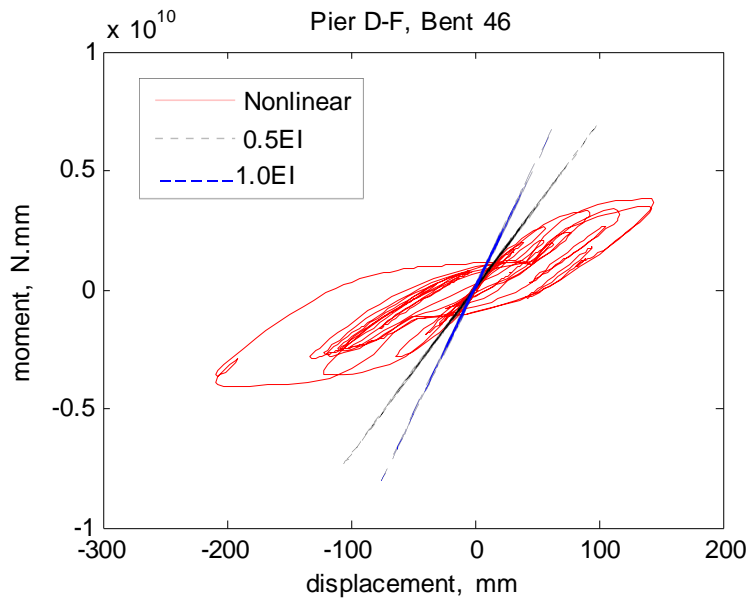


Figure 144 Graph. Sample longitudinal hysteretic response of bridge piers

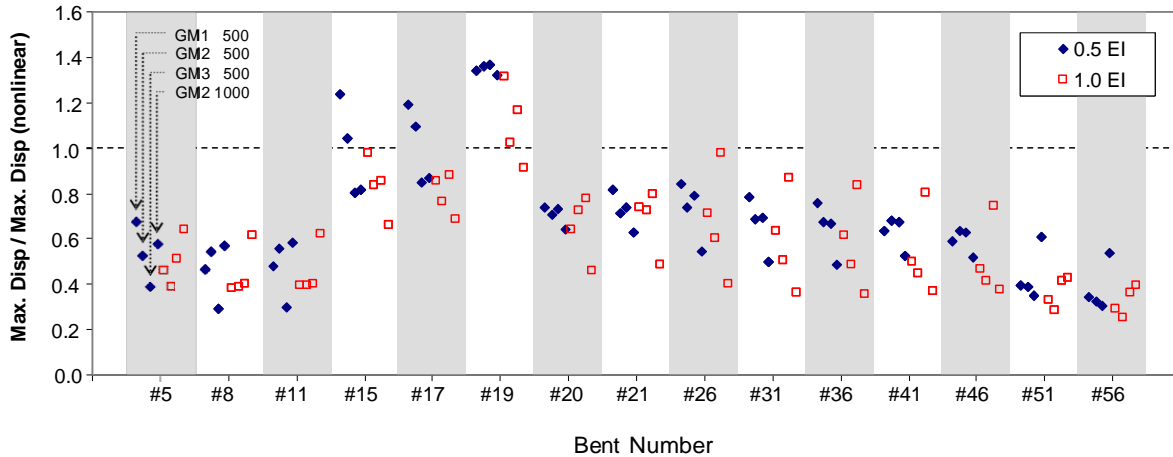


Figure 145 Graph. Normalized maximum longitudinal deck response from two elastic analyses

4.4 ASSESSMENT OF EVALUATION PROCEDURE

Two bridge structures, a Central-Eastern US regular bridge and an irregular complex 59-span bridge, are analyzed using several approximate analysis procedures. The followings are the main observations and conclusions drawn from the study.

Inelastic Response History Analysis

The inelastic behavior of structural materials, bearings, foundations, gaps, and abutments is modeled, alongside geometric nonlinearity. The response history analysis with inelastic bridge model is the most realistic method for the seismic response assessment of bridge structures as long as the inelastic characteristics of the bridge components are realistically represented. The responses of the two example bridges showed that the inelastic system is capable of representing the opening and closure of gaps, inelasticity in foundations, bearings, and structural members. The analyses also reiterate the very significant demand for computational effort. Convergence of analysis for the complex bridge which is highly irregular and contains many zero-stiffness gaps and joints was a serious challenge. Convergent solutions however represent a more reliable estimate of action and deformation demands imposed on the structure and its constituents.

Elastic Response History Analysis

Elastic response history analysis with $0.5E_cI_g$ and $1.0E_cI_g$ are conducted. In the first example, Section 3.1, the model with elastic stiffness of $0.5E_cI_g$ tends to overestimate transverse responses at low amplitude level. The model with $1.0E_cI_g$ shows better

accuracy in transverse direction at the low intensity ground motions. On the contrary, the model with $0.5E_cI_g$ performs better in longitudinal direction at low intensity motion. In the longitudinal direction, expansion bearings mobilize friction even at low intensity level. Hence overall structural period elongates right after bearings start sliding. The elastic model with $0.5E_cI_g$ can approximately represent this feature. At intermediate intensity level, the accuracy of two elastic models is very similar in both directions. In the transverse direction, around 90% of analyses cases are acceptably accurate while in the longitudinal direction around 65% are acceptable. At large intensity level, the accuracy of both elastic models is not good with acceptable analysis cases of around 30% in the transverse direction and around 10% in the longitudinal direction. In the second (complex bridge) example, the model with $0.5E_cI_g$ overestimated the transverse deck responses at all bents while the model with $1.0E_cI_g$ underestimated transverse deck response. In the longitudinal direction, both models underestimated deck responses except at a few locations.

It is clear that using elastic models could be highly inaccurate. The level of accuracy of elastic models depends on the ground motion intensity and excitation direction, which indicate that features of the bridge are influential. The difference between elastic and inelastic response history analysis can be as large as several hundred percent. Thus extreme scrutiny and engineering judgment are required in interpreting elastic analysis result. Results from elastic analysis could be conservative or unconservative, and their tendencies cannot be judged a priori.

Inelastic SDOF Response History Analysis

Inelastic SDOF response history analyses are conducted for the first bridge example. The results show that bilinear SDOF model or SDOF model with bearing and gap elements can successfully represent inelastic response of a regular bridge which behaves mostly in the first, or a single, mode. The longitudinal direction analysis of the bridge confirms that the inelastic characteristics of the SDOF system should be able to represent inelastic characteristics of the bridge. Cyclic pushover analysis of a bridge is suggested to model inelastic SDOF system.

Capacity Spectrum Methods

Two capacity spectrum methods are evaluated in this study with the first bridge example. The capacity spectrum methods are applied only to transverse direction as the capacity

curve of a bridge in longitudinal direction is very different from the pushover curves that are used to verify capacity spectrum methods in the literature. The capacity spectrum method in the transverse direction shows similar accuracy at low-to-intermediate ground motion intensity levels. At large intensity levels, the capacity spectrum method by Chopra and Goel⁽⁶⁴⁾ showed higher accuracy than the method in ATC-40⁽⁴³⁾. As the capacity spectrum methods cannot be used to estimate responses with significant higher mode effects (without further assumptions for inelastic response combination), the application of CSM is limited to a regular bridge structure. In addition, the application of CSM method to longitudinal response needs careful verification to take account of the effect of bearings, gaps, and abutments.

5 SUMMARY AND RECOMMENDATIONS

DEVELOPMENT IN DESIGN SPECIFICATIONS

1. The NCHRP 12-49 recommendations consist of much higher ground motion intensity in life safety assessment than that used in the AASHTO Standard Specifications in the concerned states of this study. This elevated design requirement may be offset by the more generous force reduction (R-factors) when advanced analysis methods are used (SPAD E). Some recent comparative studies have not taken such advantage and therefore shown tremendous increase in construction cost by using the recommended provisions.
2. The “Operational” performance objective in NCHRP 12-49 recommendations has more severe requirements than “Critical” bridges in AASHTO Standard Specifications.
3. Although the cap of site coefficient used in determination of Seismic Hazard Level reduces the design effort to a certain degree, the NCHRP 12-49 recommendations requires seismic demand analysis for bridges in a broader area than AASHTO Standard Specifications (Figure 38).
4. The AASHTO Guide Specifications 2007 (NCHRP 20-7 Task 193) uses a single level life safety assessment ground motion that is lower than the MCE used in NCHRP 12-49 recommendations. Design effort is comparable to that of the AASHTO Standard Specifications (Figure 35). It is not expected to increase construction cost of bridges.
5. The explicit displacement capacity verification (pushover analysis) is an important new analysis option (or requirement, as in AASHTO Guide Specifications) that allows the full advantage of ductile structure to be utilized. The FHWA developed a computer application (on separate funding) for quick pushover analysis to ease the implementation of the new analysis procedure.
6. Further study on the design effort and construction cost using AASHTO Guide Specifications is recommended. Since the seismic hazard specifications and design approach (displacement design) cannot be directly compared with the AASHTO Standard Specifications, a number of bridges at various locations and having different

functionalities should be investigated for this purpose to cover effect from all possible factors.

GROUND MOTION SIMULATION IN CSUS

Although definitive answers for the two questions raised in 2.2 may not yet be available at any given time due to the continuous improvement of ground motion models in the CSUS, some recommendations may be provided based on recent research results:

1. USGS seismic hazard maps are produced by including multiple models with a logic tree formalism. The 1996 update consists of only one-corner ground motion model and may not be optimized for the use in CSUS. The 2002 update includes a 2-corner model, a finite-fault model, and a hybrid model, as well as other adjustments that represent latest findings. It is recommended that the 2002 update is used for bridge design and retrofitting purpose in CSUS.
2. The site coefficients used in NCHRP 12-49 recommendations and AASHTO Guide Specifications are based on those used by NEHRP provisions. These coefficients are not produced with consistent PSHA procedure that produces the base ground motion and may not represent the unique near-surface geological composition in this area. Before more comprehensive study is done to address this discrepancy, a set of modification curves⁽¹⁸⁾ may serve as a reference for various soil layer thickness in the Mississippi Embayment area.
3. For critical bridges with vibration period close to the range of 0.3~0.5 second and located over deep soil layers, site-specific study is recommended to ensure the significant amplification from soil column resonance is captured by the design spectrum.
4. Further study on site effect in the CSUS is recommended to obtain suitable adjustment on the NEHRP site coefficients that can be used in broader area and various soil types in the CSUS.

FHWA GROUND MOTION TOOL

A computer tool that provides essential design ground motion parameters (design spectrum, SHL, SDC, etc.) is developed and provided for the bridge engineers in CSUS

free of charge. This tool uses the 2002 update of USGS seismic data and can be used for the ease of implementation of latest design and retrofitting documents.

SEISMIC VULNERABILITY AND RETROFIT OF BRIDGES

Seismic vulnerability and practice of bridge retrofit in the CSUS area are reported in Chapter 3. Based on the nonlinear dynamic analysis, seismic vulnerability of critical bridge components for 9 bridge classes is identified. The results show that each class of bridges exhibit vulnerable to earthquake loads at various parts of substructure and bearings, with an exception of single-span concrete bridges. Potential failure mechanisms include short support lengths, inadequate transverse reinforcement, and inadequate bearings, which may result in shifted superstructure/falling span, column failure, pounding damage, and bearing damage.

Recognizing the inadequate technical support for evaluating the impact of the various retrofit measures on the seismic performance of bridges in the CSUS region or selecting measures appropriate for these bridges, a comprehensive review of bridge retrofitting techniques used in the CSUS is offered in Chapter 3. Examples of the current state of practice in seismic retrofit of bridges in the CSUS are presented, with details of specific cases in each state listed in appendices. This includes protection of a number of different bridge components using a range of retrofit measures and approaches, including:

1. Column Retrofits
2. Isolation
3. Restrainers
4. Other Longitudinal Restraint and Response Modification
5. Shear Keys
6. Seat Extenders and Catcher Blocks
7. Bent Retrofits

Qualitative discussion on the level of vulnerability provides an overview on the most potent retrofitting method for specific bridge types and components. This can be a good reference to consider retrofitting techniques to be used. For example, the MSC steel girder bridges are found vulnerable to seismic loads and prone to incur damage to their

steel bearings. Replacement of these bearings would produce significant increase in resilience to earthquake. Similar discussions on various bridge types can be found in Section 3.6.2. More detailed calculation involving the cost of retrofitting and benefit through the remaining service life in dollar amount can offer quantitative support to the selection of retrofitting strategies. Results of cost-benefit analysis vary for different locations and structural systems. Fragility parameters provide critical information for necessary calculations on expected life cycle cost associated with different retrofitting strategies. Examples of such calculation can be found in Section 3.6.3.

SEISMIC PERFORMANCE EVALUATION PROCEDURES

In Chapter 4, several approximate procedures for seismic response evaluation of bridges are evaluated. Two bridge structures, one 4-span regular bridge and another irregular 59-span complex bridge, are analyzed. The analysis results from approximate procedures are compared with results from inelastic response history analysis. The comparison shows that the applicability of approximate methods highly depends on ground motion characteristics as well as dynamic characteristics of the bridge. As bridge structures are inherently very different from building structures, due to bearings, foundations, gaps, and abutments, the approximate methods especially developed and calibrated for building structures needs careful reevaluation. The inelastic response history analysis is the most realistic. Notwithstanding, the inelastic response history analysis of complex bridge is computationally demanding. Cases where the simplified procedures yielded acceptably accurate results are presented in Chapter 4 of this report.

ACKNOWLEDGEMENTS

The authors wish to thank all those that have assisted in the development of this document. In particular, we would like to acknowledge the following individuals that provided us with valuable information, access to their bridges, and contributed their time. As special thanks is extended to the following:

Mr. Ed Wasserman

Tennessee Department of Transportation

Ralph Anderson & Daniel H. Tobias

Illinois Department of Transportation

Allen Thomas

Kentucky Transportation Cabinet

Mark Capron

Jacobs Civil Inc.

Robert Turner & Brad Ridgley

Indiana Department of Transportation

REFERENCES

1. ATC/MCEER, (2002), Comprehensive Specification for the Seismic Design of Bridges, NCHRP REPORT 472.
- 2 BSSC, (2001), NEHRP Recommended Provisions for Seismic Regulations for Buildings and Other Structures.
3. Boore, D. M. (2003), "Simulation of Ground Motion Using the Stochastic Method," *Pure appl. geophys.* 160 (2003) 635–676
4. Applied Technology Council. (ATC), 1978, Tentative Provisions for the Development of Seismic Regulations for Buildings, ATC 3-06 Report, Redwood City, CA.
5. Dobry, R.; Borcherdt, R. D.; Crouse, C. B.; Idriss, I. M.; Joyner, W. B.; Martin, G. R.; Power, M. S.; Rinne, E. E.; and Seed, R. B. (2000); "New Site Coefficients and Site Classification System Used in Recent Building Seismic Code Provisions," *Earthquake Spectra*. Volume 16, No.1, February 2000.
- 6 Arthur D. Frankel, Mark D. Petersen, Charles S. Mueller, Kathleen M. Haller, Russell L. Wheeler, E.V. Leyendecker, Robert L. Wesson, Stephen C. Harmsen, Chris H. Cramer, David M. Perkins, and Kenneth S. Rukstales, (2002), Documentation for the 2002 Update of the National Seismic Hazard Maps, USGS Open File Report 02-420.
- 7 M. Ala Saadeghvaziri, (2004), Implementation of Recommended LRFD Guidelines (NCHRP 12-49) for Seismic Design of Highway Bridges in New Jersey, FHWA-NJ-2004-019 Report, December 2004
- 8 Imbsen, R.; (2001), Updating "Recommended LRFD Guidelines for the Seismic Design of Highway Bridges."
- 9 Ger, J., Straatmann, D., Patel, S., Gupta, S.; (2002), "Cost Impact Study for a Typical Highway Bridge Using Different Return Period Seismic Design Maps," *Proceedings of the Third National Seismic Conference and Workshop on Bridges and Highways*, MCEER, March 11, 2002
- 10 Panahshahi, N., Cross, W. B., Arjomandnia, N., Emami, B., Biller, J., Ivanov, G., Shrestha, S., Arab, A., Kumar, S., Marianos, Jr., W. N., Pezeshk, S.; (2004),

“Evaluation of Comprehensive Seismic Design of Bridges (LRFD) in Illinois,”
Illinois Transportation Research Center, Report No. ITRC FR 02-3, Illinois
Department of Transportation

- 11 Arthur Frankel, Charles Mueller, Theodore Barnhard, David Perkins, E.V. Leyendecker, Nancy Dickman, Stanley Hanson, and Margaret Hoppe; 1996, National Seismic-Hazard Maps: Documentation June 1996, USGS Open-File Report 96-532.
- 12 Atkinson, G.M. and D. M. Boore (1995). Ground motion relations for eastern North America, *Bull. Seism. Soc. Am.*, v. 85, pp. 17-30.
- 13 Toro, G.R., N.A. Abrahamson and J.F. Schneider (1997). A Model of Strong Ground Motions from Earthquakes in Central and Eastern North America: Best Estimates and Uncertainties. *Seismological Research Letters*, v.68, no. 1, pp. 41-57.
- 14 Atkinson, G. M. and Boore, D. M. (2006), “Earthquake Ground-Motion Prediction Equations for Eastern North America,” *Bulletin of the Seismological Society of America*, Vol. 96, No. 6, pp. 2181–2205, December 2006, doi: 10.1785/0120050245
- 15 Borchardt, Roger D., 2002, “Empirical Evidence for Site Coefficients in Building Code Provisions,” *Earthquake Spectra*, Volume 18, No. 2, pages 189–217, May 2002.
- 16 Wen, Y.K., Wu, C.L.; (2001), “Uniform Hazard Ground Motions for Mid-America Cities,” *Earthquake Spectra*. Volume 17, No.2, May 2001
- 17 Romero, S.M. and Rix, G.J. (2001). "Ground motion amplification in the Upper Mississippi Embayment." GIT-CEE/GEO-01-1, National Science Foundation Mid America Center, Atlanta.
- 18 D. Park and Y.M.A. Hashash (2004); “Integration of Probabilistic Seismic Hazard Analysis with Nonlinear Site Effects and Application to the Mississippi Embayment,” *Proc. 2004 ANSER Annual Meeting: Networking of Young Earthquake Engineering Researchers and Professionals*, July 28-30, 2004, The Sheraton Princess Kaiulani, Honolulu, Hawaii.
- 19 Pezeshk, S., Hashash, Y., Park, D.; (2004), *Non-Linear Seismic Site Response of Deep Deposits in West Tennessee*, Final Report for Tennessee Department of Transportation

- 20 Lin, T., Gambel, W.L., and Hawkins, N.M., "Seismic Behavior of Bridge Column Non-Contact Lap Splices, SRS No. 622, Department of Civil and Environmental Engineering, University of Illinois at Urbana-Champaign, June 1998.
- 21 CUSEC (2000). "Earthquake Vulnerability of Transportation Systems in the Central and Southeastern US." Central US Earthquake Consortium and US Department of Transportation.
- 22 Chai, Y. H., M. J. N. Priestley and F. Seible, 1991. Seismic Retrofit of Circular Bridge Columns for Enhanced Flexural Performance, *ACI Structural Journal (American Concrete Institute)* 88(5), 572-584.
- 23 Saiidi, M., M. Randall, E. A. Maragakis and T. Isakovic, 2001. Seismic Restrainer Design Methods for Simply Supported Bridges, *Journal of Bridge Engineering* 6, pp. 307-315.
- 24 DesRoches, R., T. Pfeifer, R. T. Leon and T. Lam, 2003. Full-Scale Tests of Seismic Cable Restrainer Retrofits for Simply Supported Bridges, *Journal of Bridge Engineering* 8, 191-198.
- 25 DesRoches, R., E. Choi, R. T. Leon and T. Pfeifer, 2004b. Seismic Response of Multiple Span Steel Bridges in Central and Southeastern United States. II: Retrofitted, *Journal of Bridge Engineering* 9.
- 26 Mackie, K. and B. Stojadinovic, 2004. Fragility Curves for Reinforced Concrete Highway Overpass Bridges, 13th World Conference on Earthquake Engineering, Vancouver, B.C., Canada, August 1-6.
- 27 DesRoches, R., E. Choi, R. T. Leon and T. Pfeifer, 2004a. Seismic Response of Multiple Span Steel Bridges in Central and Southeastern United States. I: As Built, *Journal of Bridge Engineering* 9.
- 28 FHWA, 2006. Seismic Retrofitting Manual for Highway Structures: Part 1 - Bridges, Report No. FHWA-RD (MCEER-06-xxxx), Federal Highway Administration,
- 29 Priestley, M. J. N., Seible, F., and Calvi, G. M. (1996). *Seismic Design and Retrofit of Bridges*. John Wiley and Sons, New York.

- 30 Stanton, J. F. and Roeder, C. W. (1992). "Elastomeric Bearings: An Overview." *Concrete International: Design and Construction*, 14(1), 41–46.
- 31 Wendichansky, D. A., Chen, S. S., and Mander, J. B. (1995). "In-Situ Performance of Rubber Bearing Retrofits." *National Seismic Conference on Bridges and Highways, Progress in Research and Practice*, San Diego, CA.
- 32 Koh, C. G. and Kelly, J. M. (1989). "Viscoelastic Stability Model for Elastomeric Isolation Bearings." *Journal of Structural Engineering*, 115(2), 285–302.
- 33 Cooper, J., Friedland, I. M., Buckle, I. G., Nimis, R. B., and Bobb, N. M. (1994). "The Northridge: Progress Made, Lessons Learned in Seismic Design of Bridges." *Public Roads*, 58(1).
- 34 Housner, G. W. and Thiel, Charles C., J. (1995). "The Continuing Challenge: Report on the Performance of State Bridges in the Northridge Earthquake." *Earthquake Spectra*, 11(4), 607–636.
- 35 Moehle, J., Fenves, G. L., Mayes, R., Priestley, N., Seible, F., Uang, C.-M., Werner, S., and Aschheim, M. (1995). "Highway Bridges and Tra_c Management." *Earthquake Spectra*, 11(S2), 287–372.
- 36 Saiidi, M., Maragakis, E., and Feng, S. (1996). "Parameters in bridge restrainer design for seismic retrofit." *J. Struct. Engrg., ASCE*, 122(1), 61–68.
- 37 Caltrans, 1997, *Seismic Design Criteria Retrofit of the West Approach to the San Francisco-Oakland Bay Bridge Draft #14*, California Department of Transportation, Sacramento, California
- 38 Keady, K. I., Alameddine, F., and Sardo, T. E. (2000). "Seismic Retrofit Technology." *Bridge Engineering Handbook*, W.-F. Chen and L. Duan, eds., CRC Press.
- 39 Hipley, P. (1997). "Bridge Retrofit Construction Techniques." *Second National Seismic Conference on Bridges and Highways*, Sacramento, CA.
- 40 Padgett, J., 2007. *Seismic Vulnerability Assessment of Retrofitted Bridges Using Probabilistic Methods*, thesis, Georgia Institute of Technology, Atlanta, May, 2007.

- 41 Cornell, A. C., F. Jalayer and R. O. Hamburger, 2002. Probabilistic Basis for 2000 SAC Federal Emergency Management Agency Steel Moment Frame Guidelines, *Journal of Structural Engineering* 128, 526-532.
- 42 Nielson, B. and R. DesRoches, 2007a. Probabilistic Seismic Analysis of Highway Bridges Using a Component Level Approach, *Earthquake Engineering and Structural Dynamics* In Press.
- 43 ATC-40 (1997). *Seismic Evaluation and Retrofit of Concrete Buildings*, Applied Technology Council, Redwood City, Palo Alto, California.
- 44 FEMA 306 (1998). *Evaluation of Earthquake Damaged Concrete and Masonry Wall Buildings*, Federal Emergency Management Agency, Washington D.C.
- 45 FEMA 355F (2000). State of the Art Report on Performance Prediction and Evaluation of Steel Moment-Frame Buildings, Federal Emergency Management Agency, Washington D.C.
- 46 SEAOC (1995). "Vision 2000 - A Framework for Performance Based Earthquake Engineering," Vol. 1, January, 1995.
- 47 Veletsos, A.S. and Newmark, N.M. (1960). "Effect of inelastic behavior on the response of simple systems to earthquake motions," *Proceedings of the World Conference on Earthquake Engineering*, Japan, vol. 2; 895–912.
- 48 FEMA 356 (2000). *Prestandard and Commentary for the Seismic Rehabilitation of Buildings*, Federal Emergency Management Agency, Washington D.C.
- 49 FEMA 450 (2003). NEHRP Recommended Provisions for Seismic Regulations for New Buildings and Other Structures, Federal Emergency Management Agency, Washington D.C.
- 50 Chopra, A. K. and Goel, R. K. (2002), "A Modal Pushover Analysis Procedure for Estimating Seismic Demands for Buildings," *Earthquake Engineering and Structural Dynamics*, Vol. 31, No. 3, pp. 561-582.
- 51 Bracci, J. M., Kunnath, S. K. and Reinhorn, A. M. (1997). "Seismic performance and retrofit evaluation of RC structures, ASCE, ST Division 123(1), 3–10.

- 52 Gupta, B. and Kunnath, S. K. (2000). “Adaptive spectra-based pushover procedure for seismic evaluation of structures,” *Earthquake Spectra* 16(2), 367–391.
- 53 Elnashai, A. and Papanikolaou, V. (2005). *Evaluation of conventional and adaptive pushover analysis I: Methodology*, *Journal of Earthquake Engineering*, Vol. 9, No. 6, pp. 923-941, 2005.
- 54 Elnashai, A. and Papanikolaou, V. (2005), *Evaluation of conventional and adaptive pushover analysis II: Comparative results*, *Journal of Earthquake Engineering*, Vol. 10, No. 1, pp. 127-151, 2005.
- 55 Hernández-Montes, E., Kwon, O., and Aschheim, M. A. (2004). “An energy-based formulation for first-and multiple-mode inelastic static (pushover) analyses,” *Journal of Earthquake Engineering*, Vol. 8, No. 1, p69-88.
- 56 Mander, J.B., Priestley, M.J.N., and Park, R. (1988). “Theoretical Stress-Strain Model for Confined Concrete,” *Journal of Structural Engineering*, 114 (8), pp. 1804-1826.
- 57 Elnashai, A. S., Papanikolaou, V. and Lee, D. (2002). *ZEUS NL – A System for Inelastic Analysis of Structures*, Mid-America Earthquake Center, University of Illinois at Urbana-Champaign, Program Release Sept.
- 58 Newmark, N.M. and Hall, W.J. (1982) *Earthquake Spectra and Design*. Earthquake Engineering Research Institute, Berkeley, CA.
- 59 Rosenblueth, E and Herrera, I. (1964). “On a kind of hysteretic damping,” *Journal of Engineering Mechanics Division ASCE* 90:37– 48.
- 60 Gulkan, P. and Sozen, M. (1974). “Inelastic response of reinforced concrete structures to earthquakes motions,” *ACI Journal* 71:604–610.
- 61 Hadjian, A.H. (1982). “A re-evaluation of equivalent linear models for simple yielding systems,” *Earthquake Engineering and Structural Dynamics* 10:759 –767.
- 62 Kowalsky, M.J. (1994). *Displacement-based design-a methodology for seismic design applied to RC bridge columns*. Master’s Thesis, University of California at San Diego, La Jolla, California.

- 63 Paraskeva, T.S., Kappos, A.J., and Sextos, A.G. (2006). Extension of modal pushover analysis to seismic assessment of bridges, *Earthquake Engineering and Structural Dynamics*, 35:1269-1293.
- 64 Chopra, A. K., and Goel, R. K. (1999). *Capacity-Demand-Diagram Methods for Estimating Seismic Deformation of Inelastic Structures: SDF Systems*, Report No. PEER-1999/02, Pacific Earthquake Engineering Research Center, University of California, Berkeley.
- 65 Nielson, B. G. (2005). *Analytical Fragility Curves for Highway Bridges in Moderate Seismic Zones*, PhD thesis, Georgia Institute of Technology, Atlanta, Georgia.
- 66 Kwon, O. and Elnashai, A. S. (2008a). "Seismic fragility analysis of a bridge in Central and Eastern United States," *Journal of Structure and Infrastructure Engineering*, (accepted).
- 67 Mazroi, A., Wang, L. L., and Murray, T. M. (1983). *Effective Coefficient of Friction of Steel Bridge Bearings*, Transportation Research Record 903.
- 68 Mander, J. B., Kim, D.-K., Chen, S. S., and Premus, G. J. (1996). *Response of Steel Bridge Bearings to Reversed Cyclic Loading*, Technical Report NCEER-96-0014, National Center for Earthquake Engineering Research.
- 69 McKenna, F. and Fenves, G. L. (2001). *The OpenSees command language manual, version 1.2*. Pacific Earthquake Engineering Research Center, Univ. of California at Berkeley.
- 70 Yang, Z., Lu, J. and Elgamal, A. (2005). "OpenSees Geotechnical Simulation Capabilities and User Manual", University of California San Diego, <http://cyclic.ucsd.edu/opensees/>.
- 71 Kwon, O. and Elnashai, A. S. (2008b) "Multi-platform simulation of highway over-crossing bridge with consideration of soil-structure-interaction," *Journal of Structural Engineering*, ASCE, Vol. 134, No. 4, p651-660.
- 72 Fernández, J. A. and Rix, G. J. (2006). "Soil Attenuation Relationships and Seismic Hazard Analyses in the Upper Mississippi Embayment," Submitted to *Bulletin of the Seismological Society of America*, September.

- 73 McKenna, F., Fenves, G.L., Filippou, F.C., & Mazzoni, S. 2006. Open system for earthquake engineering simulation (OpenSees). Pacific Earthquake Engineering Research Center (PEER), University of California, Berkeley, C.A.
<http://opensees.berkeley.edu/OpenSees/home/about.php>.
- 74 Mwafy, A.M., Elnashai, A.S., and Yen, W-H. (2007). “Implications of design assumptions on capacity estimates and demand predictions of multi-span curved bridges,” *ASCE J. of Bridge Engineering* 12:6, 710-726.
- 75 Elnashai, A.S., Mwafy, A., and Kwon, O. (2007). Seismic Assessment of the I-155 Bridge at Caruterville with SSI, Task C – Inelastic Soil Structure Interaction Analysis. Mid-America Earthquake Center.
- 76 Hashash, Y. (2006). Seismic site response analysis, Seismic Retrofit Study of Bridge A-1700 Route I-155, Pemiscot County, Univ. of Illinois at Urbana-Champaign, Urbana, IL.
- 77 Mwafy, A.M., Kwon, O., and Elnashai, A.S. (2008). “Inelastic Seismic Response of a 59-Span Bridge with Soil-Structure Interaction,” Proceedings of 14th World Conference on Earthquake Engineering, Beijing, China.

APPENDIX A: SEISMIC RETROFIT IN INDIANA



Figure 146 Photo. Bearing retrofits and details in Indiana: Elastomeric bearing with keeper brackets (SR 66 at Diamond – IN)



Figure 147 Photo. Bearing retrofits and details in Indiana: Elastomeric Bearings (HW50 Red Skelton – IN)



Figure 148 Photo. Bearing retrofits and details in Indiana: Isomeric Bearing with Dampers (US 41 @ Eagle Creek –IN)



Figure 149 Photo. Transverse restraining devices in Indiana: Transverse Shear Key (SR51 over White River / Carl Grey Memorial Bridge – IN)



Figure 150 Photo. Transverse restraining devices in Indiana: Transverse Restrainer Cables (SR51 over White River / Carl Grey Memorial Bridge – IN)

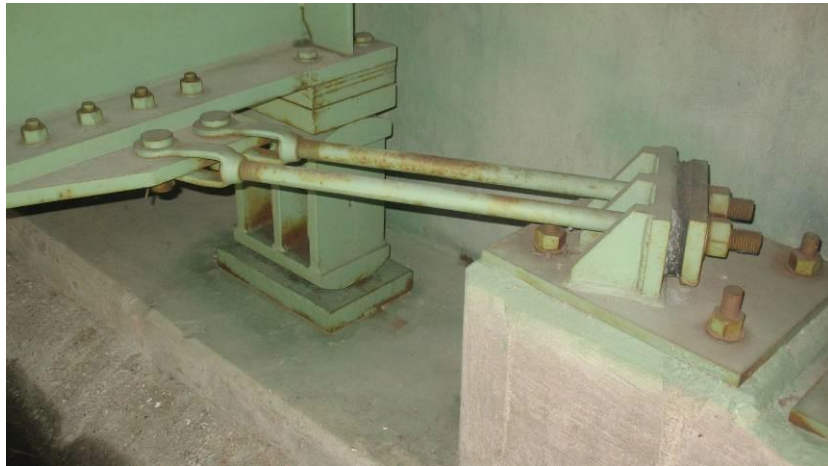


Figure 151 Photo. Transverse restraining devices in Indiana: Transverse Restrainer Bars (164 at County Road 800 - IN)

APPENDIX B: SEISMIC RETROFIT IN ILLINOIS



Figure 152 Photo. Poplar Street Retrofits in Illinois: Column Cable Wraps, Bent Cap Retrofits, Transverse Restrainer Bars (Poplar Street Complex - IL)

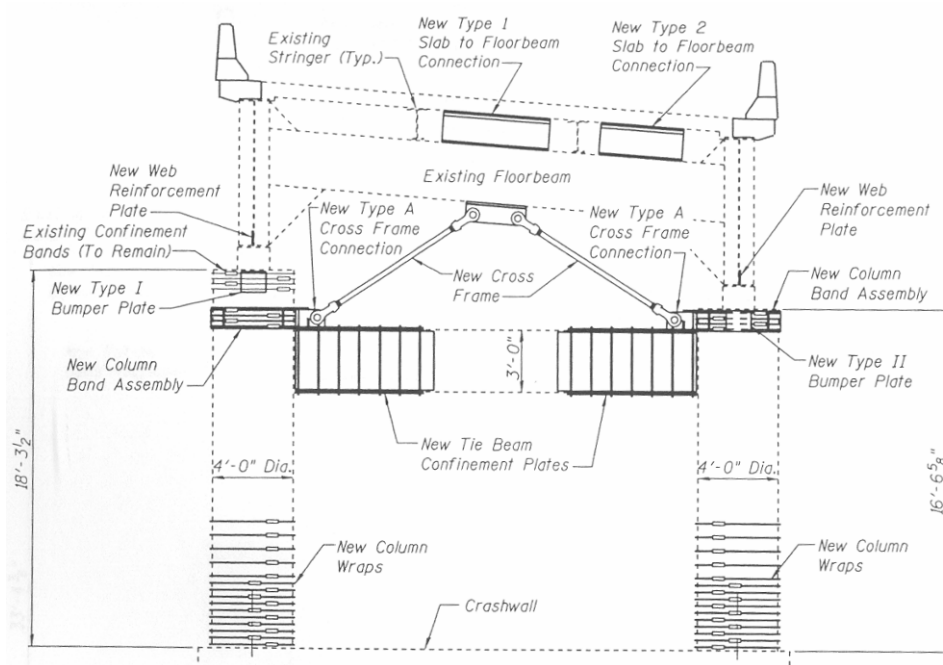


Figure 153 Photo. Poplar Street Retrofits in Illinois: Details of Cable Column Wraps, Bent Cap Retrofits, Transverse Restrainer Bars (Rte 3 Poplar Street – IL)



Figure 154 Photo. Poplar Street Retrofits in Illinois: Bent Cap Retrofit, Longitudinal Restrainer Bars, and Transverse Restraint with Turnbuckles (Poplar Street Complex – IL)

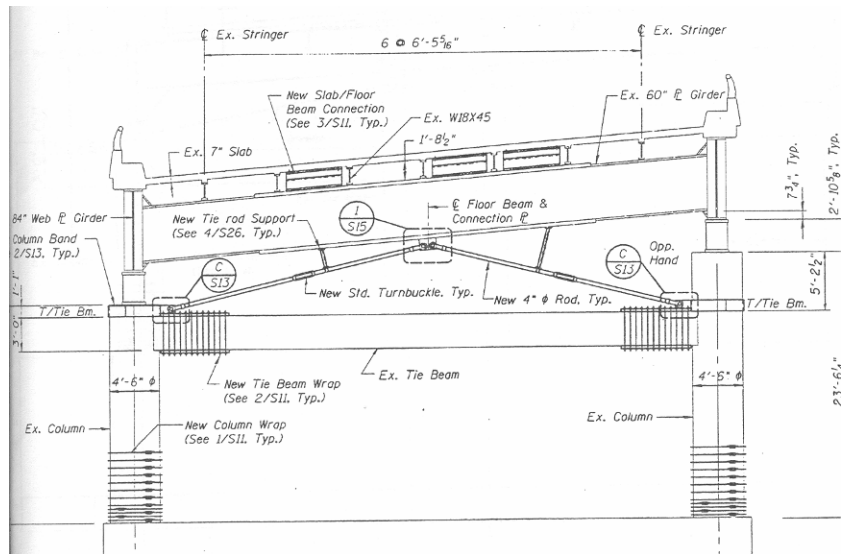


Figure 155 Photo. Poplar Street Retrofits in Illinois: Cable Column Wraps, Bent Cap Retrofits, Restrainer Bars (Rte 70 Poplar Street – IL)

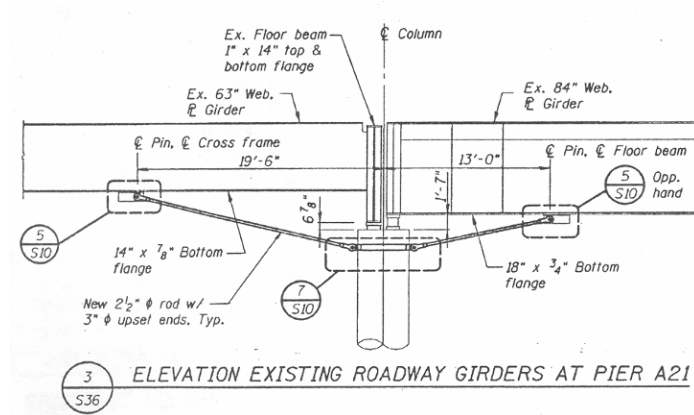


Figure 156 Photo. Poplar Street Retrofits in Illinois: Elevations (Rte 70 Poplar Street – IL)



Figure 157 Photo. Details of Column and Bent Cap Wraps in Illinois: Column Cable Wraps (Poplar Street Complex – IL)

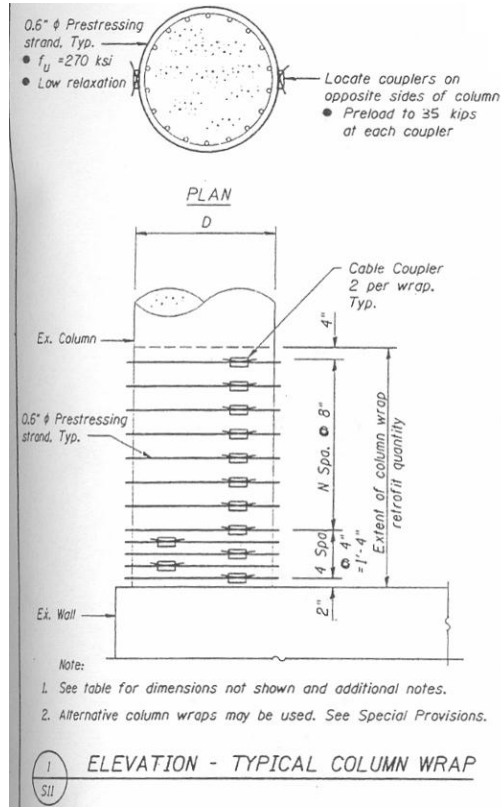


Figure 158 Illustration. Details of Column and Bent Cap Wraps in Illinois: Cable Wraps (Rte 70 Poplar Street – IL)

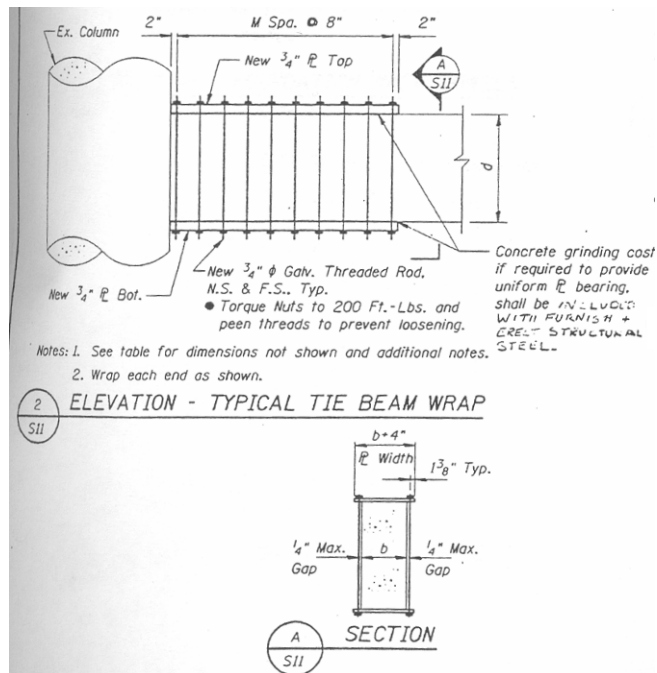


Figure 159 Illustration. Details of Column and Bent Cap Wraps in Illinois: Bent Cap Wraps (Rte 70 Poplar Street – IL)



Figure 160 Photo. Restrainer Bars and Bumpers in Illinois: Restrainer Bar (Poplar Street Complex - IL)

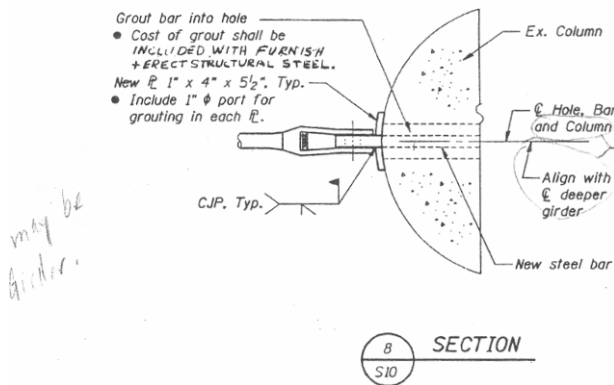
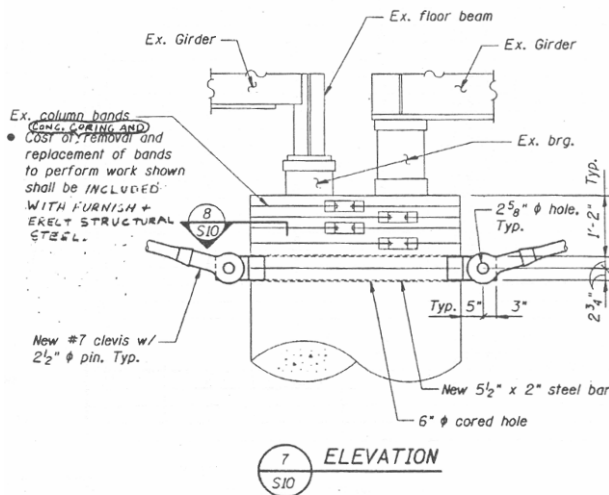


Figure 161 Illustration. Restrainer Bars and Bumpers in Illinois: Restrainer Bar Connections /Column Cable Wraps (Rte 70 Poplar Street – IL)



Figure 162 Photo. Restrainer Bars and Bumpers in Illinois: Bumpers and Restrainer Bar (Poplar Street Complex - IL)

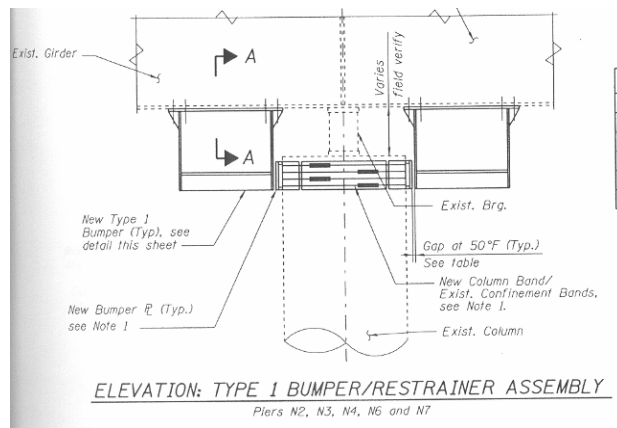


Figure 163 Illustration. Restrainer Bars and Bumpers in Illinois: Bumpers (Rte 3 Poplar Street – IL)



Figure 164 Photo. Restrainer Bars in Illinois: Restrainer Bar (Poplar Street Complex - IL)

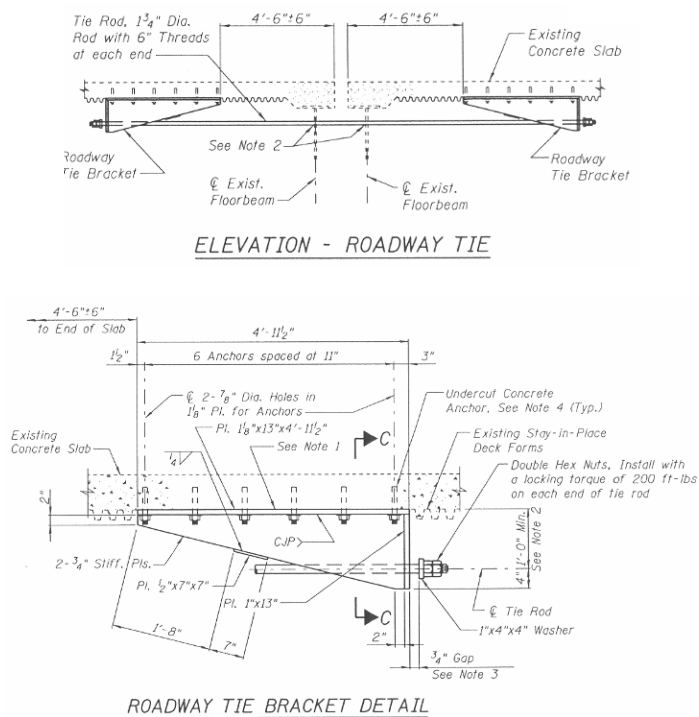


Figure 165 Illustration. Restrainer Bars in Illinois: Detail of Typical Restrainer Bars (Rte 3 Poplar Street – IL)

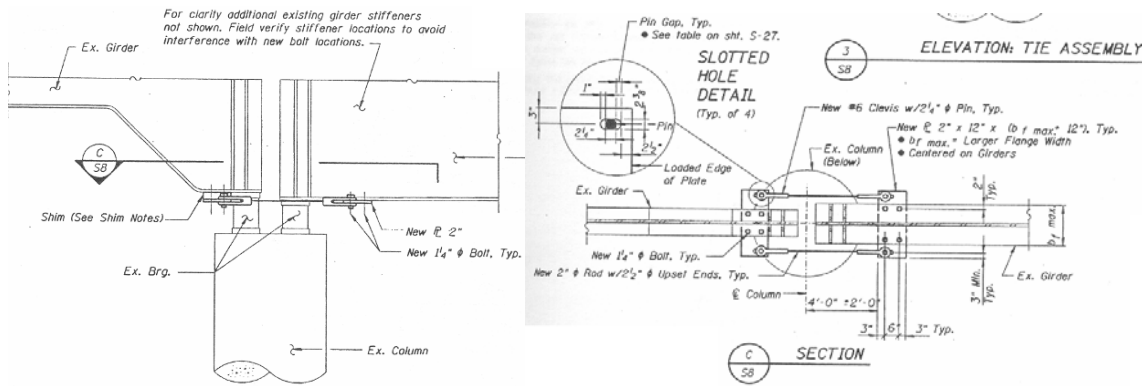


Figure 166 Illustration. Restrainer Bars in Illinois: Detail of Alternative Restrainer Bar Assembly (Rte 70 Poplar Street – IL)



Figure 167 Photo. Column Retrofits in Illinois: Fiber Composite Retrofit (Poplar Street Complex – IL)

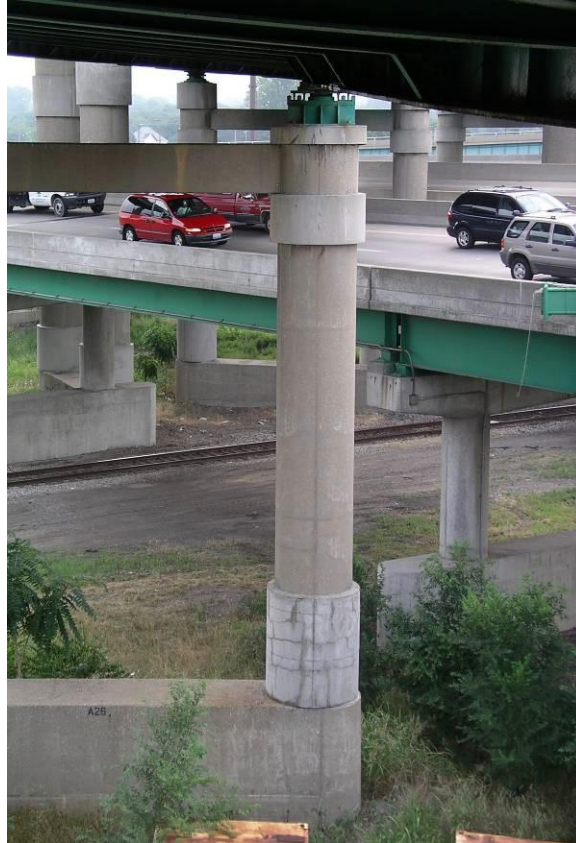


Figure 168 Photo. Column Retrofits in Illinois: Partial Column Encasement (Poplar Street Complex – IL)



Figure 169 Photo. Column Retrofits in Illinois: Fiber Composite Retrofit (Poplar Street Complex – IL)



Figure 170 Photo. Isolation in Illinois: Elastomeric Bearings and Restrainer Cables (Poplar Street Complex – IL)



Figure 171 Photo. Isolation in Illinois: Isolation Bearing (Poplar Street Complex – IL)

APPENDIX C: SEISMIC RETROFIT IN KENTUCKY



Figure 172 Photo. Different restrainer cable configurations in Kentucky: Restrainer Cables



Figure 173 Photo. Different restrainer cable configurations in Kentucky: Restrainer Cables

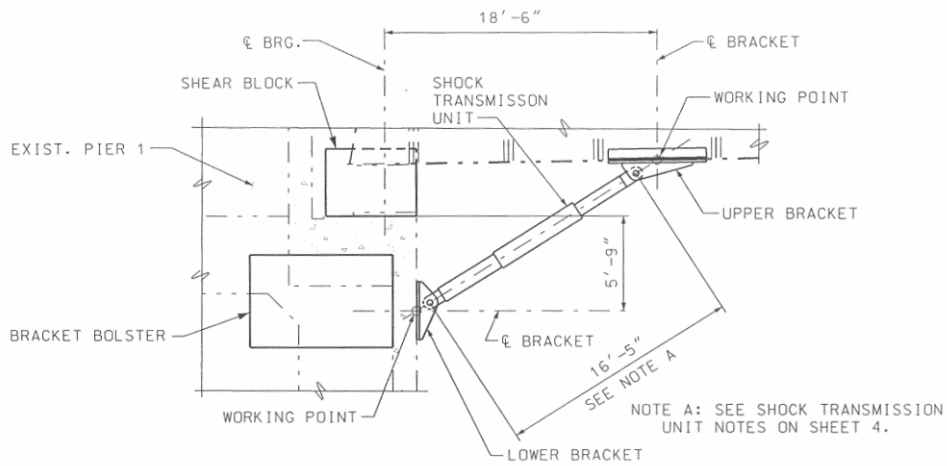


Figure 174 Photo. Different restrainer cable configurations in Kentucky: Restrainer Cables

APPENDIX D: SEISMIC RETROFIT IN MISSOURI



**Figure 175 Photo. Shear Key and Shock Transmission Unit Retrofits in Missouri:
Shear Keys and Shock Transmission Units (Poplar Street Complex – MO)**



**Figure 176 Illustration. Shear Key and Shock Transmission Unit Retrofits in
Missouri: Shock Transmission Unit and Shear Key (I70 Poplar Street – MO)**

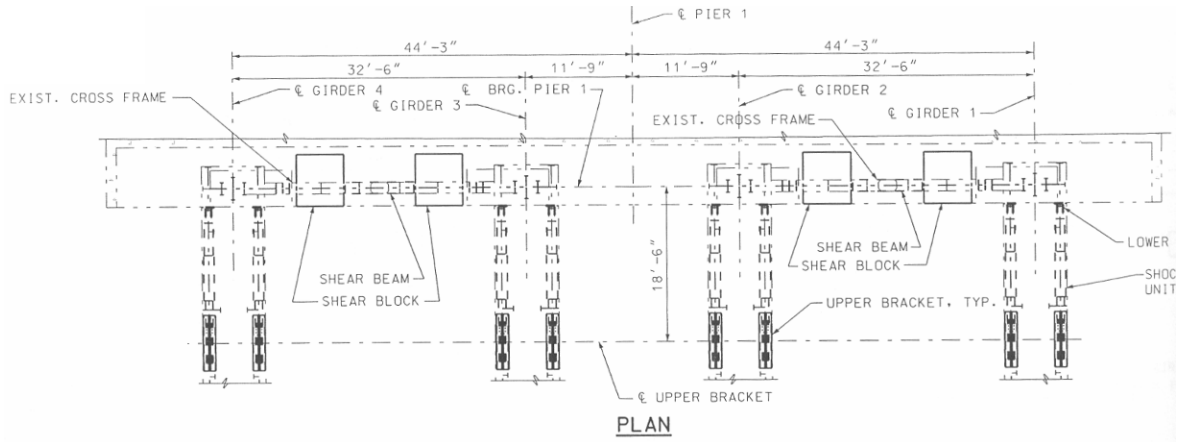


Figure 177 Illustration. Shear Key and Shock Transmission Unit Retrofits in Missouri: Shear Keys and Shock Transmission Units (I70 Poplar Street – MO)



Figure 178 Photo. Bumper, Bent Cap, and Shear Key Retrofits in Missouri: Bumpers (Poplar Street Complex – MO)

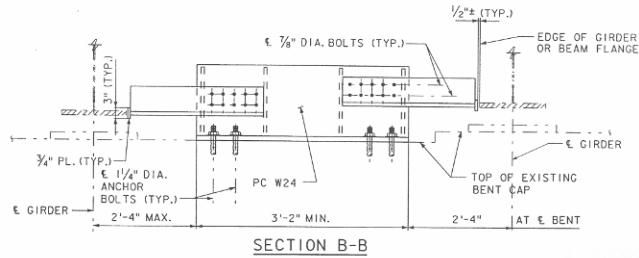
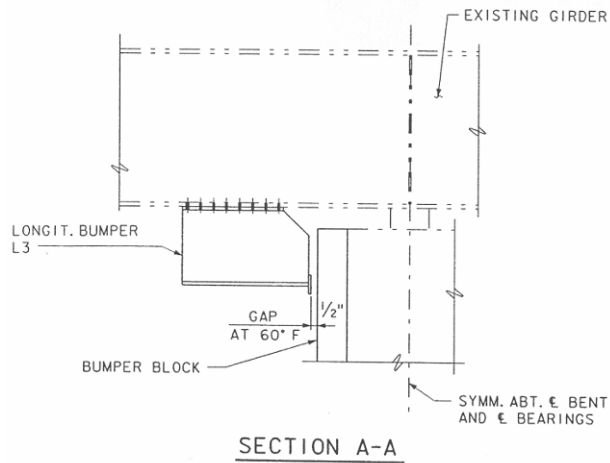


Figure 179 Illustration. Bumper, Bent Cap, and Shear Key Retrofits in Missouri: Bumpers (US40 Poplar Street – MO)

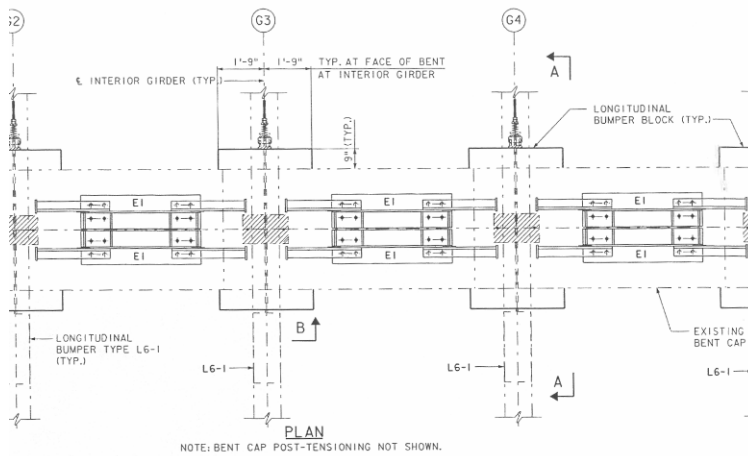


Figure 180 Illustration. Bumper, Bent Cap, and Shear Key Retrofits in Missouri: Transverse Shear Key (US40 Poplar Street – MO)



Figure 181 Photo. Bumper, Bent Cap, and Shear Key Retrofits in Missouri: Bent Cap Post-tension Retrofit



Figure 182 Photo. Longitudinal Bumper and Restrainer Retrofits in Missouri: Restrainer Bars and Bumpers (Poplar Street Complex – MO)

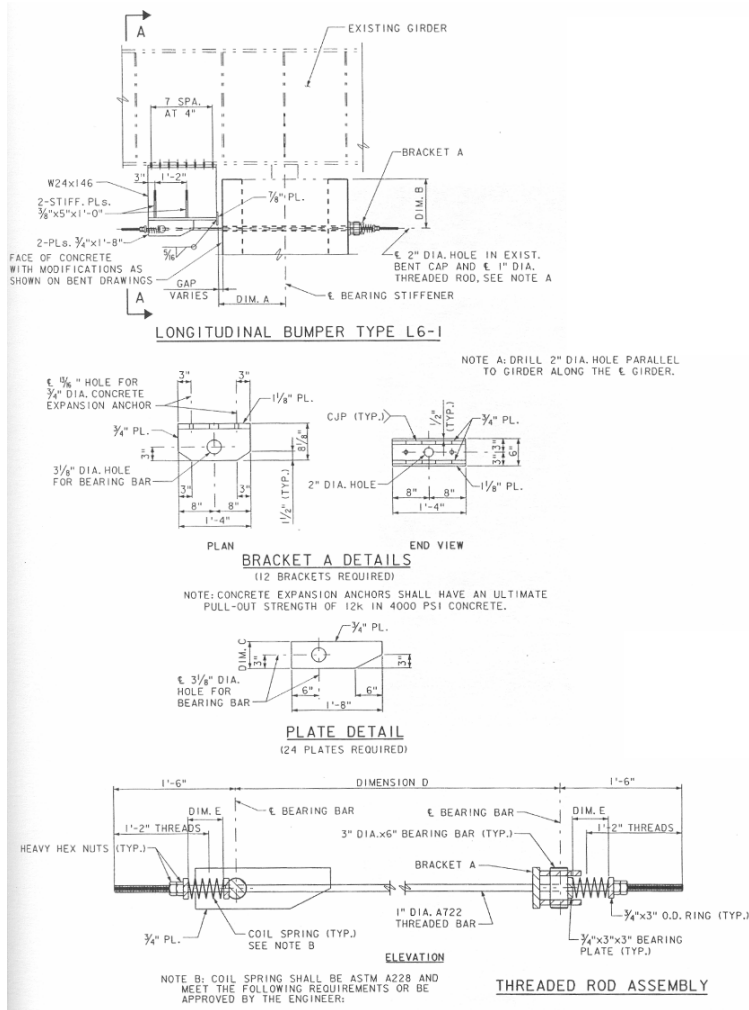


Figure 183 Illustration. Longitudinal Bumper and Restrainer Retrofits in Missouri: Bumper and Restrainer Cable (US40 Poplar Street – MO)



Figure 184 Photo. Longitudinal Bumper and Restrainer Retrofits in Missouri: Steel Jackets (Poplar Street Complex – MO)

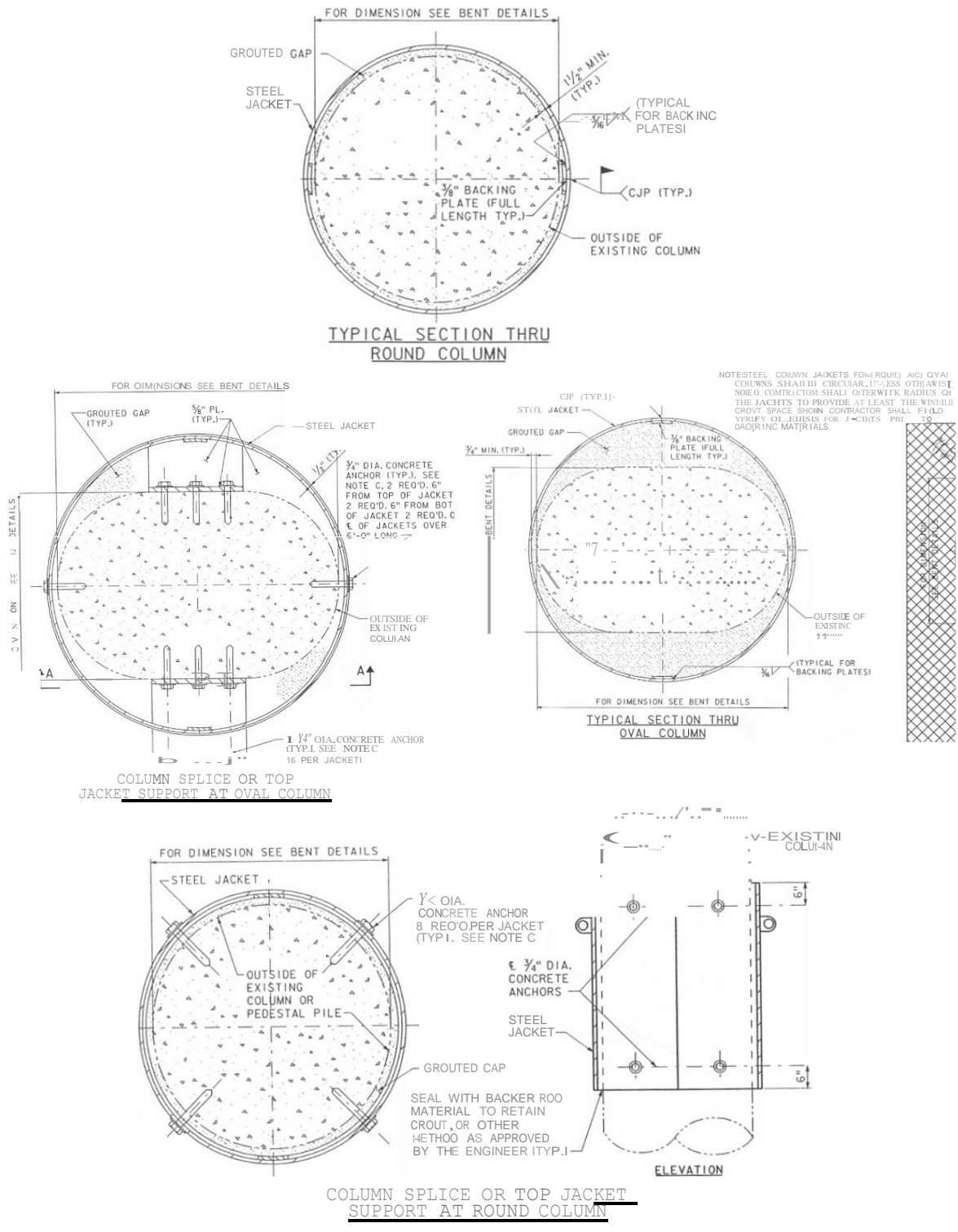


Figure 185 Illustration. Longitudinal Bumper and Restrainer Retrofits in Missouri: Steel Jacket Details (US40 Poplar Street- MO)



Figure 188 Photo. Seat Extenders and Bent Cap Retrofit in Missouri: Bent Cap Retrofit (Poplar Street Complex– MO)



Figure 189 Photo. Seat Extender and Restrainer Rods in Missouri: Seat Extenders (Poplar Street Complex – MO)

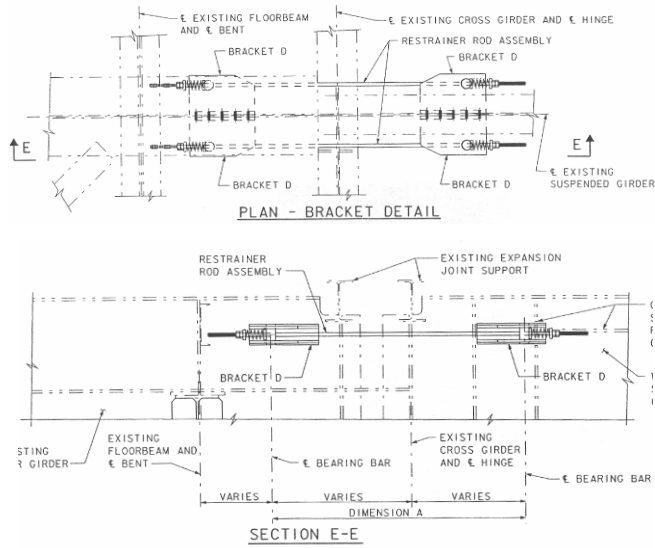


Figure 190 Illustration. Seat Extender and Restrainer Rods in Missouri: Restrainers (US40 Poplar Street – MO)

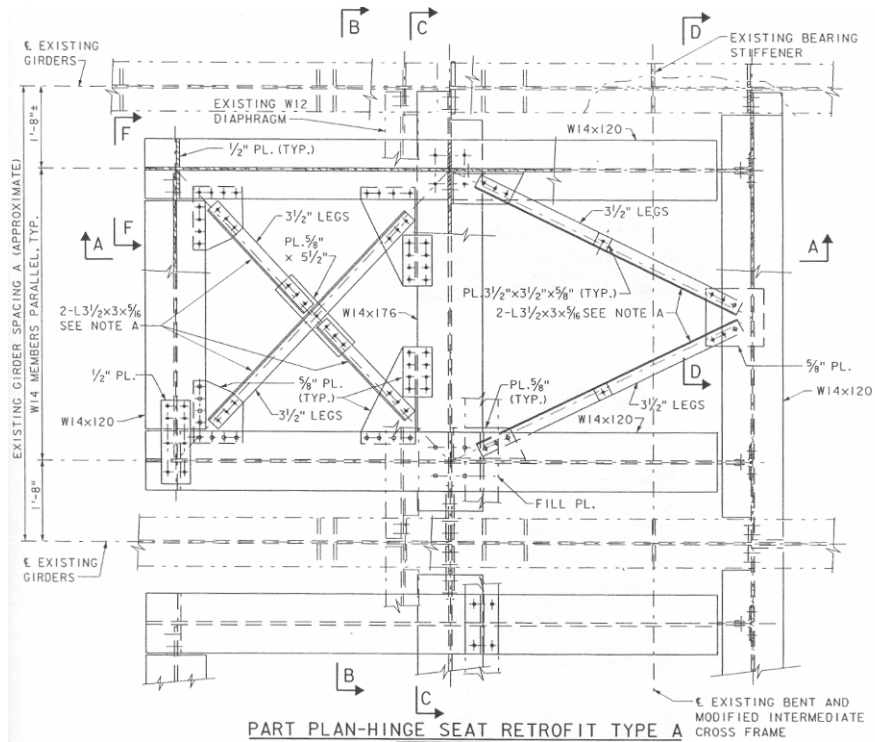
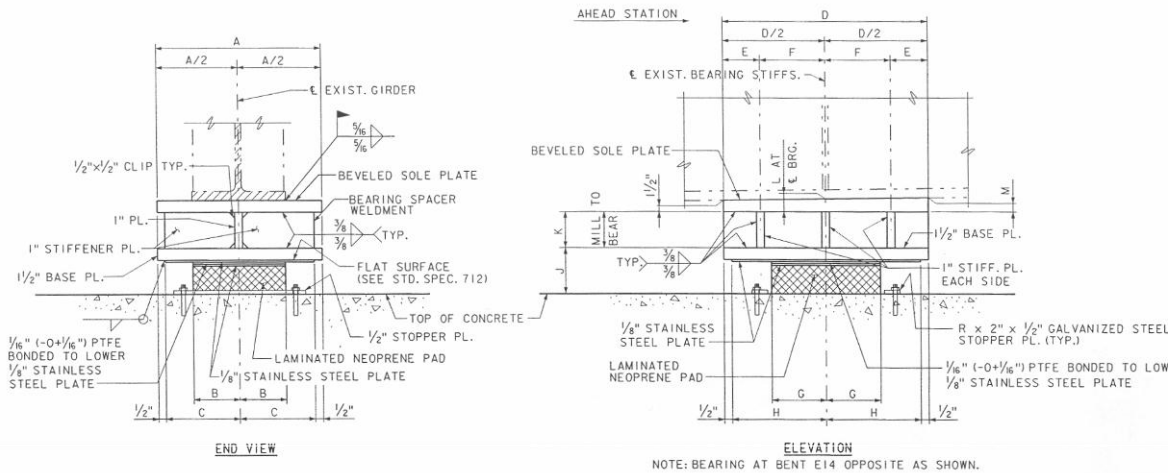


Figure 191 Illustration. Seat Extender and Restrainer Rods in Missouri: Seat Extender (US 40 Poplar Street – MO)



TYPE "N" PTFE EXPANSION BEARINGS

NOTE: FABRICATOR MAY BEVEL SOLE PLATE AS SHOWN OR TAPER WEB AND STIFFENERS OF WELDMENT TO DIMENSIONS SHOWN.

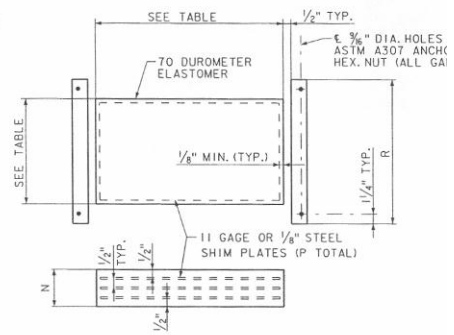
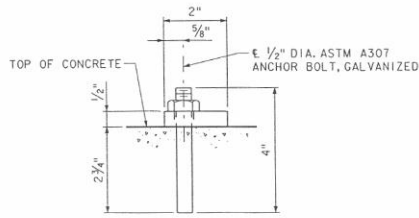


Figure 192 Illustration. Replacement with Less Vulnerable Bearings in Missouri: Bearing Replacement (US40 Poplar Street – MO)

APPENDIX E: SEISMIC RETROFIT IN TENNESSEE



Figure 193 Photo. The First Seismic Retrofit in Tennessee: First Retrofit in TN: “Uplift” and Longitudinal Restrainer Cables (SR 14 over CSX Railroad– TN)



Figure 194 Photo. The First Seismic Retrofit in Tennessee: First Retrofit in TN: “Deck Girder” Restraint Cables (SR 14 over CSX Railroad – TN)

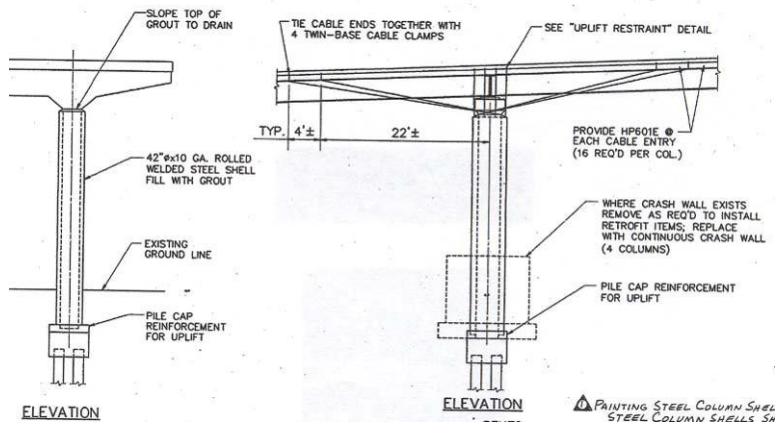


Figure 195 Illustration. The First Seismic Retrofit in Tennessee: Steel Jackets and Restrainer Cables (SR 14 over CSX Railroad – TN)

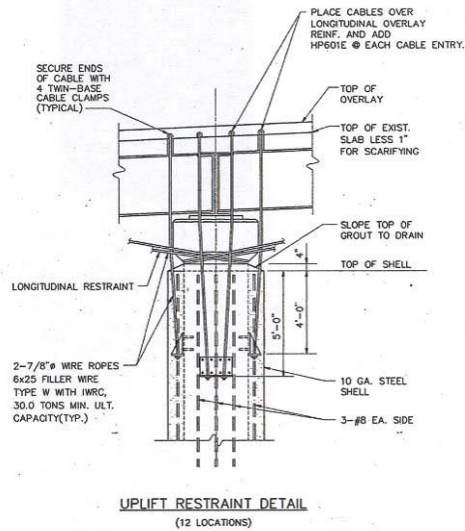


Figure 196 Illustration. The First Seismic Retrofit in Tennessee: Restrainer Cables (SR14 over CSX Railroad – TN)

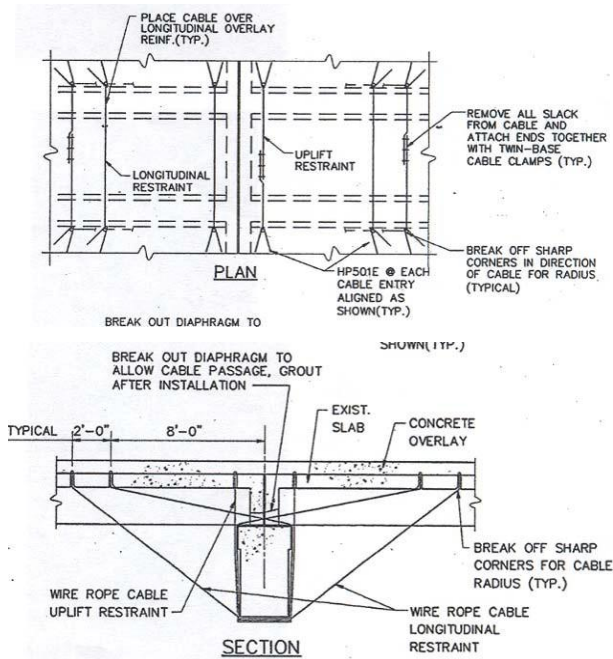


Figure 197 Illustration. The First Seismic Retrofit in Tennessee: Deck Girder Restrainer Cables (SR14 over CSX Railroad – TN)



Figure 198 Photo. Retrofit of Davies Plantation Road in Tennessee: Bent Cap Retrofit, Steel Jackets, and Shear Keys (Davies Plantation Road – TN)

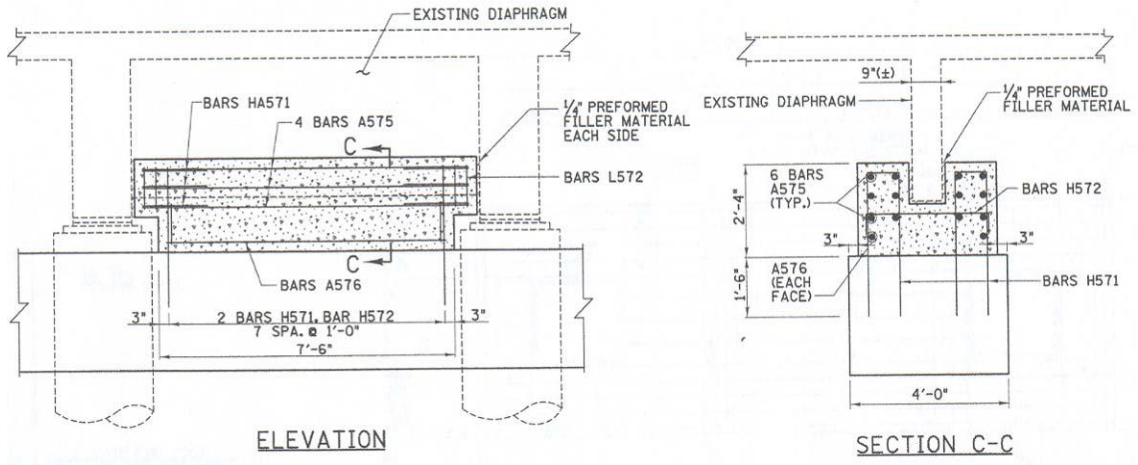


Figure 199 Illustration. Retrofit of Davies Plantation Road in Tennessee: Shear Key (Davies Plantation Road – TN)

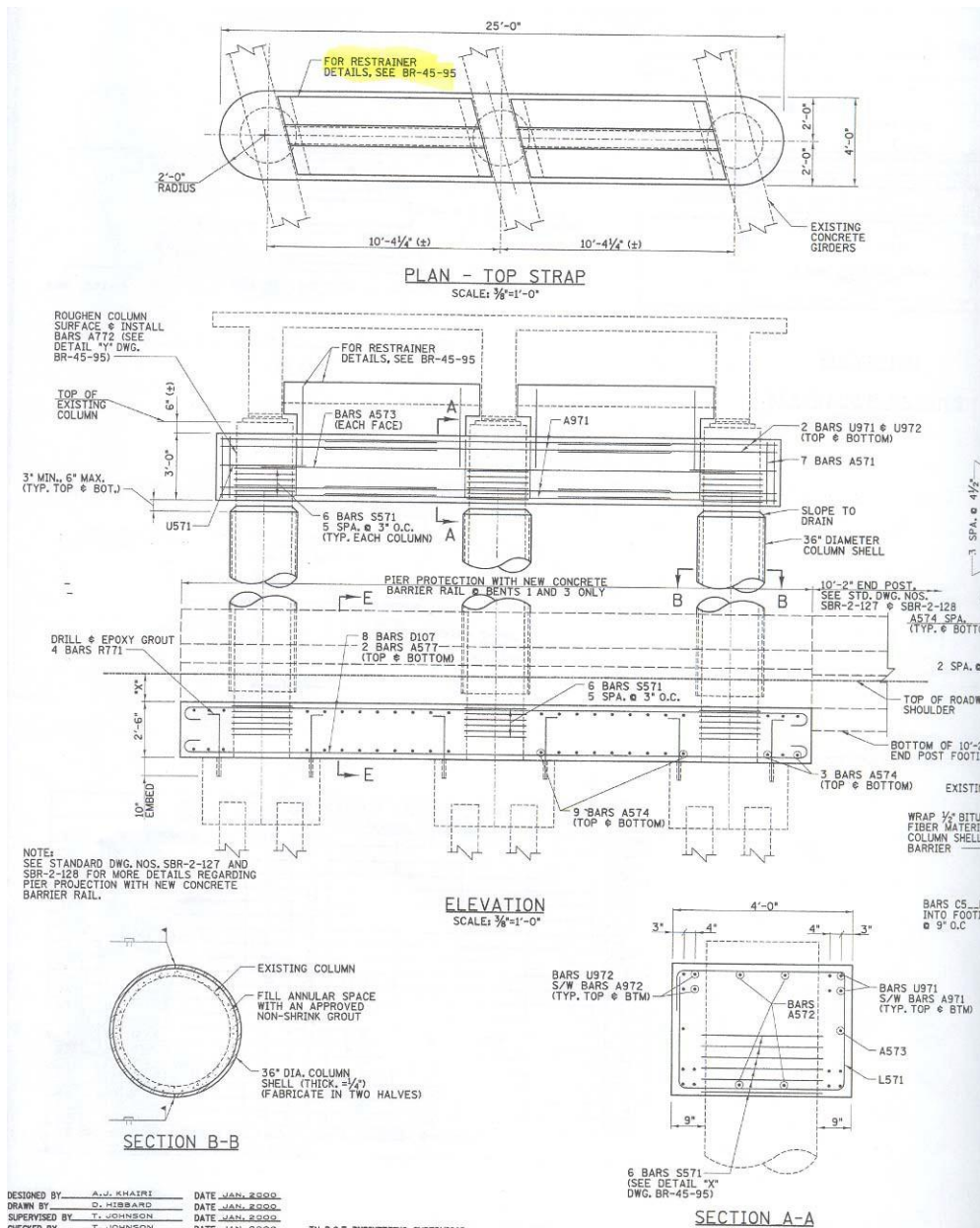


Figure 200 Illustration. Details of Bent Cap and Column Retrofit in Tennessee: Bent Cap and Steel Casing (Davies Plantation Road – TN)



Figure 201 Photo. Retrofit of Columns and Bearings in Tennessee: Painted Steel Jackets (I40 over SR 15 – TN)

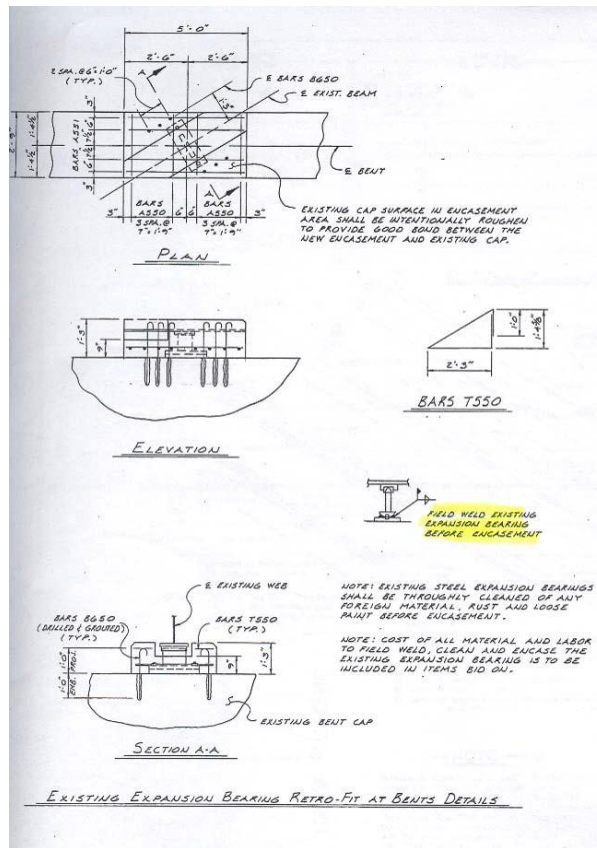


Figure 202 Illustration. Retrofit of Columns and Bearings in Tennessee: Bearing Retrofit (I40 over SR 15 – TN)



Figure 203 Photo. Retrofit of Columns and Bearings in Tennessee: Bearing Retrofit (I40 over SR 15 – TN)



Figure 204 Photo. Retrofit of Columns and Bent Caps in Tennessee: Steel Jackets and Bent Cap Retrofit (SR 196 over I40 – TN)

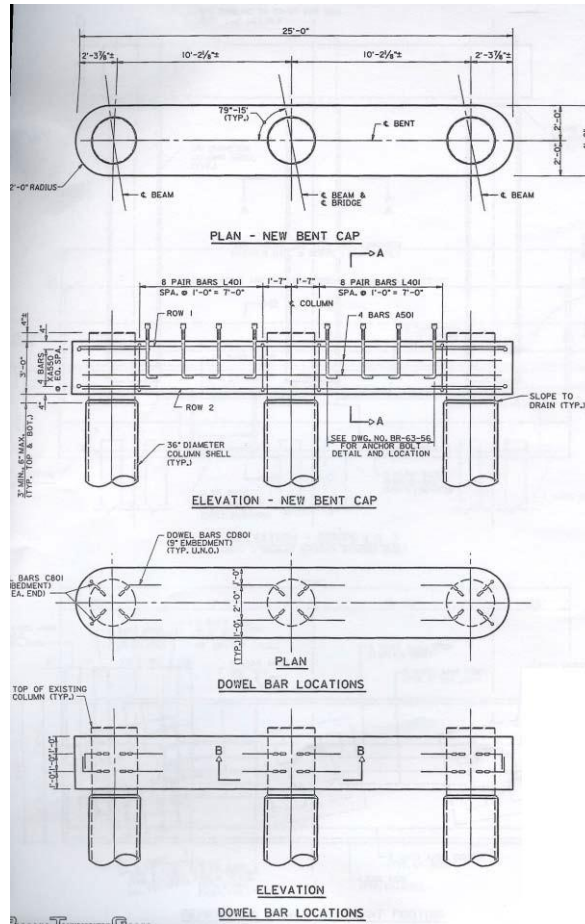


Figure 205 Illustration. Retrofit of Columns and Bent Caps in Tennessee: Bent Cap Retrofit (SR 196 – TN)

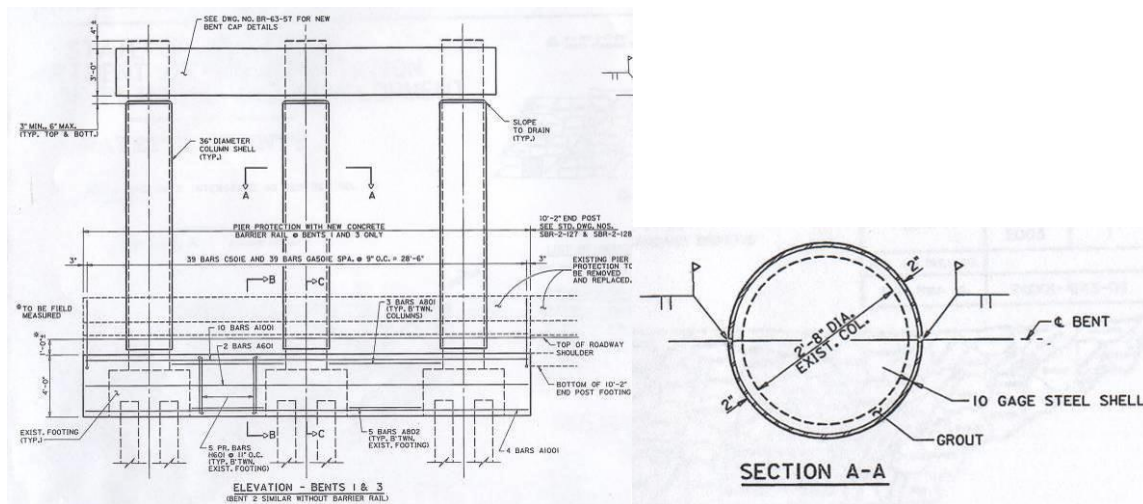


Figure 206 Illustration. Retrofit of Columns and Bent Caps in Tennessee: Steel Jackets (SR196 – TN)



Figure 207 Photo. Restrainer Cable Details in Tennessee: Restrainer Cables and Transverse Keeper Brackets (Chambers Chapel Road over I40 – TN)

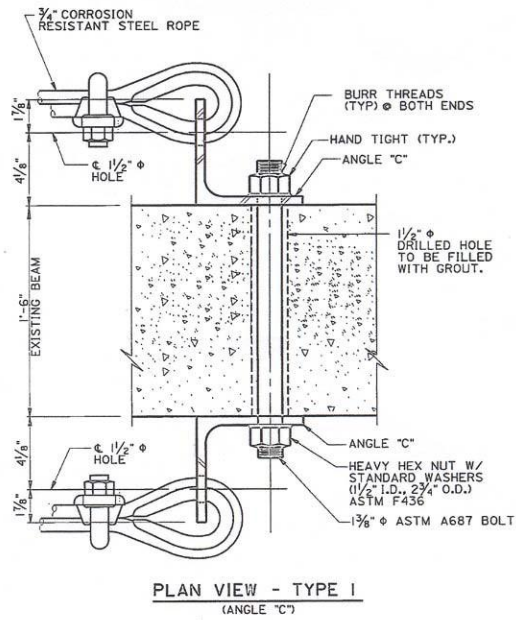


Figure 208 Illustration. Restrainer Cable Details in Tennessee: Connection for Cables (Chambers Chapel Road – TN)

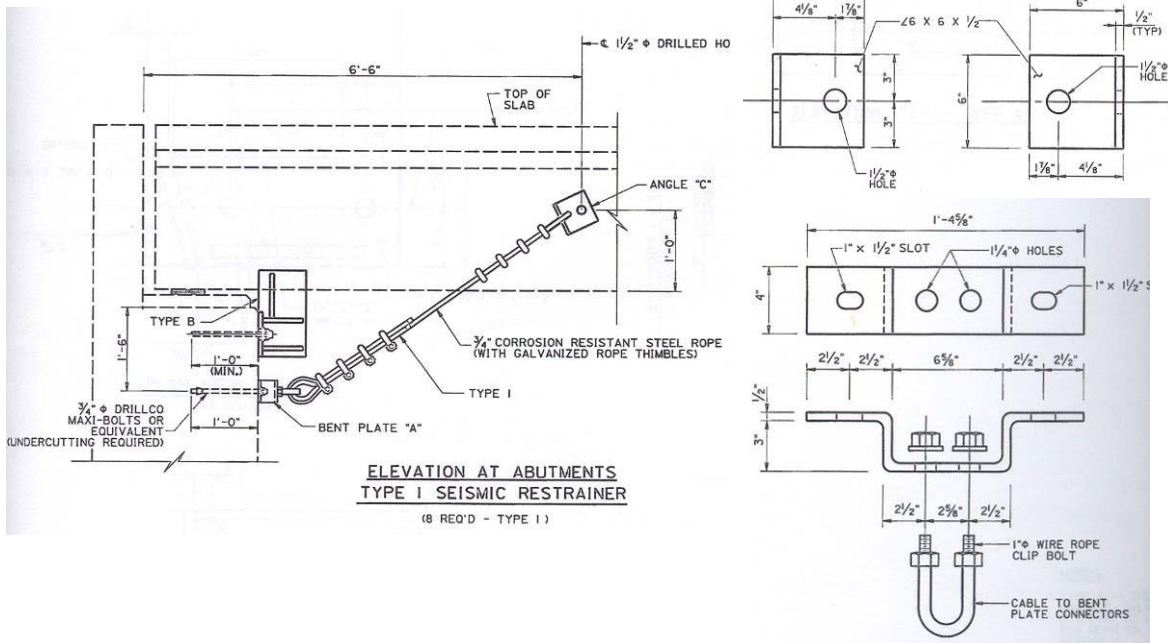


Figure 209 Illustration. Restrainer Cable Details in Tennessee: Restrainer Cable and Attachments (Chambers Chapel Road – TN)



Figure 210 Photo. Transverse Keeper Brackets (Shear Keys) in Tennessee: Transverse Keeper Brackets (Chambers Chapel Road over I40 – TN)

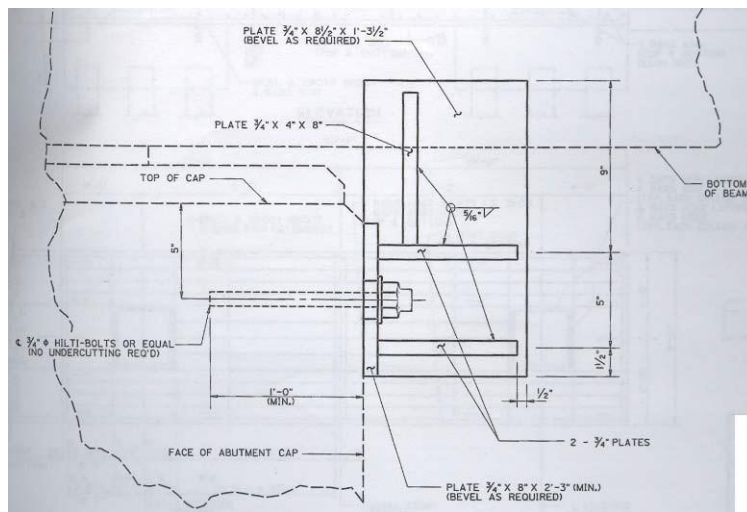
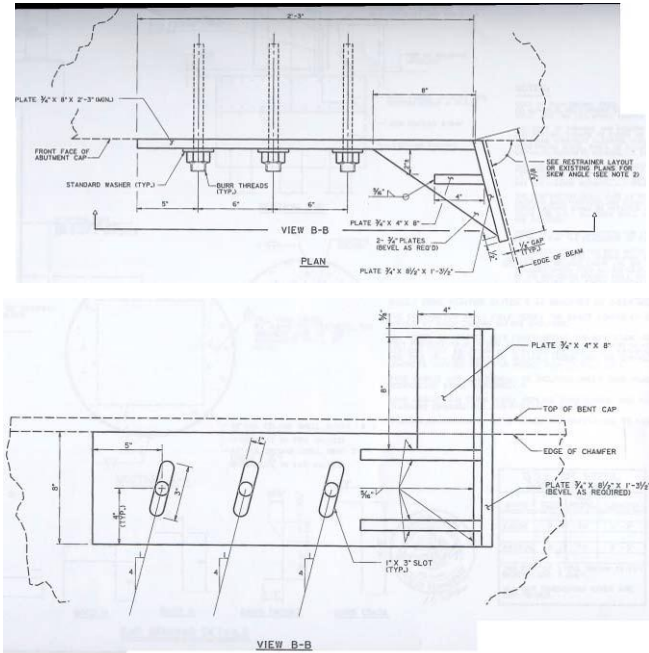
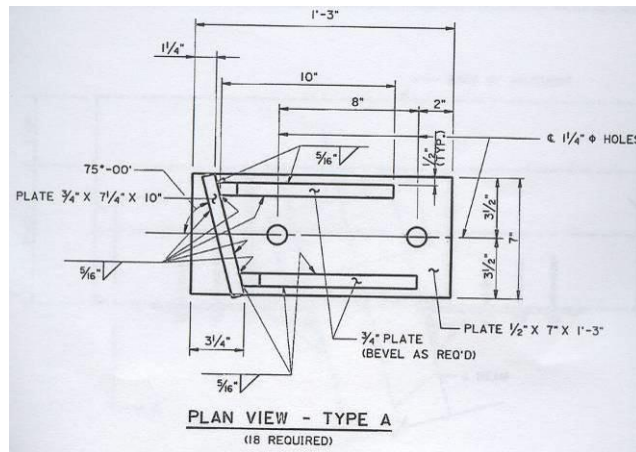
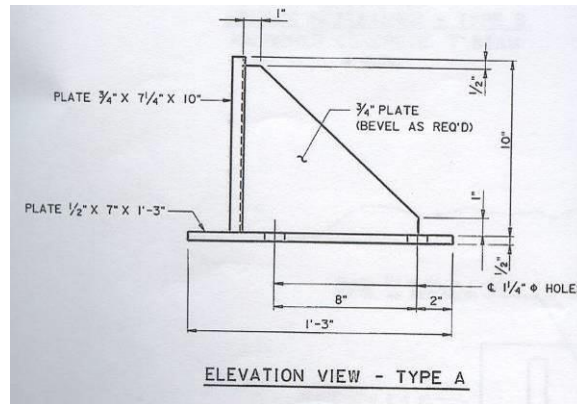
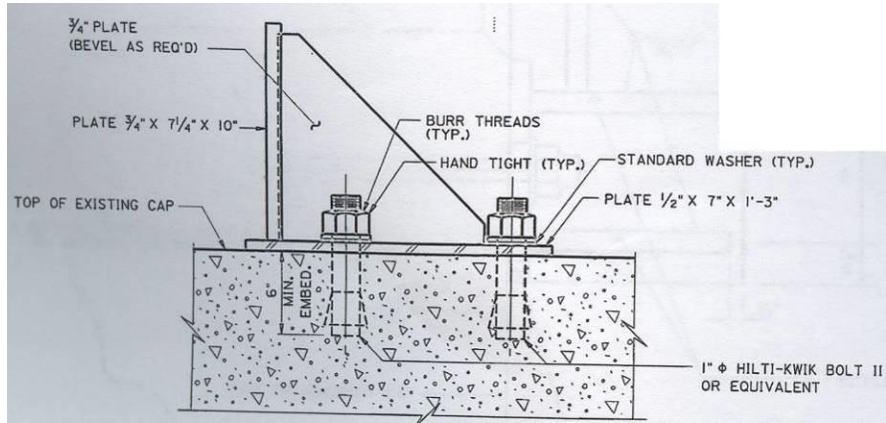


Figure 211 Illustration. Transverse Keeper Brackets (Shear Keys) in Tennessee: Keeper Bracket Details – Type B(Chambers Chapel Road – TN)



Figure 212 Photo. Transverse Keeper Brackets (Shear Keys) in Tennessee: Keeper Brackets (Chambers Chapel Road over I40 – TN)



**Figure 213 Illustration. Transverse Keeper Brackets (Shear Keys) in Tennessee:
Keeper Brackets - Type A (Chambers Chapel Road – TN)**



Figure 214 Photo. Steel Jacket and Footing Retrofit in Tennessee: Steel Column Jackets (Chambers Chapel Road – TN)

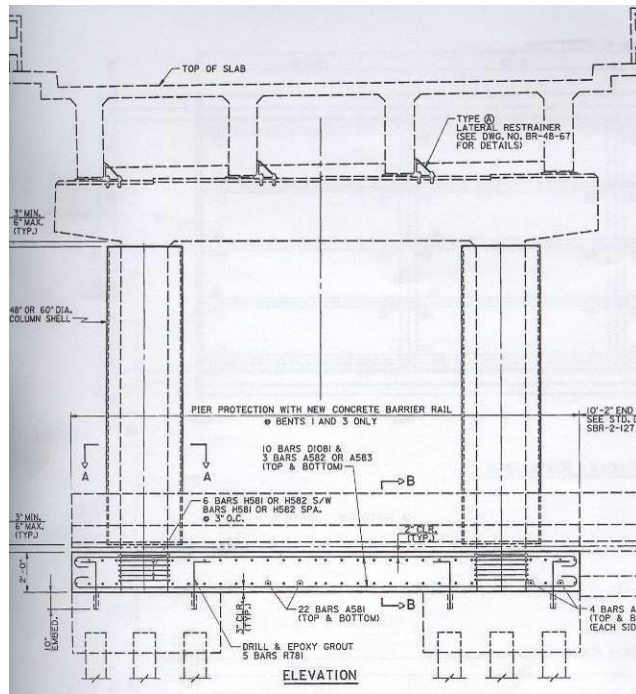


Figure 215 Illustration. Steel Jacket and Footing Retrofit in Tennessee: Steel Jacket Elevation (Chambers Chapel Road – TN)

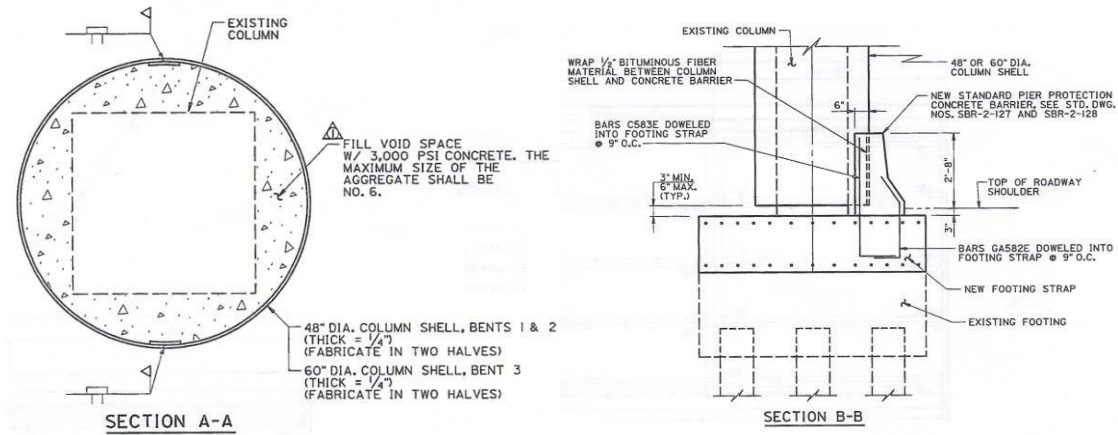


Figure 216 Illustration. Steel Jacket and Footing Retrofit in Tennessee: Steel Column Jackets and Footing Retrofit (Chambers Chapel Road – TN)



Figure 217 Photo. Concrete Shear Keys in Tennessee: Concrete Shear Keys (SR59 over I40 – TN)

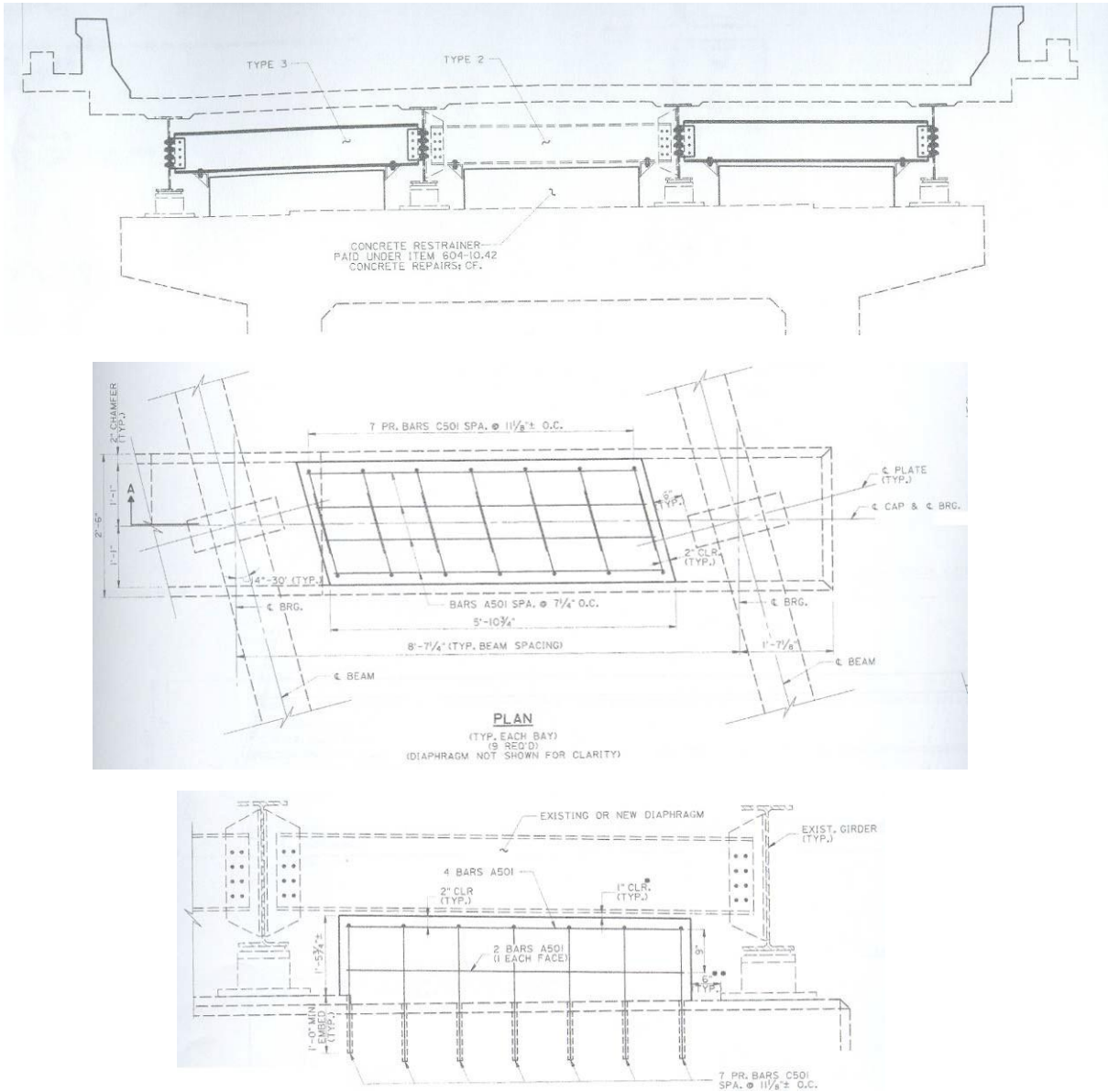


Figure 218 Illustration. Concrete Shear Keys in Tennessee: Concrete Shear Key Details (SR59 – TN)



Figure 219 Photo. Keeper Brackets in Tennessee: Keeper Brackets (SR59 – TN)

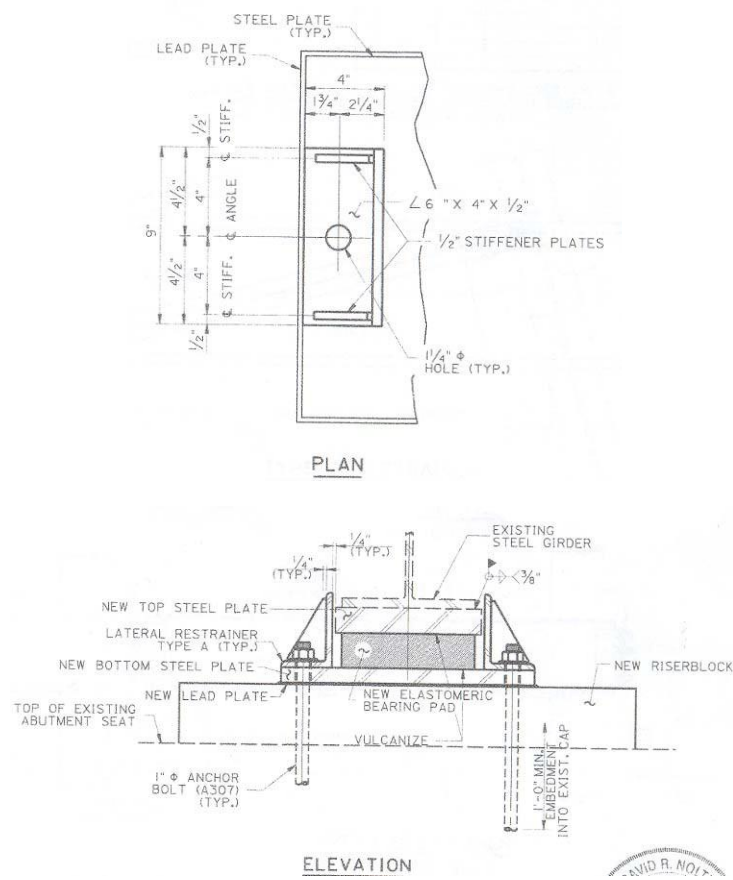


Figure 220 Illustration. Keeper Brackets in Tennessee: Keeper Bracket Details (SR59 – TN)



Figure 221 Photo. Restrainer Cables in Tennessee: Restrainer Cables (SR59 – TN)

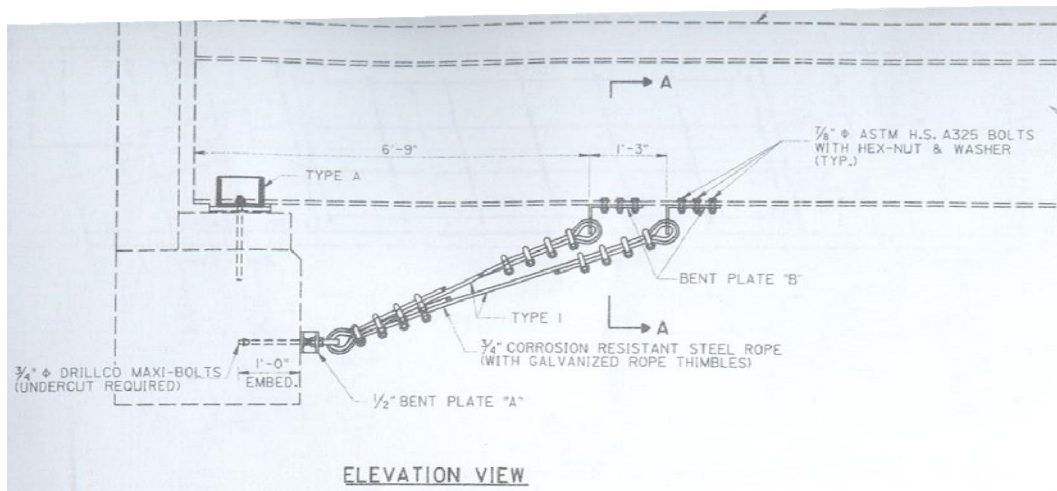


Figure 222 Illustration. Restrainer Cables in Tennessee: Restrainer Cable Detail (SR59 – TN)

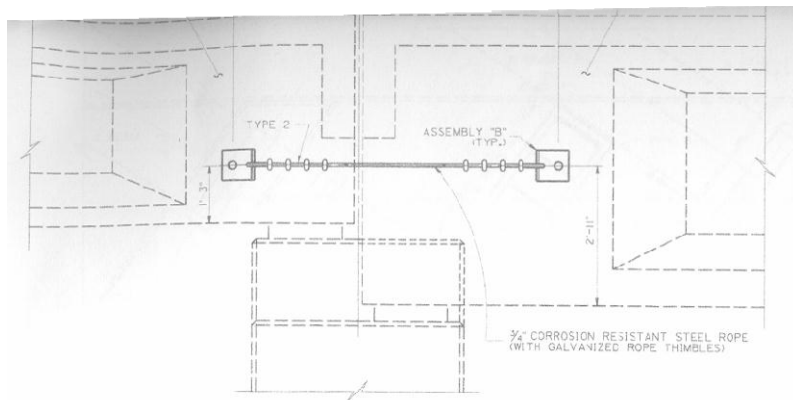
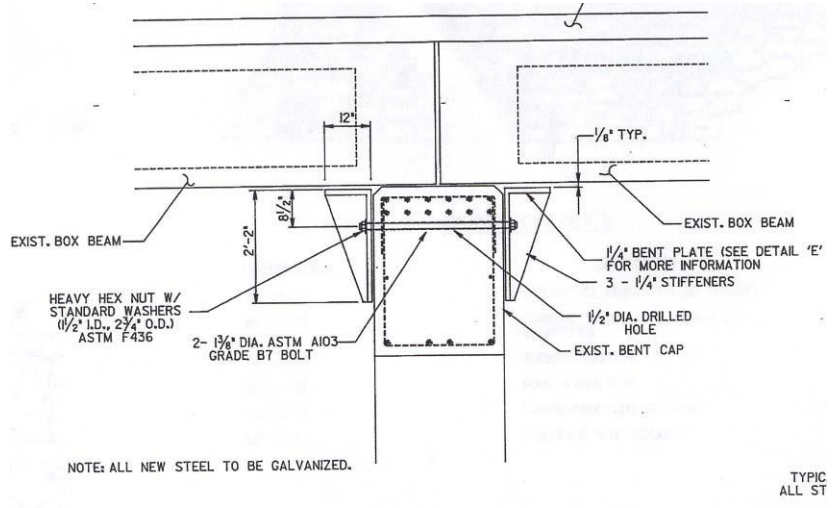


Figure 223 Illustration. Restrainer Cables in Tennessee: Alternative Restrainer Cable Detail (SR 1 over I40 – TN)



Figure 224 Photo. Seat Extenders in Tennessee: Seat Extenders (RT A026 over I40 – TN)



TYPICAL SEISMIC DETAIL AT BENT

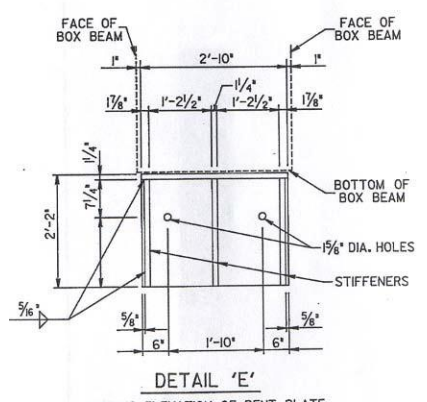


Figure 225 Illustration. Seat Extenders in Tennessee: Detail of Seat Extenders (Rte A026 – TN)

APPENDIX F: SEISMIC RETROFIT IN TENNESSEE/ARKANSAS



Figure 226 Photo. Isolation and Column Retrofit of the Hernando DeSoto Bridge Carrying I40 between Tennessee and Arkansas: Reinforced Concrete Encasement with Steel Jackets (Hernando DeSoto I40 over Mississippi River - TN)



Figure 227 Photo. Isolation and Column Retrofit of the Hernando DeSoto Bridge Carrying I40 between Tennessee and Arkansas: Friction Pendulum Isolation Bearing (Hernando DeSoto I40 Over Mississippi River – TN)



Figure 228 Photo. Isolation and Column Retrofit of the Hernando DeSoto Bridge Carrying I40 between Tennessee and Arkansas: Elastomeric Isolation Bearings (Hernando DeSoto I40 Over Mississippi River – TN)

Section 508 Text

Figure 1 Map. Transportation network. Map of the U.S. showing significant transportation facility.

Figure 2 Map. Seismic hazard in the CSUS. Map of eastern central and southeastern U.S. that shows seismicity in color code near New Madrid fault and Charleston.

Figure 3 Map. 1988 NEHRP map of 500-year return period PGA.

Figure 4 Map. 1996 MCE maps for NEHRP Provisions and upper level events for FHWA Seismic Retrofitting Manual: 0.2-sec spectral acceleration (%g) with 2% probability of exceedance in 50 years (site: NEHRP B-C boundary)

Figure 5 Map. 1996 MCE maps for NEHRP Provisions and upper level events for FHWA Seismic Retrofitting Manual: 1.0-sec spectral acceleration (%g) with 2% probability of exceedance in 50 years (site: NEHRP B-C boundary)

Figure 6 Map. 1996 MCE maps for NEHRP Provisions and upper level events for FHWA Seismic Retrofitting Manual: 0.2-sec spectral acceleration (%g) with 5% probability of exceedance in 50 years (site: NEHRP B-C boundary)

Figure 7 Map. 1996 MCE maps for NEHRP Provisions and upper level events for FHWA Seismic Retrofitting Manual: 1.0-sec spectral acceleration (%g) with 5% probability of exceedance in 50 years (site: NEHRP B-C boundary)

Figure 8 Equation. C_s is equal to $1.2 A S$ divided by T to the power of two-thirds and is not greater than 2.5 times of A .

Figure 9 Map. USGS regional workshops for earthquake hazard mapping

US map marking the location of Seattle, San Francisco, Los Angeles, Salt Lake City, Memphis, and New York City.

Figure 10 Map. Ratio between PGA of 2500-year return period and PGA of 500-year return period for the New Madrid Fault Area.

Figure 11 Map. Comparison for long period response by 1-point and 2-point spectra (1996 USGS data): Long-period response ratio $S_1/1.2PGA$ (500-yr) for the New Madrid Fault Area.

Figure 12 Map. Comparison for long period response by 1-point and 2-point spectra (1996 USGS data): (b) Long-period response ratio $S_1/1.2PGA$ (2500-yr) for the New Madrid Fault Area.

Figure 13 Map. Comparison for short period response by 1-point and 2-point spectra (1996 USGS data): Short-period response ratio $S_s/2.5PGA$ (500-yr) for the New Madrid Fault Area.

Figure 14 Map. Comparison for short period response by 1-point and 2-point spectra (1996 USGS data): Short-period response ratio $S_s/2.5PGA$ (2500-yr) for the New Madrid Fault Area.

Figure 15 Map. Comparison of PGA values between 1988 and 1996 USGS maps: 1988 map (unit: percent of g) for the New Madrid Fault Area.

Figure 16 Map. Comparison of PGA values between 1988 and 1996 USGS maps: 1996 map (unit: g) for the New Madrid Fault Area.

Figure 17 Map. Ratio of long-period design spectral value (S_{D1}) for 2-point/1-point methods—Site B/S1

Figure 18 Map. Ratio of long-period design spectral value (S_{D1}) for 2-point/1-point methods—Site B/S1

Figure 19 Map. Ratio of short-period design spectral value (S_{Ds}) for 2-point/1-point methods—site B/S1

Figure 20 Map. Ratio of short-period design spectral value (S_{Ds}) for 2-point/1-point methods—site E/S4

Figure 21 Graph. Changed power of T in NCHRP 12-49 recommendations: The dashed line shows the long-period branch of design spectrum from Division I-A of AASHTO Standard Specifications (proportional to $T^{-2/3}$). The solid line shows the long-period branch of design spectrum from NCHRP 12-49 recommendations (proportional to T^{-1}).

Figure 22 Map. Ratio of spectral values between 2500-year return period and 500-year return period (2002 data)—PGA

Figure 23 Map. Ratio of spectral values between 2500-year return period and 500-year return period (2002 data)—Short period response (0.2-sec)

Figure 24 Map. Ratio of spectral values between 2500-year return period and 500-year return period (2002 data)—Long period response (1-sec)

Figure 25 Map. Ratio of 2002 data to 1996 data—PGA 2500-year return period

Figure 26 Map. Ratio of 2002 data to 1996 data— S_s 2500-year return period

Figure 27 Map. Ratio of 2002 data to 1996 data— S_1 2500-year return period

Figure 28 Map. 500-year return period PGA from 1988 map for New Jersey.

Figure 29 Map. 500-year return period PGA from 1996 update data for New Jersey.

Figure 30 Map. Seismic Hazard Level in accordance with NCHRP 12-49 recommendations for New Jersey.

Figure 31 Map. Seismic Hazard Level in accordance with NCHRP 12-49 recommendations for New Jersey.

Figure 32 Graph. Map. Sample hazard curves in CSUS (Memphis) and western U.S. (Los Angeles). The curve for Memphis is in red dashed line, while that for Los Angeles is in blue solid line. The horizontal axis is the return period (year) in logarithm scale. The vertical axis is PGA in g. The peak ground acceleration of frequent events (on the left of the graph) at Memphis is much lower than that at Los Angeles. The rare events shown on the right end of the graph have similar intensity at the two locations.

Figure 33 Map. Sites for cost comparison of design based on NCHRP 12-49 recommendations and Standard specifications. The three sites are Johnson County Bridge, St. Clair County Bridge, and Pulaski County Bridge.

Figure 34 Map. Sites to compare the increase of construction cost in Missouri (Contour: $S_1/1.2$ PGA—500-yr). The four sites are shown as Locations A, B, C, and D.

Figure 35 Map. Ratio between PGA of 1000-year return period and PGA of 500-year return period for the New Madrid Fault Area.

Figure 36 Map. Range of Applicability study in NCHRP 20-7 Task 193⁽⁸⁾(GuideSpec). Even under relatively high site amplification for Site Class D, the area that requires “Seismic Demand Analysis” by the NCHRP 20-7 (193) recommendations is of similar size to the “No Analysis” area by AASHTO Standard Specifications.

Figure 37 Map. Seismic Hazard Levels by NCHRP 12-49 recommendations for New Madrid Fault area.

Figure 38 Map. Seismic Hazard Levels by Guide Specifications for New Madrid Fault area.

Figure 39 Map. Seismic Hazard Levels by FHWA Seismic Retrofit Manual (left), Guide Specifications (middle), and NCHRP 12-49 recommendations (right).

Figure 40 Graph. Generic rock/stiff soil shear wave velocity profile used to produce USGS maps. A magnified view shows the top 0~30m layer.

Figure 41 Graph. Samples of ground motion relationships—Frankel et al., 1996

Figure 42 Graph. Samples of ground motion relationships— Atkinson and Boore, 1995 (2-corner)

Figure 43 Graph. Samples of ground motion relationships—Toro et al., 1997 (1-corner)

Figure 44 Graph. Samples of ground motion relationships—Atkinson and Boore, 2006(finite fault)

Figure 46 Graph. Comparison of UHRS to NEHRP spectra for Memphis, St. Louis, and Cabondale⁽¹⁶⁾

Figure 47 Map. Locations where PSHA is performed to produce ground motions for the purpose of site amplification analysis^(18, 19)

Figure 48 Graph. Normalized site coefficients for varying soil layer thickness (left: F_a , right: F_v)

Figure 49 Empirical formulae for modification of site coefficients (left: short period, right: long period)

Figure 50 Screenshot. Opening screen of the ground motion tool

Figure 51 Screenshot. Return period and design/retrofitting documents

Figure 52 Screenshot. Site class

Figure 53 Screenshot. Design spectral values and display of the curve

Figure 54 Illustration. Typical Multi-Span Simply Supported Bridge in Mid-America (*redrawn from TN Department of Transportation Bridge Plans*)

Figure 55 Illustration. Rocker and Fixed Bearings Commonly Found in Mid-America Bridges (*redrawn from IL Department of Transportation Bridge Plans*).

Figure 56 Photo. Typical vulnerabilities found in bridges in the Central and Southeastern US, Including (a) short support lengths, (b) inadequate transverse reinforcement, and (c) inadequate bearings.

Figure 57 Illustration. Analytical Model of Bridge Used in Nonlinear Dynamic Analysis. Top: Line model of a 3-span simply-supported bridge. Bottom: Detailed spring-dashpot models for end joint, intermediate joint, and foundation.

Figure 58 Photo. Damage to steel girder bridges in past earthquake events: (a) pounding damage in Northridge, (b) column damage and (c) shifted superstructure in Kobe, and (d) bearing damage in Nisqually (courtesy of WDOT).

Figure 59 Photo. CSUS bridge retrofits: (a) steel jackets in TN, (b) elastomeric isolation bearings in IL, (c) restrainer cables in KY, (d) seat extenders and (e) shear keys in TN.

Figure 60 Graph. Effect of confinement on concrete. Shaded area shows a relatively small energy dissipation by unconfined concrete.

Figure 61 Graph. Force deformation of column without and with steel jacket⁽²⁹⁾. Graph on the left shows limited hysteresis for column without steel jacket. Graph on the right shows significant hysteresis for steel-jacketed columns.

Figure 62 Illustration. Typical steel jacket retrofit details: (a) full height, (b) typical section.

Figure 63 Photo. Examples of (a) partial height steel jackets in MO and (b) full height steel jackets in TN.

Figure 64 Photo. Concrete column overlay (a) during construction in TN and (b) as a partial encasement in IL.

Figure 65 Photo. Other column retrofits with (a) cable wraps or (b and c) fiber composites performed in IL.

Figure 66 Photo. Column cable wraps, bent cap retrofits, restrainer bars (Poplar Street Complex - IL)

Figure 67 Photo. Steel jacket details (US40 Poplar Street – MO)

Figure 68 Photo. (left) Typical elastomeric bearing adapted from Priestley et al.⁽²⁹⁾, (right) deformed bearing during experimental test.

Figure 69 Graph. Acceleration and displacement response spectrum showing the shift in periods with isolation systems.

Figure 70 Photo. Potentially vulnerable existing steel (a) fixed and (b) rocker bearings.

Figure 71 Photo. Elastomeric bearing isolation systems found in the CSUS.

Figure 71 Photo. Elastomeric bearing isolation systems found in the CSUS.

Figure 72 Photo. Sliding isolation systems used in the Central and Southeastern US.

Figure 73 Photo. (a) Elastomeric bearings with keeper plates, and (b) Bearings with dampers.

Figure 74 Illustration. Examples of restrainer connection details (a) (via the bent cap), or (b) from girder to girder.

Figure 75 Graph. Load-deformation from Caltrans restrainer cable testing⁽³⁷⁾.

Figure 76 Photo. Common CSUS restrainer cable retrofit details as performed in TN.

Figure 77 Photo. Examples of restrainer cables connected between adjacent girders.

Figure 78 Photo. Example of restrainer cables wrapped around bent cap.

Figure 79 Photo. Example of high strength bar restrainers in the Central and Southeastern US.

Figure 80 Photo. Connection details for high strength restrainer bars.

Figure 81 Photo. Connection details for high strength restrainer bars used to restrain motion in the longitudinal and transverse directions.

Figure 82 Photo. Retrofits performed using bumper elements.

Figure 83 Photo. Application of shock transmission units at the intermediate span of a bridge.

Figure 84 Photo. Transverse restraint provided by (a) concrete shear keys and (b) keeper brackets.

Figure 85 Photo. Concrete block transverse shear keys in (a) Indiana (SR51 over White River/Carl Grey Memorial Bridge – IN) and (b) Missouri (Poplar Street Complex – MO).

Figure 86 Photo. (a) Concrete shear keys among other retrofits (Davies Plantation Road – TN) and (b) elevation view of shear key details.

Figure 87 Photo. (a) Steel transverse shear keys along with bent cap retrofit in MO (Poplar Street Complex – MO), and keeper bracket retrofits in TN (b) (SR59 – TN) and (c) (Chambers Chapel Road over I40 – TN)

Figure 88 Illustration. Corbel and bracket seat extender details.

Figure 89 Photo. (a) Traditional seat extender retrofit in TN (RT A026 over I40 – TN), (b) beam extender in MO, and (c) catcher block (Poplar Street Complex – MO).

Figure 90 Photo. Detail of steel bracket type seat extenders like those shown in Figure 89(a) (Rte A026 – TN).

Figure 91 Photo. Steel seat extenders (Poplar Street Complex – MO).

Figure 92 Photo. Bent cap retrofit using post tensioning rods.

Figure 93 Photo. Bent cap retrofit focused on shear reinforcement and confinement of the bent cap end regions.

Figure 94 Photo. Bent cap retrofits with reinforced concrete encasement.

Figure 95 Photo. Bent cap retrofits with reinforced steel encasement

Figure 96 Equation. Probability P_r subscript failure

Figure 97 Equation. Conditional probability P , bracket, “D greater than C” under the condition of IM, close bracket.

Figure 98 Equation. S subscript d equals to a I M superscript b

Figure 99 Equation. Conditional probability P , bracket, DS under the condition PGA, close bracket equals ϕ parenthesis numerator: natural log PGA minus natural log med subscript sys, denominator: beta subscript sys, close parenthesis.

Figure 100 Graph. Fragility curves for the MSSS Concrete girder bridge class, comparing the as-built and retrofitted bridge fragility for each damage state.

Figure 101 Graph. Comparison of as-built and retrofitted median fragility values for each damage state for the (a) MSSS Steel, (b) MSC Steel, and (c) MSC Concrete girder bridges.

Figure 102 Graph. Fragility curves constructed from the lognormal parameters listed in Table 20 for the MSC steel bridge class, comparing the as-built and retrofitted failure probabilities.

Figure 103 Graph. Illustration of (a) comparing the percent change in the median value and (b) comparing other percentiles for assessing retrofits.

Figure 104 Equation. PGA subscript x percent equals med subscript sys exponential parenthesis beta subscript sys times ϕ inverse x-percent, close parenthesis.

Figure 105 Equation. Benefit subscript r equals to E bracket LCC subscript as-built close bracket minus E bracket LCC subscript r close bracket.

Figure 106 Equation. CBR subscript r equals to Benefit subscript r divided by Cost subscript r

Figure 107 Equation. $E, \text{ bracket, } LCC, \text{ close bracket equals } 1 \text{ divided by } \alpha T \text{ times parenthesis } 1 \text{ minus } e \text{ to the power of minus } \alpha T \text{ close parenthesis times capital sigma for } j \text{ from } 1 \text{ to } 4 \text{ parenthesis minus } C \text{ subscript } j \text{ bracket natural log parenthesis } 1 \text{ minus } P \text{ subscript } T \text{ f } j \text{ close parenthesis minus natural log parenthesis } 1 \text{ minus } P \text{ subscript } T \text{ f } j \text{ plus } 1 \text{ close parenthesis close bracket close parenthesis}$

Figure 108 Equation. $P \text{ subscript } T, f, j \text{ equals } 1 \text{ minus parenthesis } 1 \text{ minus } P \text{ subscript AF close parenthesis superscript } T$

Figure 109 Graph. Cost-benefit ratios for retrofit of the case-study bridges, at different locations.

Figure 110 Graph. Performance objectives of buildings and bridges

Figure 111 Illustration. Steel and concrete models used in inelastic response history analysis

Figure 112 Illustration. Discretization of reinforced concrete sections for frame analysis

Figure 113 Illustration. Modeling of gaps with asymmetric spring between two units

Figure 114 Equation. $\Delta \text{ subscript } i \text{ equals } C \text{ capital delta subscript } e$

Figure 115 Equation. $C \text{ for } T \text{ less than } T \text{ subscript } a : C \text{ equals } \mu \text{ when } T \text{ is less than } T \text{ subscript } a. T \text{ subscript } a \text{ is equal to one-thirty-thirds second.}$

Figure 116 Equation. $C \text{ for } T \text{ between } T \text{ subscript } a \text{ and } T \text{ subscript } b. C \text{ equals to } \mu \text{ divided by parenthesis } 2 \mu \text{ minus } 1 \text{ close parenthesis superscript } \beta \text{ when } T \text{ subscript } a \text{ is less than } T \text{ and } T \text{ is less than } T \text{ subscript } b. T \text{ subscript } b \text{ is } 0.125 \text{ second.}$

Figure 117 Equation. $C \text{ for } T \text{ between } T \text{ subscript } b \text{ and } T \text{ subscript } c \text{ prime. } C \text{ equals to } \mu \text{ divided by square root } 2 \mu \text{ minus } 1 \text{ (end square root) when } T \text{ subscript } b \text{ is less than } T \text{ and } T \text{ is less than } T \text{ subscript } c.$

Figure 118 Equation. $C \text{ for } T \text{ between } T \text{ subscript } c \text{ prime and } T \text{ subscript } c. C \text{ equals to } T \text{ subscript } c \text{ divided by } T.$

Figure 119 Equation. $C \text{ equals to } 1 \text{ for } T \text{ greater than } T \text{ subscript } c$

Figure 120 Graph. Estimation of inelastic response from elastic response

Figure 121 Illustration. Configuration of the studied bridge

Figure 122 Illustration. Configuration of typical bents and foundations

Figure 123 Illustration. FE model of the bridge and connectivity of structural components

Figure 124 Graph. Analytical models of bridge components

Figure 125 Graph. Monotonic and cyclic pushover curves of bridge

Figure 126 Graph. Response of full inelastic and bilinear SDOF models in transverse direction

Figure 127 Graph. Maximum transverse response from different analysis methods

Figure 128 Graph. Maximum transverse responses from approximate methods (normalized by inelastic response history results)

Figure 129 Graph. Response of full inelastic and bilinear SDOF models in longitudinal direction

Figure 130 Graph. Maximum longitudinal response from various analysis methods

Figure 131 Graph. Maximum longitudinal responses from approximate methods (normalized by inelastic response history results)

Figure 132 Illustration. Overview of the Caruthersville Bridge⁽⁷⁷⁾

Figure 133 Graph. Spring models for bridge bearings and expansion joints

Figure 134 Illustration. OpenSees model and sample results of Bent 2 foundation system

Figure 135 Graph. Input ground motions with 500 year return period

Figure 136 Illustration. Monitored bents during response history analysis

Figure 137 Illustration. Monitoring points at each bents

Figure 138 Graph. Sample transverse response history of bridge decks, GM2-500

Figure 139 Graph. Sample foundation response in transverse direction

Figure 140 Graph. Sample transverse hysteretic response of bridge piers

Figure 141 Graph. Normalized maximum transverse deck response from two elastic analyses

Figure 142 Graph. Sample longitudinal response history of bridge decks, GM2-1000

Figure 143 Graph. Sample foundation response in longitudinal direction

Figure 144 Graph. Sample longitudinal hysteretic response of bridge piers

Figure 145 Graph. Normalized maximum longitudinal deck response from two elastic analyses

Figure 146 Photo. Bearing retrofits and details in Indiana: Elastomeric bearing with keeper brackets (SR 66 at Diamond – IN)

Figure 147 Photo. Bearing retrofits and details in Indiana: Elastomeric Bearings (HW50 Red Skelton – IN)

Figure 148 Photo. Bearing retrofits and details in Indiana: Isomeric Bearing with Dampers (US 41 @ Eagle Creek –IN)

Figure 149 Photo. Transverse restraining devices in Indiana: Transverse Shear Key (SR51 over White River / Carl Grey Memorial Bridge – IN)

Figure 150 Photo. Transverse restraining devices in Indiana: Transverse Restrainer Cables (SR51 over White River / Carl Grey Memorial Bridge – IN)

Figure 151 Photo. Transverse restraining devices in Indiana: Transverse Restrainer Bars (164 at County Road 800 - IN)

Figure 152 Photo. Poplar Street Retrofits in Illinois: Column Cable Wraps, Bent Cap Retrofits, Transverse Restrainer Bars (Poplar Street Complex - IL)

Figure 153 Photo. Poplar Street Retrofits in Illinois: Details of Cable Column Wraps, Bent Cap Retrofits, Transverse Restrainer Bars (Rte 3 Poplar Street – IL)

Figure 154 Photo. Poplar Street Retrofits in Illinois: Bent Cap Retrofit, Longitudinal Restrainer Bars, and Transverse Restraint with Turnbuckles (Poplar Street Complex – IL)

Figure 155 Photo. Poplar Street Retrofits in Illinois: Cable Column Wraps, Bent Cap Retrofits, Restrainer Bars (Rte 70 Poplar Street – IL)

Figure 156 Photo. Poplar Street Retrofits in Illinois: Elevations (Rte 70 Poplar Street – IL)

Figure 157 Photo. Details of Column and Bent Cap Wraps in Illinois: Column Cable Wraps (Poplar Street Complex – IL)

Figure 158 Illustration. Details of Column and Bent Cap Wraps in Illinois: Cable Wraps (Rte 70 Poplar Street – IL)

Figure 159 Illustration. Details of Column and Bent Cap Wraps in Illinois: Bent Cap Wraps (Rte 70 Poplar Street – IL)

Figure 160 Photo. Restrainer Bars and Bumpers in Illinois: Restrainer Bar (Poplar Street Complex - IL)

Figure 161 Illustration. Restrainer Bars and Bumpers in Illinois: Restrainer Bar Connections /Column Cable Wraps (Rte 70 Poplar Street – IL)

Figure 162 Photo. Restrainer Bars and Bumpers in Illinois: Bumpers and Restrainer Bar (Poplar Street Complex - IL)

Figure 163 Illustration. Restrainer Bars and Bumpers in Illinois: Bumpers (Rte 3 Poplar Street – IL)

Figure 164 Photo. Restrainer Bars in Illinois: Restrainer Bar (Poplar Street Complex - IL)

Figure 165 Illustration. Restrainer Bars in Illinois: Detail of Typical Restrainer Bars (Rte 3 Poplar Street – IL)

Figure 166 Illustration. Restrainer Bars in Illinois: Detail of Alternative Restrainer Bar Assembly (Rte 70 Poplar Street – IL)

Figure 167 Photo. Column Retrofits in Illinois: Fiber Composite Retrofit (Poplar Street Complex – IL)

Figure 168 Photo. Column Retrofits in Illinois: Partial Column Encasement (Poplar Street Complex – IL)

Figure 169 Photo. Column Retrofits in Illinois: Fiber Composite Retrofit (Poplar Street Complex – IL)

Figure 170 Photo. Isolation in Illinois: Elastomeric Bearings and Restrainer Cables (Poplar Street Complex – IL)

Figure 171 Photo. Isolation in Illinois: Isolation Bearing (Poplar Street Complex – IL)

Figure 172 Photo. Different restrainer cable configurations in Kentucky: Restrainer Cables

Figure 173 Photo. Different restrainer cable configurations in Kentucky: Restrainer Cables

Figure 174 Photo. Different restrainer cable configurations in Kentucky: Restrainer Cables

Figure 175 Photo. Shear Key and Shock Transmission Unit Retrofits in Missouri: Shear Keys and Shock Transmission Units (Poplar Street Complex – MO)

Figure 176 Illustration. Shear Key and Shock Transmission Unit Retrofits in Missouri: Shock Transmission Unit and Shear Key (I70 Poplar Street – MO)

Figure 177 Illustration. Shear Key and Shock Transmission Unit Retrofits in Missouri: Shear Keys and Shock Transmission Units (I70 Poplar Street – MO)

Figure 178 Photo. Bumper, Bent Cap, and Shear Key Retrofits in Missouri: Bumpers (Poplar Street Complex – MO)

Figure 179 Illustration. Bumper, Bent Cap, and Shear Key Retrofits in Missouri: Bumpers (US40 Poplar Street – MO)

Figure 180 Illustration. Bumper, Bent Cap, and Shear Key Retrofits in Missouri: Transverse Shear Key (US40 Poplar Street – MO)

Figure 181 Photo. Bumper, Bent Cap, and Shear Key Retrofits in Missouri: Bent Cap Post-tension Retrofit

Figure 182 Photo. Longitudinal Bumper and Restrainer Retrofits in Missouri: Restrainer Bars and Bumpers (Poplar Street Complex – MO)

Figure 183 Illustration. Longitudinal Bumper and Restrainer Retrofits in Missouri: Bumper and Restrainer Cable (US40 Poplar Street – MO)

Figure 184 Photo. Longitudinal Bumper and Restrainer Retrofits in Missouri: Steel Jackets (Poplar Street Complex – MO)

Figure 185 Illustration. Longitudinal Bumper and Restrainer Retrofits in Missouri: Steel Jacket Details (US40 Poplar Street – MO)

Figure 186 Photo. Seat Extenders and Bent Cap Retrofit in Missouri: Beam Seat Extender (Poplar Street Complex – MO)

Figure 187 Illustration. Seat Extenders and Bent Cap Retrofit in Missouri: Seat Extender Section (US40 Poplar Street – MO)

Figure 188 Photo. Seat Extenders and Bent Cap Retrofit in Missouri: Bent Cap Retrofit (Poplar Street Complex – MO)

Figure 189 Photo. Seat Extender and Restrainer Rods in Missouri: Seat Extenders (Poplar Street Complex – MO)

Figure 190 Illustration. Seat Extender and Restrainer Rods in Missouri: Restrainers (US40 Poplar Street – MO)

Figure 191 Illustration. Seat Extender and Restrainer Rods in Missouri: Seat Extender (US 40 Poplar Street – MO)

Figure 192 Illustration. Replacement with Less Vulnerable Bearings in Missouri: Bearing Replacement (US40 Poplar Street – MO)

Figure 193 Photo. The First Seismic Retrofit in Tennessee: First Retrofit in TN: “Uplift” and Longitudinal Restrainer Cables (SR 14 over CSX Railroad – TN)

Figure 194 Photo. The First Seismic Retrofit in Tennessee: First Retrofit in TN: “Deck Girder” Restrainer Cables (SR 14 over CSX Railroad – TN)

Figure 195 Illustration. The First Seismic Retrofit in Tennessee: Steel Jackets and Restrainer Cables (SR 14 over CSX Railroad – TN)

Figure 196 Illustration. The First Seismic Retrofit in Tennessee: Restrainer Cables (SR14 over CSX Railroad – TN)

Figure 197 Illustration. The First Seismic Retrofit in Tennessee: Deck Girder Restrainer Cables (SR14 over CSX Railroad – TN)

Figure 198 Photo. Retrofit of Davies Plantation Road in Tennessee: Bent Cap Retrofit, Steel Jackets, and Shear Keys (Davies Plantation Road – TN)

Figure 199 Illustration. Retrofit of Davies Plantation Road in Tennessee: Shear Key (Davies Plantation Road – TN)

Figure 200 Illustration. Details of Bent Cap and Column Retrofit in Tennessee: Bent Cap and Steel Casing (Davies Plantation Road – TN)

Figure 201 Photo. Retrofit of Columns and Bearings in Tennessee: Painted Steel Jackets (I40 over SR 15 – TN)

Figure 202 Illustration. Retrofit of Columns and Bearings in Tennessee: Bearing Retrofit (I40 over SR 15 – TN)

Figure 203 Photo. Retrofit of Columns and Bearings in Tennessee: Bearing Retrofit (I40 over SR 15 – TN)

Figure 204 Photo. Retrofit of Columns and Bent Caps in Tennessee: Steel Jackets and Bent Cap Retrofit (SR 196 over I40 – TN)

Figure 205 Illustration. Retrofit of Columns and Bent Caps in Tennessee: Bent Cap Retrofit (SR 196 – TN)

Figure 206 Illustration. Retrofit of Columns and Bent Caps in Tennessee: Steel Jackets (SR196 – TN)

Figure 207 Photo. Restrainer Cable Details in Tennessee: Restrainer Cables and Transverse Keeper Brackets (Chambers Chapel Road over I40 – TN)

Figure 208 Illustration. Restrainer Cable Details in Tennessee: Connection for Cables (Chambers Chapel Road – TN)

Figure 209 Illustration. Restrainer Cable Details in Tennessee: Restrainer Cable and Attachments (Chambers Chapel Road – TN)

Figure 210 Photo. Transverse Keeper Brackets (Shear Keys) in Tennessee: Transverse Keeper Brackets (Chambers Chapel Road over I40 – TN)

Figure 211 Illustration. Transverse Keeper Brackets (Shear Keys) in Tennessee: Keeper Bracket Details – Type B (Chambers Chapel Road – TN)

Figure 212 Photo. Transverse Keeper Brackets (Shear Keys) in Tennessee: Keeper Brackets (Chambers Chapel Road over I40 – TN)

Figure 213 Illustration. Transverse Keeper Brackets (Shear Keys) in Tennessee: Keeper Brackets - Type A (Chambers Chapel Road – TN)

Figure 214 Photo. Steel Jacket and Footing Retrofit in Tennessee: Steel Column Jackets (Chambers Chapel Road – TN)

Figure 215 Illustration. Steel Jacket and Footing Retrofit in Tennessee: Steel Jacket Elevation (Chambers Chapel Road – TN)

Figure 216 Illustration. Steel Jacket and Footing Retrofit in Tennessee: Steel Column Jackets and Footing Retrofit (Chambers Chapel Road – TN)

Figure 217 Photo. Concrete Shear Keys in Tennessee: Concrete Shear Keys (SR59 over I40 – TN)

Figure 218 Illustration. Concrete Shear Keys in Tennessee: Concrete Shear Key Details (SR59 – TN)

Figure 219 Photo. Keeper Brackets in Tennessee: Keeper Brackets (SR59 – TN)

Figure 220 Illustration. Keeper Brackets in Tennessee: Keeper Bracket Details (SR59 – TN)

Figure 221 Photo. Restrainer Cables in Tennessee: Restrainer Cables (SR59 – TN)

Figure 222 Illustration. Restrainer Cables in Tennessee: Restrainer Cable Detail (SR59 – TN)

Figure 223 Illustration. Restrainer Cables in Tennessee: Alternative Restrainer Cable Detail (SR 1 over I40 – TN)

Figure 224 Photo. Seat Extenders in Tennessee: Seat Extenders (RT A026 over I40 – TN)

Figure 225 Illustration. Seat Extenders in Tennessee: Detail of Seat Extenders (Rte A026 – TN)

Figure 226 Photo. Isolation and Column Retrofit of the Hernando DeSoto Bridge Carrying I40 between Tennessee and Arkansas: Reinforced Concrete Encasement with Steel Jackets (Hernando DeSoto I40 over Mississippi River - TN)

Figure 227 Photo. Isolation and Column Retrofit of the Hernando DeSoto Bridge Carrying I40 between Tennessee and Arkansas: Friction Pendulum Isolation Bearing (Hernando DeSoto I40 Over Mississippi River – TN)

Figure 228 Photo. Isolation and Column Retrofit of the Hernando DeSoto Bridge Carrying I40 between Tennessee and Arkansas: Elastomeric Isolation Bearings (Hernando DeSoto I40 Over Mississippi River – TN)